



**HAL**  
open science

## Contributions for parametric identification and observation of powered two-wheeler vehicles

Majda Fouka

► **To cite this version:**

Majda Fouka. Contributions for parametric identification and observation of powered two-wheeler vehicles. Automatic. Université Paris-Saclay, Université d'Evry Val-d'Essonne, 2019. English. NNT : 2019SACLE033 . tel-02453899

**HAL Id: tel-02453899**

**<https://hal.science/tel-02453899>**

Submitted on 24 Jan 2020

**HAL** is a multi-disciplinary open access archive for the deposit and dissemination of scientific research documents, whether they are published or not. The documents may come from teaching and research institutions in France or abroad, or from public or private research centers.

L'archive ouverte pluridisciplinaire **HAL**, est destinée au dépôt et à la diffusion de documents scientifiques de niveau recherche, publiés ou non, émanant des établissements d'enseignement et de recherche français ou étrangers, des laboratoires publics ou privés.

# Contributions to Parametric Identification and Observation of Powered Two-Wheeler Vehicles.

Thèse de doctorat de l'Université Paris-Saclay  
préparée à l'Université d'Evry-Val-d'Essonne

Ecole doctorale n 580 Sciences et Technologies de l'Information et de la  
Communication (STIC)  
Spécialité de doctorat : Automatique

Thèse présentée et soutenue à Evry, le 5 decembre 2019, par

**MAJDA AMINA AIDA FOUKA**

Composition du Jury :

Andreas Rauh Professeur des Universités, Rostock, Allemagne	Rapporteur
Roberto Lot Professeur des Universités, Padova, Italie	Rapporteur
Philippe Chevrel Professeur des Universités, IMT Atlantique, France	Rapporteur
Cristina Stoica Maniu Professeur des Universités, CentraleSupélec, L2S, Paris	Présidente
Hichem Arioui Maître de Conférences-HDR, UEVE, Evry	Directeur de thèse
Lamri Nehaoua Maître de Conférences, UEVE, Evry	Co-directeur de thèse
Saïd Mammam Professeur des Universités, UEVE, Evry	Invité



## *Acknowledgements*

Many persons have given me help, guidance, and inspiration during my thesis at university of Evry Val d'Essonne and Paris-Saclay. I would like to express my gratitude to all of them who have made this thesis possible. First, I would like to express heartfelt thanks to my advisor Hichem Arioui, for his research direction and encouragement during my doctoral study. No person I met has a deeper sense of understanding and better ability to explain his ideas. I consider a great honor to have him as a advisor and I look forward to many more years of collaboration. I am especially grateful to my supervisor Lamri Nehaoua, for his patience, and support during my thesis in the Research Laboratory. Besides his technical skills, which I had the possibility to appreciate during my research work, I wish to thank him for his insightful comments that have exemplified the work during the development of my thesis. I have to express also my gratitude to my co-advisor, Said Mammam, for his valuable advices, for encouraging my research and for allowing me to grow as a research scientist. His advice on my thesis work as well as my career has been priceless.

The most fortunate event in my thesis has been meeting professors Sergio Savaresi, Simone Gelmini and Mara Tanelli. I would like to thank them, for having accepted me for an internship in their University of Politecnico di Milano, Polimi in Italy. During this experience, I benefited from their vast industrial and research experience, but also from a new perspective on my work.

I would also like to extend my thank to professor Hermann Winner, for having accepted me in their laboratory (FZD, Group of motorcycle safety, Darmstadt University of Technology in Germany). My gratitude thanks go to doctor engineers Raphael Pleß for involving me in many challenging research projects related to motorcycle dynamics. During my stay they have also been friendly and I sincerely hope we find opportunities in the future to work together once again.

My deepest thanks go the dissertation committee members. I would like to thank Andreas Rauh, Professor at the University of Rostock Germany, Roberto Lot, Professor at the University of Padoue Italy, and Philippe Chevrel, Professor at IMT Atlantique, for the honor they have given me by accepting to be reporters of this thesis. I would also express my gratitude to Cristina Stoica Maniu, Professor at the University Paris-Sud, and to Mr. Mohammed M'saad, Professor at ENSICAEN, who kindly accepted to be examiners.

I am grateful to my current and past office-mates in the IBISC Laboratory: Fida Benabdallah, Rayane Benyoucef, Eslam abouselima, Sara Ifqir and Sushil sharma for the fun we had together in many occasions in the lab and outside during all this time. I only make an exception for Dr. Pierre Marie Damon who deserves a special treatment, he helped me so many times in learning the software dedicated to study the behavior of the motorcycle during these years. Above anyone else I would like to thank, Mahtout Imane. She has been giving me her personal and professional unwavering support and encouraged me to strive towards my goal.

Finally, I would like to thank my parents for their support through all my life. Words cannot express how grateful I am to my mother for all of her support and sacrifices. She has been and will always be a model for my life. A special thanks goes to my sisters Farah and Sarah and my aunt Sadia and other people close to me. They have been a tremendous emotional and psychological support to me throughout these years and for that I am eternally thankful.

Last but not least, I owe special thanks to my husband, Said Boudkhal, to which this dissertation is dedicated. His smiles and jokes are always of great fun and support for me, in all occasions. I deeply thank him for being my pillar that encourages me to overcome hardships, his encouragement were a great comfort to me and contributed to the success of this work.



## *Abstract*

Nowadays, Powered Two-Wheeled Vehicles (PTWV) are an increasingly popular means of transport in daily urban and rural displacements, especially for the possibilities it offers to avoid traffic congestion. However, riders are considered as the most vulnerable road users. In fact, the unstable nature of the PTWV makes them more susceptible to loss of control. This problem is even more complex during emergency braking or on cornering maneuvers. As matter of fact, passive and active safety systems such as Anti-Lock Braking (ABS), Electronic Stability Control (ESP), seat belts, airbags developed in favour of passenger vehicles have largely contributed to the reduction of risks on the road. However, the delay in the development of security systems for motorcycles is notable. Moreover, despite some existing systems, motorcycle riders use them badly or they don't use them at all. Therefore, it is not trivial that this delay, in the development of Advanced Rider Assistance Systems (ARAS), coming from a delay in the development of theoretical and research tools.

This thesis fits into the context of designing ARAS for PTWV. Our work deals with observation and identification techniques to estimate the PTWV dynamic states and physical parameters. These latter are fundamental for risk quantification and to assess the safety of the PTWV, which are the main focus of our research work. The first part of the thesis concerns classical identification techniques for estimating the physical parameters of PTWV. The second part deals with model-based observers proposed to estimate the dynamic states of the PTWV. We proposed an unknown input observer (UIO) for steering and road geometry estimation and an interconnected fuzzy observer (IFO) for both longitudinal and lateral dynamics. An alternative methods to identification algorithms are observer-based identifier which allow both the parameters identification and the states estimation. Therefore, a Luenberger adaptive observer (LAO) for lateral dynamic states and pneumatic stiffness as well as a delayed unknown inputs observer (DUIO) with an arbitrary relative degree, have been developed in this thesis.

As matter of fact, all these techniques allow to estimate the motorcycle dynamics while reducing the number of sensors and overcoming the problem of non-measurable states and parameters. These proposed methods require a simple combination of sensors and take into account realistic assumption like the longitudinal speed variation. Among others, this manuscript introduces a self calibration algorithm for Inertial Measurement Units (IMUs) alignment. Such a self-calibration method is used for telematic boxes (e-Boxes) installed on two-wheeled vehicles, whose IMUs' axes are often result not to be aligned with the vehicle reference system. Finally, objective indicators are setting up to quantify the riding risks. These functions were studied for ARAS purpose. To highlight the performance of these approaches, we have acquired data from high-fidelity motorcycle simulator or even with data from real motorcycles. To conclude, we have drawn up a comparison tables with the proposed approaches. The results of both the numerical simulations and the performed experimentation seem to be quite promising.



# Contents

<b>Contents</b>	<b>v</b>
<b>List of Figures</b>	<b>ix</b>
<b>List of Tables</b>	<b>xiii</b>
<b>List of Abbreviations</b>	<b>xv</b>
<b>List of Symbols</b>	<b>xvii</b>
<b>General Introduction</b>	<b>1</b>
<b>I Context &amp; PTW Vehicle Modeling</b>	<b>7</b>
<b>1 Road fatalities and ARAS for PTWV</b>	<b>9</b>
1.1 Road Traffic Fatalities . . . . .	9
1.1.1 Fatal Accident Statistics . . . . .	10
1.2 Fatal Risk Factors . . . . .	12
1.3 Motorcycles Safety Issues . . . . .	13
1.3.1 Attractiveness of PTWV . . . . .	14
1.3.2 Dynamic Specification of Motorcycles . . . . .	14
1.3.3 Vulnerability of PTWV users . . . . .	17
1.4 Intelligent Transportation Systems . . . . .	18
1.4.1 Overview on Road Safety Systems . . . . .	18
1.4.2 Towards Motorcycles ITS . . . . .	19
1.5 State of the art of Motorcycle ITS . . . . .	20
1.5.1 Advanced Rider Assistance Systems . . . . .	20
1.5.2 On-Bike Information Systems . . . . .	21
1.5.3 Vision Enhancement for Crash Avoidance . . . . .	21
1.5.4 Motorcycle Autonomous Emergency Braking . . . . .	22
1.5.5 Antilock Braking System Technology . . . . .	22
1.5.6 Precrash Systems and External Airbags . . . . .	22
1.5.7 Curve Speed Warning . . . . .	23
1.5.8 Roadway Departure Warning Motorcycle . . . . .	23
1.5.9 Electronic Stability Program . . . . .	23
1.5.10 Inter-Vehicle Communication System for Motorcycle . . . . .	23
1.5.11 Helmet-Mounted Display . . . . .	24
1.5.12 Longitudinal Control System . . . . .	24
1.5.13 Gaps in ITS for Motorcycle Safety . . . . .	24
1.6 VIROLO++ Project Overview . . . . .	24
1.7 Conclusions . . . . .	26

<b>2</b>	<b>PTW Vehicle Modeling</b>	<b>27</b>
2.1	Overview of PTW Vehicle	27
2.2	PTWV Description	29
2.3	Tire-Ground Interactions	30
2.4	Tire's kinematics	30
2.5	Pneumatic efforts	32
2.5.1	The Magic Formula	32
2.5.2	Lateral Force	33
2.5.3	Longitudinal Force	34
2.5.4	Vertical Forces	35
2.5.5	Self-Alignment Moment	35
2.5.6	Overturning Moment	36
2.5.7	Rolling Resistance Moment	37
2.6	Literature of Motorcycle Dynamics Modeling	37
2.7	PTWV Dynamics Modeling	38
2.7.1	Motorcycle Description	38
2.7.2	Virtual Power Principle	40
2.7.3	Technical Simplification for Implementation Purpose	42
2.8	Two-Body Model for the Lateral Dynamics	42
2.8.1	Assumptions	42
2.8.2	Rear and Front Body Kinematics	43
2.8.3	Rear and Front Tire-Road Contact Point Kinematics	45
2.8.4	Non-Conservative Generalized Efforts	48
2.9	Linearisation and State Space Models	48
2.9.1	Out-of-Plane Motion	49
2.9.2	Road Consideration	50
2.9.3	One-Body Model of Lateral Dynamic	52
2.9.4	In-Plane Motion	52
2.10	Stability and Handling	53
2.10.1	Gyroscopic effect	53
2.10.2	Vibration Modes	53
2.10.3	PTWV Control	54
2.11	Motorcycle Instrumentation and Data Calibration	55
2.12	Instrumented Lab's Motorcycle	55
2.13	Inertial Sensor Calibration	56
2.13.1	Overview of Calibration	56
2.13.2	Self-Calibration Algorithm	57
2.13.3	Experimental Results	60
2.13.4	Final Remarks	63
2.14	Conclusions	63
<b>II</b>	<b>Parametric Identification of PTWV</b>	<b>65</b>
	Introduction	67
<b>3</b>	<b>Identification of a Single Rigid-Body model</b>	<b>69</b>
3.1	Parametric Identification-Geometric Approach	69
3.2	Gradient Decent Algorithm	71
3.3	Algebraic Identification Approach	73
3.4	Experimental Result	75
3.4.1	Static Test	75
3.4.2	Dynamic Test	77
3.4.3	Algebraic Identification	78
3.4.4	Gradient Method	79
3.5	Conclusions	81
<b>4</b>	<b>Identification of Two-bodies model</b>	<b>82</b>
4.1	Multi-Objective Optimization	82
4.1.1	Identification Problem Formulation	83

4.1.2	Optimization Problem Formulation	84
4.1.3	Simulation Results	85
4.2	Levenberg-Marquardt (LM) Algorithm	88
4.2.1	Problem Statement	88
4.2.2	Simulation Results	89
4.3	Final Remarks	93
4.4	Comparison and analysis	93
Conclusions		95
<b>III Model-based Observers for PTWV Estimation and Identification</b>		<b>96</b>
Introduction		98
<b>5</b>	<b>Road and Steering Dynamics Reconstruction</b>	<b>100</b>
5.1	LPV Observer Design	100
5.2	Unknown Input Estimation	104
5.3	Experimental Results	105
5.4	Conclusions	109
<b>6</b>	<b>Delayed Unknown Input Observer</b>	<b>110</b>
6.1	Problem Statement	110
6.2	Augmented State Space	111
6.3	Observer Design	112
6.4	Extension to the PTWV case	115
6.4.1	Problem Statement	115
6.4.2	Augmented Model	117
6.4.3	Observer Design	117
6.5	Application for PTWV Estimation	119
6.6	Simulations Results	120
6.7	Conclusions	124
<b>7</b>	<b>Adaptive Observer for PTWV</b>	<b>125</b>
7.1	Model Description	125
7.1.1	Parameter-Dependent Model	126
7.1.2	Problem Statement	127
7.2	Observer Design	128
7.2.1	Observability Analysis	128
7.2.2	Adaptive Observer	128
7.2.3	Polytopic Form	131
7.3	Simulation Results	132
7.4	Observer Sensitivity and Robustness	135
7.4.1	Observer Sensitivity against Sensors' Noise	135
7.4.2	Observer Robustness against Modeling Uncertainties	135
7.5	Motorcycle Experimental Test	136
7.6	Conclusions	139
<b>8</b>	<b>Interconnected Observers for PTWV</b>	<b>140</b>
8.1	Complete PTWV Model	140
8.1.1	State Space Representation	140
8.2	Observer Design	142
8.2.1	Preliminaries	143
8.2.2	State Estimation	143
8.3	Observer Evaluation and Simulation	147
8.4	Final Remarks	151
8.5	Comparison and Analysis	151
Conclusions		153

<b>IV Risk Assessment: Steering Behavior</b>	<b>155</b>
Introduction	157
<b>9 On Steady-State Cornering Analysis</b>	<b>159</b>
9.1 Lateral Motorcycle Dynamics	159
9.2 Steady Steering behavior and Handling Analysis	160
9.3 Side Slip Dynamics	161
9.4 Neutral Path Detection Algorithm	163
9.5 Simulation Results	164
9.5.1 Scenario 1	165
9.5.2 Scenario 2	166
9.5.3 Results Discussion	168
9.6 Conclusions	168
<b>10 Lane Crossing Tracking</b>	<b>170</b>
10.1 Problem Statement	170
10.2 Vision-based Information	171
10.3 Lane Crossing Point Tracking	172
10.3.1 Straight predicted vehicle trajectory ( $\delta = 0$ )	172
10.3.2 Circular predicted vehicle trajectory ( $\delta \neq 0$ )	172
10.4 Simulation Results	176
10.4.1 Case 1: Straight road with zero steering	176
10.4.2 Case 2: Curved roads with constant steering	177
10.5 Conclusions	178
<b>General Conclusions &amp; Perspectives</b>	<b>180</b>
<b>Appendices</b>	<b>187</b>
<b>A Definitions of observability and detectability</b>	<b>187</b>
A.0.1 LTI system properties	187
A.0.2 LTV/LPV system properties	188
<b>B Motivating example of DUIO</b>	<b>190</b>
B.0.1 The noise-free case	190
B.0.2 The noisy outputs case	190
<b>C Numerical Values of the PTWV</b>	<b>193</b>

# List of Figures

1.1	Fatalities statistics and global target in France (ONSIR, 2018).	10
1.2	Trends per road users categories in France	11
1.3	Monthly number of road fatalities: Killed in 30 days per year in France.	12
1.4	Annual Global Road Crash Statistics (ZindaLawGroup, 2015).	13
1.5	In Bangladesh, riding a PTWV has become an efficient solution for urban mobility (Dhaka Tribune, December 2017).	14
1.6	Gendarme dead in Trieux, Meurthe-et-Moselle, 2015.	14
1.7	Honda's self-balancing motorcycle (Honda, 2017)	15
1.8	Loss of control in curve (Machézal, Loire, July 2012)	15
1.9	Counter-steering phenomenon.	16
1.10	Motorcycle wheelie and stoppie situations.	16
1.11	Mortality by road user category (WHO, 2018).	17
1.12	Motorcycles Accidents (Oliveira, 2013).	18
1.13	Safety System.	18
1.14	ARAS Systems for PTWV.	19
1.15	Rider Assistance System Architecture.	20
1.16	Classification of ARAS for PWTv.	21
1.17	VIROLO++ French ANR Research Project.	25
2.1	Two-Wheeler Vehicles.	28
2.2	Motorcycle components.	29
2.3	Geometry for handling of of two-wheeled vehicle.	30
2.4	Effort generated by the pneumatic.	31
2.5	Normalised magic Formula or Pacejka model.	33
2.6	The influence of $\gamma$ on the normalized $F_y$ .	33
2.7	Longitudinal tire force as a function of the longitudinal slip ratio.	34
2.8	Self-alignment Moment, $M_z$ .	36
2.9	Overturning moment, $M_x$ .	36
2.10	Rolling resistance Moment, $M_y$ .	37
2.11	Geometry of the eight-body model of the PTWV with rider.	39
2.12	Orientation of PTWV coordinate systems.	40
2.13	Geometry of the two-body model of the PTWV and its rider.	43
2.14	Front tire contact point.	46
2.15	Schematic side view of the PTWV two-body model with notation, Sharp equivalent model.	50
2.16	Motorcycle geometry with road banking angle.	51
2.17	Kinematic representation of PTWV.	52
2.18	Lateral stability curve of PTWV.	54
2.19	Motorcycle-Road-Environment.	55
2.20	Instrumented Scooter at the IBISC Lab, university of Evry.	56
2.21	An overview of the experimental setup used to validate the algorithm.	57
2.22	The alignment of the axes $x$ , $y$ , $z$ to the tern $x''$ , $y''$ , $z''$ .	57
2.23	The flowchart of the self-calibration algorithm.	58

2.24	Self-calibration and experimental measurements: (left) the raw acceleration vector, (right) the acceleration vector along the virtual aligned axes. . . . .	61
2.25	Sensitivity analysis: an overview of the sensitivity analysis of the averaging window for the estimate of $\varphi$ and $\vartheta$ . It is evident that with at least 4000 samples, the error computed in the estimate is very small with respect to the one estimated when the vehicle is standing still. . .	62
2.26	Sensitivity analysis: the RLS convergence is compared with the averaged LS. Estimates converge in less than 400 samples. Steady state error results to be smaller than 0.92 deg. . . . .	62
3.1	Single body geometry of motorcycle. . . . .	70
3.2	The balance of forces - Motorcycle on the slope in the opposite direction. . . . .	70
3.3	The position of the CoG o of the motorcycle and the rider. . . . .	71
3.4	Functional diagram of Gradient Descent. . . . .	72
3.5	The instrumented Kawasaki ER6N PTWV. . . . .	75
3.6	Measurement environment . . . . .	76
3.7	Steering angle, chirp flying input. . . . .	78
3.8	System outputs. . . . .	78
3.9	Parameters convergence. . . . .	79
3.10	Parameters convergence . . . . .	79
3.11	Turning at the roundabout. . . . .	80
3.12	Steering angle input. . . . .	80
3.13	Validation of the model: turning at the roundabout. . . . .	81
4.1	Riders torque and motorcycle path. . . . .	85
4.2	Comparison between the roll, steer angles and lateral speed of the identified model and the <i>BikeSim</i> motorcycle data. . . . .	86
4.3	Comparison between the identified model and the <i>BikeSim</i> motorcycle data. . . . .	86
4.4	Comparison between the identified model and the <i>BikeSim</i> motorcycle data. . . . .	87
4.5	Block diagram of the LM method. . . . .	89
4.6	Test manoeuvrer : double line change, $v_x = 100$ km/h in circle road, on high-friction surface $\mu = 0.85$ : Rider torque $\tau$ - Longitudinal velocity - Path. . . . .	90
4.7	Generic responses (acceleration angles) estimation in initial parameters value $\theta_0$ compared to actual responses. . . . .	90
4.8	Generic responses (acceleration angles) estimation after updating parameters estimates value $\theta_i$ , compared to actual responses . . . . .	90
4.9	Combined inertial parameters estimates $\hat{\theta}_i, \hat{\theta}_6$ . . . . .	91
4.10	Correlation graph for white noise and residual error. . . . .	91
4.11	Test manoeuvrer 2: oncoming variable speed, in road course with $\mu = 0.85$ : Rider torque $\tau$ - Longitudinal velocity - Path. . . . .	91
4.12	Generic responses (acceleration angles) estimation in initial parameters value $\theta_0$ compared to actual responses. . . . .	92
4.13	Generic responses (acceleration angles) estimation after updating parameters estimates value $\theta_i$ , compared to actual responses. . . . .	92
4.14	Combined inertial parameters estimates. . . . .	92
4.15	Correlation graph for white noise and residual error. . . . .	92
5.1	Longitudinal velocity . . . . .	105
5.2	States estimation (gray) compared to actual measurement (orange). . . . .	106
5.3	Unmeasurable states estimation of Scooter. . . . .	107
5.4	Unknown inputs estimation. . . . .	107
5.5	State estimation validation: $F_{yf}, F_{yr}, F_{\phi_r}$ from the estimated lateral acceleration (dashed gray) compared to the IMU lateral acceleration (orange). . . . .	108
5.6	State estimation validation: $\hat{v}_y$ from the lateral acceleration (dashed gray) compared to the IMU lateral acceleration (orange). . . . .	108
5.7	State estimation validation: $\phi, \phi_r$ estimated (gray) from the IMU roll angle measurement (orange). . . . .	108
5.8	Front and Rear Sidelip angles. . . . .	109
6.1	Steering torque input (chirp signal). . . . .	120
6.2	Actual measures (blue) and their estimation (dashed red). . . . .	121

6.3	Observer validation. . . . .	121
6.4	Actual parameters (dashed red) and estimated parameters (blue). . . . .	122
6.5	Slalom maneuver at constant speed 40 km/h. . . . .	122
6.6	Test 1: Updated state (dashed red) compared to actual measurement (blue). . . . .	123
6.7	An oncoming traffic with variable speed. . . . .	123
6.8	Test 2: Updated state (dashed red) compared to actual measurement (blue). . . . .	124
7.1	Schematic overview of estimation methodology. . . . .	128
7.2	<i>BikeSim</i> scenario: the rider's steering torque input $\tau$ , the forward speed $v_x$ , and the vehicle's trajectory. . . . .	133
7.3	<i>BikeSim</i> sensor (red) and observer estimation (dashed blue). . . . .	133
7.4	Unmeasurable states estimation. . . . .	133
7.5	<i>BikeSim</i> sensor (red) and observer estimation (dashed blue). . . . .	134
7.6	Estimation performance of tire cornering stiffness. . . . .	134
7.7	Robustness to noise: observer states estimation in presence of IMU measurements noise. . . . .	136
7.8	Experimental test: Vehicle trajectory, rider steering torque and longitudinal velocity. . . . .	137
7.9	Test 2: Scooter Experimental test: Unmeasurable states estimation. . . . .	138
7.10	Test 2: Scooter Experimental test : Actual measures (red) and their estimation (dashed blue). . . . .	138
7.11	Real measurements (red) and observer estimation (dashed blue). Test 2: Scooter Experimental test: State estimates validation ( $v_y$ , $F_{yf}$ , $F_{yr}$ ) from the lateral acceleration and the additional measurement; and $\phi$ from IMU roll angle. . . . .	138
8.1	General diagram of the interconnected estimation of longitudinal and lateral dynamics . . . . .	142
8.2	Maneuver 1: Inputs. . . . .	147
8.3	Maneuver 1: <i>BikeSim</i> measured states. . . . .	147
8.4	Maneuver 1: Actual states (in blue) compared to estimated states (dashed red). . . . .	148
8.5	Maneuver 1: Validation of the estimated states. . . . .	148
8.6	Maneuver 2: Inputs. . . . .	149
8.7	Maneuver 2: Measured states. . . . .	149
8.8	Maneuver 2: Actual states (in blue) compared to estimated states (dashed red). . . . .	150
8.9	Maneuver 2: Validation of the estimated states. . . . .	150
7.12	Test 2: Scooter Experimental test: Tire cornering stiffness Convergence $\hat{\theta}_i = \hat{C}_{(f,r)i} - C_{(f,r)i_0}$ ( $f, r = \text{front, rear and } i = (1, 2, 3, 4)$ ). . . . .	154
9.1	Motorcycle kinematics. . . . .	160
9.2	Motorcycle sensitivity gain. . . . .	161
9.3	Over and Under steering situations. . . . .	163
9.4	Memory block . . . . .	164
9.5	(right) Rider torque and steering angle (left) Neutral Path Departure. . . . .	165
9.6	Steady Steering behavior: outputs and steering errors. . . . .	165
9.7	Alarm and corrections. . . . .	166
9.8	Steering behavior: Rider torque and steering angle. . . . .	167
9.9	Trajectory departure errors. . . . .	167
9.10	Noisy outputs. . . . .	167
9.11	Risk functions, alarm and corrections. . . . .	168
10.1	Captured camera image with reprojected road lanes, predicted trajectories and LCP . . . . .	171
10.2	Scheme of the vehicle circular path prediction . . . . .	173
10.3	Road bird-eye-view with predicted vehicle trajectories and tracked LCP . . . . .	175
10.4	DLC for straight PTWV trajectory on straight road . . . . .	177
10.5	DLC for circular PTWV trajectory on curved road. . . . .	178
B.1	Input-Estimation Errors- Parameters convergence. The convergence is compared with $RMS = (0.0731, 0.2165, 0.0150)$ , $MSE = (0.0053, 0.047, 2.236 \cdot 10^{-4})$ . . . . .	191
B.2	State Estimation: Actual state (red) their estimates (blue) . . . . .	192
B.3	The noise-corrupted case . . . . .	192



# List of Tables

1.1	Annual number of road fatalities in France. . . . .	10
1.2	Fatalities per age group in France . . . . .	11
1.3	Fatalities per road users categories in France (ONSIR, 2018). . . . .	12
1.4	Monthly number of road fatalities in France (ONSIR, 2018). . . . .	12
2.1	Analysis of the estimated angles for the different boxes for all the tests conducted. . . . .	61
2.2	Analysis of the estimated angles for all the boxes with different initial conditions. In all the cases, the the standard deviation does not exceed 0.6 deg. . . . .	63
2.3	Correlation analysis of the rotated axes different boxes against all the considered tests. . . . .	63
3.1	Weight measurements $F_{zf}$ and $F_{zr}$ for Kawasaki ERN6 and identification results. . . . .	76
3.2	Identification Result: Geometric parameters $a, b, h(m), m(kg)$ for Kawasaki. . . . .	77
3.3	Geometric parameters $a, b, h(m), m(kg)$ for Scooter . . . . .	77
3.4	Inertial parameters identification result for one body PTWV model. . . . .	80
4.1	Multi-Objective-Optimisation method. . . . .	86
4.2	Analysis of the estimated states for the tests conducted. . . . .	87
4.3	LM identification results . . . . .	93
4.4	Comparison table: Advantages/disadvantages of the presented parametric identification for PTWV. . . . .	94
5.1	Analysis of the estimated state. . . . .	106
6.1	Analysis of the estimation method for the new tests conducted. . . . .	123
7.1	Parameters Mean values comparison . . . . .	135
7.2	Robustness to motorcycle mass ( $m^+ = m + 50, m^- = m - 50$ ), and tire parameters variation ( $C_{fr_i}$ ). . . . .	137
7.3	Scooter Parameters Mean values comparison . . . . .	137
8.1	Comparison table: Advantages / disadvantages of the presented observers for estimating of PTWV states and parameters. . . . .	152
C.1	Parameters expressions and numerical values . . . . .	193
C.2	Matrices expressions . . . . .	194
C.3	Motorcycle parameters and numerical values . . . . .	194



# List of Abbreviations

<b>ABS</b>	<b>Anti-lock Braking System</b>
<b>ADAS</b>	<b>Advanced Driver Assistance Systems</b>
<b>ARAS</b>	<b>Advanced Rider Assistance Systems</b>
<b>BS</b>	<b>BikeSim</b>
<b>CoG</b>	<b>Center of Gravity</b>
<b>DLC</b>	<b>Double Change de Line</b>
<b>DoF</b>	<b>Degree of Freedom</b>
<b>DUIO</b>	<b>Delayed Unknown Inputs Observer</b>
<b>ESP</b>	<b>Electronic Stability Program</b>
<b>ECU</b>	<b>Electronic Control Unit</b>
<b>FHWA</b>	<b>Federal Highway Administration's</b>
<b>GPS</b>	<b>Global Positioning Systems</b>
<b>GNSS</b>	<b>Global Navigation Satellite Systems</b>
<b>IMU</b>	<b>Inertial Measurement Unit</b>
<b>ISpS</b>	<b>Input to State Practical Stability</b>
<b>IFO</b>	<b>Interconnected Fuzzy Observer</b>
<b>ITS</b>	<b>Intelligent Transportation System</b>
<b>IVIS</b>	<b>In-Vehicle Information Systems</b>
<b>IBISC</b>	<b>Informatique, Biologie Intégrative et Systèmes Complexes</b>
<b>LMI</b>	<b>Linear Matrix Inequality</b>
<b>LPV</b>	<b>Linear Parameter Varying</b>
<b>LTI</b>	<b>Linear Time Invariant</b>
<b>LTV</b>	<b>Linear Time Variant</b>
<b>LAO</b>	<b>Luenberger Adaptive Observer</b>
<b>LM</b>	<b>Levenberg-Marquardt</b>
<b>MSC</b>	<b>Motorcycle Stability Control</b>
<b>NHTSA</b>	<b>National Highway Traffic Safety Administration</b>
<b>ONISR</b>	<b>National Inter-ministerial French Road Safety Observatory</b>
<b>PRBS</b>	<b>Pseudo-Random Binary Sequence</b>
<b>PTWV</b>	<b>Powered Two-Wheeled Vehicles</b>
<b>P4WV</b>	<b>Powered Four-Wheeled Vehicles</b>
<b>RMSE</b>	<b>Root Mean Square Error</b>
<b>SDG</b>	<b>Sustainable Development Goals</b>
<b>TS</b>	<b>Takagi Sugeno</b>
<b>UI</b>	<b>Unknown Input</b>
<b>UIO</b>	<b>Observer with Unknown Inputs</b>
<b>VRU</b>	<b>Vulnerable Road Users</b>
<b>WHO</b>	<b>World Health Organization</b>



# List of Symbols

$\mathbb{Z}$	The set of integers
$\mathbb{R}$	The set of real numbers
$\mathbb{R}^+$	The set of non-negative real numbers
$\mathbb{R}_{>0}$	The set of positive real numbers
$\mathbb{R}^n$	$N$ -dimensional vector space over the field of the real numbers
$A^T, A^\dagger$	Matrix transpose, left pseudo-inverse
$A > 0, (< 0)$	Matrix positive (negative) definiteness
$\ A\ $	The Euclidean norm of $A$
$I_n, 0_n$	Identity and Zero matrix of $n$ dimension
$\theta$	Unknown parameter
$\Theta$	Set of unknown parameters
$\zeta$	The vector of $n_\zeta$ known time-varying parameters
$(\cdot)^\dagger$	The left pseudo-inverse $\left( [(\cdot)^T(\cdot)]^{-1} (\cdot)^T \right)$ of the matrix $(\cdot)$
$c_\alpha$	Cosine of $\alpha$
$s_\beta$	Sine of $\beta$
$t_\gamma$	Tangent of $\gamma$
$g$	Gravity $9.81 \left[ \frac{m}{s^2} \right]$
$v_x, v_y$	Longitudinal and Lateral speeds
$\phi, \psi, \delta$	Roll, Yaw, Steering angles
$\dot{\phi}, \dot{\psi}, \dot{\delta}$	Roll, Yaw, Steering rates
$a_x, a_y$	Longitudinal and Lateral accelerations
$\omega_f, \omega_r$	Wheel rotational speed
$\tau$	Rider steering torque
$B_f, B_r$	The front and rear braking torques applied to the tires
$T$	The total engine torque applied only to rear wheel
$F_{yf}, F_{yr}$	Cornering front and rear forces
$F_{xf}, F_{xr}$	Longitudinal front and rear forces
$F_{zf}, F_{zr}$	Vertical front and rear forces
$F_y^0, F_x^0$	The steady-state value of the lateral and longitudinal forces
$F_a$	the aerodynamic force
$F_{rr}$	Rolling resistance force
$\lambda_f, \lambda_r$	Front and rear longitudinal slips
$\alpha_f, \alpha_r$	Front and rear lateral slip angles
$\sigma_f, \sigma_r$	Front and rear tire relaxation
$\mu$	Road adherence
$G_t$	Center of gravity of the vehicle (rigid body)
$G_f, G_r$	Center of gravity of the front and the rear frames
$m_f, m_r$	Mass of the front and the rear frame
$m$	Mass of the whole motorcycle
$j, h, k, e$	Linear dimensions
$l_f, l_r$	Front and rear wheelbase

$a, b, h$	Geometric variables (rigid body)
$C_{f1}, C_{r1}$	Front and rear tire cornering stiffness
$C_{f2}, C_{r2}$	Front and rear tire camber stiffness
$I_f, I_r$	Front and rear body inertia
$i_{fy}, i_{ry}$	Polar moment of inertia of front and rear wheels
$I_{fx}, I_{rx}$	Front and rear frame inertias about $X$ axis
$I_{fz}, I_{rz}$	Front and rear frame inertias about $Z$ axis
$C_{rxz}$	Rear frame product of inertia, $X$ and $Z$ axis
$I_x, I_z$	Moment of inertia along the $x$ and $z$ axis (rigid body)
$R_f, R_r$	Front and rear wheel radius
$\epsilon$	Caster angle
$\eta$	Mechanical trail
$C_d$	Drag coefficient
$f_w$	Rolling resistance coefficient

# General Introduction

The powered two-wheeler vehicles (PTWV) which include motorcycles, scooters and mopeds has been constantly increasing much faster than the passenger cars. The technological progress of PTWV brought a noteworthy convenience to its users through a significant reduction of transportation journey, especially for the opportunities it offers in avoiding congestion. Nonetheless, their proliferation has highlighted serious safety issues as well. Therewith, it is necessary to adopt safety interventions and assistive systems targeting this mode of transport. As a matter of fact, the growing vehicle traffic has increased the number of accidents and road fatalities. The global status report 2018 (WHO, 2018) on road safety highlights that the number of annual world road traffic deaths has reached 1.35 million. Henceforth, the road traffic accident is the 8<sup>th</sup> leading cause of violent death, after everyday accidents. As well, road crashes statistics reveal that more than half of all road traffic deaths are among Vulnerable Road Users, VRU, (Otte, Facius, and Brand, 2018). Although pedestrians, cyclists and riders of powered two and three-wheelers are more vulnerable as a result of being less protected than car occupants, the heavy burden of deaths arisen from these road users is also a reflection of infrastructure and vehicle design that prioritizes cars and other motorized transport. The study of road accidents shows that human factors (57%) appear far before the meteorological or technical issues. The two most frequent human causes (alcohol and speed) are respectively responsible for 31% and 25% of fatal accidents. Distraction and tiredness are also an important human factors in a road accident, that can be seen in unsuitable lane crossing or abnormal steering behavior. In the scope of improving road safety, insight into preventable causes of road accidents is of interest.

Currently, intelligent safety technologies have mainly targeted four-wheeled vehicles and continue to be developed and tested primarily for passenger cars and commercial vehicles. Unlike four-wheeled vehicles, the design of motorcycles does not include primordial components that inherently increase safety. As a result, the consequences of a motorcycle crash are often quite serious for the motorcyclists. Besides, road accident statistics underline the importance of improving motorcycle safety and highlight key safety concerns, that new safety technologies should target. Notwithstanding the high risks associated with motorcycle use, relatively little research on motorcycle safety design has been carried out. In spite of that, with the increasing popularity of this transport mode and increasing casualty levels, new safety systems, traffic laws, national and international attentions are currently being given to this area. Towards this end, many research broadly surveyed a wide range of Intelligent Transportation Systems (ITS) technologies with the potential to advance motorcycle safety. The integration of Advanced Rider Assistance Systems (ARAS) and ITS for PTWV is one of the forward objectives of automakers and suppliers, to help making a partial automated riding and serve as safety system to support/alert the rider of potentially hazardous situations. Further, the integration of various safety systems into one architecture can lead to an unexpected behavior in hazardous riding situations. The supply of road safety for PTWV riders remains useless, as long as some driving rules are not always adapted to riding psycho-physical capacity, like the visual fields, distance assessment, dynamics evaluation and loss of attention. Hence, the development of ARAS to improve rider safety should integrate riding experience and vehicle controllability in different riding situations.

On-board roadway departure assistance systems are already integrated in modern car. In order to avoid damage or even fatal crashes in dangerous steering situations, these systems make the vehicles more autonomous, allowing to inspect the surrounding vehicle's position and to detect the driver hypo-vigilance. In spite of this fact, departure lane systems are not yet developed for motorcycles and those implemented for

four-wheeled vehicles are not entirely transferable to motorcycles. As a matter of fact, the PTWV size can be seen as a weakness. They tend to frequently change travel direction and speed, regardless number of lanes or their width. Therefore, departure avoidance systems for motorcycles are the next step, aimed to detect as early as possible, when the motorcycle is involuntary getting out of the lane. Needless to say, designing warning systems for motorcycles or even vehicles requires risk quantification function, which can be used to warn the rider, in the case of passive assistance or engage the control action in the case of active assistance. Car Departure Lane Assist (DLA) system usually defines a Lane Crossing Time (TLC) and Distance to Lane Crossing (DLC) as a risk index, to assess the time for involuntary trespassing the boundaries. An estimation of the DLC provide with a clear view of emerging traffic situations, so that if rider makes a mistake, he will have more time to respond, more space to maneuver and correct the trajectory. Among other, steady-state analysis and handling capabilities issues are also very related to vehicle safe trajectory and roadway departure. The analysis of the handling properties highlights certain dynamic aspects that are important to define dangerous/safe stability threshold conditions, as the neutral, overturning or underturning behavior. Nevertheless, there is a lack of warning systems related to the problem of Lane Crossing Point (LCP) detection for motorcycles. Therefore, DLA systems for motorcycles need more thorough investigations to be embedded in modern two-wheelers.

In the last decade, the challenge of creating more accurate models for active safety systems has increased. Concerning PTWV, which are highly dynamic, nonlinear and coupled systems, many models have been developed in the literature, with various levels of complexity and completeness. In fact, the uncertainties, caused by the environment and induced by the aerodynamic phenomena as well as the motorcycle's intrinsic unstable platform and complex tire/road interaction make the modeling task more challenging. Withal, even if a parametric model can be derived, the parameters values are not always available. Indeed, it is well recognized in the automotive research community that knowledge of the real-time pertinent vehicles parameters can be extremely valuable for active safety applications. In this scope, a thorough improvement of this systems requires accurate motorcycle states information. Nevertheless, the measurement of all dynamic states and inputs with conventional sensors is inconceivable for economic or technical reasons. To counter the latter, virtual sensors are one of the key research fields using model-based estimators to overcome previous shortcomings in providing estimates of unmeasured states and relevant parameters of the PTWV's dynamics. Besides, the emergence of new applications in many fields of mobile systems and robotics has promoted the development of various approaches for estimation and identification. Nonetheless, each approach is suitable for a class of mathematical representation of the system under consideration. Hence, developing ARAS for PTWV remains a high theoretical and technical challenge because of the self-unstable characteristic of PTWV, which gives rise to various difficulties in design of identification and observation methods of the motorcycle. This topic is one of our research interest which intends to develop these systems starting from a minimum set of vehicle self-integrated sensors to acquire measured states.

Withal, parametric identification is the process of finding a set of optimal system's parameters, from available input-output data, and a prior knowledge of the system's structure. Several research works attempt to solve the identification problem for a predefined class of systems. Among others, these techniques are designed for a specific systems form and their direct transposition to the more general case is a complex task. Furthermore, the identification problem is formulated assuming that all the system states are measured, which is really untruthfully. Usually, identification is performed offline where online identification lays with some challenges. Hence, enabling efficient solution of an identification experiment is conditioned by a purposeful set of input signals related to persistence of excitation in order to reach an optimal solution. Hence, suitable rich input signals should be considered, while in practice, these signals can not be freely applied to excite the PTWV due to the system constraints, and the global optimization problem can settle to a set of incompatible parameters. Alternative approaches suggest the use of observer-based identification. In this scope, observers based identifier presents a convenient approach to deal with both dynamics states and parameters estimation.

In most of the references, the estimation of the PTWV dynamics is done by considering restrictive assumptions regarding riding motorcycle practices, constant longitudinal speed, parameters variation, road geometry and/or neglected tire-road contact and also by considering a known tire friction. Indeed, the coupling motion of the lateral and longitudinal dynamics of two-wheeled vehicle has not received much attention in the literature related to motorcycle. All these assumptions simplify the estimation problem but lead to an inaccurate estimation with respect to the real dynamics. Furthermore, it is commonly known that a physical system may include unknown parts and subjected to various intrinsic parameters and external perturbations. In this context, designing a virtual sensor for these systems has got significant consideration.

Withal these approaches, almost real systems subjected to unknown inputs, parameters and/or disturbances, the matching condition does not hold every time. The motorcycle model is one of these complex systems which does not fulfill the requirement to design a classical observer. Several open topics related to PTWV field of research need more thorough investigations as for structural constraints and the convergence of the state estimates jointly with a parametric identification.

Concerning instrumentation and data acquisition, axes calibration is a mandatory operation when inertial sensors mounted within some sort of Electronic Control Unit (ECU) installed on a vehicle must be used for measuring or estimating variables of interest for vehicle control and/or estimation purpose. In fact, inertial sensors are strongly affected by mounting angles, and the correct rotation to be applied in order to recover an alignment which is consistent with the vehicle motion is paramount to obtain sensible data to be employed as representative of the variables of interest. In general, the aim of the calibration is to align axes of sensors present in various aftermarket equipment, which may be installed in non-standard positions, and for which the internal alignment of the sensors is also in general not known. In two-wheeled vehicles, such a calibration step becomes even more crucial than in cars, as space and vibration constraints often do not allow installations of the needed inertial measurement unit (IMU) in such a way to obtain a nearly natural alignment with the direction of motion, so that the mounting angles can result in being quite significant.

For all these reasons, this thesis manuscript provides several contributions to the identification and estimation of the dynamics of powered two-wheelers vehicles. In this particular context, the objective of this thesis is to identify the main problems related to PTWV and to study its critical cases. A part of this PhD is dedicated to identification algorithms, these techniques are designed to estimate the unknown parameters of the motorcycle parametric models. The second part deals with model-based observers proposed to estimate the dynamic states of the PTWV. An alternative methods to identification approaches are observer based identifier which allows both the parameters identification and the states estimation. Further, this manuscript introduces a self calibration algorithm for Inertial Measurement Units (IMUs) alignment. The last part of this thesis deals with objective indicators for risk quantification.

## Thesis Organisation

This manuscript is organized as follows:

**Part I:** presents the general context and the motivation of these three years of research.

- *Chapter 1* provides a state of the art on road accident analysis and road safety systems as well as the important features of these systems for powered two-wheeler vehicles.
- *Chapter 2* offers a brief review of PTWVs and we show the motivation of our choice to consider the motorcycle as typical vehicles for the research study. Indeed, this chapter provides mathematical modeling of tire-ground forces and moments as well as, the powered two-wheeler vehicle kinematic and dynamic modeling. For the sake of validation, we present the instrumented motorcycle (Scooter lab's) and we introduce a self calibration algorithm to align Inertial Measurement Units (IMUs) data.

**Part II:** is dedicated to open-ended questions related to parameter identification for motorcycle. With regard to the modeling scope, we have studied two structures of models according to the expected fineness. The first is a rigid body model (Inverted pendulum), then we have extended the model to two-body model according to our requirements. This part is divided in two chapters:

- *Chapter 3* considers the identification of the rigid one-body motorcycle model. Three design methods are studied in this chapter: using static test, an algebraic identification approach compared to an iterative gradient descent algorithm.
- *Chapter 4* focuses on the identification of a mathematical two-bodies model of a two-wheeled vehicle. Two methods were proposed: a cascade, multiple-objective optimization algorithm and a Levenberg-Marquardt (LM) identifier.

**Part III:** focuses on the states estimation and the parameters identification of the PTWV dynamics with observers synthesized from the two-bodies PTWV model. To this end, four observers are introduced:

- *Chapter 5* introduces Unknown Input Observer (UIO): for road and steering dynamics reconstruction.
- *Chapter 6* addresses an original method for designing a delayed unknown input observer (DUIO) for nonlinear system with mismatched condition.
- *Chapter 7* proposes an LPV Luenberger Adaptive Observer (LAO) for the PTWV dynamics states estimation and tires' cornering stiffness identification.
- *Chapter 8* presents Interconnected fuzzy Observer (IFO) for PTWV: both lateral and longitudinal dynamics estimation of the two-wheelers.

**Part IV:** aims at identifying objective indicators for the quantification of risk as well as carry out and discuss the design of possible warning system for riders of PTW vehicles. To do this, we divided this part into two chapters:

- *Chapter 9* presents a neutral-path departure (NPD) algorithm towards getting circular stationary states and analytical handling conditions.
- *Chapter 10* focuses on Lane Crossing Prediction (LCP) for PTWV.

This design requires a precise knowledge of the various dynamic states and parameters of the motorcycle as well as the external effort acquired either from measurement, estimation or identification techniques.

**Last chapter** provides a general conclusion to end-up this thesis and introduces the perspectives opened by the work presented in this manuscript.

## List of publications

### Accepted articles:

- (Fouka et al., 2017b): M. Fouka, L. Nehaoua, H. Arioui & S. Mammar. "Parametric Identification of a Powered Two-Wheeled Vehicles : Algebraic Approach ", IEEE 25th Mediterranean Conference on Control and Automation, Malte, 2017.
- (Fouka et al., 2017a): M. Fouka, L. Nehaoua, H. Arioui & S. Mammar. "Mutiple-Gradient Descent Algorithm for Parametric Identification of a Powered Two-Wheeled Vehicles ", IEEE International Conference on Systems, Man and Cybernetics (SMC), Banff, Canada, 2017.
- (Fouka et al., 2018e): M. Fouka, L. Nehaoua, H. Arioui & S. Mammar. "Simultaneous Parameters Identification and State Estimation based on Unknown Input Observer for a class of LPV Systems. ", American Control Conference (ACC), 2018.
- (Fouka et al., 2018b): M. Fouka, L. Nehaoua, H. Arioui & S. Mammar. "A Motorcycle inertial parameters identification via algorithmic computation of state and disign sensitivities ", The IEEE Intelligent Vehicles Symposium (IV'18), 2018.
- (Fouka et al., 2018c): M. Fouka, L. Nehaoua, H. Arioui & S. Mammar. "Road Geometry and Steering Reconstruction for Powered Two Wheeled vehicles. ", The IEEE International Conference on Intelligent Transportation Systems (ITSC), 2018.
- (Fouka et al., 2018a): M. Fouka, L. Nehaoua, H. Arioui & S. Mammar. "Adaptive Observer for Motorcycle State Estimation and Tire Cornering Stiffness Identification ", IEEE Conference on Decision and Control (CDC), 2018.
- (Fouka et al., 2018d): Simone Gelmini, Majda Fouka, Silvia Strada, Mara Tanelli, & Sergio Savaresi. "Analysis and development of an IMU axes self-calibration algorithm for motorcycles. ", The IEEE International Conference on Intelligent Transportation Systems (ITSC), 2018.
- (Fouka et al., 2019b): M. Fouka, L. Nehaoua, H. Arioui & S. Mammar. "Interconnected Observers for a Powered Two-Wheeled Vehicles: Both Lateral and Longitudinal Dynamics Estimation", IEEE International Conference on Networking, Sensing and Control (ICNSC), 2019.
- (Fouka et al., 2019c): M. Fouka, L. Nehaoua, H. Arioui & S. Mammar. "On Steady-State Cornering Analysis for Motorcycles ", The IEEE International Conference on Intelligent Transportation Systems (ITSC), 2019.
- (Damon et al., 2019): P-M Damon, M. Fouka, L. Nehaoua, H. Arioui & S. Mammar. "Vision-Based Lane Crossing Point Tracking for Motorcycles", The IEEE International Conference on Intelligent Transportation Systems (ITSC), 2019.
- (Fouka et al., 2019a): M. Fouka, L. Nehaoua, H. Arioui & S. Mammar. "Full Order Observer with Unmatched Constraint: Unknown Parameters Identification", IEEE Control Systems Letters (L-CSS), 2019.

### Under revision:

- M. Fouka, L. Nehaoua, Hichem Arioui & Saïd Mammar. "Motorcycle State Estimation and Tire Cornering Stiffness Identification Applied to Road Safety: Using Observer Based Identifiers", IEEE Transactions on Intelligent Transportation Systems (T-ITS).
- M. Fouka, L. Nehaoua, Hichem Arioui & Saïd Mammar. " How to recover Unsatisfied Matching Condition based on Delayed Outputs : State Estimation and Parameters Identification for Motorcycles", IEEE Transactions on Intelligent Vehicles.

**Reports:**

- (Arioui, Damon, and Fouka, 2017): H. Arioui, M. Fouka, P-M Damon, « Identification de Paramètres et Estimation des Etats dynamiques des véhicules à deux roues motorisés (V2RM) », Bilan Scientifique du laboratoire IBISC dans le cadre du projet ANR *VIROLO*<sup>++</sup>, 2017.
- (Arioui, Damon, and Fouka, 2019): H. Arioui, M. Fouka, P-M Damon, « Quantification de risque pour les véhicules a deux-roues motorisés (V2RM): Aspects d'Estimation & de Perception », Bilan Scientifique du laboratoire IBISC dans le cadre du projet ANR *VIROLO*<sup>++</sup>, 2019.

**Presentations:**

- MED 2017. Presentation of an article in the Mediterranean Conference on Control and Automation held on Valletta, Malta.
- ICNSC 2019. Presentation of an article in the IEEE International Conference on Networking, Sensing and Control held in Banff, a national park in Alberta, Canada.
- Groupe de Travail Automatique et Automobile (GTAA), Amiens, France, 2017. Presentation of my researches concerning the identification algorithm applied to the motorcycle safety systems. <https://home.mis.u-picardie.fr/evenement/GTAA2017/index.html>
- Groupe de Travail Automatique (JAMACS), Nantes, France, 2018. Presentation of my researches concerning motorcycle state estimation and tire cornering stiffness identification using adaptive observer based identifier. <https://jamacs2018.ec-nantes.fr/>

**Others:**

- **Members of the Research Commission:** *PhD student representative.* Sector 1: Science and Technology, The lists "UEVE FUTURE VISION", College G.
- **Members of the Research Project:** *National project Virolo++*, for the training of novice motorcycle riders. Development of tools to evaluate the cornering ability.

## Part I

# Context & PTW Vehicle Modeling



# Chapter 1

## Road fatalities and ARAS for PTWV

### Abstract

Limited access to certain territories, the environmental and climatic urgency, the ever-increasing daily transportation needs, faced to these challenges, it is time for a general overhaul of transportation policy and to rethink new mobility solutions for forthcoming decades. In France, the mobility orientation project is started in 2018 and is structured around four main objectives: to provide all and everywhere alternative solutions to the individual cars, to develop innovation and new mobility solutions, to reduce the environmental footprint of transport and to invest more to improve the infrastructures. While waiting for those promised solutions, several alternatives have already been democratized all over the world to simplify mobility and especially two-wheeled vehicles. The practice of such vehicles is no longer exclusive to a few crops or cultures. Using bicycles and motorcycles is an economic and social reality. However, from a road safety point of view, the increase in the traffic of two-wheeled vehicles has not been foreseen in time and the lack of security systems and adequate infrastructure testifies this.

This chapter gives a review of road fatalities and safety of ground vehicles and in particular the Powered Two-Wheeled Vehicle (PTWV) to show the motivation of our choice to consider the PTWV as typical vehicles for our research study. In section 1.1 road accident analysis is studied. Section 1.2 discusses the most frequent factors contributing to PTWV crashes. They are described following the interaction between the three basic components of the traffic system: PTW riders and other road users, road environment and vehicle factors. Indeed, section 1.4 describe the existing methods in the literature of Advanced Rider Assistance Systems (ARAS), also we present their limits and recommendations to future works to improve the reliability and safety of motorcycle rider. Our motivations and the specific challenges within the framework of VIROLO++ project are highlighted in section 1.6.

### 1.1 Road Traffic Fatalities

In roadway safety, the road traffic accident is the usual term used to describe a collision between two vehicles or a fixed/mobile obstacle. It refers to any accident occurring on a road open to public circulation, and in which at least one person is injured or unfortunately killed.

The road accidentology consists essentially of decrypting the accident reports in order to identify their causal factors, consequences, and to suggest corrective measures at potential location (Faheem, 2017). This can be achieved by an in-depth knowledge of accidentology and statistical methods to evaluate the number and the severity of accident and also their frequency and circumstances. Several risk variables including population, road kilometer, distance traveled and economic cost are considered in the accidentology analysis. The statistical analysis of accidents is carried out periodically at critical locations or road stretches which will

help to arrive at suitable measures to effectively decrease accident rates. The interpretation of the statistical data is very important to provide insight to the accidentology problem (Faheem, 2017).

In France, the National Inter-ministerial French Road Safety Observatory (ONISR) is in charge of the National Road Traffic Accident database (BAAC) and leads various research programs about road safety. It quantifies results and elements of assessment on roadway users' behavior, public authorities' actions and comparison at the international level<sup>1</sup>.

### 1.1.1 Fatal Accident Statistics

The road traffic accident is now the 8<sup>th</sup> leading cause of violent death, after everyday accidents, suicides, surpassing HIV/AIDS, tuberculosis and diarrhoeal diseases (Pietrasik, 2018). It is the first cause of death for children and young adults aged between 5-29 years old<sup>2</sup>.

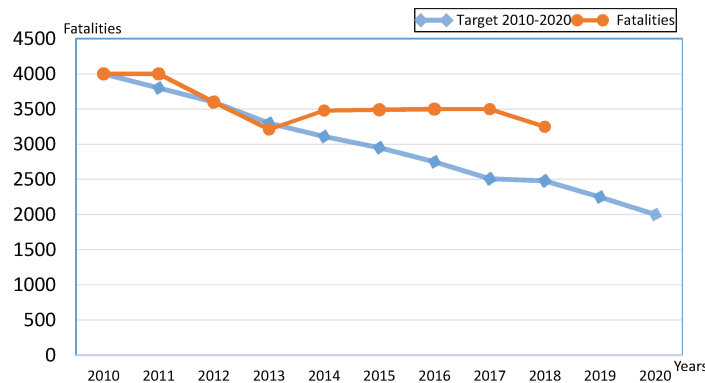


FIGURE 1.1: Fatalities statistics and global target in France (ONSIR, 2018).

According to the World Health Organization, traffic accidents claim around 1.35 million lives annually (WHO, 2018). Additionally, accidents lead to an estimated annual cost of around 500 billion euros, or 3% of the world Gross Domestic Product (GDP). In 2018, the ONISR reports that nearly 3,259 people died on french roads with light decrease with respect to 2017 (−189 or −5.5%), this is also the case for the remaining indicators: injury accidents −4.8% and injured people −5.4% (Table 1.1).

TABLE 1.1: Annual number of road fatalities in France.

Result for the year 2018	Injury accidents	Killed within 30 days	Injured people	Inc hospitalized 24h
2018 estimates	55800	3259	69434	20864
2017 final results	58613	3448	73384	27732
Difference 2018/2017	−2813	−189	−3950	−6868
Variation 2018/2017	−4.8%	−5.5%	−5.4%	−24.8%

Despite these alarming statistics, it should be noted that after four years of rising or stagnating road deaths in France, the year 2018 recorded the lowest mortality numbers in the history of Road Safety statistics as shown in Figure 1.2 and Table 1.2. The decrease in road traffic fatalities between 2010 and 2018 is estimated at −18.4% which represents 733 lives saved in 2018 compared with 2010.

Another remark concerns the fatalities among young people aged between 18 to 24 which decreased by 12% in 2018 and nearly 41% with respect to 2010. This decrease in fatalities and serious injuries is particularly pronounced for young riders. Notwithstanding, it has increased again among young motorcyclists, particularly inside built-up areas and on motorways. Nonetheless, in spite of ascertainment, this age group remains the most exposed to road risks.

<sup>1</sup><https://www.onisr.securite-routiere.interieur.gouv.fr/>

<sup>2</sup>[https://www.who.int/violence\\_injury\\_prevention/road\\_traffic/en/](https://www.who.int/violence_injury_prevention/road_traffic/en/)

TABLE 1.2: Fatalities per age group in France

	0-17 year	18-24 year	25-34 year	35-49 year	50-64 year	>+65 year	Total
2010	291 7%	831 21%	547 18%	704 20%	809 15%	592 19%	3992 100%
2013	199 6%	636 19%	547 17%	666 20%	532 16%	688 21%	3268 100%
2017	205 6%	562 16%	571 17%	638 19%	603 17%	869 25%	3448 100%
2018	190 6%	493 15%	523 16%	621 19%	580 18%	852 26%	3259 100%
Variation 2017-2018	-7%	-12%	-8%	-3%	-4%	-2%	-5.5%
Variation 2013-2018	-5%	-22%	-4%	-7%	+9%	+24%	-0.3%
Variation 2010-2018	-35%	-41%	-26%	-23%	-2%	+12%	-18.4%

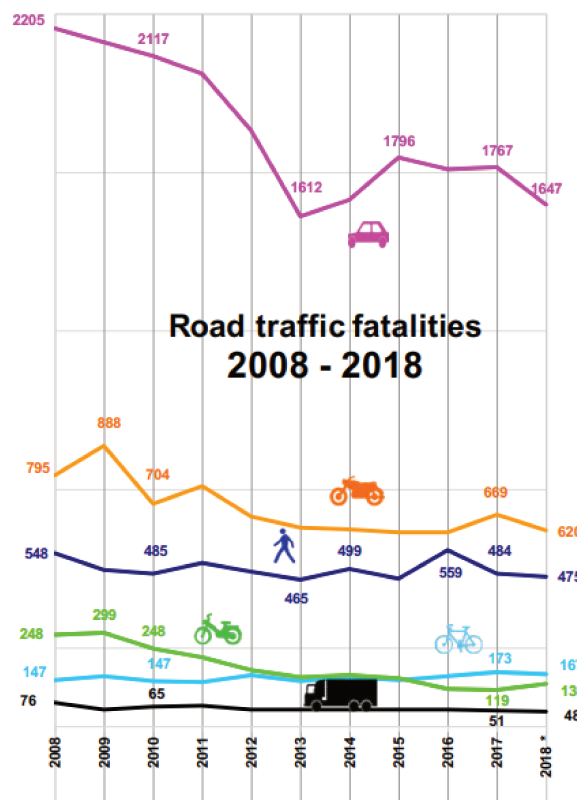


FIGURE 1.2: Trends per road users categories in France

As reported in Table 1.3, the car user fatalities represent the majority of the fatalities in France. While using passive security system can largely improve the safety of road users, it is concluded that the miss of a proper use of seat belts is the major death factor<sup>3</sup>. Make a seat-belt reduces the risk of death or serious injuries by 50% for the driver and the front seat occupant, and by 25% for the rear seat occupants. On the other side, the number of fatalities among PTWV is still significant with 620 case in 2018. Compared to 2017, fatalities have decreased by -7% among motorcyclists, -3% among pedal-cyclist and -2% for pedestrian but it increased by more than +14% among moped riders. As for car users, failure to take a helmet concerns half of fatalities while wearing a helmet decrease the risk of fatal injuries by 42%.

<sup>3</sup><https://www.securite-routiere.gouv.fr>

TABLE 1.3: Fatalities per road users categories in France (ONSIR, 2018).

	Pedestrians 人	Pedal-cyclist 🚲	Moped user 🛵	Motorcyclist 🏍️	Car users 🚗	HGV users 🚚	Other users ■	Total
2010	485 12%	147 4%	248 6%	704 18%	2117 53%	65 2%	226 6%	3992 100%
2013	465 14%	147 4%	159 5%	631 19%	1612 49%	57 2%	197 6%	3268 100%
2017	484 14%	173 5%	119 3%	669 19%	1767 51%	51 1%	185 5%	3448 100%
2018	475 15%	167 5%	136 4%	620 19%	1647 51%	48 1%	166 5%	3259 100%
Variation 2017-2018	-2%	-3%	+14%	-7%	-7%	-6%	-10%	-5
Variation 2013-2018	2%	14%	-14%	-2%	+2%	+16%	-16%	0
Variation 2010-2018	-2%	-14%	-45%	-12%	-22%	-26%	-27%	-18%
Variation 2000-2018	-44%	-39%	-70%	-35%	-69%	-61%		-60%

Particular weather conditions can affect road mortality. In winter, the number of road fatalities decreases (Figure 1.3), road users avoid hazardous weather situations. However, July is extremely marked by road fatalities. In fact, good weather conditions lead to an increase in travel, especially for vulnerable road users as motorcycles. On the other hand, degraded weather conditions can increase the individual risk of each user's for many reasons as poor visibility, loss of grip in case of rain, ice storm. It is therefore generally difficult to point the influence of meteorology on mortality month by month apart from the most extreme variations.



FIGURE 1.3: Monthly number of road fatalities: Killed in 30 days per year in France.

Furthermore, a strong increase in road victims is recorded in February 2019 compared to 2018 as shown in (Figure 1.3). According to preliminary estimates of the ONISR<sup>4</sup> (Table 1.4), 253 people died on the roads, against 216 in February 2018 (Figure 1.3). The same conclusion can be formulated for the remaining indicators: the number of injured persons and accidents. Also, this increase in road mortality concerns mainly pedestrians, cyclists, young people between 18 – 24 years old and seniors aged 65 and over<sup>5</sup>.

TABLE 1.4: Monthly number of road fatalities in France (ONSIR, 2018).

	February			
	2019	2018	Difference	Variation
Accidents	4091	3345	+746	+22.3%
Victims	5274	4348	+926	+21%
Killed	253	216	+37	+17.1%
Injured	5021	4132	+889	+21.5%

## 1.2 Fatal Risk Factors

Research investigation and analysis show that human-inherent errors by distraction, drowsiness or under evaluation of driving situation are the primary fatal risk factors in most of the accidents (WHO, 2018).

<sup>4</sup><https://www.securite-routiere.gouv.fr>

<sup>5</sup><https://www.europe1.fr/societe/securite-routiere-le-nombre-de-morts-sur-les-routes-en-hausse-de-171-en-fevrier-3881783>



### 1.3.1 Attractiveness of PTWV

Beyond the fun side, PTWV have specific features that make them an effective means of transportation. In urban areas, PTWV have the potential to go relatively quickly by their capacity to overtake vehicles and the use of traffic ways dedicated for other public transportation. In addition, PTWV users save time when searching for a parking place, by parking legally or not very close to their destination. In rural areas, they offer mobility options for users who do not have access to a car and where public transport is sometimes non-existent. PTWV can bring benefits from an environmental perspective with respect to car vehicles, less fuel consumption and less emissions. The emergence of electric PTWV, which are much cheaper than electric cars, may bring additional environmental benefits.



FIGURE 1.5: In Bangladesh, riding a PTWV has become an efficient solution for urban mobility (Dhaka Tribune, December 2017).

However, PTWV have also a number of drawbacks compared to car vehicles: vulnerability, more riskier, less comfort, less visible and very few riding assistance system. PTWV riders have a higher risk of injury due to their greater vulnerability, resulting from a lack of protection compared to passenger cars, which can lead to very severe consequences in the event of collisions above a given speed. Safety measures that are already well-recognized, such as helmets, protective clothes, etc., have diminished this vulnerability, but further progress still needs to be made. Indeed, motorcycles exhibit other intrinsic difficulty of riding due to the necessity to balance the vehicle, its lower friction capacity and its great sensitivity to the environmental perturbations (wind, gravel, any change in road surface, etc.) which may destabilize the vehicle. Also, PTWVs are a significant source of noise.



FIGURE 1.6: Gendarme dead in Trieux, Meurthe-et-Moselle, 2015.

### 1.3.2 Dynamic Specification of Motorcycles

As discussed in the previous section, PTWV presents a different dynamics behavior due its design and motorization. Unlike car vehicles, a PTWV is inherently unstable and can't be balanced without rider actions. They also exhibit a non-minimum phase steering behavior and non-linearities due to the steering geometry and tire-road interactions. Generally, the stability of the vehicle is guaranteed by a combination of

several effects that depend on the geometry, mass distribution, riding torque applied on the handlebar and forward speed. The PTWV's balance issue is one of the biggest challenges to develop active safety systems.



FIGURE 1.7: Honda's self-balancing motorcycle (Honda, 2017)

Beside the motorcycle's balance difficulty, the lateral motion of the PTWV is also a complex dynamics of PTWV. This dynamics arises from the rotation of the handlebar or the inclination of the vehicle. It includes cornering, driving in a roundabout, overtaking, etc. The lateral motion of a PTWV are controlled by the steering torque applied to the handlebar. The latter is directly linked to the front wheel (via the suspension system) without reduction stage. While for four wheeled vehicles, the driver controls the lateral dynamics through the steering angle of the steering wheel which is connected to the wheel by a reduction gear. In addition, the steering angle is, in general, very low especially at high speed. As a result, the PTWV rider feels more the effort resulting from the road on the steering mechanism. Also, the rider can act with the inclination of his bust/posture to better control the lateral dynamics which is an additional degree of freedom of control. In addition, the PTWV must lean during a turn to compensate the generated lateral force at the tire/road contact. Whereas the roll angle is limited by suspensions geometry in car vehicle, it can reach  $60^\circ$  in competition motorcycles.

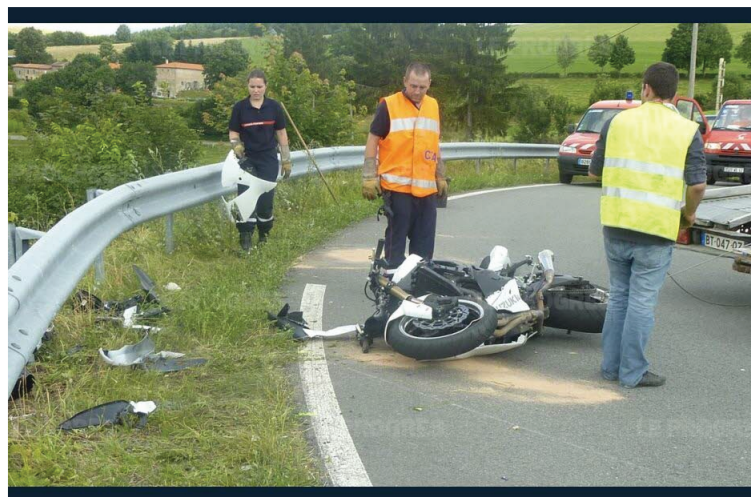


FIGURE 1.8: Loss of control in curve (Machézal, Loire, July 2012)

Counter-steering is a transient phenomenon which results from gyroscopic effects which contribute to generate a roll motion of the front wheel. Thus, a right steering motion generates a rolling moment on the left and conversely. Nevertheless, the amplitude of the rolling moment is small compared to other moments acting on the wheels, but its transient nature is very important when cornering.



FIGURE 1.9: Counter-steering phenomenon.

Among others, the rider to the motorcycle mass ratio is much higher for PTWV than for cars. It is a very important factor to consider, particularly for the robustness of the estimation and control algorithms. The weight of a PTWV varies between 50 *kg* for moped vehicles up to 400 *kg* for high-end motorcycles. As a result, PTWV are very sensitive to the rider's posture and its riding style which highly affects the roll and the lateral dynamics.

Moreover, due to the geometry of the PTWV, and in particular the position of the Center of Gravity (CoG), the load transfer between the front and rear wheels is more important. It leads sometimes to dangerous situations such as the stoppie or the wheelie (Figure 1.10). These phenomena are often neglected in automotive ITS systems due to less load transfer. This can be explained first by the lower position of the car CoG and also by the heavy mass of the vehicle compared to the driver. Nevertheless, the load transfer must be taken into account when designing ITS systems for motorcycles, as this may cause instability, the fall of the motorcycle and may affect the braking efficiency.



FIGURE 1.10: Motorcycle wheelie and stoppie situations.

Consequently, riding a PTWV may exhibit a specific behavior pattern on the road which is different from the car drivers of four-wheeled vehicles. Such atypical behavior may surprise other road users. For example, overtaking within a small space, turning on the incorrect side, positioning on one side of the lane, great acceleration, are common practices which can be judged very hazardous for other road users and alter their perception experience and decision making.

All these factors have attracted a great attention from transportation and research communities. From control point of view, many interesting features are investigated such as instability, vibration mode, out-of-plane control, non-linearities and the counter-steering concept. From behavior point of view, rider modeling is a very active research field which aims to give more insight comprehension about PTWV stabilization and rider's risk assessment mechanisms.

### 1.3.3 Vulnerability of PTWV users

Vulnerable Road Users are defined in the ITS Directive as *non-motorised* road users, such as pedestrians, cyclists, PTWV road user, as well as all persons with disabilities or reduced mobility. More than half of all road traffic deaths are among vulnerable road users. In this context, pedestrians and cyclists represent 26%, PTWV users 28% while 29% for car's users (Otte, Facius, and Brand, 2018). In addition, being less protected than car occupants, accidents involving this class of users are of heavy consequences. The legacy reflections in designing infrastructure have amplified this vulnerability and, despite the prominence of vulnerable road users worldwide, the measures considered during the last years are still insufficient to significantly reduce their mortality<sup>7</sup>.

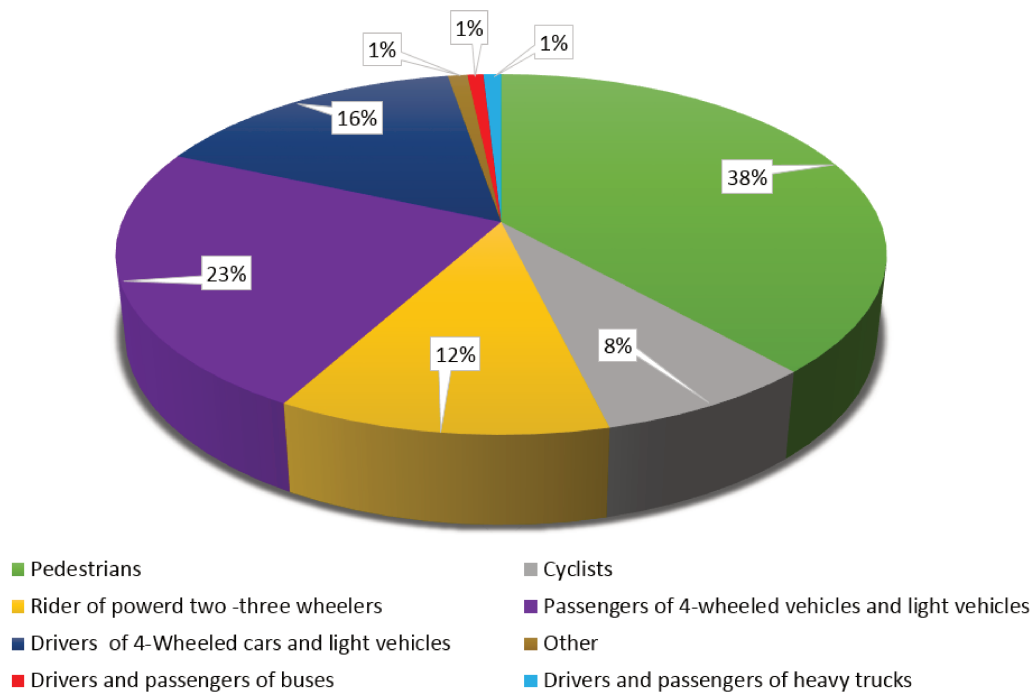


FIGURE 1.11: Mortality by road user category (WHO, 2018).

Very few studies are published about the impact of vulnerability in fatal accidents. MAIDS, Motorcycle Accidents In Depth Study, has conducted a very interesting study whose results are published in ([penumaka2014depth](#)). Also, according to the NHTSA, National Highway Traffic Safety Administration, PTWV riders accounted for 14% of traffic mortality in 2016. The analysis prepared by the Insurance Information Institute, five main factors influence the outcome of fatal motorcycle crashes<sup>8</sup>. It is showed that in 37.4% of PTWV accidents, the responsibility of the rider is highly engaged whereas in 50.5% this responsibility is endorsed by other users category. Next, the loss of PTWV control accounts for 32% and non adapted speed for 34%. Also, one among four of PTWV riders involved in fatal crashes don't hold a valid license<sup>9</sup>, compared to 13% for passenger car drivers.

<sup>7</sup><https://ec.europa.eu/transport/themes/its>

<sup>8</sup><https://www.iii.org/fact-statistic/facts-statistics-highway-safety>

<sup>9</sup><https://visual.ly/community/infographic/health/motorcycle-accidents>

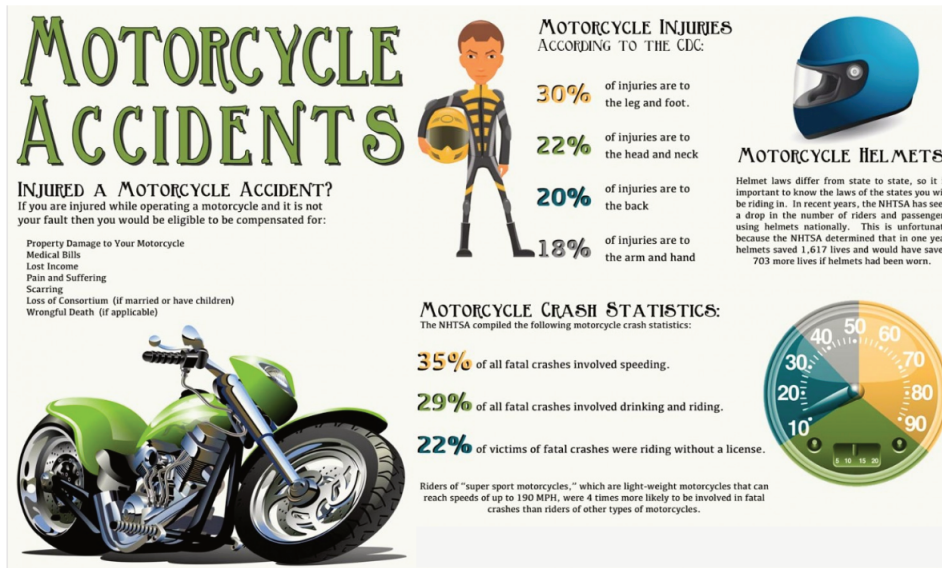


FIGURE 1.12: Motorcycles Accidents (Oliveira, 2013).

### 1.4 Intelligent Transportation Systems

Transport has always been crucial and challenging for society. Research explores new approaches to transport, in order to ensure its social, economic and environmental sustainability. In this context, this section discusses the potential of ITS systems to reduce motorcycle safety issues. From the literature related to PTWV ARAS and ITS, we present the gaps in motorcycle research and ARAS design.



FIGURE 1.13: Safety System.

#### 1.4.1 Overview on Road Safety Systems

Reducing the number of road accidents involves designing and developing safety systems to improve road safety and ensure passengers integrity. Intelligent systems have a crucial role to play within the new vision of

mobility. These ITS include a broad range of concepts, systems, and application of advanced technologies that aim to reduce the number of accidents and optimize the use of infrastructure (Alam, Ferreira, and Fonseca, 2016). Almost worldwide, the use of assistance systems including ADAS and In-Vehicle Information Systems (IVIS) is quite commonplace. But traditionally, the road safety systems can be classified into two categories: passive or active. Passive safety systems aim to reduce severe injuries and to protect the vehicle occupants from strong impacts (Flanigan et al., 2018). Systems like airbags, seatbelt and active head restraint are deployed from several decades ago on each sold vehicle. Nowadays, researches focus mainly on new chassis more able to absorb accident shocks. Despite all these, the passive road safety remains restricted regarding human behavior, driving skills limits and vehicle technical failure. On the other hand, the active safety systems embed different level of intelligence to prevent rider from hazardous driving situation or even to act directly on the car actuators. Many active safety systems have been developed and widely implemented to improve the controllability of the vehicle and get the best dynamic behavior almost driving situations, from the most common to the most unexpected.

In particular, these systems help the driver by informing him about the driving conditions (Gordon, 2016). For these reasons, car manufacturers are now able to develop ADAS that automate some low level driving tasks. Figure 1.13 shows a summarized cartography of the main conventional active safety systems.

### 1.4.2 Towards Motorcycles ITS

Intelligent safety technologies have mainly targeted truck and car vehicles, while only a limited ARAS for PTWV have been developed. These systems are named ARAS, Advanced Rider Assistance Systems and OBIS, On-Bike Information Systems. Nowadays, several researches try to evaluate the possibility and the potential to transfer ADAS, developed for cars, towards PTWV (Figure 1.14).



FIGURE 1.14: ARAS Systems for PTWV.

The literature review, presented in (Flanigan et al., 2018) gives a thorough analysis and revealed a series of trends and gaps in the current state of research on motorcycle safety and ITS. According to this review, the ITS services focus on the following categories of investigation:

1. Adaptive Front Lighting and Daytime Running Lights,
2. Advanced Driver Assistance Systems (ADAS),
3. Anti-lock Braking Systems (ABS),
4. Collision Warning and Avoidance Systems,
5. Curve Speed Warning,
6. Electronic Stability Programs,
7. Inter-Vehicle Communication Systems and Motorcycle Detection Systems.

## 1.5 State of the art of Motorcycle ITS

### 1.5.1 Advanced Rider Assistance Systems

ARAS are assistance systems for PTW riders. They provide automated assistance for riding tasks such as steering, braking, collision avoidance, lane departure warning, lane keeping, and adaptive cruise control. ARAS can be classified as an informing systems, warning systems, active assistance systems, or autonomous systems.

Almost of literature related to PTWV ARAS focused entirely on the safety benefits of ARAS for motorcycles (Cossalter et al., 2006b; Slimi et al., 2009; Popov, Rowell, and Meijaard, 2010; Touliou et al., 2012; Sharp, 2012; Kooijman and Schwab, 2013; Beanland et al., 2013). In the European Commission's SAFERIDER project (Montanari, Borin, and Spadoni, 2011), five key ARAS functions for motorcycles are identified, speed alert, curve warning, frontal collision warning, improving safety at intersections, and lane change support.

In addition, these works focus on the technical advancement of ARAS for motorcycles where dynamics modeling occupies a prime place. It aims to study new models of motorcycle steering control, handling, and roll motion, which can be used to better adapt ARAS to motorcycles. Among other, many works focused on the development of high-end motorcycle riding simulators to test the effectiveness of ARAS. Other important issues are also investigated, aiming to evaluate the acceptability of ARAS by PTWV riders (Touliou et al., 2012). Acceptability is a major obstacle for ARAS, these two concepts do not bring together a consensus among the whole bikers community.

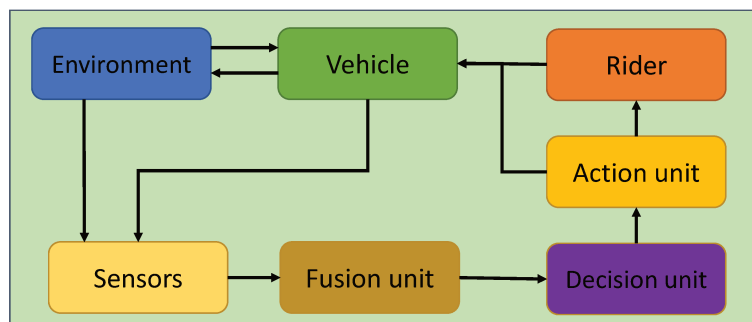


FIGURE 1.15: Rider Assistance System Architecture.

Figure 1.15 shows the general architecture of a rider assistance system. It is based on the perception of the environment through proprioceptive and exteroceptive sensors which provide measurements of the vehicle dynamics and collect information relating to the external environment. Each acquired data is then forwarded to the fusion unit for processing to get an accurate knowledge about the current riding situation. Next, the data processed by the fusion unit is transmitted to the decision module which analyzes them and decide for the adequate actions according to the environment, the rider's behavior and the risk level. Finally, these actions are sent to the action module, which produces either visual, sonore and/or haptic warnings, or an active intervention to correct the vehicle trajectory.

According to Figure 1.16, we can also classify ARAS systems with respect to the intrusion level (Kuschefski, Haasper, and Vallese, 2009). Informing and Warning systems have an indirect influence on the driving task and allows to inform the driver about the current driving situation. Assisting systems indicate driving errors to prevent an hazardous driving situation. Partly autonomous system acts partially to assist the driver to recover a safety riding situation, however, the driver is the only responsible for decision making and hence can simply disable the system or readjust its risk function. Fully autonomous systems have a great margin of decision and operate directly on the low-level vehicle actuators, hence they cannot be disabled by the driver as in case of the ABS.

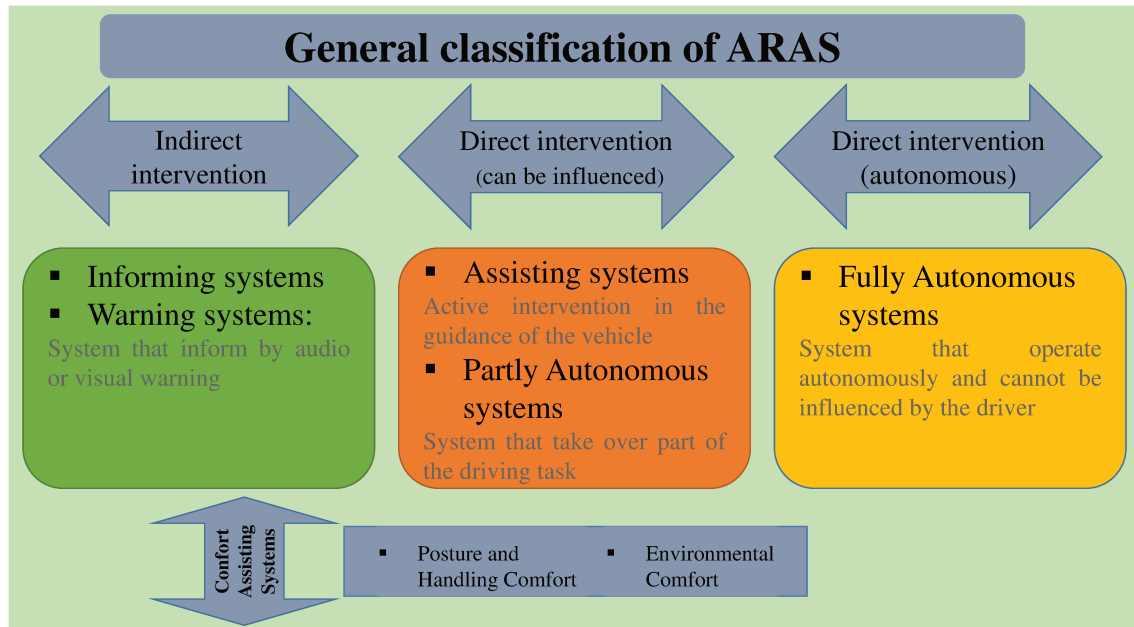


FIGURE 1.16: Classification of ARAS for PWTv.

### 1.5.2 On-Bike Information Systems

OBIS provide important information on weather conditions, as well as, they improve the vehicle visibility through intelligent communication interfaces (Touliou et al., 2012 and Diederichs et al., 2010).

The four OBIS functions having the highest impact for PTWV safety are listed in SAFERIDER project<sup>10</sup>. *eCall system* requires the capacity of PTWV to detect and remotely provide information, as the location of a crash. *Tele-diagnostics services* monitor constantly the functioning conditions of the vehicle. *Navigation & Route Guidance* provides a key function for novice riders by integrating OBIS and positioning data. *Weather, traffic & black spot warnings* integrate the navigation system with weather, traffic and accident data, in order to warn the vehicle occupant about potential dangers along the road.

### 1.5.3 Vision Enhancement for Crash Avoidance

This service deals with poor visibility riding conditions and aims to improve the road perception. It allows to avoid potential collisions with other vehicles, railings, pedestrians, or obstacles and assist the driver in complying with traffic signals and signs. Such examples are AFS and DRL technologies which focus on the visibility problem. Almost research works aim to better understand the effect of AFS and DRL on motorcycle conspicuity and their effectiveness (Cavallo and Pinto, 2014; Varlakati, Yogaraja, and Sudharsan, 2013; Cavallo and Pinto, 2012).

- AFS, Adaptive Front-lighting System, is an active safety system providing an optimized vision to the driver during night and poor-visibility riding conditions. AFS adjust dynamically the vehicle headlight position and intensity according to the daytime, lean angle, the vehicle speed, road type, environment and the position of other vehicles.

<sup>10</sup>[www.saferider-eu.org](http://www.saferider-eu.org)

- DRL, Daytime Running Lights is a lighting device on the front of the vehicle in which a multicolor lights are emitted to increase the visibility of the vehicle during daylight conditions.

#### 1.5.4 Motorcycle Autonomous Emergency Braking

The Collision Warning and Avoidance Systems are known as Motorcycle Autonomous Emergency Braking (MAEB). MAEB refer to systems that detect objects in the roadway through sensors embedded in the front of the vehicle and alert the rider if objects become a potential collision risk. In most cases, MAEB would then apply autonomous emergency braking if the rider does not answer to the collision risk warn (Tanelli et al., 2009a; Savino et al., 2013a).

- FCW, Forward Collision Warning, detects the distance between the vehicle and a potential obstacle using laser sensors or camera. When a vehicle is approaching too close to the obstacle, it provides alerts via an IHM.
- LatCA, Lateral Collision Avoidance, assists the rider to avoid collisions by providing warnings and/or controlling the vehicle in imminent situation.
- LRM, Lateral and Rear Monitoring, aims to improve driver perception to reduce the risk of side and rear collision.
- LgCA, Longitudinal Collision Avoidance, the same as LatCA but it concerns the front or rear of the vehicle.
- ICA, Intersection Collision Avoidance, assists the rider to avoid potential collisions at intersections.

In SAFERIDER project, FCW is identified as one of the five key ARAS functionalities suitable to develop and implement on a motorcycle prototype. It is shown that this system has a good predictive capability under different riding styles and collision scenarios. However, the acceptability of this system reminds further research.

#### 1.5.5 Antilock Braking System Technology

ABS is a legacy safety system that allows vehicles to maintain contact with the road surface according to driver inputs while braking and hence, preventing wheels locking up (Gail et al., 2009; Muller and Yildirim, 2011; Huang and Shih, 2011).

The ABS technology was firstly implemented on a PTWV motorcycles in the 1980s and it is a mandatory system since 2016. Many works related to motorcycle conduct statistical analysis of crash data to determine the safety benefits of ABS-enabled motorcycles (Roll, Hoffmann, and Konig, 2009; Rizzi et al., 2015). Among other, some works have focused on improving the braking distance and time for motorcycles with ABS or adapting ABS to lighter PTWV. It is proven that ABS technology has a great potential for motorcycle safety due to its relatively widespread acceptance among the motorcycle community.

#### 1.5.6 Precrash Systems and External Airbags

Precrash systems combine the active and passive collision avoidance technologies (Georgi et al., 2009).

- Airbag Jackets: functioning as a collision protection system for motorcyclists. When a motorcyclist is thrown from the motorcycle during a crash, the airbag jacket instantly inflates to protect the rider's upper body.
- External Airbags: act to disperse the force of the crash more slowly rather than directly protecting the occupant, they prevent collision force from reaching the motorcycle.

### 1.5.7 Curve Speed Warning

CSW, Curve Speed Warnings, is a warning system for excessive cornering speed in particular when approaching a turn (Yuen, Karim, and Saifizul, 2014; Huth et al., 2012; Biral et al., 2010). The literature review concludes that this system has a good applicability and a real effectiveness for the PTWV safety.

### 1.5.8 Roadway Departure Warning Motorcycle

The roadway departure warning system provides assistance by alerting the driver of an inadvertent line crossing due to driver inattention or fatigue. This system uses information from a video sensor and road line detection algorithms to define the vehicle position and orientation in the lane. This makes possible to compute a risk indicator, almost the lane departure time such TLC or DLC. If TLC is below a threshold value, the system issues an alert.

- LKA, Lane Keeping Assist, and DWS, Departure Warning Systems, detects distance and time to line crossing in order to generate a lane departure warning (Chiu and Lin, 2005, Lord et al., 2011).
- LDW, Lane crossing warning system, provides lateral control to correct the vehicle position within its lane when the rider unintentionally cross the markings (Marumo and Katagiri, 2011a).
- Following Distance Warning detects other vehicles in the front of the driver and generates a warning when the inter-distance becomes under a predefined threshold. This technology may be combined with collision avoidance warning system and adaptive cruise control (Katagiri, Marumo, and Tsunashima, 2008a).
- RDCWS, Warning system to prevent road exit, a combination between CSW and LDW systems. It provides a warning signal when with respect to the vehicle speed when approaching a turn. It allows also to warn the rider for an excessive lateral displacement. It was developed as part of the RDCW FOT project (LeBlanc, 2006).

### 1.5.9 Electronic Stability Program

ESP is an electronic control system for dynamic stability or trajectory control. It allows to keep control of the vehicle despite the hazards of the road, (Kidane et al., 2009; De Filippi et al., 2011a; Murakami, Nishimura, and Zhu, 2012; Seiniger, Schröter, and Gail, 2012). Most of these research studied the implementation and performance of ESP systems during challenging maneuvers while braking, on curves, and on rough roads.

### 1.5.10 Inter-Vehicle Communication System for Motorcycle

IVCS facilitates communications between vehicles, e.g., car-to-car or motorcycle-to-car. It is also a key part of evolving connected vehicle technologies V2X (Manzoni et al., 2010; Rajab, Othman, and Refai, 2012; Ling, Gibson, and Middleton, 2013; Maruyama et al., 2014). Few researchers have been working to design the Motorcycle Approaching Indication (MAI) function in V2V systems for automobiles. These technologies offer considerable safety benefits to motorcyclists because they reduce the risk of automobile-motorcycle crashes.

- Motorcycle Detection Systems use inter-vehicle communications to detect nearby vehicles and notify the driver of potential risks or other relevant information (i.e., motorcycle in a truck's blind spot).
- Road Surface Condition uses sensor systems that collect information on road surface conditions and communicate that information to the driver via V2I and V2V systems (Svendenius, 2007; Savino et al., 2013b).

Future research efforts should investigate motorcycle-based communication and detection technologies as well, especially given that human-machine interfaces for these technologies will need to be specially designed for motorcyclists.

### 1.5.11 Helmet-Mounted Display

Helmet-Mounted Displays is a system that projects alerts, warnings and any possible other information such as speed onto a helmet visor or as audible speech. Sensors in a helmet that sense light conditions, adjust the darkness of the visor, and provide night vision capabilities in very dark conditions (Dee, 2009).

### 1.5.12 Longitudinal Control System

Riding in heavy traffic and maintaining the correct distance to the vehicle in front takes a great deal of concentration and is strenuous over longer periods. As an example, ACC which maintains a safe distance between the vehicle and another preceding it. This is made possible by an on-board sensors, radar or laser, that detects the presence of a vehicle on the same track and measures the distance of the vehicle ahead as well as its speed.

The Saspence (SAfe SPEed and Safe DistaNCE) project (Bertolazzi et al., 2009) develops a system capable of helping the driver to maintain the maximum authorized speed and safety distance according to the given driving conditions (road geometry, traffic situation and meteorological conditions). This system serves to avoid the risk of accidents due to excessive speed and inappropriate distance in a particular situation.

### 1.5.13 Gaps in ITS for Motorcycle Safety

As crash causes for motorcycle safety issues are more precisely defined, Intelligent Transportation System (ITS) solutions can be designed to address them, and improve safety issues across all users. The literature presented in (Flanigan et al., 2018) revealed important gaps in current research on ITS for motorcycle safety. Significant progress can be expected towards the development of devices for active and passive safety by investigating future perspectives such that:

- Complete prototype systems for motorcycles allow assessing the safety benefits of such ITS and evaluate their acceptability.
- Motorcycle safety data to overcome the lack of robust data sets. Improving safety also implies an in-sight knowledge of PTWV by investing in the collection of crash data.
- Harmonization of ITS to address the important issue of ITS interoperability as well as, multi-sector collaboration.
- Connectivity is as an important ITS application for the near-term behind connected vehicle technology for automobiles and ensures that motorcycles are considered and included in the development of such technologies.

## 1.6 VIROLO++ Project Overview

Many research programs have been undertaken in Europe and abroad to understand the factors contributing to crashes. In particular, the *MAIDS* and *RIDER* projects allowed to characterize accidents situations (Penumaka et al., 2014), which paved the way to other projects such as *SAFERIDER* (Evangelos, 2010) for the development of ITS. *2BESAFE* aimed to study the motorcyclists behavior and ergonomic factors contributing to motorcycle crashes (Ng et al., 2018). The French ANR/Predit *SUMOTORI* and *DAMOTO* collaborative projects proposed an automatic fall detection algorithm for early inflating of a wireless air-bag jacket. *SIM2CO+* aimed at identifying the risky situations experienced by novice motorcyclists who have just passed their test, in order to improve pre-test training in France (ANR, 2014).

The VIROLO++ Project is a French ANR project, proposed to emphasize on bend-taking maneuvers. The aim is to fill the knowledge gap on bend-taking practices for a group of experienced and novice riders, to understand how riders enter a bend, maintain control and exit a bend. This system is mainly intended to operate on highways, national and departmental roads and in adverse conditions. In particular, the goal of this project is to develop tools and methods suitable for the study of the riders' behavior and for the understanding of the way they interact with their vehicle when negotiating a bend (Figure 1.17).

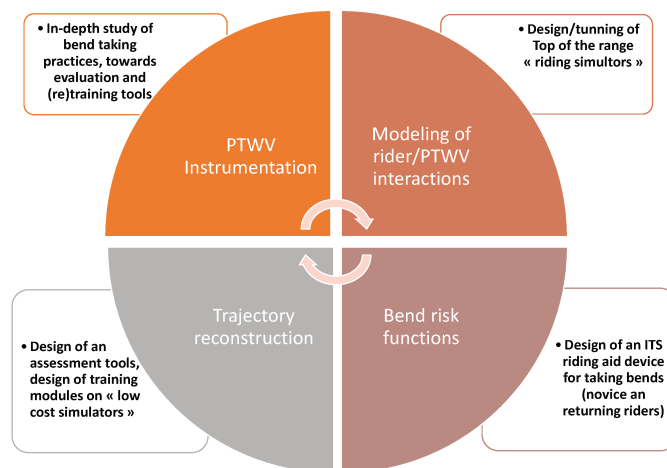


FIGURE 1.17: VIROLO++ French ANR Research Project.

The design of riding aid devices, and the training of riders to use them, are at the core of the VIROLO++ research project. The consortium's ambition is to mitigate PTWV rider road fatalities and injuries linked to a loss of control in bends, through the study of bend-taking behavior of motorbike riders application to training and intelligent transport systems is undertaken by the the VIROLO++ research project.

The project looks for more knowledge about how motorcyclist effectively take bends. Experiments were objectively measure the motorcyclist behavior and the rider-vehicle interaction. A cybernetic model of steering control is expected that will represent the rider control mechanism. The trajectory reconstruction is one of the important way to improve turn riding by comparing them to safe reference trajectories.

The project is organized into six work-packages (WP). WP1 deals with the PTWV instrumentation. The goal is to design an embedded architecture for the acquisition and recording of data. This embedded system will work in real riding situation to collect information about the rider behavior, vehicle behavior and driver/vehicle interaction in real-time. The WP is organized in four different tasks:

1. Deploy the embedded logger on two motorcycles belonging to the national gendarmerie in order to measure and evaluate trajectories;
2. Add on a third motorcycle a sensor system to measure forces exerted by the rider on the PTWV;
3. Design an IHM based on tablet or a smartphone application to display on-line information and the different warning signals;
4. Design a minimal low-cost sensor architecture.

WP2 concerns the estimation of the PTWV dynamic states and trajectory in turn or lane change. This task allows identifying the relevant parameters for a better reconstruction of dynamic states and external actions applied to the motorcycle. In order to of validate observations, several track tests must be carried out. This validation requires good instrumentation, something that is already widely available on the target prototypes.

In WP3, the rider-motorcycle interaction is studied to propose cybernetic model for the steering control task. Measurements on test track will be conducted with the instrumented vehicles in the WP1 in order to investigate the practices of a diverse population of riders and compare how these riders describe their control strategies with how they actually perform.

WP4 concerns the development of a risk function by defining objective indicators to quantify a hazardous

riding situation. The risks considered here is related to unsuitable approach speeds, leading to a possible loss of control or a collision with a third party. The risk functions to be synthesized will be mainly based on purely dynamic considerations of the lateral dynamics and the mobilized adhesion. However, the implementation of the road-risk assessment function requires the best possible knowledge of the various dynamic states of the motorcycle and the external effort.

WP5 develops application to training and safe bend-taking. This covers the development of products for industry based on the results of all previous WP, mainly targeting innovative training applications for safe bend-taking: off-line and on-line devices for the evaluation of motorbike paths, and new scenarios for the low-cost riding simulators. These new products will be evaluated by riding trainees and experienced riders.

WP6 deals mainly with project management. All partners will contribute to this work package, to define the dissemination strategy and its execution during the project.

## 1.7 Conclusions

Throughout this chapter, we have discussed the context and motivations of the thesis. In summary, Powered Two-Wheelers riders are the most vulnerable road users. The accident analysis studies have shown that reducing the number of road accidents requires designing and developing safety systems to ensure passengers safeness. Nevertheless, assistive systems for cars are well known and increasingly popular but for PTW riders the development of Advanced Rider Assistance Systems and On-Bike Information Systems have not progressed far enough yet. The lack of consideration of these users explains these alarming statistics. To overcome these problems, it is necessary to improve vehicles and road network infrastructure through the proposal of intelligent systems. Now and in many countries, the use of safety-enhancing assistive systems for passenger and commercial vehicles, including advanced driver assistance systems and In-Vehicle Information Systems are quite commonplace. Nevertheless, only a limited amount of the PTW equivalents systems have been developed so far. A better understanding of rider behavior would make it possible to sensitize experienced riders who show good practice, but also to set up new training and retraining measures, to improve the road design, to amend the highway code, and to identify areas for the design and/or assessment of driving assistance devices dedicated to PTWVs. Finally, knowledge of the interaction between riders and their PTWVs is critical for the tuning of riding simulators, which can then be used by a broader set of the rider population. The above analysis of safety gaps indicates several opportunities to advance the state of research on motorcycle safety and Intelligent Transportation Systems by addressing key gaps and needs. To help take action to address the identified gaps and challenges in research on ITS for motorcycle safety many recommended areas of research were identified to enhance ITS for motorcycle safety, include: synthesizing ITS technology and implementation with the already successful technology of antilock braking systems (ABS) in motorcycles, rider-motorcycle interface, motorcycle safety data including preparations to take full advantage of big data moving forward, applied research and assessments of safety benefits; and the harmonization of ITS technologies and standards such as inter-operable connected vehicles.

This thesis fits into this context by proposing a contribution to the development of rider assistive systems for motorcyclists, also known as Advanced Rider Assistance Systems. During these three years of research, within the VIROLO++ project, we have placed so much emphasis on the development of realistic solutions and their validations. In this validation process, we used the *BikeSim* software and the experimental platforms of the laboratory. Therewith, to accomplish ARAS design, the main elements of the PTWV structure and the basic phenomena at the origin of its specific dynamic behavior are discussed. Indeed, to characterize the behavior of the two wheeled vehicles, it is important to understand the V - I - R (Vehicle - Infrastructure - Rider) system. These characteristics have to be considered in the synthesis of PTWV model, estimation and control problems. In the next chapter, we present a detailed kinematic and dynamics modeling of the motorcycle, taken into account various factors influencing this dynamic.

# Chapter 2

## PTW Vehicle Modeling

### Abstract

Accurate modeling is important to analyze and understand the behavior of a system, to validate and test the effectiveness of various control strategies and estimation methods. Henceforth, this chapter deals with the mathematical modeling of powered two wheeled vehicle (PTWV). Since there is no affordable way to measure the pneumatic forces and moments of a PTWV, a tire modeling is studied with respect to different characteristics that have a strong influence on tire/road interaction. As a first step, an overview of PTWVs is given in section 2.1. Thereby, we introduce the issues related to tire modeling for a dynamic model in section 2.4. A brief description of the tire/road contact forces is introduced based on the magic formula of Pacejka to understand the tire dynamics and consequently the parameters of the tire model in section 2.5. The expressions of the pneumatic moments are also derived. In section 2.6 a short review is presented showing the progress of the PTWV modeling. Some important preliminaries are presented in section 2.7. Some technical simplifications for the sake of implementation are reported in section 2.8. The different motorcycles/rider models are introduced in section 2.9. In order to have an experimental platforms, used as a reference for the validation of the two-wheeled models and algorithms, we will present the motorcycle (Scooter lab's), the different sensors and their characteristics in section 2.12. Last, we introduce a new procedure for data calibration in section 2.13. Such a self-calibration method is focused for telematic boxes (e-Boxes) installed on two-wheeled vehicles, whose IMUs' axes often result not to be aligned with the vehicle reference system.

### 2.1 Overview of PTW Vehicle

PTWV is a two or three-wheeled motorized vehicle such that motorcycle, bike, motorbike, cycle, scooters and mopeds (Figure 2.1). They have gained popularity as an efficient transportation way especially in urban areas. The PTWV design varies greatly to fit a wide range of different purposes: long distance travel, commuting, cruising, sport including racing, and off-road riding. More and more people are giving up their four-wheeled vehicles and embracing life on two wheels vehicles. Motorcycles can be seen as a form of transportation or as a way to be free to enjoy the open road. Furthermore riding a motorcycle offers several advantages over driving a four wheeled vehicles. The most obvious, and greatest, advantage of traveling by motorcycle, is the ability to get through traffic faster in highly congested areas. There are many fun elements in owning a motorcycle but also a great disadvantage since the rider is most exposed to danger in an accident and he is less protected from serious injuries.

Therewith, the involvement of PTWV in the daily life transportation has attracted the attention of industrial and research laboratories around the world to face the new arising challenges. They are seriously thinking



FIGURE 2.1: Two-Wheeler Vehicles.

about exploiting the promising capabilities of these vehicles, which may highly affect the global vehicle economy. Although most of the topics have already been discussed for several decades ago, the particularity of the two-wheeled vehicle has made some classical issues such as stability and maneuverability always a very active research topic until nowadays. Several research groups are specialized in a specific topic related to the PTWV riding assistance systems and the related embedded solution for perception and control such that the obstacles detection and avoidance, vision-based landing, localization techniques, data fusion and others.

The history of the study of motorcycle dynamics is nearly as old as the bicycle itself. In 1817, Karl Drais invented the *Laufmaschine*<sup>1</sup>, or the running machine known later as the velocipede or draisine. This machine showed that a rider could balance his device by steering the front wheel. But the first meaningful overview about PTWV dynamics are undertaken first at the Imperial College by the Robin Sharp works, in the early of 1970s. He investigated regularly the stability behavior of motorcycles by studying its dynamics to deals with the so-called instability modes. Next, the team of Vitore Cossalter at the university of Padova is invested in an extensive research works for about two decades to analyze stability, handling, maneuverability and control of the PTWV. Their research, both experimental and numerical, has covered riding simulators, vehicle modeling, tire modeling, suspension design and optimal time maneuver<sup>2</sup>.

Other institution are also interested to the PTWV. The Automotive Systems Engineering, FZD<sup>3</sup>, at the university of Darmstadt focuses mainly on the concepts for motorcycle rider assistance by developing new active safety systems and by analyzing test results. Also, at the Polimi laboratory of Milano Polytechnic institute, the research team is interested by the implementation and the evaluation of new motorcycle prototype<sup>4 5</sup>.

At IBISC laboratory of Evry university, the first works on PTWV goes back to the ANR project SIMACOM. This project is intended to define the main specifications for designing a riding simulator for learning the relevant behaviors in emergency braking situations, and for PTWV with or without braking assistance system. Since, several works have followed concerning the analysis of PTWV dynamics, estimation and observation of dynamic states, motorcycle cornering towards ITS implementation. Recently, the VIROLO++ project<sup>6</sup> aims to better understand the causes and effects related to loss of control in curves. It includes tools and methods for studying driving behaviors and understanding driver/vehicle interactions. This research is structured around the use of instrumented motorcycles to reconstruct a precise trajectories and to compute risk function based on the collected data.

<sup>1</sup><https://www.cyclinguk.org/cycle/draisienne-1817-2017-200-years-cycling-innovation-design>

<sup>2</sup><https://www.unipd.it/en/saferider>

<sup>3</sup><https://www.tu-darmstadt.de/adda/partner/fzd/index.de.jsp>

<sup>4</sup><http://www.sport.polimi.it/en/motostudent>

<sup>5</sup><https://www.move.deib.polimi.it/>

<sup>6</sup><https://www.ibisc.univ-evry.fr/portfolio/virolo/>

## 2.2 PTWV Description

The PTWV is a complex system that involves a set of mechanical parts connected to each other by several links. These components are engineered, manufactured, and assembled in order to produce a particular motorcycle model with the desired performance, design, and cost to better adapt and to cover all riders' tastes and needs. The key components of a PTWV are presented in this section.

The first part is the principal body or the chassis assembly which includes the frame and the engine. The front and rear suspensions are connected to the chassis by a suspension arrangement and serves to enhance the passengers comfort by filtering undesirable vertical vibrations arising from the road irregularities. They also highly contribute to braking and handling the vehicle. Beside the main chassis, we find the steering mechanism composed by the front fork and the vehicle's handlebar. The front fork holds the front suspension and is connected to the front wheel through the wheel hub which houses the brake system. For handling, the front body is the most critical part of a motorcycle since the combination of rake and trail determines how stable the vehicle is. Finally, wheels and tires are the most important characteristic since they are the only way of the vehicle to road interaction. The tire ensures a permanent contact within its patch and provides the necessary friction for acceleration and braking.

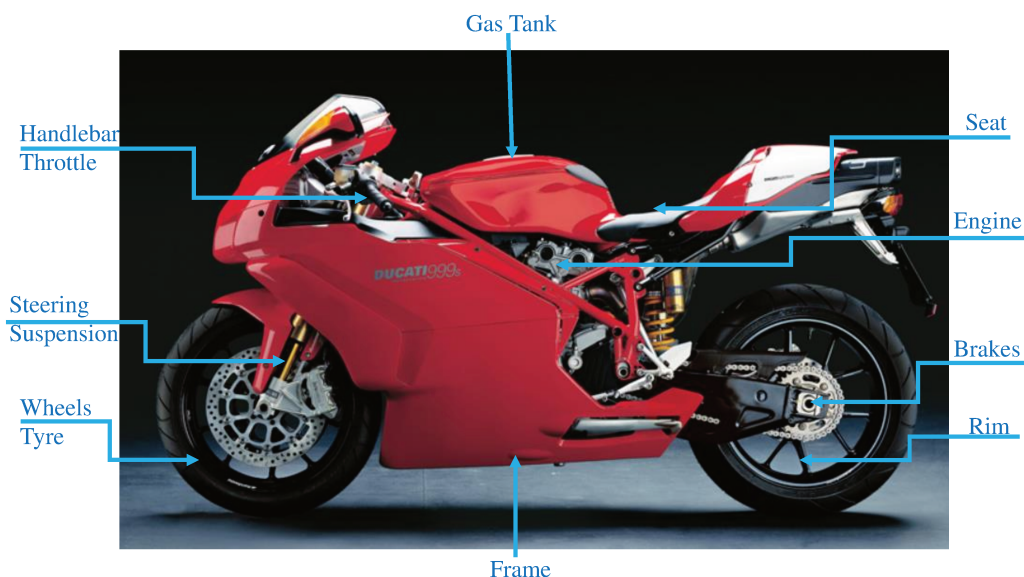


FIGURE 2.2: Motorcycle components.

The parameters that describe the geometry of a PTWV are defined in figure 2.3. The key parameters are wheelbase, caster angle, and trail. These parameters have a significant effect on the vehicle handling and varies with respect to the vehicle type, long distance travel, cruising, sport including racing, and off-road. For example, a cruiser motorcycle is often identified by its long and extended front forks with more lean angle, whereas motorbikes has shorter and less extended front forks.

Figure 2.3 shows a vehicle with a positive caster geometric trail which means that the contact point between the front wheel and the road is behind the intersection point between the extension of the steer axis and the road. The caster or rake angle determines the steering ability of a motorcycle. A smaller caster angle means the motorcycle will be easier to corner but less stable in a straight line.

The wheelbase length is an intrinsic property of the vehicle and determines the length between the two vehicle's axles. Longer wheelbase entails more stability while a shorter one means that the vehicle is more agile in turn. Besides the wheelbase, the geometric trail is defined as the horizontal distance when the motorcycle is upright with zero steer angle. The trail length is what ultimately decides the tire contact patch area. The contact patch is the part of the tire which remains in contact with the road. A greater trail length means more straight line stability but it will be more difficult to maintain balance while cornering or in curve maneuver.

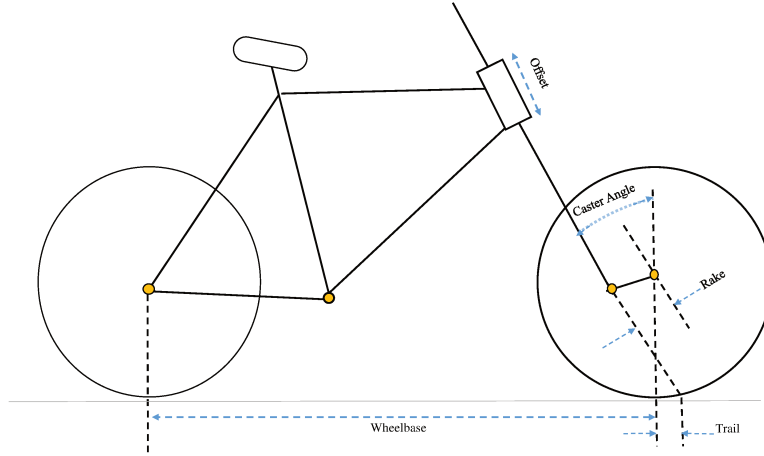


FIGURE 2.3: Geometry for handling of of two-wheeled vehicle.

## 2.3 Tire-Ground Interactions

The vehicle dynamics is governed mainly by the tire/road interactions. Due to tire materials, the pneumatic deformations allow to generate the longitudinal and lateral forces necessary to accelerate, to brake and to make a direction change when steering. These forces, combined to the rider actions, dictate the vehicle dynamics and the limit of its handling.

However, the interaction between tires and ground is a complex phenomenon and can make the dynamics modeling a hard task. For this, tire-road interaction can be represented by three efforts, the lateral cornering forces, the longitudinal braking or acceleration forces and the self-aligning moment (Pacejka and Sharp, 1991; Pacejka, 2005). This decomposition simplifies the mathematical description of the pneumatic efforts with respect to the vehicle's kinematics variables such that slip angles and the vehicle speed. Also, various intrinsic and extrinsic parameters are necessary for the evaluation of the pneumatic efforts in particular, road friction, tire cornering stiffness, steering geometry and the vertical load. Road friction, or adhesion, translates the capacity of the tire to transform the normal force, at the tire-road contact, to a pneumatic forces. So, the loss of adhesion can leads to the motorcycle fall and the under-evaluation of this entity can be fatal for the rider safety.

Beyond the tire-road interaction, the vehicle is also subject to other external forces. Gravitational, aerodynamic and rolling friction are some examples of efforts which can highly modify the vehicle dynamics behavior and also have an indirect impact on the pneumatic generated forces. we detail these aspects in the remaining of this chapter.

## 2.4 Tire's kinematics

In this section, the PTWV wheels are considered as rigid, thin disks where the tire-road contact is located at the point  $C$ . Also, we assume that there is no lateral displacement of the contact point. At this point, a local coordinate frame is introduced and denoted  $\mathfrak{R}_T(C, i_T, j_T, k_T)$  to describe the tire motion. The vector  $k_T$  is the normal vector to the road surface. The vector  $i_T$  is obtained by the cross product between the wheel rolling axis  $j_\theta$  and the vector  $k_T$  as  $i_T = j_\theta \times k_T$ . Last, the vector  $j_T$  completes the reference axis.

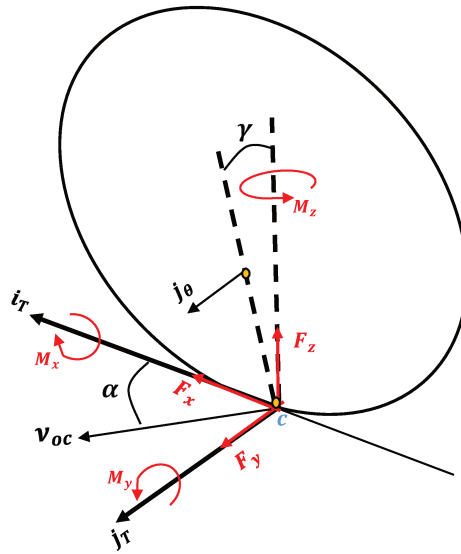


FIGURE 2.4: Effort generated by the pneumatic.

As shown in figure 2.4, the camber angle  $\gamma$  is the angle formed by the two vectors  $j_\theta$  and  $k_T$ . This angle plays an important role in the PTWV stabilization and handling. This angle is expressed by the following scalar product:

$$\sin \gamma = k_T \cdot j_\theta \quad (2.1)$$

Due to the tire deformation, the tire-road contact point velocity  $v_{oc}$  is no longer along the  $i_T$  axis. It forms an angle  $\alpha$  known as the sideslip angle. Also, during acceleration and braking phases, the relative velocity between the linear velocity generated by the wheel rotation  $\dot{\theta}$  and the forward speed at the tire-road contact causes the well known longitudinal slip ratio usually denoted  $\kappa$ . The two slip variables are defined by the following equations:

$$\begin{aligned} \kappa &= -\frac{V_C - r_W \dot{\theta}}{\max(V_C, r_W \dot{\theta})} \\ \alpha &= \arctan\left(\frac{j_T \cdot v_{oc}}{i_T \cdot v_{oc}}\right) \end{aligned} \quad (2.2)$$

where  $r_W$  the effective wheel's dynamic radius and  $V_C = \|v_{oc}\|$  is the speed at the contact point  $C$ . Moreover, assuming that the contact point  $C$  must still belong to the road surface, the vertical deformation of the tire can be calculated with the following equation:

$$\varpi = k_T \cdot r_{VC} \quad (2.3)$$

with  $r_{VC}$  is the position vector between the contact point  $C$  and the origin of the vehicle reference frame  $\mathfrak{R}_V$  which will be defined later. This deformation allows to calculate the normal load necessary to avoid wheeling.

Once the tire's kinematics variables are defined, the equivalent pneumatic effort can be computed at the wheel center  $R$  by the following expressions:

$$\begin{aligned} F_T &= F_x i_T + F_y j_T + F_z k_T \\ M_T &= M_x i_T + M_y j_T + M_z k_T + F_T \times r_{CR} \end{aligned} \quad (2.4)$$

Where  $F_x$  is the longitudinal force generated by the longitudinal slip  $\kappa$  and assumed to be positive during acceleration phase and negative when braking.  $F_y$  is the lateral force generated by the sideslip angle  $\alpha$ .  $F_z$  corresponds to the normal force at the tire-road contact point.  $M_x$  is the tilting moment around  $i_T$ ,  $M_y$  is the rolling resistance moment around  $j_T$  and  $M_z$  is the self-alignment moment around the vertical axis  $k_T$ . In the next section 2.5, more details about the expressions of these forces and moments associated with the model (2.4) are given.

## 2.5 Pneumatic efforts

The simulated motorcycle dynamics depend on the mathematical tire forces and moments (Sharp, Evangelou, and Limebeer, 2004). In the literature, several theoretical, semi-empirical or experimental tire effort representations are developed with respect to the intended complexity level.

### 2.5.1 The Magic Formula

The magic formula or Pacejka model is a non-linear representation of the pneumatic forces and moments, introduced by Pacejka in 1993 (Pacejka, 2005). This model is the most widespread used for modeling tires of land vehicles and also the PTWV (Sharp, Evangelou, and Limebeer, 2004). It is also an empirical approach which allows to reflect the real tire behavior including tire saturation. According to Pacejka model, the longitudinal force, the lateral force, and the self-alignment moment can be computed from the following generic equation:

$$F(\vartheta) = D_\vartheta \sin \left( C_\vartheta \operatorname{atan} \left( B_\vartheta \vartheta - E_\vartheta (B_\vartheta \vartheta - \operatorname{atan} (B_\vartheta \vartheta)) \right) \right) \quad (2.5)$$

with  $B_\vartheta$  is called the stiffness factor,  $C_\vartheta$  is the shape factor,  $D_\vartheta$  is the peak value and  $E_\vartheta$  is the curvature factor. These factors are related to the pneumatic intrinsic characteristics and determined empirically.  $\vartheta$  is a generic variable which corresponds to the sideslip  $\alpha$ , longitudinal slip  $\kappa$  or the wheel camber  $\gamma$ . The tire stiffness is the slope of the curve in its linear region as in figure 2.5.

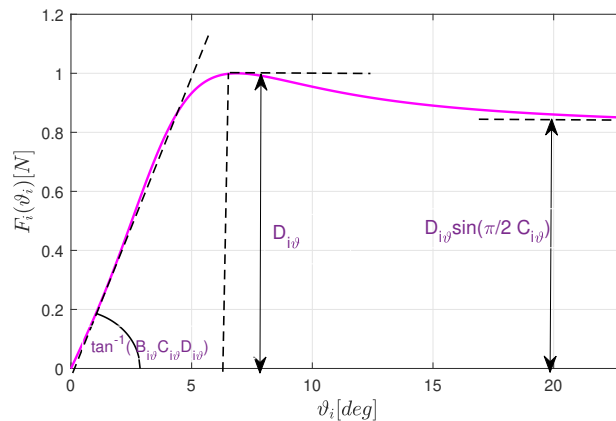
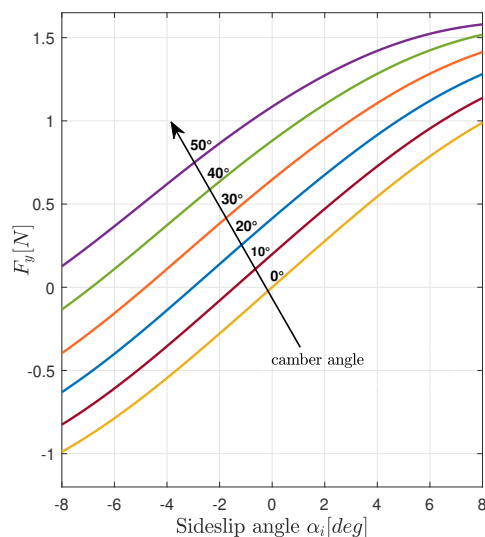


FIGURE 2.5: Normalised magic Formula or Pacejka model.

### 2.5.2 Lateral Force

Unlike a car vehicle, the camber angle is directly related to the PTWV roll angle and can reach significant values depending on the forward speed and path curvature. Then, when cornering, the contribution of the tire lateral force  $F_y$  depends mainly on the tire sideslip angle  $\alpha$  and the camber angle  $\gamma$  which is a geometric angle (Pacejka and Sharp, 1991, Bakker, Nyborg, and Pacejka, 1987). Figure 2.6 shows the effect of the camber angle on the generated lateral force  $F_y$  as a function of the sideslip angle  $\alpha$ .

The choice of a specific representation for tire lateral force requires some attention since it impacts the stability analysis of the PTWV (Cossalter et al., 2006b). If the tire is in its linear region, an additional amount of the tire force can be generated and hence the vehicle remains controllable, however, in saturation region, the tire force is at its maximum and the rider will lose vehicle control.

FIGURE 2.6: The influence of  $\gamma$  on the normalized  $F_y$ .

However, in control and estimation problems, the use of the magic formula is cumbersome. For small values of sideslip and camber angles, the lateral force can be approximated by a linear model of the following form:

$$F_y = C_\alpha \alpha + C_\gamma \gamma \quad (2.6)$$

The parameters  $C_\alpha$  and  $C_\gamma$  are respectively the sideslip and camber cornering stiffness expressed in  $\frac{N}{rad}$ .

The previous magic formula or its corresponding linear form describes only the static behavior of the pneumatic efforts. However, due to its elastic deformation, a transient behavior occurs. To consider this transient phenomenon, almost literature includes a first order low-pass filter to the model, known as the tire relaxation given by:

$$\frac{\sigma}{v_x} \dot{F}_y = -F_y + F_y^0 \quad (2.7)$$

where,  $\sigma$  is the relaxation length which models the transient time.  $F_y^0$  is the steady-state value of the lateral force obtained by applying the magic formula (2.5) or the linear form (2.6). By solving the differential equation (2.7), we get the instantaneous lateral force.

### 2.5.3 Longitudinal Force

During acceleration or braking, a corresponding torque is applied to the tire which generates a longitudinal force. Figure 2.7 shows the evolution of the tire longitudinal force with respect to the slip ratio. Generally, the longitudinal slip is considered as the normalized ratio as shown in the equation (2.2).

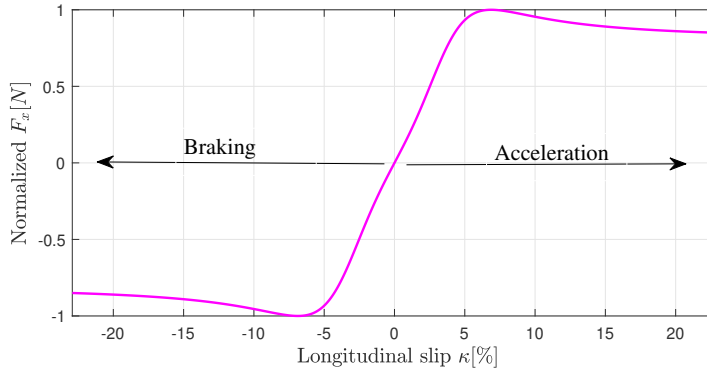


FIGURE 2.7: Longitudinal tire force as a function of the longitudinal slip ratio.

As for the tire lateral force, for small longitudinal slips ratio, linear formulation is possible where:

$$F_x = C_\kappa \kappa \quad (2.8)$$

$C_\kappa$  is the coefficient of stiffness which depends on the vertical force  $F_z$  according to the relation  $C_\kappa = k_\kappa F_z$  where  $k_\kappa$  is the normalized stiffness.

To consider the transient phenomenon, the tire relaxation, introduced in the previous section, can also be applied here as following:

$$\frac{\sigma}{v_x} \dot{F}_x = -F_x + F_x^0 \quad (2.9)$$

where,  $\sigma$  is the relaxation length which model the transient time.  $F_x^0$  is the steady-state value of the longitudinal force obtained by applying the magic formula (2.5) or the linear form (2.8). By solving the differential equation (2.9), one can get the instantaneous longitudinal force.

### 2.5.4 Vertical Forces

The vertical force  $F_z$  is the image of the load force applied on the tire at its contact point with the road. This force is very important since it governs the maximum values of the generated tire longitudinal and lateral forces. The distribution of the vertical forces between the two tires depends mainly on the position of the vehicle's gravity center (CoG) and on the longitudinal acceleration.

In vehicle dynamics, the distribution of the vertical force is commonly referred to as static load balancing and the load transfer. If we write  $F_{zf}$ ,  $F_{zr}$  the vertical force on both tires,  $\Delta F_z$  the amount of the load transfer and,  $F_{zf0}$ ,  $F_{zr0}$  the static vertical forces then it comes:

$$\begin{aligned} F_{zf} &= F_{zf0} - \Delta F_z \\ F_{zr} &= F_{zr0} + \Delta F_z \end{aligned} \quad (2.10)$$

$\Delta F_z$  is positive in acceleration phase and negative in braking phase. The expression of the dynamic vertical forces  $F_z$  as a function of the longitudinal acceleration of the PTWV and its geometry is obtained from equations of equilibrium forces:

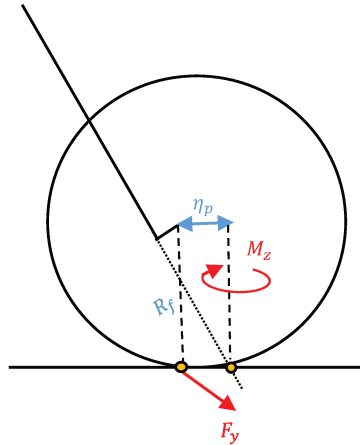
$$\begin{aligned} F_{zr} &= \frac{m(l_f g + h a_x)}{l_f + l_r} \\ F_{zf} &= \frac{m(l_r g - h a_x)}{l_f + l_r} \end{aligned} \quad (2.11)$$

where  $m$  is the PTWV mass,  $g$  is the gravity constant,  $a_x$  the longitudinal acceleration,  $h$  the high of the CoG and,  $l_f$ ,  $l_r$  are respectively the longitudinal distance between the vehicle's CoG and the front and rear tires contact point. It goes that  $l_f + l_r$  is the vehicle's wheelbase.

It should be noted that the PTWV are characterized by a low wheelbase and a relatively high CoG position. This is why load transfer is much more important compared to passenger cars. It can lead to dangerous phenomenon such as the wheelie or stoppie.

### 2.5.5 Self-Alignment Moment

In addition to the pneumatic forces, the tire generates moments about its different axes. These moments are often neglected because of their small contributions. Nevertheless, pneumatic moments can be introduced to compensate for simplistic modeling assumptions. Indeed, in section 2.4, the PTWV wheels are considered as rigid, thin disks where the tire-road contact is dot shaped. Such considerations are not real even for a simple modeling task. To overcome this limitations, three main moments are introduced and discussed.

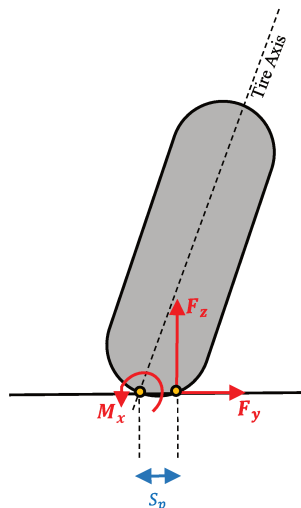
FIGURE 2.8: Self-alignment Moment,  $M_z$ .

We start with the most important moment for the PTWV dynamics which is the self-alignment. The distribution of the tire lateral forces generated by the sideslip angle is not symmetric. Hence, the lateral force is applied at a different point from that corresponding to the vertical projection of the wheel center on the ground as shown in Figure 2.8. The resulting offset, called geometric trail  $\eta_p$ , generates a stabilizing moment that tends to rotate the wheel by the following equation:

$$M_z = -\eta_p F_y \quad (2.12)$$

### 2.5.6 Overturning Moment

This moment is introduced to compensate for no lateral displacement of the contact point assumption. With regard to the geometry of the PTWV tires, the real tire-road contact point  $C$  moves transversely because of the camber and hence it is located at a distance  $S_p$  from the conventional contact point defined by the vertical projection of the wheel center on the ground. As in figure 2.9, due to this lateral deviation, the vertical force  $F_z$  creates a moment called the overturning moment  $M_x$  which has a destabilizing effect.

FIGURE 2.9: Overturning moment,  $M_x$ .

The overturning moment is expressed by the following linear equation:

$$M_x = -S_p F_z \quad (2.13)$$

### 2.5.7 Rolling Resistance Moment

If we consider a wheel that rolls without sliding on a flat surface then the rolling radius  $R$  is defined as the ratio between the longitudinal speed  $v_x$  of the vehicle and the rotation speed of the wheel  $\dot{\theta}$ . It comes:

$$R = v_x \dot{\theta} \quad (2.14)$$

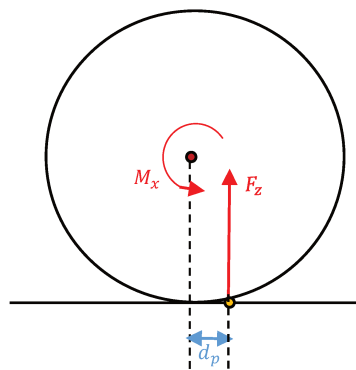


FIGURE 2.10: Rolling resistance Moment,  $M_y$ .

The effective rolling radius is generally lower than the radius without load because of the deformation of the tire. The latter depends on the type of tire, its radial stiffness, its inflation pressure, the vertical force and the longitudinal speed of the vehicle. This difference, noted  $d_p$ , between the effective radius and the initial radius generates a rolling resistance moment of the vehicle  $M_y$  as in figure 2.10. It is expressed by the following linear equation:

$$M_y = d_p F_z \quad (2.15)$$

## 2.6 Literature of Motorcycle Dynamics Modeling

The PTWV design coupled to the complex tire-road interaction makes the dynamics modeling a challenging task. In fact, the dynamics study of the two-wheeled vehicles has been started for long time ago. Several mathematical models have been proposed in the literature, with various levels of complexity and details. In the following, a brief review is presented focusing on the progress of the modeling methodology. The choice of a modeling methodology is very important since it affects the dynamics behavior analysis, the number of degrees of freedom and the usefulness of the resulting model for the final application such as the control application.

The first attempt to analyze the two-wheeled vehicle dynamics is published in (Rankine, 1869). Early work progressed slowly and many conflicting conclusions were drawn initially. The main substantial contribution was the work of Whipple presented in (Whipple, 1899). In this work, the two-wheeled vehicle is a bicycle modeled as a set of two rigid bodies linked via the rotation axis of the handlebar. A system of nonlinear

differential equations describing the motion of a bicycle including the rider are established. At this time, the numeric computers were not available to solve effectively these nonlinear differential equations. Hence, Whipple has linearized the model and study it for small disturbances around the straight-line equilibrium at a given constant speed.

However, the works cited above deal only with the dynamics of the bicycles which is very different from a PTWV in a manner of factors such : weigh, power, maximum speed, aerodynamics, and tire-road interaction. In 1971, Sharp's model is presented and it is considered as the most relevant reference in the PTWV dynamics modeling field (Sharp, 1971). In this work, the dynamics of the PTWV in free control is detailed to perform a stability analysis from straight line equilibrium. Sharp highlights the presence of three unstable vibration modes namely the capsize, the weave and the wobble. In the work published in (Eaton, 1975), the auto-alignment and overturning moments are introduced by modifying Sharp's equations. Nevertheless, there were an inconsistency in the tire equations between the analytical and physical results. This work will be taken over in (Segel and Wilson, 1975) to develop a more refined model of tire. Aerodynamic efforts are considered in (Cooper, 1974) to demonstrate their importance on the performance and the stability of the PTWV in particular at high speeds. Afterward, Sharp includes the vehicle acceleration (Limebeer, Sharp, and Evangelou, 2001) and the aerodynamic load transfer (Sharp and Jones, 1977) in the lateral dynamics to prove their effects on the out-of-plane stability. Unfortunately, this is not enough to explain the discrepancy between theory and practice.

Weir introduces the rider control in his modeling (Weir and Zellner, 1978) which presents the first motorcycle stabilization approach (Weir and Zellner, 1978). In (Koenen, 1983), the author look for the influence of the roll degree of freedom on the coupling between the in-plane and the out-of-plane vibration. (Katayama, Aoki, and Nishimi, 1988) study the actions of the rider on the motorcycle control. The results indicate that the PTWV is mainly controlled by the handlebar steering torque while it is always possible to control the vehicle with a small movements of the rider's lower part. Sharp proposed an improvement of his first model to evaluate the influence of the rider and bodies flexibilities on the unstable vibration modes (Sharp, 1994).

With the development of high-end numerical solutions, more complex modeling approach have emerged. (Imaizumi, Fujioka, and Omae, 1996) consider a set of twelve rigid bodies to model the PTWV dynamics. The rider actions have been applied via the proportional controller. Sharp proposed a multibody model integrating the suspension and a more elaborate representation of the road-tire contact and the pneumatic efforts are computed by using the magic formula (Sharp, 2001). This model allowed to study the PTWV dynamics over large motions around equilibrium conditions and to better understand the coupling between longitudinal, lateral and vertical dynamics. Cossalter presents an eleven degrees of freedom using a modeling approach called the natural coordinates approach (Cossalter and Lot, 2002). In this model, the front and rear chassis, steering system, suspensions and tires are considered and a more original tire model was developed, which takes into account the geometric shape of tires and the elastic deformation of tire carcasses. A realistic representation of the vehicle wheel is showed in (Sharp, Evangelou, and Limebeer, 2004) where the geometry of the rim and the tire width are taken into account. This model was the most complete of the literature and it constitutes the base of the PTWV simulation environment *BikeSim*.

## 2.7 PTWV Dynamics Modeling

### 2.7.1 Motorcycle Description

In its mid-scale decomposition, the PTWV can be represented as the interconnection of a set of six bodies. The rear body  $G_r$  includes the saddle, the engine and the fuel tank. The upper front body  $G_f$  includes the handlebar and the upper part of the suspension assembly. The lower front body  $G_l$  represents the lower part of the suspension assembly and the brake system. The swing arm body  $G_s$  contains the swing arm mass and the rear brake system. Finally,  $R_f$  and  $R_r$  represent, respectively, the front and the rear-wheel bodies. Note that we can also consider further bodies such that the rider upper body  $G_{d_u}$  and rider lower body  $G_{d_l}$  as in Figure 2.11. To characterize the PTWV motion, we should introduce a set of natural coordinates (Damon, 2018) as follows:

- the longitudinal, lateral and vertical positions  $(x, y, z)$  of the chassis,
- the roll, pitch and yaw orientation  $(\phi, \theta, \psi)$  of the the chassis,

- the steering angle  $\delta$  of the front steering system,
- the front suspension travel  $\lambda_f$  and the swing arm rotation  $\mu$ ,
- and finally, the front and rear wheels spinning,  $\theta_f$  and  $\theta_r$ .

Next, we consider the Earth-fixed frame  $\mathfrak{R}_O(O, i_O, j_O, k_O)$  and the vehicle reference frame  $\mathfrak{R}_V(V, i_V, j_V, k_V)$  in which the vehicle dynamics will be expressed. The axes  $i_V$  and  $j_V$  are respectively along the longitudinal and the transverse axis of the vehicle. For the axis  $k_V$ , there are two main standards defining the configuration of reference frame used for modeling ground vehicles, the the ISO 8855 and the SAE J670e standards. They differs mainly in the direction of the  $z$ -axis. Point  $V$  corresponds to the projection of the point  $P$  at the ground along the symmetry plan of the vehicle where  $P$  is the link attachment point of the swing arm.

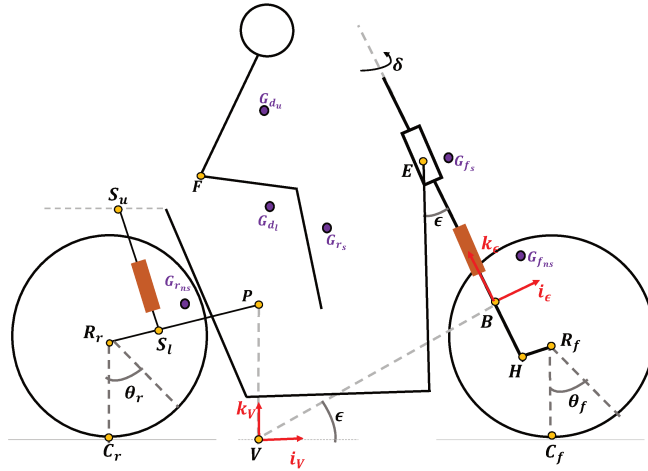


FIGURE 2.11: Geometry of the eight-body model of the PTWV with rider.

The motion of the PTWV is referred to the inertial reference frame  $\mathfrak{R}_O$  by a set of generalized velocities  $v_x, v_y$  of point  $V$ , and the yaw rotation  $\psi$  around the  $z$ -axis of the inertial reference frame. Starting from the reference frame  $\mathfrak{R}_V$ , the orientations of the other reference frames are defined in figure 2.12. The first rotation corresponds to the roll  $\phi$  about  $i_V$  which gives an intermediate reference frame  $\mathfrak{R}_\phi(V, i_\phi, j_\phi, k_\phi)$ . The second rotation is the pitch motion around  $j_\phi$  and gives another reference  $\mathfrak{R}_\theta(P, i_\theta, j_\theta, k_\theta)$ . Then, a geometric rotation  $\epsilon$  around  $j_\theta$  leading to the reference  $\mathfrak{R}_\epsilon(P, i_\epsilon, j_\epsilon, k_\epsilon)$ . Finally, the steering rotation  $\delta$  around  $k_\epsilon$  gives the reference  $\mathfrak{R}_\delta(B, i_\delta, j_\delta, k_\delta)$ . At the same time, the rotation of the swing arm  $\mu$  around  $j_\phi$  gives  $\mathfrak{R}_\mu(P, i_\mu, j_\mu, k_\mu)$ .

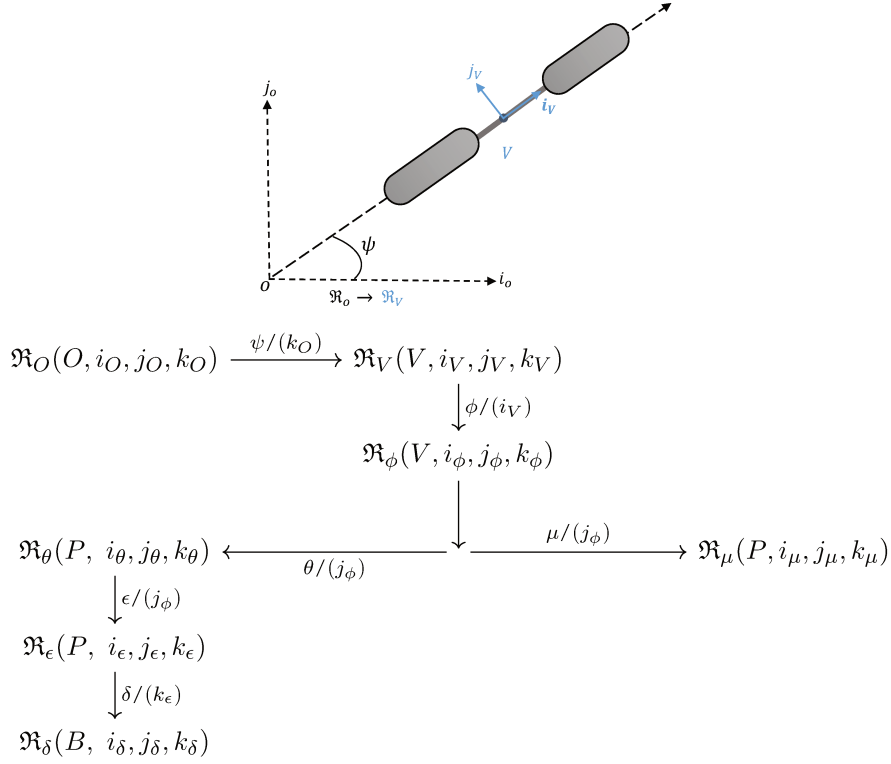


FIGURE 2.12: Orientation of PTWV coordinate systems.

The velocity vector of each body in the vehicle reference frame  $\mathfrak{R}_V$  is given by (Nehaoua et al., 2013a) :

$$\begin{aligned} v_{OG_i} &= v_{OV} + \omega_{OV} \times r_{VG_i} + \dot{r}_{VG_i} \\ \omega_{OG_i} &= \omega_{OV} + \omega_{VG_i} \end{aligned} \quad (2.16)$$

where  $v_{OV} = [v_x, v_y, 0]^T$  and  $\omega_{OV} = [0, 0, \dot{\psi}]^T$  are respectively the linear and the angular velocity vector of point  $V$ . Also, the acceleration vector of each body in the vehicle reference frame  $\mathfrak{R}_V$  is given by :

$$\begin{aligned} a_{OG_i} &= \dot{v}_{OV} + \varepsilon_{OV} \times r_{VG_i} + \ddot{r}_{VG_i} + \omega_{OV} \times (v_{OG_i} + \dot{r}_{VG_i}) \\ \varepsilon_{OG_i} &= \dot{\omega}_{OV} + \omega_{OV} \times \omega_{VG_i} + \dot{\omega}_{VG_i} \end{aligned} \quad (2.17)$$

where  $\dot{v}_{OV} = [\dot{v}_x, \dot{v}_y, 0]^T$  and  $\dot{\omega}_{OV} = [0, 0, \ddot{\psi}]^T$ .

By using equations (2.16) and (2.17), all kinematic quantities for all bodies can be defined easily. The next section discusses the basics of the virtual power principle for dynamic modeling of PTWV.

## 2.7.2 Virtual Power Principle

The virtual power principle is a dual formulation of the fundamental principle of Newton-Euler's dynamics. As stated by the third Newton law, when a body exerts a force on another body, the former simultaneously exerts a force equal in magnitude and opposite in direction. So, the power of the constraint in this case is null and we say that the constraint is compatible or conservative with the direction of motion. Then, the

virtual powers in a virtual motion provided by conservative constraint forces  $F_{G_i,c}$  and moments  $M_{G_i,c}$  is null:

$$\sum_{i=1}^n \{ \Delta v_{OG_i} F_{G_i,c} + \Delta \omega_{OG_i} M_{G_i,c} \} = 0 \quad (2.18)$$

with  $n$  the number of bodies,  $\Delta v$  and  $\Delta \omega$  are virtual variation in linear and angular velocities.

From Newton/Euler dynamics principle, the conservative efforts  $F_{G_i,c}$  and  $M_{G_i,c}$  can be separated from the system motion and the external applied efforts  $F_{G_i,a}$  and  $M_{G_i,a}$  such that:

$$\begin{aligned} F_{G_i,c} &= m_{G_i} a_{OG_i} - F_{G_i,a} \\ M_{G_i,c} &= \mathfrak{J}_{G_i} \epsilon_{OG_i} + \omega_{OG_i} \times \mathfrak{J}_{G_i} \omega_{OG_i} - M_{G_i,a} \end{aligned} \quad (2.19)$$

with  $m_{G_i}$  and  $\mathfrak{J}_{G_i}$  are respectively the mass and the inertial matrix of the body  $i$  in its  $CoG_i$ . Moreover, from equations (2.16) and (2.17), the velocity and acceleration vectors of each body  $G_i$  can be written as follows:

$$\begin{aligned} v_{OG_i} &= \frac{\partial v_{OG_i}}{\partial \vartheta} \vartheta \\ \omega_{OG_i} &= \frac{\partial \omega_{OG_i}}{\partial \vartheta} \vartheta \\ a_{OG_i} &= \frac{\partial v_{OG_i}}{\partial \vartheta} \dot{\vartheta} + a_R \\ \epsilon_{OG_i} &= \frac{\partial \omega_{OG_i}}{\partial \vartheta} \dot{\vartheta} + \epsilon_R \end{aligned} \quad (2.20)$$

where  $\vartheta$  denotes the vector of generalized velocities and the partial derivatives are called Jacobian matrices of the velocity vector with respect to the generalized velocities vector. Vectors  $a_R$  and  $\epsilon_R$  are referred as the residual acceleration terms.

Finally, by combining equations (2.18), (2.19) and (2.20) and after some algebraic manipulations, the system dynamics can be described by the following first-order differential equation (Nehaoua et al., 2013a):

$$\mathcal{M} \dot{\vartheta} = Q_a - Q_R \quad (2.21)$$

with  $\dot{\vartheta}$  is the derivative of the vector of generalized velocities.  $\mathcal{M}$  denotes the mass matrix:

$$\mathcal{M} = \sum_{i=1}^n \left\{ m_{G_i} \left( \frac{\partial v_{OG_i}}{\partial \vartheta} \right)^T \frac{\partial v_{OG_i}}{\partial \vartheta} + \left( \frac{\partial \omega_{OG_i}}{\partial \vartheta} \right)^T \mathfrak{J}_{G_i} \frac{\partial \omega_{OG_i}}{\partial \vartheta} \right\} \quad (2.22)$$

$Q_a$  is the applied generalized effort vector and  $Q_R$  is the residual generalized effort vector:

$$Q_a = \sum_{i=1}^n \left\{ \left( \frac{\partial v_{OG_i}}{\partial \vartheta} \right)^T F_{G_i,a} + \left( \frac{\partial \omega_{OG_i}}{\partial \vartheta} \right)^T m_{G_i,a} \right\} \quad (2.23)$$

$$Q_R = \sum_{i=1}^n \left\{ m_{G_i} \left( \frac{\partial v_{OG_i}}{\partial \vartheta} \right)^T a_R + \left( \frac{\partial \omega_{OG_i}}{\partial \vartheta} \right)^T (\mathcal{J}_{G_i} \varepsilon_R + \omega_{OG_i} \times \mathcal{J}_{G_i} \omega_{OG_i}) \right\} \quad (2.24)$$

### 2.7.3 Technical Simplification for Implementation Purpose

The PTW multibody representation of the previous section is suitable for the simulation and the validation of the vehicle's dynamics behavior. In the other hand, the resulting mathematical model is strongly nonlinear and highly complex which does not make it a suitable candidate to solve control, estimation and identification problems.

A first approach consists to choose a reduced number of bodies with the minimum set of generalized coordinates. Then, the lateral and longitudinal dynamics decoupling will simplify greatly the model. In both cases, the front and rear wheels are assimilated to virtual masses but their rotation dynamics are considered in the development of the models. Also, the upper and lower front bodies are merged into one body and the swing arm is included into the rear body. This yields to a two bodies representation with decoupled longitudinal and lateral dynamics. This issue will be the subject of the next section.

## 2.8 Two-Body Model for the Lateral Dynamics

This section presents the development of the lateral dynamics by considering the PTWV and its rider as a set of two bodies: the front body and the rear body. Once established, a linearization around a straight line trajectory is discussed.

### 2.8.1 Assumptions

In this section, the PTWV and its rider are represented by a set of two bodies linked by the steering mechanism. We distinguish the front body  $G_f$ , including the front wheel, the fork and the handlebars. The rear body  $G_r$  includes the chassis, the tank, the rider, the swing arm, the engine and the rear wheel. By this simplifications, the dynamics of the suspensions is not taken into account which eliminates the pitch dynamics and load transfer. Also, the longitudinal velocity is considered to be constant or at least it varies very slowly allowing to neglect the longitudinal slip ratio for both tires.

For the development of the two-body model, we define a vehicle reference  $\mathfrak{R}_A = (A, i_A, j_A, k_A)$  attached to the PTWV at point  $A$  according to the ISO standard. The origin  $A$  corresponds to the projection of the rear body CoG on the ground along the longitudinal plane of symmetry as in figure 2.13. Starting from the vehicle reference  $\mathfrak{R}_A$ , a roll rotation  $\phi$  around  $i_A$  gives an intermediate reference  $\mathfrak{R}_\phi(A, i_\phi, j_\phi, k_\phi)$ . Next, a rotation  $\epsilon$  around  $j_\phi$  gives  $\mathfrak{R}_\epsilon(A, i_\epsilon, j_\epsilon, k_\epsilon)$ . Finally, a steering rotation  $\delta$  around  $k_\epsilon$  gives  $\mathfrak{R}_\delta(B, i_\delta, j_\delta, k_\delta)$ .

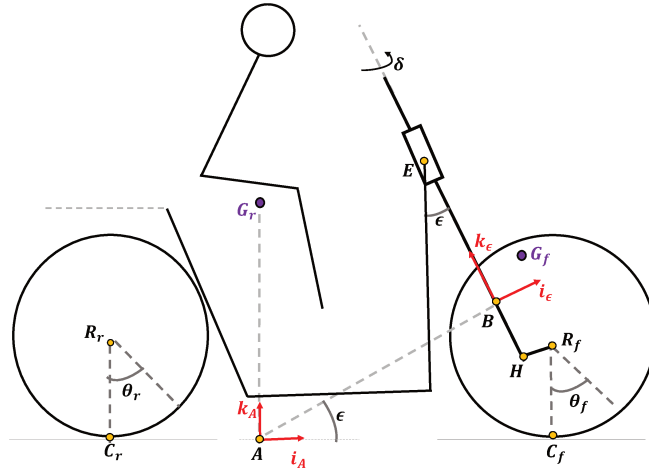


FIGURE 2.13: Geometry of the two-body model of the PTWV and its rider.

The resulting model allows the simulation of 4 DoF namely the yaw  $\psi$ , the roll  $\phi$ , the steer  $\delta$  and the lateral speed  $v_y$  with respect to the rider torque applied on the vehicle's handlebar. So, we choose a set of four generalized velocities:

$$\vartheta = [v_y \quad \dot{\psi} \quad \dot{\phi} \quad \dot{\delta}]^T \quad (2.25)$$

### 2.8.2 Rear and Front Body Kinematics

The position of the CoG of the rear body in its local reference frame  $\mathfrak{R}_\phi$  is a constant vector  $r_{AG_r}^\phi = [0, 0, z_{G_r}]^T$ . Then, in the vehicle reference we have:

$$r_{AG_r} = R_\phi r_{AG_r}^\phi \quad (2.26)$$

By differentiating the equation (2.26), we can express the vector of the relative linear velocities by:

$$\dot{r}_{AG_r} = \omega_\phi \times r_{AG_r} \quad (2.27)$$

where  $\omega_\phi = [\ddot{\phi}, 0, 0]^T$ . A second differentiation, the vector of the relative linear accelerations is:

$$\ddot{r}_{AG_r} = \dot{\omega}_\phi \times r_{AG_r} + \omega_\phi \times \dot{r}_{AG_r} \quad (2.28)$$

By using equations (2.16) and (2.17), we can express the rear body kinematics in the vehicle reference as follows:

$$\begin{aligned}
v_{OG_r} &= v_{OA} + \omega_{OA} \times r_{AG_r} + \dot{r}_{AG_r} \\
\omega_{OG_r} &= \omega_{OA} + \omega_{AG_r} \\
a_{OG_r} &= \dot{v}_{OA} + \varepsilon_{OV} \times r_{AG_r} + \ddot{r}_{AG_r} + \omega_{OA} \times (v_{OG_r} + \dot{r}_{AG_r}) \\
\varepsilon_{OG_r} &= \dot{\omega}_{OA} + \omega_{OA} \times \omega_{AG_r} + \dot{\omega}_{AG_r}
\end{aligned} \tag{2.29}$$

where  $\omega_{AG_r} = \omega_\phi$  and  $\dot{\omega}_{AG_r} = [\dot{\omega}_\phi, 0, 0]^T$ . We recall that  $\omega_{OA} = [0, 0, \dot{\psi}]^T$  and  $v_{OA} = [v_x, v_y, 0]^T$ . By the set of equations (2.29), it is straightforward to define the velocity Jacobian matrices for the rear body as:

$$\begin{aligned}
\frac{\partial v_{OG_r}}{\partial \vartheta} &= [j_A \quad k_A \times r_{AG_r} \quad i_A \times r_{AG_r} \quad 0_{3,1}] \\
\frac{\partial \omega_{OG_r}}{\partial \vartheta} &= [0_{3,1} \quad k_A \quad i_A \quad 0_{3,1}]
\end{aligned} \tag{2.30}$$

and the residual acceleration terms:

$$\begin{aligned}
a_{R,G_r} &= \omega_{OA} \times (v_{OG_r} + \dot{r}_{AG_r}) + \omega_\phi \times \dot{r}_{AG_r} \\
\varepsilon_{R,G_r} &= \omega_{OA} \times \omega_\phi
\end{aligned} \tag{2.31}$$

The front body has only 1 DoF relative to the rear body  $G_r$  corresponding to the steering angle  $\delta$ . The position of the CoG of the front body in its local reference frame  $\mathfrak{R}_\delta$  is a constant vector  $r_{BG_f}^\delta = [x_{G_f}, 0, z_{G_f}]^T$ . Also, the position of  $B$  in its local reference frame  $\mathfrak{R}_\epsilon$  is a constant vector  $r_{AB}^\epsilon = [x_B, 0, 0]^T$ . Then, in the vehicle reference frame we have:

$$r_{AG_f} = r_{AB} + r_{BG_f} = R_{\phi,\epsilon} r_{AB}^\epsilon + R_{\phi,\epsilon,\delta} r_{BG_f}^\delta \tag{2.32}$$

By differentiating the equation (2.32), we can express the vector of the relative linear velocities by:

$$\dot{r}_{AG_f} = \dot{r}_{AB} + \dot{r}_{BG_f} = \omega_\phi \times r_{AB} + \omega_{\phi,\delta} r_{BG_f} \tag{2.33}$$

where  $\omega_{\phi,\delta} = \omega_\phi + \omega_\delta$  and  $\omega_\delta = R_{\phi,\epsilon}[0, 0, \dot{\delta}]^T$ . A second differentiation, the vector of the relative linear accelerations is:

$$\ddot{r}_{AG_f} = \dot{\omega}_\phi \times r_{AB} + \omega_\phi \times \dot{r}_{AB} + \dot{\omega}_{\phi,\delta} \times r_{BG_f} + \omega_{\phi,\delta} \times \dot{r}_{BG_f} \tag{2.34}$$

where  $\dot{\omega}_{\phi,\delta} = \dot{\omega}_\phi + \dot{\omega}_\delta$  and  $\dot{\omega}_\delta = R_{\phi,\epsilon}[0, 0, \ddot{\delta}] + \omega_\phi \times \omega_\delta$ .

By using equations (2.16) and (2.17), we can express the front body kinematics in the vehicle reference frame as follows:

$$\begin{aligned}
v_{OG_f} &= v_{OA} + \omega_{OA} \times r_{AG_f} + \dot{r}_{AG_f} \\
\omega_{OG_f} &= \omega_{OA} + \omega_{AG_f} \\
a_{OG_f} &= \dot{v}_{OA} + \varepsilon_{OV} \times r_{AG_f} + \ddot{r}_{AG_f} + \omega_{OA} \times (v_{OG_f} + \dot{r}_{AG_f}) \\
\varepsilon_{OG_f} &= \dot{\omega}_{OA} + \omega_{OA} \times \omega_{AG_f} + \dot{\omega}_{AG_f}
\end{aligned} \tag{2.35}$$

where  $\omega_{AG_f} = \omega_{\phi,\delta}$  and  $\dot{\omega}_{AG_f} = \dot{\omega}_{\phi,\delta}$ . By the set of equations (2.35), it is straightforward to define the velocity Jacobian matrices for the front body as:

$$\begin{aligned}
\frac{\partial v_{OG_f}}{\partial \vartheta} &= [j_A \quad k_A \times r_{AG_f} \quad i_A \times r_{AG_f} \quad k_\delta \times r_{BG_f}] \\
\frac{\partial \omega_{OG_f}}{\partial \vartheta} &= [0_{3,1} \quad k_A \quad i_A \quad k_\delta]
\end{aligned} \tag{2.36}$$

and the residual acceleration terms:

$$\begin{aligned}
a_{R,G_f} &= \omega_{OA} \times (v_{OG_f} + \dot{r}_{AG_f}) + \omega_\phi \times \dot{r}_{AB} + (\omega_\phi \times \omega_\delta) \times r_{BG_f} + \omega_{\phi,\delta} \times \dot{r}_{BG_f} \\
\varepsilon_{R,G_f} &= \omega_{OA} \times \omega_{\phi,\delta} + \omega_\phi \times \omega_\delta
\end{aligned} \tag{2.37}$$

### 2.8.3 Rear and Front Tire-Road Contact Point Kinematics

The position of the rear tire-road contact point  $C_r$  in its local reference  $\mathfrak{R}_\phi$  is a constant vector  $r_{AC_r}^\phi = [x_{R_r}, 0, 0]^T$ . Then, in the vehicle reference frame, we have:

$$r_{AC_r} = R_\phi r_{AC_r}^\phi \tag{2.38}$$

By differentiating the equation (2.38), we can express the vector of the relative linear velocities by:

$$\dot{r}_{AC_r} = \omega_\phi \times r_{AC_r} \tag{2.39}$$

By using equations (2.16) we can express the rear tire-road contact point linear velocity in the vehicle reference frame as follows:

$$v_{OC_r} = v_{OA} + \omega_{OA} \times r_{AC_r} + \dot{r}_{AC_r} \tag{2.40}$$

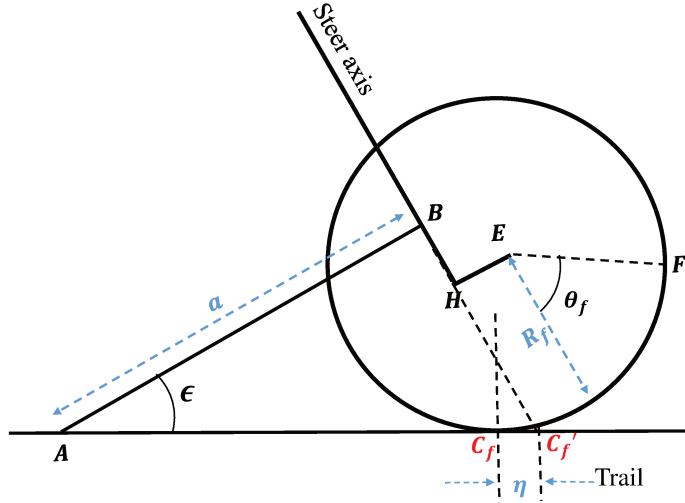


FIGURE 2.14: Front tire contact point.

Nevertheless, the computation of the front tire-road contact point kinematics is quite clever. As presented in figure 2.14, the position of the front tire-road contact point  $C_f$  in the vehicle reference frame is given by:

$$r_{AC_f} = r_{AC'_f} + r_{C'_f C_f} \quad (2.41)$$

where  $C'_f$  is the intersection point of the steering axis with the ground. The position vector  $r_{AC'_f}$  remains constant in the vehicle reference frame since it is not influenced by the steering rotation. Then, from figure 2.14, we can express that position as:

$$r_{AC'_f} = \begin{bmatrix} x_{R_f} + \frac{\eta}{\cos \epsilon} \\ 0 \\ 0 \end{bmatrix} \quad (2.42)$$

where  $\eta$  is the geometric trail. The position of the front contact point  $C_f$  with respect to  $C'_f$  in its local reference  $\mathfrak{R}_\delta$  is a constant vector  $r_{C'_f C_f}^\delta = [-\eta, 0, -\eta \tan \epsilon]^T$ . Then, in the vehicle reference, the position of the front contact point  $C_f$  with respect to  $A$  is :

$$r_{AC_f} = r_{AC'_f} + R_{\phi, \epsilon, \delta} r_{C'_f C_f}^\delta \quad (2.43)$$

By differentiating the equation (2.43), we can express the vector of the relative linear velocities by:

$$\dot{r}_{AC_f} = \omega_{\phi, \delta} \times r_{C'_f C_f} \quad (2.44)$$

By using equation (2.16) we can express the front tire-road contact point linear velocity in the vehicle reference frame as follows:

$$v_{OC_f} = v_{OA} + \omega_{OA} \times r_{AC_f} + \dot{r}_{AC_f} \quad (2.45)$$

From equations (2.40) and (2.45), we can define the sideslip angle  $\alpha$  for both rear and front tire.

Finally, the last issue in this section concerns the gyroscopic effect of both wheels. We assumed that the front and rear wheels are mass-less bodies, hence, their contribution in the mass matrix is null. So, it is useless to compute the linear velocity Jacobian matrices and also the linear residual acceleration. However, each wheel is supposed to rotate about its axis with a given inertia. To count with the gyroscopic effect, we should express the angular velocity Jacobian matrices and the angular residual acceleration.

The rear wheel rotates about  $j_{\theta_r}$  with an angular velocity  $\omega_{\theta_r} = \dot{\theta}_r j_{\theta_r}$ . Then, the angular velocity vector of the rear wheel with respect to the vehicle reference frame is given by:

$$\omega_{AR_r} = \omega_\phi + \omega_{\theta_r} \quad (2.46)$$

where, in the vehicle reference frame  $j_{\theta_r} = R_\phi[0, 1, 0]^T$ . By differentiating the equation (2.46), we get the relative angular acceleration vector:

$$\dot{\omega}_{AR_r} = \dot{\omega}_\phi + \dot{\omega}_{\theta_r} \quad (2.47)$$

where  $\dot{\omega}_{\theta_r} = \ddot{\theta}_r j_{\theta_r} + \omega_\phi \times \omega_{\theta_r}$ .

As for the rear wheel, the front wheel rotates about  $j_{\theta_f}$  with an angular velocity  $\omega_{\theta_f} = \dot{\theta}_f j_{\theta_f}$ . Then, the angular velocity vector with respect to the vehicle reference is given by:

$$\omega_{AR_f} = \omega_\phi + \omega_\delta + \omega_{\theta_f} \quad (2.48)$$

where, in the vehicle reference frame  $j_{\theta_f} = R_{\phi, \epsilon, \delta}[0, 1, 0]^T$ . By differentiating the equation (2.48), we get the relative angular acceleration vector:

$$\dot{\omega}_{AR_f} = \dot{\omega}_\phi + \dot{\omega}_\delta + \dot{\omega}_{\theta_f} \quad (2.49)$$

where  $\dot{\omega}_{\theta_f} = \ddot{\theta}_f j_{\theta_f} + (\omega_\phi + \omega_\delta) \times \omega_{\theta_f}$ .

By using equations (2.16) and (2.17) we can express the angular kinematics of both wheels in the vehicle reference frame as follows:

$$\begin{aligned}
\omega_{OR_r} &= \omega_{OA} + \omega_{AR_r} \\
\omega_{OR_f} &= \omega_{OA} + \omega_{AR_f} \\
\varepsilon_{OR_r} &= \dot{\omega}_{OA} + \omega_{OA} \times \omega_{AR_r} + \dot{\omega}_{AR_r} \\
\varepsilon_{OR_f} &= \dot{\omega}_{OA} + \omega_{OA} \times \omega_{AR_f} + \dot{\omega}_{AR_f}
\end{aligned} \tag{2.50}$$

Finally, we can deduce the residual acceleration terms by:

$$\begin{aligned}
\varepsilon_{R,R_r} &= \omega_{OA} \times (\omega_\phi + \omega_{\theta_r}) + \omega_\phi \times \omega_{\theta_r} \\
\varepsilon_{R,R_f} &= \omega_{OA} \times (\omega_\phi + \omega_\delta + \omega_{\theta_f}) + \omega_\phi \times \omega_\delta + (\omega_\phi + \omega_\delta) \times \omega_{\theta_f}
\end{aligned} \tag{2.51}$$

### 2.8.4 Non-Conservative Generalized Efforts

The PTWV is subject to various force and torque elements. In this section, we account for the gravity force, rider steering torque, steer damper torque and tire lateral force on the front and rear tire contact points.

To express the contribution of gravity force in the generalized effort vector  $Q_a$ , we can make use of equation (2.23):

$$Q_{a,g} = \left\{ m_r \left( \frac{\partial v_{OG_r}}{\partial \vartheta} \right)^T + m_f \left( \frac{\partial v_{OG_f}}{\partial \vartheta} \right)^T \right\} \begin{bmatrix} 0 \\ 0 \\ -g \end{bmatrix} \tag{2.52}$$

In the same way, the contribution of the tire/road contact efforts into the generalized effort vector is given by:

$$Q_{a,T} = \sum_{i=r,f} \left\{ \left( \frac{\partial v_{OR_i}}{\partial \vartheta} \right)^T F_{T_i} + \left( \frac{\partial \omega_{OR_i}}{\partial \vartheta} \right)^T (F_{T_i} \times r_{C_i R_i}) \right\} \tag{2.53}$$

where  $F_{T_i}$  are defined in equation (2.4).

Afterward, to evaluate the contribution of the rider steering torque  $\tau$  and the steer damper torque  $K_\delta \dot{\delta}$  in the generalized effort vector, it may be tedious to use equation (2.23). Therefore, it is most convenient to find the virtual power done by each effort and hence its associated contribution. So, it is more simple to write :

$$Q_{a,h} = \left( \frac{\partial \delta}{\partial \vartheta} \right)^T \begin{bmatrix} 0 \\ 0 \\ \tau - K_\delta \dot{\delta} \end{bmatrix} \tag{2.54}$$

## 2.9 Linearisation and State Space Models

For PTWV dynamics, we distinguish two classes of motions around the equilibrium. The first one is the *in-plane* motion which relates to the longitudinal motion of the vehicle in its plane of symmetry. It is mainly

affected by acceleration, braking, suspension motions and irregularities of the road. The other one is the *out-of-plane* motion which refers to the lateral motion in turns and hence to the roll, the yaw, the steering and the lateral displacement degrees of freedom. Besides these two main classes, other subdivisions can be done by separating braking and acceleration phases from the turning ones (Cossalter et al., 2006b). Actually, in the real world these phases happen together in a coupled way so that the result is that the vehicle turns while it is braking or accelerating. Also, *neutral* phase occurs when the vehicle is going on a coast down condition. Usually neutral phase is not developed in mathematical models.

The objective of this section is to set up PTWV dynamic models taking into account the triplet motorcycle-rider-environment. Motorcycle models can be accomplished in several ways depending on the use that will be made and the desired precision. These models should represent all dynamics of interest as simply as possible.

- The out-of-plane model: incorporates the most important parameters and dynamic states of the motorcycle. It is used to understand the lateral motion and estimate the included variables, which is the topic of interest for this work.
- The one-body lateral model: is studied in a motorcycle-fixed reference frame with the origin located at the Centre of Gravity (CoG). It is used in the sake of identifying the CoG and the total mass of the motorcycle/rider. It allowed also to design a steady-state risk function to detect the abnormal steering behavior.
- The in-plane model: describes the braking and acceleration dynamics. It is used in estimating the complete dynamic and the coupling between the longitudinal and lateral motions.

The differences between these models are the number of bodies, flexibility and degrees of freedom. These requirements are imposed by the application. In this context, selecting a suitable model structure is prerequisite before its estimation and identification. This selection is also constrained by the availability of the motorcycle measurements. Based on what is developed in section 2.8, these dynamics models are given in the following sections.

### 2.9.1 Out-of-Plane Motion

The large number of accidents on the bend motivates the fact that many of our works deal with lateral dynamic model. This model is widely used for the development of estimation and control algorithms of the PTWV dynamics. Therewith, a linearized version of the lateral dynamics model representing small motions in the neighborhood of the straight motion is derived which leads to a four degree-of-freedom (4 Dof) model. This representation considers that the main frame is subject to lateral motion, roll motion about the  $x$  - *axis*, yaw motion about the  $z$  - *axis* and the front frame is subject to steering motion, due essentially to the effect of pneumatic forces acting on the front and rear wheels ( $F_{yf}$  and  $F_{yr}$ ) with tire relaxation.

By neglecting the nonlinearities associated with the products between dynamic variables, the motions are expressed by the following dynamic equations:

$$\left\{ \begin{array}{l} \text{Lateral motion} \quad e_{33}\dot{v}_y + e_{34}\ddot{\psi} + e_{35}\ddot{\phi} + e_{36}\ddot{\delta} = a_{34}\dot{\psi} + \sum F_y \\ \text{Yaw motion} \quad e_{34}\dot{v}_y + e_{44}\ddot{\psi} + e_{45}\ddot{\phi} + e_{46}\ddot{\delta} = a_{44}\dot{\psi} + a_{45}\dot{\phi} + a_{46}\dot{\delta} + \sum M_z \\ \text{Roll motion} \quad e_{35}\dot{v}_y + e_{45}\ddot{\psi} + e_{55}\ddot{\phi} + e_{56}\ddot{\delta} = a_{54}\dot{\psi} + a_{56}\dot{\delta} + \sum M_x \\ \text{Steering motion} \quad e_{36}\dot{v}_y + e_{46}\ddot{\psi} + e_{56}\ddot{\phi} + e_{66}\ddot{\delta} = a_{64}\dot{\psi} + a_{65}\dot{\phi} + a_{66}\dot{\delta} + \sum M_s \\ \text{Front lateral force motion} \quad \dot{F}_{yf} = a_{71}\dot{\phi} + a_{72}\dot{\delta} + a_{73}v_y + a_{74}\dot{\psi} + a_{76}\dot{\delta} + a_{77}F_{yf} \\ \text{Rear lateral force motion} \quad \dot{F}_{yr} = a_{81}\dot{\phi} + a_{83}v_y + a_{84}\dot{\psi} + a_{88}F_{yr} \end{array} \right. \quad (2.55)$$

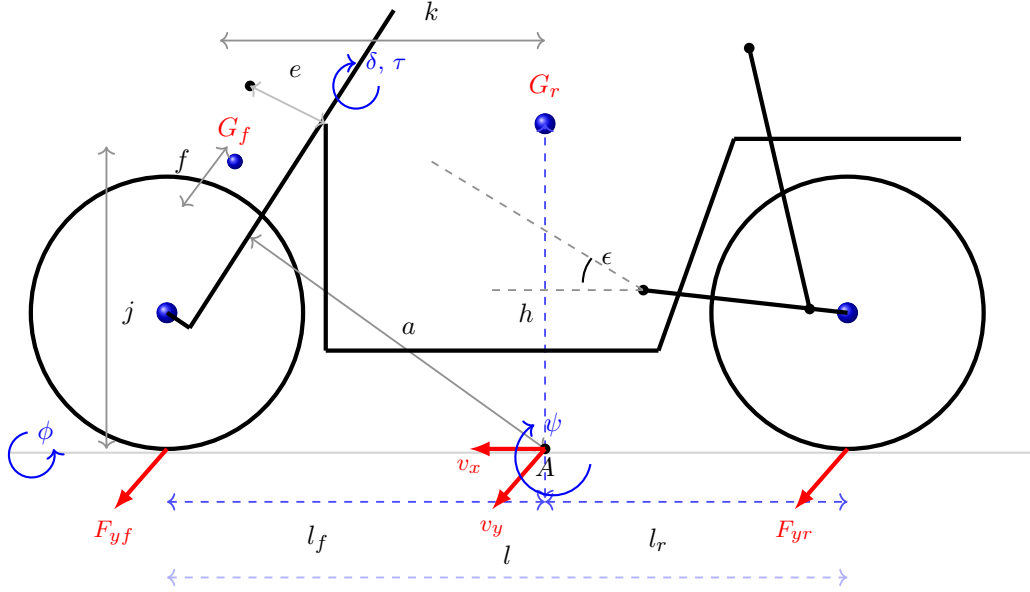


FIGURE 2.15: Schematic side view of the PTWV two-body model with notation, Sharp equivalent model.

where:

$$\begin{cases} \sum F_y = F_{yf} + F_{yr} \\ \sum M_z = a_{47}F_{yf} + a_{48}F_{yr} \\ \sum M_x = a_{51}\phi + a_{52}\delta \\ \sum M_s = a_{61}\phi + a_{62}\delta + a_{67}F_{yf} + \tau \end{cases}$$

Nevertheless, there is an interesting alternative to consider the nonlinearities of the roll and the steering angle due to the potential energy. The expression (2.56) becomes:

$$\begin{cases} \sum F_y = F_{yf} + F_{yr} \\ \sum M_z = a_{47}F_{yf} + a_{48}F_{yr} \\ \sum M_x = a_{51}\sin(\phi) + a_{52}\sin(\delta) \\ \sum M_s = a_{61}\sin(\phi) + a_{62}\sin(\delta) + a_{67}F_{yf} + \tau \end{cases}$$

For further details on the motorcycle parameters ( $e_{ij} - a_{ij}$ ) and expressions refer to the appendix C .

The motorcycle dynamic model given by equation (2.55-2.56) can be expressed by the following descriptor model:

$$\begin{cases} E\dot{x} = M(v_x)x + R\tau \\ y = Cx \end{cases} \quad (2.56)$$

whereas  $x = [\phi, \delta, v_y, \psi, \dot{\phi}, \dot{\delta}, F_{yf}, F_{yr}]^T$  denotes the state vector, the matrix  $M(v_x)=[a_{ij}]_{8 \times 8}$  is parameter varying,  $R$  is a constant matrix,  $y$  is the vector of measures and  $C$  is the observation matrix  $E=[e_{ij}]$  is a constant nonsingular matrix, its inverse  $E^{-1}$  exists. Let us consider  $\zeta(t) = v_x(t)$ . The Linear Parameter Varying (LPV) structure is expressed by:

$$\begin{cases} \dot{x}(t) = A(\zeta)x(t) + Bu(t) \\ y = Cx(t) \end{cases} \quad (2.57)$$

where  $x(t) \in \mathbb{R}^n$ ,  $u(t) = \tau(t) \in \mathbb{R}^m$ , and  $y(t) \in \mathbb{R}^{n_y}$ . The matrix  $A(\zeta) = E^{-1}M(\zeta) \in \mathbb{R}^{n \times n}$ , the matrices  $C \in \mathbb{R}^{n_y \times n}$ ,  $B = E^{-1}R \in \mathbb{R}^{n \times m}$ . Whereas,  $n = 8$ ,  $m = 1$ ,  $p = 6$ ,  $n_y = 5$ .

## 2.9.2 Road Consideration

This section extends the model in section 2.9.1, taking into account the road bank angle, denoted  $\phi_r$  at which the road is inclined about its longitudinal axis with respect to the horizontal one. It has the effect of transferring a portion of the gravity force to lateral tire forces keeping the motorcycle in its path. Also, it

tilts the motorcycle in the direction of the curve to take a safer turn, to avoid skidding and overturning of motorcycle, this force is noted  $F_{\phi_r} = mg \sin(\phi_r)$ .

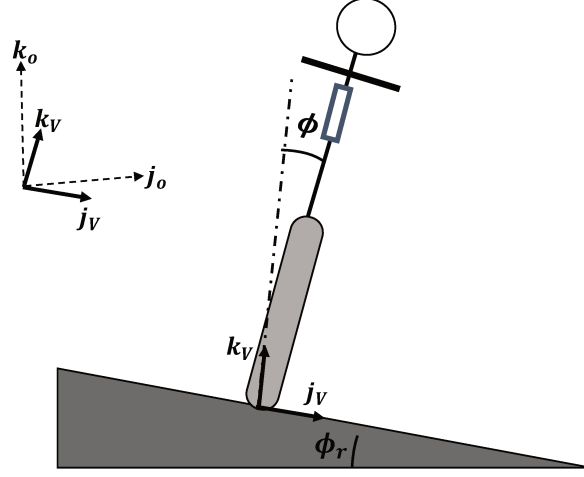


FIGURE 2.16: Motorcycle geometry with road banking angle.

**Assumption 2.1.** *The road bank angle is constant piecewise or varies slowly.*

Under this assumption, the motions of the motorcycle can be described by the following equations

$$\left\{ \begin{array}{l} e_{33}\dot{v}_y + e_{34}\ddot{\psi} + e_{35}\ddot{\phi} + e_{36}\ddot{\delta} = a_{34}\dot{\psi} + F_{yf} + F_{yr} - mg \sin(\phi_r) \\ e_{34}\dot{v}_y + e_{44}\ddot{\psi} + e_{45}\ddot{\phi} + e_{46}\ddot{\delta} = a_{44}\dot{\psi} + a_{45}\dot{\phi} + a_{46}\dot{\delta} + a_{47}F_{yf} + a_{48}F_{yr} \\ e_{35}\dot{v}_y + e_{45}\ddot{\psi} + e_{55}\ddot{\phi} + e_{56}\ddot{\delta} = a_{51} \sin(\phi + \phi_r) + a_{52} \sin(\delta) + a_{54}\dot{\psi} + a_{56}\dot{\delta} \\ e_{36}\dot{v}_y + e_{46}\ddot{\psi} + e_{56}\ddot{\phi} + e_{66}\ddot{\delta} = a_{61} \sin(\phi + \phi_r) + a_{62} \sin(\delta) + a_{64}\dot{\psi} + a_{65}\dot{\phi} + a_{66}\dot{\delta} + a_{67}F_{yf} + \tau \\ \dot{F}_{yf} = a_{71}(\phi + \phi_r) + a_{72}\delta + a_{73}v_y + a_{74}\dot{\psi} + a_{76}\dot{\delta} + a_{77}F_{yf} \\ \dot{F}_{yr} = a_{81}(\phi + \phi_r) + a_{83}v_y + a_{84}\dot{\psi} + a_{88}F_{yr} \end{array} \right. \quad (2.58)$$

The mathematical formulas of lateral front and rear forces  $F_{yf}$  and  $F_{yr}$ , expressed in the motorcycle-related reference frame, are given by :

$$\left\{ \begin{array}{l} \frac{\sigma_f}{v_x} \dot{F}_{yf} = -F_{yf} - C_{f1}\alpha_f + C_{f2}(\phi + \phi_r + \delta \sin(\epsilon)) \\ \frac{\sigma_r}{v_x} \dot{F}_{yr} = -F_{yr} - C_{r1}\alpha_r + C_{r2}(\phi + \phi_r) \end{array} \right. \quad (2.59)$$

with

$$\alpha_f = \left( \frac{v_y + l_f \dot{\psi} - \eta \dot{\delta}}{v_x} \right) - \delta \cos(\epsilon), \quad \alpha_r = \left( \frac{v_y - l_r \dot{\psi}}{v_x} \right) \quad (2.60)$$

$C_{fi}$  and  $C_{ri}$  refer to the tire forces coefficients (stiffness and camber coefficients  $i = (1, 2)$ ),  $\epsilon$  refers to the caster angle,  $\eta$  is the mechanical trail,  $l_f$  (resp.  $l_r$ ) represents the distance between the center of mass and the front and rear axis. Considering the lateral forces in their linear form is not restrictive because we are targeting urban scenarios where the camber and slip angles remain in the linear domain of the lateral forces.

### 2.9.3 One-Body Model of Lateral Dynamic

In this part, the lateral dynamics of the PTWV is reconsidered by simplifying the two-body model, leading to a rigid one-body model. The inertial parameters of the motorcycle are generally represented by: its mass  $m$ , the moments of inertia  $I_x, I_y, I_z$  and the position of its center of gravity  $CoG$ . Let us consider the following one body motorcycle model with 3 DoF giving the lateral, the yaw and the roll motion dynamics:

$$\begin{cases} m(v_y + \dot{\psi}v_x) = F_{yf} + F_{yr} \\ I_z\dot{\psi} = aF_{yf} - bF_{yr} \\ I_x\ddot{\phi} + mh(v_y + \dot{\psi}v_x) = mgh\phi \end{cases} \quad (2.61)$$

and the tire relaxation dynamics

$$\begin{cases} \dot{F}_{yf} = -\frac{v_x}{\sigma}F_{yf} + C_{f1}(\delta - \frac{v_y - \alpha\dot{\psi}}{v_x}) + C_{f2}\gamma \\ \dot{F}_{yr} = -\frac{v_x}{\sigma}F_{yr} - C_{r1}(\frac{v_y - b\dot{\psi}}{v_x}) + C_{r2}\gamma \end{cases} \quad (2.62)$$

Let  $x = [v_y, \psi, \phi, \dot{\phi}, F_{yf}, F_{yr}]^T$ . We conclude the following Linear Parameter Varying (LPV) system :

$$\begin{cases} \dot{x} = A(\zeta)x + Bu + Q(\zeta)d \\ y = Cx \end{cases} \quad (2.63)$$

where the input  $u(t)$  is the steering angle  $\delta$  and  $d(t)$  is the nonlinear part of the lateral forces, with  $\zeta = v_x$ ,  $A(\zeta) = E^{-1}M(\zeta)$ ,  $B = E^{-1}N$  and  $Q(\zeta) = E^{-1}F(v_x)$ .

### 2.9.4 In-Plane Motion

The *in-plane* motion is related to the longitudinal dynamic of the vehicle in its plane of symmetry. It refers to the vehicle's ability to accelerate and brake. Hence, the behavior of the motorcycle during straight-line movements depends on longitudinal pneumatic and aerodynamic forces. It is mainly affected by acceleration, braking, suspension motions and irregularities of the road. The in-plane model is given by the following equations:

$$\begin{cases} m(v_x - v_y\dot{\psi}) = F_{xf} + F_{xr} - F_a - F_{rr} \\ i_{fy}\dot{\omega}_f = -R_f F_{xf} + B_f \\ i_{ry}\dot{\omega}_r = -R_r F_{xr} + T + B_r \end{cases} \quad (2.64)$$

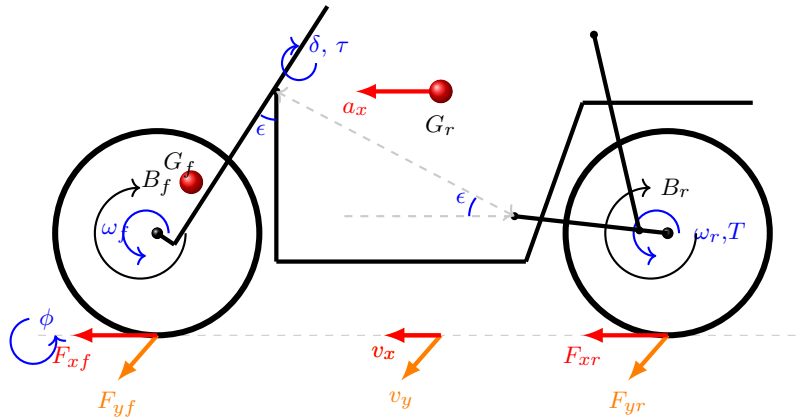


FIGURE 2.17: Kinematic representation of PTWV.

- $F_a = C_d v_x^2$  is the aerodynamic force with  $C_d$  is the drag coefficient.

- $F_{rr} = f_w F_z$  is the rolling resistance force with  $f_w$  is the rolling resistance coefficient (Cossalter et al., 2006b).
- $B_f$  and  $B_r$  are the braking torques applied to the front and rear wheels,  $T$  is the total engine torque applied only to rear wheel.
- $\omega_{f,r}$  is the wheel rotational speed,  $i_{(f,r)y}$  the moment of inertia of the wheels,  $R_{f,r}$  are the wheel radius.

## 2.10 Stability and Handling

The role of the gyroscopic effect in bike designs is to help steer the front wheel. This phenomenon is called precession. The rate at which an object precesses is inversely proportional to its rate of spin. At low speeds, the precession of the front wheel is quick, causing an uncontrolled bike's tendency to oversteer. At high speeds, the precession is usually too slow, contributing to an uncontrolled bike's tendency to. This tendency is very easy for riders to counteract. Another reason of gyroscopic effects is a roll moment generated by the front wheel during countersteering. This effect is presented in Figure 4. The moment is smaller than the moment generated by the out-tracking front wheel, but begins as soon as the rider applies torque to the handlebars and so can be used even when the front tire does not have contact with a ground. The magnitude of this moment is proportional to the moment of inertia of the front wheel, its spin rate, the rate of torque that the rider applies to the handlebars, the cosine of the angle between the steering axis and the vertical.

### 2.10.1 Gyroscopic effect

Any object rotating about a spin axis is subject to the gyroscopic effect which refers to the ability of this object to keep in balance its rotation axis. Henceforth, the PTWV gyroscopic effect arises from the front wheel speed. This physical effect is prominent to ensure the motorcycle balance in straight line and when steering (Cossalter et al., 2010; Grzegożek and Weigel-Milleret, 2015). It is worth noting that its amplitude is relatively small compared to other moments, but its transitory character is crucial in cornering. Once the wheel is in rotation with a given angular speed, the gyroscopic effect can be generated by one or by the combination of three motion: steer, roll and yaw. First, the gyroscopic steer-lean effect is created by a steering maneuver. For example, to initiate a left turn, the motorcycle's handlebar is turned in the counter sense allowing the vehicle to lean in the turn direction. When the desired angle of the lean is reached, the handlebar is brought back to its neutral position to get a balance trajectory within turn. Second, the gyroscopic roll-steer effect is generated by the motorcycle roll independently of any handlebar motion. Then, the gyroscopic yaw-righting effect arises from the circular motion of the vehicle as those generated by rotation of the wheels in a constant turn. This is the only gyroscopic effect that tends to destabilize the vehicle.

### 2.10.2 Vibration Modes

While in motion, single track vehicle and its rider remain in an unstable equilibrium like an inverted pendulum (Cossalter et al., 2006a). The term *stable* means that the vehicle remains at its steady equilibrium at constant speed without falling. Therewith, the safe ranges of stability are determined by the vehicle characteristic, the forward speed and the rider actions.

A PTWV maintains a state of equilibrium as long as the applied external efforts are balanced with the generated tire/road efforts. In a straight line, this stability is provided when the rider is controlling the forward speed and applying a suitable handlebar torque to reject perturbations or to control the roll angle of the PTWV. On the other hand, this also can be done by a lateral displacement of the rider body with respect to the vehicle's main body. However, for an uncontrolled motorcycle, three main modes of instability arises with respect to the vehicle forward speed (Sharp, 1971).

From Figure 2.18, the first non-oscillating vibration mode called capsizes, is a well damped mode that appears at low speed. In this mode, the front wheel is steered toward the direction of the roll but not enough to avoid a fall. Next, a second mode named weave appears as a slow oscillatory mode between the rear wheel and the front steering wheel. This mode has a frequency ranging from  $0.2Hz$  at low speed and up to  $4Hz$  at high speed. It is unstable at low speeds less than  $5m/s$ , well damped at medium speed and moderately damped in high-speed and stable beyond  $30m/s$ . It affects the whole vehicle whose trajectory undulates,

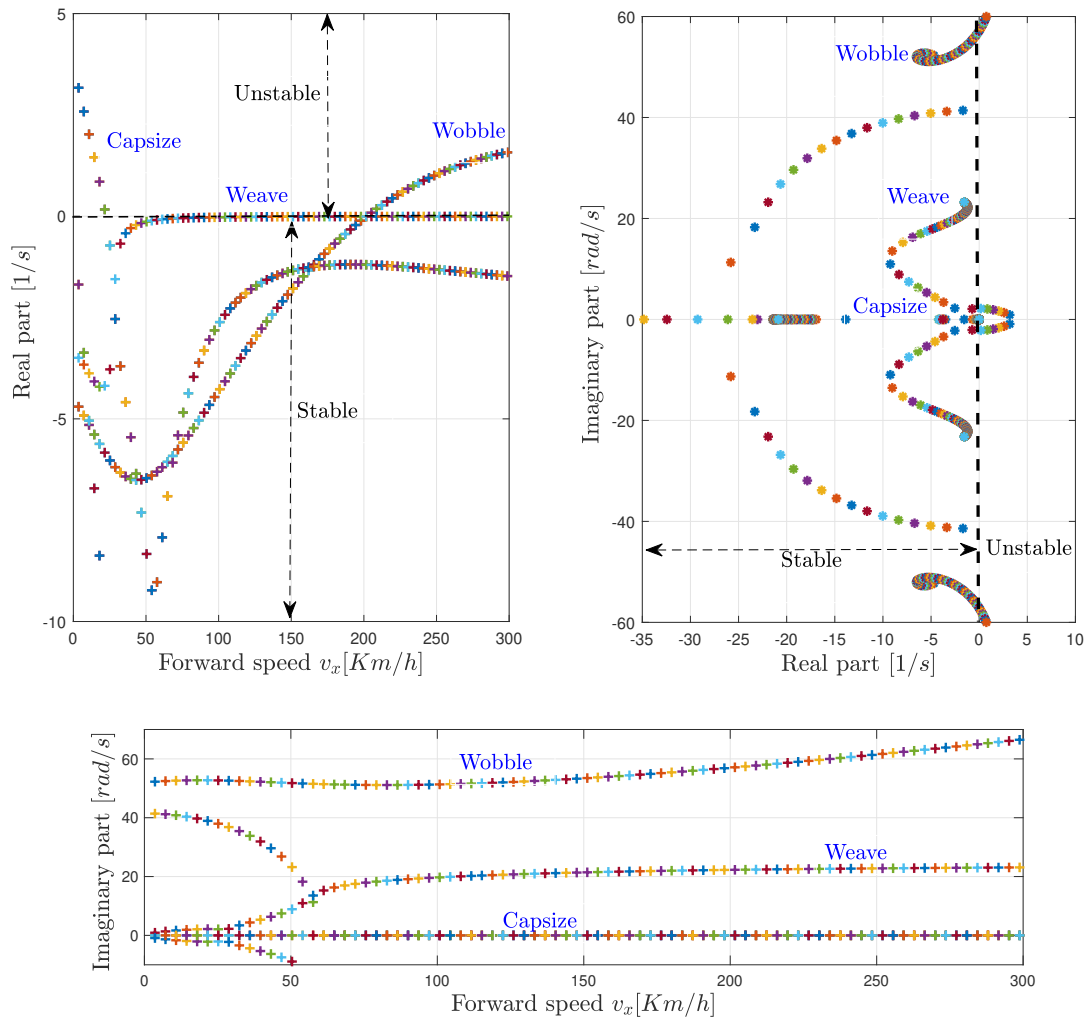


FIGURE 2.18: Lateral stability curve of PTWV.

the steering is 180 deg out of phase with the yaw and it is 90 deg out of phase with the roll. Last, wobble mode describes a fast vibration oscillation of the steering body with a frequency of  $8Hz$  to  $10Hz$  which is independent of the vehicle speed. In this mode, the vehicle's handlebar starts to swing from one side to the other until fall. This unstable mode is naturally present on the PTWV mainly at high speed and it can be damped by adding a suitable steering damper.

Figure 2.18 shows also the concept of the critical speed, under which the vehicle self-stabilization is not possible. Also, unstable modes are well differentiated and separated over the all speed range. In (Limebeer, Sharp, and Evangelou, 2001), the authors studied the influence of other parameters on the out-of-plane stability of PTWV in particular the effect of the front and rear suspensions.

### 2.10.3 PTWV Control

Riding a PTWV is not as simple and intuitive as driving a car vehicle. In normal riding conditions, the PTWV is an unstable system which requires the presence of the rider to stabilize his motorcycle and correct its trajectory. Also, with a comparable dynamics, the vehicle power to the rider mass ratio is very important and hence, each riding style gives rise to a specific control strategy which changes from one to another rider depending on his sensation and his perception of the external driving environment. So, reproducing the rider control behavior with a mathematical model is difficult and it is still the subject of several research works.

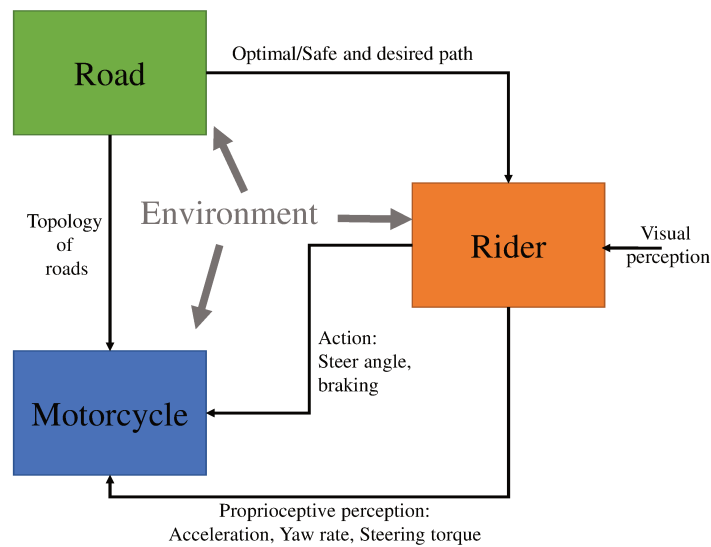


FIGURE 2.19: Motorcycle-Road-Environment.

Therefore, the PTWV, the rider and the driving environment constitute a complex system operating in a closed loop. The rider receives information from the environment on one hand and the motorcycle states on the other hand, after, the rider decides the control actions to be applied to its vehicle (Lauffenburger, 2002). Also, many other factors have a significant impact on the riding behavior, which are difficult to quantify and to model as mathematical equations. These factors are generally related to the rider's state evaluation, its experience and riding skills. The mis-evaluation of a correct environment perception and self riding skills can lead the motorcycle to ride beyond the limits that result in hazardous riding situations.

Now, after setting up PTWV dynamic models, the main focus will be to validate these models with the real riding behavior and to design estimation concepts for the unknown variables of these models. For the sake of validation, we require realistic instrumentation with sensors or high-end simulator. Usually, sensors are assumed to be placed near the Gravity Center (CoG) of the motorcycle and the data measurements are directly available in the reference frame used for the dynamic modeling of the PTWV. Nonetheless, sensors provide the measurements in the sensor reference frame attached to the vehicle that is mostly different from the body reference frame. Henceforth, these sensors are strongly affected by mounting angles, and the correct rotation to be applied in order to recover an alignment to the PTWV motion. In this context, section 2.11 proposes a practical procedure to align the measurement data.

## 2.11 Motorcycle Instrumentation and Data Calibration

In this section, we will first present the motorcycle (Scooter lab's), the different sensors and their characteristics as well as the instrumentation procedure in section 2.12. These sensors are used either to measure the physical quantities of the dynamics behavior in order to validate the mathematical model, or for the identification of the statico-dynamic parameters and for the states estimation of the motorcycle.

The second part proposes a self calibration algorithm described in section 2.13 for the estimation of the three mounting angles roll, pitch, and yaw of accelerometers and gyroscopes within Inertial Measurement Units (IMUs), whose IMUs' axes often are not aligned with the vehicle reference system.

### 2.12 Instrumented Lab's Motorcycle

For experimentation, a fully electric propulsion scooter is instrumented with various sensors as in figure 2.20. It is equipped with a DC motor, powered by three battery packs, for a total weight of about 115 kg and allowing a maximum speed of 45 km/h. The rear suitcase encloses an Intel Core i7-3610QM embedded computer manufactured by Neosys Technology dedicated to embedded applications, which also integrates a GPS receiver to measure the speed and position of the PTWV. A digital-analogue input-output card from

National Instrument (PCIe-6353) is plugged to interface the various sensors and actuators. On the other hand, a high-end Inertial Measurement Unit, SBG IG-500A is installed near the rear body center of mass. It incorporates an accelerometer, a gyroscope and a magnetometer providing accurate measurements of the three Euler angles and their associated rates and the three axes acceleration. Also, the steering system is equipped with an IOV GA210 absolute encoder directly installed on the steering column without reduction stage, and offering a 10-bit resolution for 1024 steps per revolution. This sensor measures the handlebar position seen by the actuator axle. For wheel rotational speed, optical encoder has been selected. Data acquisition is performed at 100 Hz except for the computer-integrated GPS which is slower with a maximum frequency of 10 Hz (Damon et al., 2017).



FIGURE 2.20: Instrumented Scooter at the IBISC Lab, university of Evry.

## 2.13 Inertial Sensor Calibration

The results of this section were obtained during an internship at PoliMi laboratory (Politecnico di Milano, Italy), lasted two months (April-May 2018). The work was published in (Fouka et al., 2018d).

### 2.13.1 Overview of Calibration

IMU axes calibration is an important step when installing on a vehicle to get accurate and significant measurements of the different degrees of freedom of interest (Maeder and Morari, 2011; Syed et al., 2008; Boniolo, Savaresi, and Tanelli, 2009b; Syed et al., 2007). In fact, IMU are strongly affected by mounting angles with respect to the vehicle reference frame and this relative positioning should be recovered by an alignment method (Syed et al., 2008; Groves, 2015; Vinande, Axelrad, and Akos, 2010). IMU calibration is even more essential for PTWV than cars vehicle since the roll angle can reach  $50^\circ$ . Also, the narrow space occupied largely by the vehicle's engine does not simplify the installation of the IMU closer to the center of mass of the vehicle. So, natural alignment with the vehicle's direction of motion may be impossible and significant differences can be observed between measured variables and the real ones.

To perform such a calibration, some of the existing methods use the Global Navigation Satellite System (GNSS) to compare positioning data with the IMU outputs (De Tommasi, 2014). However, these methods imply that the GNSS must be always active and running at its highest possible frequency to cover all possible measured signals bandwidth. This results have a significant increase in energy consumption, as an accelerometer/gyroscope pair requires approximately 1 mA at 3 V, thus an energy of 3 mW, while GNSS consumes 10 – 20 mA at 3 V, thus 30 – 60 mW. In applications where energy consumption is critical, as it is in two-wheeled vehicles, and in general in electric vehicles, algorithms that make sporadic use of the GNSS or even avoid the GNSS are to be preferred. Furthermore, GNSS data are subject to errors which affect the measurement precision (Groves, 2013).

In the present work, a self-calibration, energy-efficient, algorithm for triaxial IMU installed on motorcycles is proposed. Also, this looks for limiting the use of geo-localization data. The objective is to estimate the

mounting angles defined as the angles between the IMU and the vehicle reference system, assumed constant over time. Next, the estimated angles serve to virtually recalibrate the measured accelerations and angular velocities according to the conventional vehicle longitudinal, lateral and vertical axes, denoted respectively as  $x_v$ ,  $y_v$ ,  $z_v$ . The proposed approach is inspired from (Vinande, Axelrad, and Akos, 2010) which is extended to provide practical conditions for data selection and methods for an online implementation.

An experimental setup, under mixed traffic conditions, on a *Piaggio* MP3 scooter has been carried-out to prove the effectiveness of the proposed approach. This setup makes use of telemetry e-Boxes, equipped with an IMU with a sampling frequency of 400 Hz, and a GNSS unit with a sampling frequency of 10 Hz. As shown in figure 2.21, three e-Boxes are installed on the vehicle, two of them named *e-Box 1* and *e-Box 3* are mounted according to the vehicle's reference system, while the last one *e-Box 2* is mounted under-seat on a flat surface and slightly misaligned with respect to the vehicle's  $x - y$  axis.

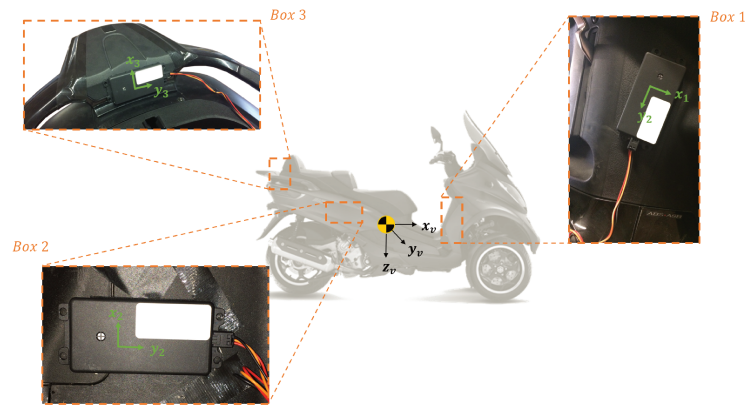


FIGURE 2.21: An overview of the experimental setup used to validate the algorithm.

### 2.13.2 Self-Calibration Algorithm

Given a rotation matrix  $R \in \mathbb{R}^{3 \times 3}$ , where  $R^T R = I$ , a vector  $\mathbf{v}$  expressed in a reference frame  $R_1(X_1, Y_1, Z_1)$  can be projected to another reference frame  $R_2(X_2, Y_2, Z_2)$  by using the following equation (Shabana, 2013):

$$\mathbf{v}_1^2 = R \cdot \mathbf{v}_1^1 \quad (2.65)$$

Otherwise, Euler theorem states that a general rotation of a rigid body about a fixed axis is equivalent to a successive three elementary rotations  $(\varphi, \vartheta, \psi)$  expressed by three direction cosine matrices (DCM):

$$DCM_\varphi = \begin{bmatrix} 1 & 0 & 0 \\ 0 & \cos(\varphi) & \sin(\varphi) \\ 0 & -\sin(\varphi) & \cos(\varphi) \end{bmatrix}, \quad DCM_\vartheta = \begin{bmatrix} \cos(\vartheta) & 0 & -\sin(\vartheta) \\ 0 & 1 & 0 \\ \sin(\vartheta) & 0 & \cos(\vartheta) \end{bmatrix}, \quad DCM_\psi = \begin{bmatrix} \cos(\psi) & \sin(\psi) & 0 \\ -\sin(\psi) & \cos(\psi) & 0 \\ 0 & 0 & 1 \end{bmatrix}$$

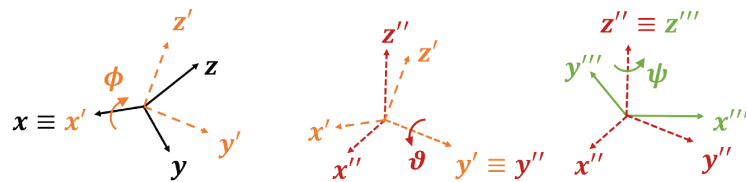


FIGURE 2.22: The alignment of the axes  $x$ ,  $y$ ,  $z$  to the tern  $x''$ ,  $y''$ ,  $z''$ .

The problem of aligning the measurement axis with respect to the vehicle reference frame axis is formulated as the problem of estimating the angles  $(\varphi, \vartheta, \psi)$ . We adopt the  $(\mathbf{X} - \mathbf{Y} - \mathbf{Z})$  convention, as illustrated in

figure 2.22, so the rotation matrix  $R$  becomes:

$$R = \begin{bmatrix} c_\psi c_\vartheta & c_\vartheta s_\psi & -s_\vartheta \\ c_\psi s_\varphi s_\vartheta - c_\varphi s_\psi & c_\varphi c_\psi + s_\varphi s_\psi s_\vartheta & c_\vartheta s_\varphi \\ s_\psi s_\varphi + c_\varphi c_\psi s_\vartheta & c_\varphi s_\psi s_\vartheta - c_\psi s_\varphi & c_\varphi c_\vartheta \end{bmatrix}. \quad (2.66)$$

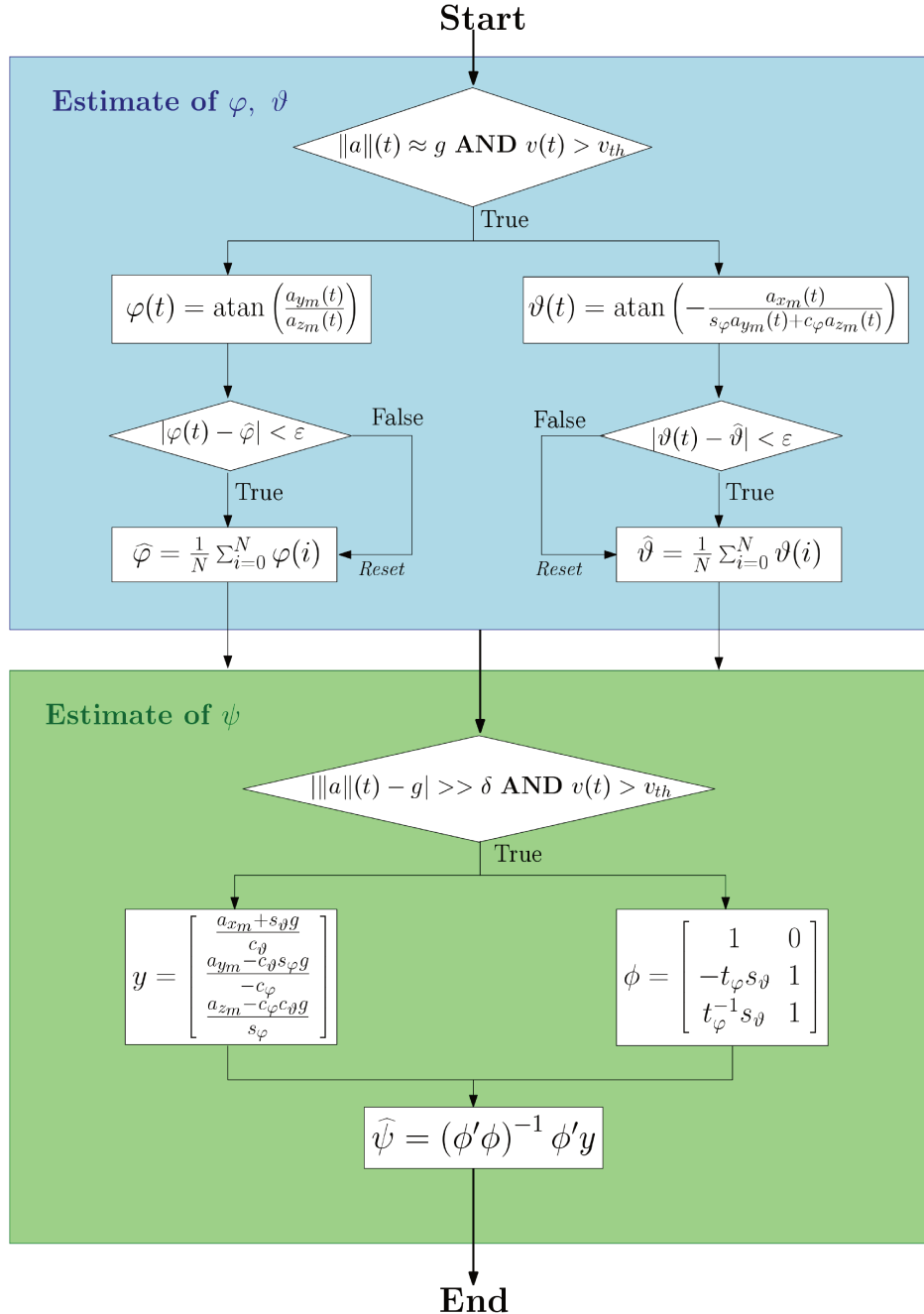


FIGURE 2.23: The flowchart of the self-calibration algorithm.

As illustrated in figure 2.23, the estimation of the mounting angles is achieved in two steps. First, the roll  $\varphi$  and the pitch  $\vartheta$  angles are estimated by aligning the vertical axis with respect to gravity vector. Then, axes  $X$  and  $Y$  are aligned by estimating  $\psi$  angle which is achieved by exploiting a prior knowledge about the vehicle longitudinal dynamics.

To estimate  $\varphi$  and  $\vartheta$ , we assume that the vehicle is moving at a constant speed on a flat surface. Also, the

case of standing still is not taken into account to avoid an extra rotation due to the PTWV kickstand, not present in car vehicles.

Under these assumptions, the acceleration in the vehicle reference system can be expressed as

$$a_v = \begin{bmatrix} 0 \\ 0 \\ g \end{bmatrix}, \quad (2.67)$$

where  $g$  is gravity. However, since the telematic box is not aligned with the vehicle's frame, the IMU's acceleration vector  $a_m$  is rotated by  $R$ . Defining  $a_{x_m}$ ,  $a_{y_m}$ , and  $a_{z_m}$  as the accelerations measured by the IMU,  $a_m$  can be expressed in the vehicle reference frame by:

$$a_m = R \cdot \hat{a}_v = \begin{bmatrix} -s_\vartheta g \\ c_\vartheta s_\varphi g \\ c_\varphi c_\vartheta g \end{bmatrix} = \begin{bmatrix} a_{x_m} \\ a_{y_m} \\ a_{z_m} \end{bmatrix} \quad (2.68)$$

It is clear that the gravity vector and the mounting angles ( $\varphi$ ,  $\vartheta$ ) influence the measured acceleration along the three axes. To estimate these two angles, a quadratic cost function  $J_g$  is defined as the sum of the squared error between  $a_v$  and  $a_m$  as:

$$J_g(\varphi, \vartheta) = (a_{x_m} + s_\vartheta g)^2 + (a_{y_m} - c_\vartheta s_\varphi g)^2 + (a_{z_m} - c_\varphi c_\vartheta g)^2. \quad (2.69)$$

The estimation of the pitch  $\hat{\vartheta}$  and the roll  $\hat{\varphi}$  angles is obtained by minimizing the following cost function:

$$\begin{bmatrix} \hat{\varphi} \\ \hat{\vartheta} \end{bmatrix} = \arg \min_{\varphi, \vartheta} J_g(\varphi, \vartheta) \quad (2.70)$$

The optimization problem can be solved making  $\frac{\partial J_g(\varphi, \vartheta)}{\partial \vartheta} = 0$  and  $\frac{\partial J_g(\varphi, \vartheta)}{\partial \varphi} = 0$  which gives the following closed form expression:

$$\begin{cases} \varphi = \arctan\left(\frac{a_{y_m}}{a_{z_m}}\right) \\ \vartheta = \arctan\left(\frac{-a_{x_m}}{s_\varphi a_{y_m} + c_\varphi a_{z_m}}\right) \end{cases} \quad (2.71)$$

Before moving to the second part of the algorithm, few considerations need to be addressed:

- thanks to the result obtained in (2.71), at each new sample we obtain the value of the two angles which minimize the mismatch, according to the assumptions made (numerically defined in (2.67)). Because of sensor's noise and drifts, the estimate is never constant. To remove these undesired effects, since the mounting angles are assumed not changing over time, the estimated values are averaged;
- estimations of  $\varphi$  and  $\vartheta$  strongly depend on the assumption made. This means that, a data selection is needed in order to limit the estimate to only the samples which satisfy the assumptions. This is done checking that the acceleration norm (i.e.,  $\|a\| = \sqrt{a_{x_m}^2 + a_{y_m}^2 + a_{z_m}^2}$ ) is approximately equal to gravity (i.e.,  $|a| \approx g$ );
- during the averaging process, significant variations of the two angles may correspond to variations of road slope, banking or any tilting action performed by the driver. To avoid the estimate to be biased, any detected outlier is removed by resetting the average process.

To estimate the yaw, the vehicle longitudinal dynamics is used, then in the vehicle reference frame the vehicle acceleration vector is  $a_v = [a_{x_v}, 0, g]$ . the IMU's acceleration vector  $a_m$  can be expressed in the vehicle reference frame by:

$$a_m = R \cdot a_v = \begin{bmatrix} c_\psi c_\vartheta a_{x_v} - s_\vartheta g \\ (c_\psi s_\varphi s_\vartheta - c_\varphi s_\psi) a_{x_v} + c_\vartheta s_\varphi g \\ (s_\varphi s_\psi + c_\varphi c_\psi s_\vartheta) a_{x_v} + c_\varphi c_\vartheta g \end{bmatrix} \quad (2.72)$$

in which  $\varphi$  and  $\vartheta$  can be substituted with their estimates. The previous equation can be rearranged in the following form:

$$\begin{bmatrix} a_{x_m} \\ a_{y_m} \\ a_{z_m} \end{bmatrix} = \begin{bmatrix} c_\psi c_\vartheta & -s_\vartheta \\ (c_\psi s_\varphi s_\vartheta - c_\varphi s_\psi) & c_\vartheta s_\varphi \\ (s_\varphi s_\psi + c_\varphi c_\psi s_\vartheta) & c_\varphi c_\vartheta \end{bmatrix} \begin{bmatrix} a_{x_v} \\ g \end{bmatrix}. \quad (2.73)$$

Thanks to the estimated pitch and roll angles, gravity can be compensated on the measured angles, as

$$\begin{bmatrix} a_{x_m} + s_\vartheta g \\ a_{y_m} - c_\vartheta s_\varphi g \\ a_{z_m} - c_\varphi c_\vartheta g \end{bmatrix} = \begin{bmatrix} c_\psi c_\vartheta \\ (c_\psi s_\varphi s_\vartheta - c_\varphi s_\psi) \\ (s_\varphi s_\psi + c_\varphi c_\psi s_\vartheta) \end{bmatrix} a_{x_v}. \quad (2.74)$$

By factorizing  $c_\psi$ ,  $s_\psi$ , we obtain

$$\underbrace{\begin{bmatrix} \frac{a_{x_m} + s_\vartheta g}{c_\vartheta} \\ \frac{a_{y_m} - c_\vartheta s_\varphi g}{-c_\varphi} \\ \frac{a_{z_m} - c_\varphi c_\vartheta g}{s_\varphi} \end{bmatrix}}_y = \underbrace{\begin{bmatrix} 1 & 0 \\ -t_\varphi s_\vartheta & 1 \\ t_\varphi^{-1} s_\vartheta & 1 \end{bmatrix}}_\phi \underbrace{\begin{bmatrix} c_\psi a_{x_v} \\ s_\psi a_{x_v} \end{bmatrix}}_\theta \quad (2.75)$$

which can now be rewritten as a least squares (LS) problem  $y = \phi \cdot \theta$ .

Once vector  $\theta$  is estimated from equation (2.75), the ratio of the two parameters is equal to  $\frac{\theta(1)}{\theta(2)} = \frac{c_\psi a_{x_v}}{s_\psi a_{x_v}} = \frac{c_\psi}{s_\psi}$ . Which is the tangent of  $\psi$ . Hence,  $\psi$  is then obtained by computing the inverse tangent of the parameters ratio  $\psi = \text{atan} \left( \frac{\theta(2)}{\theta(1)} \right)$ .

### 2.13.3 Experimental Results

The proposed algorithm is tested offline by using experimental data collected over few hours of driving and thus by considering three scenarios. Figure 2.24 shows a comparison between IMU raw data and aligned (rotated) data obtained from the estimated mounting angles. Differences in the accelerations are due to the forces experienced in the different locations of the vehicle. In Table 2.1, the estimated angles are compared for the different datasets, proving that the estimated angles converge to a very narrow range.

Location	Test #	$\varphi$ [deg]	$\vartheta$ [deg]	$\psi$ [deg]
Box 1	1	-74.79	-23.94	22.48
	2	-74.47	-23.93	22.93
	3	-74.66	-23.81	22.98
Box 2	1	4.02	3.56	38.53
	2	3.92	3.66	39.03
	3	3.93	3.69	39.68
Box 3	1	2.51	68.99	-1.94
	2	2.35	68.84	-2.51
	3	1.93	69.06	-2.16

TABLE 2.1: Analysis of the estimated angles for the different boxes for all the tests conducted.

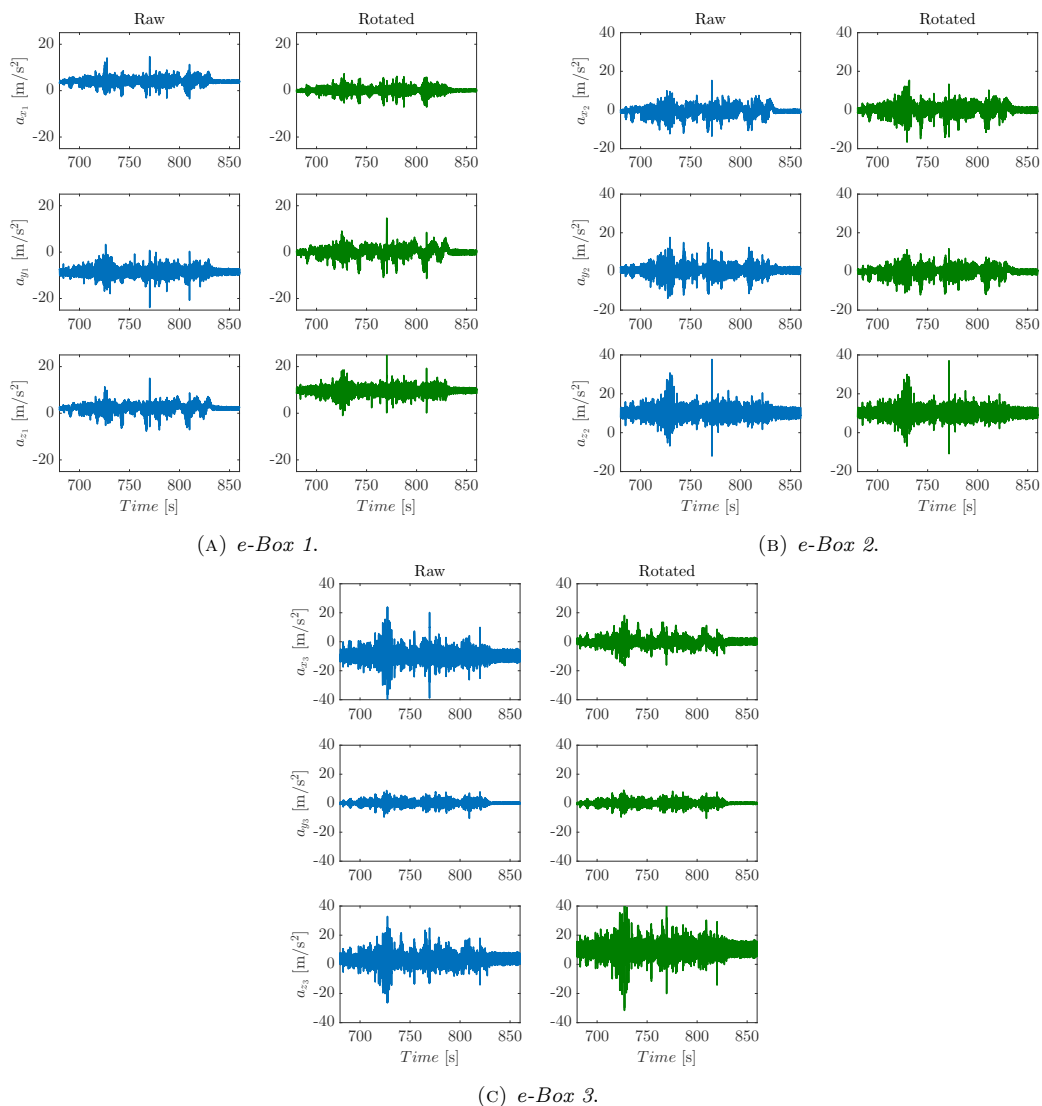


FIGURE 2.24: Self-calibration and experimental measurements: (left) the raw acceleration vector, (right) the acceleration vector along the virtual aligned axes.

A sensitivity analysis has been performed on the averaging window, as shown in Figure 2.25. The estimate of the two angles converges in a close range even with few samples, but it settles for a window length of 4000 useful samples.

In order to study the estimation convergence rate of  $\psi$ , the least square (LS) problem is compared with its recursive (RLS) version depicted in figure 2.26. The RLS converges to the final estimate with 400 useful

samples, an order of samples smaller than the number of samples required in the averaging process of  $\varphi$  and  $\vartheta$  (4000 samples). However, it must be remarked that the estimate of  $\psi$  depends heavily on data selection and this explains the small mismatch between the LS averaged and the three conducted tests.

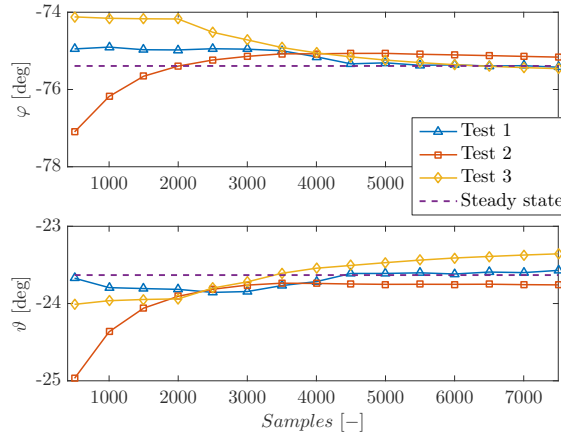


FIGURE 2.25: Sensitivity analysis: an overview of the sensitivity analysis of the averaging window for the estimate of  $\varphi$  and  $\vartheta$ . It is evident that with at least 4000 samples, the error computed in the estimate is very small with respect to the one estimated when the vehicle is standing still.

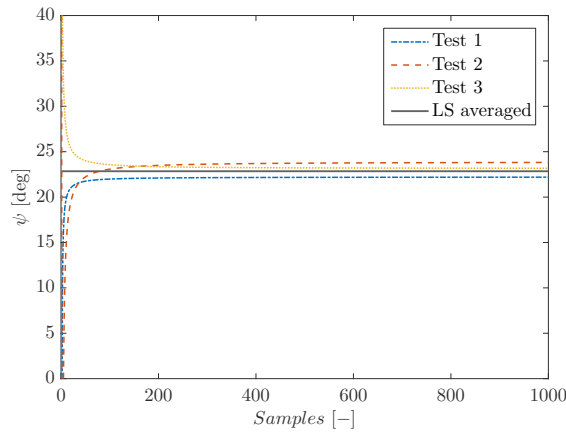


FIGURE 2.26: Sensitivity analysis: the RLS convergence is compared with the averaged LS. Estimates converge in less than 400 samples. Steady state error results to be smaller than 0.92 deg.

The last step is to test the robustness of the proposed algorithm. To do so, the self-calibration algorithm is performed considering different initial conditions for all e-Boxes. This test procedure is iterated fifty times for each dataset and the results are summarized in Table 2.2. We found that the standard deviation of the estimated angles is within  $0.6^\circ$  except for the  $\psi$  angle. In fact, the former is more sensitive to sensors biases and drifts. This is particularly more striking for the *e-Box 2* configuration, in which the pitch and roll angles are small to break up the vertical axis from the one of the vehicle's reference system. In this case, the  $\psi$  estimation is more sensitive to any bias in sensors measuring  $a_x$  and  $a_y$ .

In the other hand, to check the consistency of the virtually aligned axes, the rotated signals are compared by computing the cross-correlation between the three boxes. So, given two random signals  $x$  and  $y$ , the cross-correlation is a similarity metric defined as  $R_{x,y}(k, l) = \mathbb{E}\{x(k)y(k+l)^T\}$ , where  $l$  represents the delay between the two signals (Verhaegen and Verdult, 2007). The cross-correlation coefficient can be normalized with respect to the auto-correlation of the two signals, leading to:

$$R_{x,y, norm}(k, l) = \frac{1}{R_{x,x}(0)R_{y,y}(0)} \mathbb{E}\{x(k)y(k+l)^T\} \quad (2.76)$$

which is 0 when the two signals are orthogonal and 1 when they are completely correlated.

Location	Test #	$\varphi$ [deg]		$\vartheta$ [deg]		$\psi$ [deg]	
		Mean	Std	Mean	Std	Mean	Std
<i>e-Box 1</i>	1	-74.57	0.15	-24.06	0.11	23.33	0.52
	2	-74.31	0.12	-23.95	0.06	23.65	0.60
	3	-74.77	0.08	-23.76	0.04	23.69	0.37
<i>e-Box 2</i>	1	3.98	0.03	3.59	0.06	8.60	2.51
	2	3.94	0.02	3.59	0.08	12.47	3.75
	3	3.92	0.04	3.82	0.05	11.15	2.89
<i>e-Box 3</i>	1	2.31	0.08	68.01	0.29	-1.83	1.25
	2	2.24	0.21	68.83	0.24	-2.01	0.81
	3	1.93	0.08	68.91	0.28	-1.88	0.90

TABLE 2.2: Analysis of the estimated angles for all the boxes with different initial conditions. In all the cases, the the standard deviation does not exceed 0.6 deg.

The normalized cross-correlation coefficient is computed on the rotated signals of all the e-Boxes and for performed test. Results are listed in Table 2.3. The  $z$ -axis results to be perfectly aligned, with a high value of the normalized cross-correlation coefficient. Besides, it has proved to be less excited, meaning that its estimate is less influenced by the location of the device. Axes  $x$  and  $y$  show also a significant correlation with the relative location of the e-Box. However, this mismatch is limited and the results can be considered satisfying which proves that the effectiveness of the proposed algorithm can be considered to be independent from the mounting location and orientation.

Location <sub>1</sub>	Location <sub>2</sub>	Test #	Cross – correlation		
			$a_x$	$a_y$	$a_z$
<i>e-Box 1</i>	<i>e-Box 2</i>	1	89.57	97.55	100
		2	92.34	59.69	95.66
		3	78.40	88.63	100
	<i>e-Box 3</i>	1	88.02	83.38	100
		2	95.15	78.70	100
		3	80.89	82.43	100
<i>e-Box 2</i>	<i>e-Box 3</i>	1	81.23	82.54	100
		2	84.68	95.29	95.64
		3	77.15	71.68	100

TABLE 2.3: Correlation analysis of the rotated axes different boxes against all the considered tests.

### 2.13.4 Final Remarks

This study focused on setting up the experimental platform. First, we presented the instrumentation of the scooter from a practical point of view (sensors, mini PC, acquisition card, input / output ...), their characterization and implementation on the vehicle prototype (scooter). After that, we presented an algorithm to align the three axes of an arbitrarily mounted IMU on motorcycles. The algorithm consists in estimating three mounting angles which allow to virtually align the sensing axes with respect to the vehicle's reference frame. The algorithm has been tested and validated against real experimental data. Results favourably prove the effectiveness of the proposed approach, limiting the amount of energy needed with respect to more classical methods due to the reduced use of GNSS system.

## 2.14 Conclusions

In this chapter, we presented the dynamic modeling of the motorcycle. It should be noted that tire modeling is a key step for the derivation of a complete dynamic model of PTWV. In fact, tires-ground interaction plays a crucial role in the stability of PTWV. Thereby, we have seen that the forces generated by each tire can be decomposed into a set of three forces and three moments. We used Pacejka's magic formula to introduce the expressions of these efforts (section 2.3). Withal, to accomplish the safety requirements of motorcycles, a stability and handling analysis of PTWV dynamic is also required. Due to their special characteristics,

which allow to evaluate a various automatic tools, we focus on particular on the physical phenomena that characterize two-wheeled category and in particular the instability modes.

Furthermore, the PTWV modeling deals with the derivation of a multi-body model of motorcycle dynamics. First, we briefly presented the eight bodies motorcycle/rider model. Despite its high complexity and numerous nonlinearities, this model simulates very closely the dynamic behavior of the motorcycle/rider system. It allows the simulation of 16 Degrees of Freedom (DoF). In addition, it takes into account the coupling effects between the longitudinal and lateral dynamics. In the following works, this model was used indirectly during simulations and validations with the *BikeSim* software. Indeed, *BikeSim* uses this eight-body model in the "dynamic engine" of the software simulations. Although, the fidelity of the eight-body model discussed above, the latter is much more complex for the synthesis of control and observation algorithms. This is why we proposed the derivation of simpler models based on the principle of Jordan, with one or two-bodies, for the modeling of the lateral or longitudinal dynamics (section 2.8). To derive each of these models, we have established the kinematic relations for each of the model's bodies based on the principle of Jordan. Then, from these expressions, we have explained the steps to calculate the mass matrix, and the vector of generalized forces (non-conservative and residual efforts).

Then, we proposed a linearization of the equations around a straight line trajectory (section 2.9). This allowed us to find the famous Linear Parameter-Varying (LPV) two-body model originally introduced in (Sharp, 1971). Note that Sharp used Lagrange's formalism to derive his model. Furthermore, this dynamic models are the starting point for observer design or explicit identification algorithms in the following chapters. The two-body model has been used in all model-based observation and/or identification approaches proposed later in this manuscript (Chapters 5, 6, 7, 8). Indeed, we studied the one-body model of lateral dynamics either in the identification of CoG (chapter 3) or in the derivation of the risk function related to steering behavior in steady state situation in chapter 9. Finally, the in-plane model is presented to describe the longitudinal dynamic. The derivation of this model allowed us to tackle an important subject, namely the load transfers. In extreme cases, these phenomenon are also known as stoppie or wheelie respectively corresponding to the detachment of the rear or the front wheel. This model was used in the estimation the interconnected motion in chapter 8.

On the other hand, even if the one and two-body models seem simple in theory, identifying their parameters is a hard problems in practice. Indeed, some of the dynamic states or parameters are accessible to measurement while others require the use of advanced techniques. It is important to note that in parallel to the model choice, definition of the parameters is also important. The terms of the matrix  $A(v_x)$  and the vector  $B$  must be well informed according to the characteristics of the vehicle. Although the Sharp model is quite faithful to the behavior of the motorcycle in cornering, it contains no less than 34 parameters to identify. This issue is complex since the Sharp's model takes into account two types of parameters:

- Static parameters: masses, geometric parameters (wheelbase, position of gravity centers, etc.),
- Dynamic parameters: the inertia of the wheels, the front body and the rear body.

Some of these parameters are very difficult to estimate using conventional identification methods. If we take the example of the inertia of different bodies (wheels, front body, etc.), they can be estimated through a digital model by Computer Aided Design (CAD). This method can be very laborious. Otherwise, automatic techniques of identification are perfectly suited to this problem. In this context, chapter 3 and 4 studies parameters estimation problems. To go even further, we proposed observers able to estimate the dynamic states and simultaneously identify the parameters, this will be introduced in chapter 6 and 7.

Furthermore, we have proposed a novel calibration approach for inertial sensors mounted on motorcycles. This algorithm was validated on experimental data collected during tests performed with a motorcycle equipped with three e-Boxes mounted in different positions and orientations. Finally, we thoroughly analyses the experimental tests carried out to assess the performance of the approach, which favorably witness its capability of performing calibration for subsequent use of the accelerations in various applications.

## Part II

# Parametric Identification of PTWV



## Introduction

OVER the last few decades, the challenge of creating more accurate models for active safety systems is increased. However, without a precise knowledge of the system's parameters, any modelling effort stay insufficient to evaluate the system's dynamics. In the automotive research, the ability to get the pertinent vehicles parameters, a prior or in real-time, allows to develop attractive efficient active safety applications or model based vehicle control (Limroth, 2009 and Edwards, 2008).

The parametric identification consists in determining the best values of system's parameters. It can be formulated as an optimization problem where its resolution can becomes quickly arduous as the number of parameters to be identified increases. One can distinguish two main classes of techniques to solve an optimization problem. The first class are based on gradient computation of the objective function to be minimized while the other class uses stochastic methods (Bartoli and Del Moral, 2001). The choice of the optimization method depends strongly on the complexity of the model. Usually, gradient descent methods are simple to implement and often gives good identification results, thus, they are generally applied in practical applications (Khubotov, 1987, Møller, 1993). Furthermore, multi-objective techniques applied to model identification have achieved great results in many cases, as shown in (Yousefi, Handroos, and Soleymani, 2008, Herrero et al., 2007 and Rodriguez-Vazquez and Fleming, 1998). Among others, algebraic identification method have been investigated to obtain an accurate model of real system modelled as continuous-time linear transfer function (Fliess and Sira-Ramírez, 2003) and, it has been widely applied for electrical and mechanical applications like flexible robots estimation, mass-spring-damper model, DC Motor and others (Mamani et al., 2007, Becedas et al., 2007b, Becedas et al., 2007a, Reger and Jouffroy, 2009). This approach does not require initial conditions and the algorithm can be implemented on-line. Further, almost references, the identification methods are designed under consideration for a specific systems form and their direct transposition to the more general problem case is not straightforward for many reasons. Furthermore, the parameter identification problem is closely related to persistence of excitation in order to enable the parameters to reach an optimal solutions (Hildebrand and Gevers, 2002). Hence, for identification process, suitable rich input signals should be considered.

It is common belief that ITS use various vehicle parameters to produce a correct assistance and to minimize the likelihood of false warning. If some parameters are easy to obtain such that vehicle's mass, CoG position and inertia, identifying or estimating others is much more complex especially in real-time like tire cornering stiffness. For the PTWV, a great effort has focused on state estimation of the vehicle dynamics and several works are published since many years ago (Gasbarro et al., 2004a, Teerhuis and Jansen, 2012a, Ichalal et al., 2012, Dabladji et al., 2013, De Filippi et al., 2011b, Nehaoua et al., 2013b). However, to the author's best knowledge, a very few works deals with the PTWV parameters identification. In fact, the motorcycle is a complex and strongly nonlinear system. Almost attempt for parameters identification used behavioural models and statistical methods. Also, the persistence is difficult to respect since it is not possible to freely apply rich excitation signals to solicit the different dynamics due to the PTWV's mechanical constraints and instability.

For example, in (James, 2002), the author considers an auto-regressive model to describe the motorcycle lateral dynamics behaviour and next used to estimate a state space representation which has no relation with the physical parameters. Also, (Savaresi et al., 2008) and (Savaresi et al., 2006) have used a regression-based estimation methods to recover the available road friction. Moreover, non model-based identification method is described in (Corno and Savaresi, 2010), where the authors present a black-box identification. This method allows to directly estimate the input/output engine-to-slip dynamics of sport motorbike from experiments, instead of using the classical approach of multi-body modelling. In (Cossalter et al., 2006a), the authors deal with the identification of the vibration characteristics of motorcycle riders. This work presents an analysis to identify the properties of a rider multi-body model, which is used to fit the experimental data excited by means of stepped sine testing. On the other hand, studies have shown that semi-active steering dampers for motorcycles can be used in the design of innovative control strategies to improve two-wheeled vehicles stability. In the study (Tanelli et al., 2009b), an analytical model of a two-wheeled vehicle tuned to capture the weave and wobble modes to study steering related instabilities. The model is derived from first principles and its parameters tuned to fit a hyper-sport motorcycle based on a grey-box identification procedure. Also, in (Schwab et al., 2012; Schwab, De Lange, and Moore, 2012), the authors assume a linear PID controller for the rider control model. First, this parametric control model is fitted to the experimental data using black-box finite impulse response (FIR) model. After that, a grey box model is fitted to the response of the

FIR model to identify the PID feedback gains. Then, these gains are used to compute the specific optimal control linear-quadratic regulator (LQR) which the rider is using to control the two-wheelers.

Braking and traction control systems are commonly designed considering an integrated step of identification. In the study of (Cabrera et al., 2014), the authors consider wheel slip control when excessive torque is applied on driving wheels, using a fuzzy logic control block. The parameters that define the fuzzy logic controller have been tuned, first according to experience, then, by means of an evolutionary algorithm in order to design an augmented traction controller.

Other approaches have been investigated to study electric two-wheelers, in Wilhelm et al., 2012, the author describes an algorithms based on a grey-box model for estimating four characteristic parameters of a linear dynamics model, then the physical meaning has been interpreted from the identified parameter values.

Past works have been interested in motorcycle suspension system based on estimation theory. The recursive least squares algorithm which incorporates a fault detection scheme can be a suitable approach to estimate the time varying dynamics as proposed in (Ledwidge, 1995). It is shown using software simulations, a mass, spring and damper model are selected to represent the dynamics of the suspension system, these parameters were estimated from static tests. Further, motorcycle simulator prototype has been investigated in the recent decades, due to the rising concern of the rider safety. Their modelling claims informations about different parameters, as reviewed in (Nehaoua and Arioui, 2008), where, the authors present the dynamics modelling and parameters identification of a motorcycle simulator's platform. The identified parameters can be used to improve control scheme, adapted to driving simulation application. Also, the roll motion parameters of a motorcycle simulator prototype were studied in (Shahar et al., 2014).

To summarize, parameters identification is a main step in motorcycle studies, either for control requirements, safety purpose or even in behaviour and stability analysis. Previous studies have used various approaches with some assumptions according to the model and the available driving data. However, the robustness of these approaches across different motorcycle architecture, models and riding behaviour still needs a thorough improvements. Withal, most of these works have been devoted at identifying only part of the dynamics. Nonetheless, the identification of the full dynamic is a real challenge.

This part deals with the parameter identification for motorcycle model parameters. In the previous chapter 2, we have studied two lateral dynamics models, one rigid body and two-bodies model (Sharp's model). For Sharp's model, more than 30 unknown parameters needs to be identified which is a hard task. We'll describe several approaches for motorcycle parameters identification where the conventional methods have failed or are difficult to apply. To do this, we divided this part into two chapters. The first one deals with the rigid body model, we'll discuss static identification, gradient decent algorithm and algebraic identification method The second chapter studied the two-rigid bodies model. We'll present multi-objective optimization and Levenberg-Marquardt algorithms.

# Chapter 3

## Identification of a Single Rigid-Body model

### Abstract

This chapter proposed an identification procedure based on the motorcycle geometry and the rigid body dynamic model. In this part, we aim to identify motorcycle center of gravity (CoG) position and the inertial parameters in order to conduct a preliminary study of the simulated behaviour and interpret the motorcycle dynamics while riding. The motorcycle planar motion equations are first synthesized in the modelling step. Then, the basic-principles of static is used to define the motorcycle CoG from the measured forces on the static tests. When the geometric parameters are computed, gradient decent algorithm and an algebraic identification method are applied to estimate the dynamic parameters. Indeed, in order to be able to identify the parameters, persistent inputs should excite the associated modes. Unfortunately, some modes can be solicited only through manoeuvres generally very difficult to achieve with or without riders. To get some feedback parameters, *BikeSim* model parameters are considered for the comparison. On this software, some experimental measurements are carried on to record data for excitation. Simulations in *BikeSim/Matlab* environment is useful to verify if the proposed methods are capable of identifying motorcycle parameters. The theoretical aspects and the practical validation of this idea were published in Fouka et al., 2017b.

The chapter is organized as follows. Section 3.1 presents a static method to identify geometric parameters for a PTWV single body model. We describe the static equations of forces and moments in different configurations thanks to the fundamental principle of static. After that, we define an operating mode that makes it possible to estimate these parameters.

Afterwards, section 3.2 and 3.3 deal with the identification of the inertial parameters of the motorcycle body model using two estimation methods. First, section 3.2 describes the gradient optimization algorithm which intended to minimize a differentiable real function while processing of input/output data through a recursive method. The results of this method are compared with an algebraic identification approach introduced in section 3.3, this section presents a step by step the algebraic method for continuous-time linear system modeled by a rational transfer function. After the identification methods are outlined, simulations results are presented in order to confirm the accuracy of the parameters estimation in sections 3.4.

### 3.1 Parametric Identification-Geometric Approach

The geometry of the frame, as well as the weight distribution, are features that influence stability, handling and manoeuvrability (Cossalter and Lot, 2002). The definition of the properties of manoeuvrability and stability of a PTWV depend among others, on the following geometric parameters: the wheelbase, the caster angle, the trail, and the CoG position. For example, the wheelbase affects the load transfer between the two wheels and enhance the vehicle stability but in the same time, it makes the vehicle less manoeuvrable

in curves with small curvature radius. Also, the position of the CoG has a significant influence on the PTWV dynamic behaviour. So, a forward CoG makes over-steer in curves while a rear CoG promotes under-steering. Moreover, high CoG makes the vehicle to lift in acceleration/braking while a low position amplifies the rear and front wheel slip in acceleration/braking.

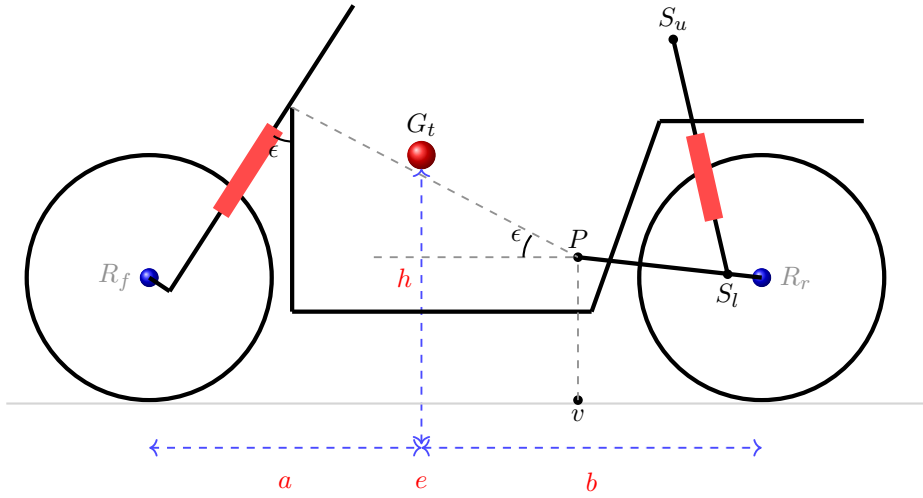


FIGURE 3.1: Single body geometry of motorcycle.

In this section, we aim to identify the CoG position by considering a single body representation of the motorcycle as in figure 3.1. The position of the CoG,  $G_t$ , is characterized by three geometric parameters  $a$ ,  $b$  and  $h$ . First, the front and rear wheel load is measured where the two wheel's contact point are on the same flat surface. Next, the same measurement is done by tilting the motorcycle with a given known angle  $\alpha$  as shown in figure 3.2. The first scenario allows to determine  $a$  and  $b$  and the total motorcycle mass. In the inclined scenario, front and rear masses  $m_f$ ,  $m_r$  and CoG's height  $h$  can be calculated.

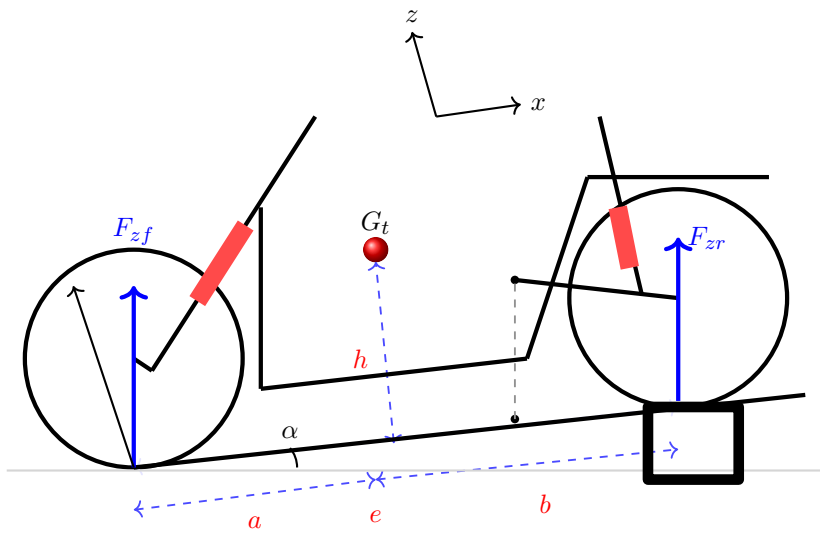


FIGURE 3.2: The balance of forces - Motorcycle on the slope in the opposite direction.

In the horizontal scenario, we have the static equilibrium of vertical forces  $F_{zf} + F_{zr} = mg$  and the corresponding moments  $aF_{zf} = bF_{zr}$ , where  $F_{zf}$  and  $F_{zr}$  are respectively the vertical force applied on the front and the rear wheels.  $m$  is the total vehicle mass. So, in the horizontal configuration, the distance between the front and rear contact point and the position of CoG is estimated by:

$$b = \frac{F_{zf}}{mg}e \quad \text{and} \quad a = \frac{F_{zr}}{mg}e \quad (3.1)$$

For the inclined configuration of figure 3.2, the static equilibrium for two different slope angle  $\alpha_1$  and  $\alpha_2$  allows to write:

$$\begin{aligned} mgh \sin \alpha_1 + (F_{zf_1}a - F_{zr_1}b) \cos \alpha_1 &= 0 \\ mgh \sin \alpha_2 + (-F_{zf_2}a + F_{zr_2}b) \cos \alpha_2 &= 0 \\ F_{zf_1} + F_{zr_1} &= mg \\ F_{zf_2} + F_{zr_2} &= mg \end{aligned} \quad (3.2)$$

By solving this set of linear equations with respect to  $a$ ,  $b$  and  $h$ , we get the motorcycle CoG position :

$$\begin{cases} a = \frac{F_{zr_1} + F_{zr_2}}{2mg}e \\ b = e - a \\ h = \frac{F_{zr_1}b - F_{zf_1}a}{mg \tan \alpha} \end{cases} \quad (3.3)$$

In experimental test, the previous procedure is iterated by taking into account the rider to measure the position of the new CoG as in figure 3.3.

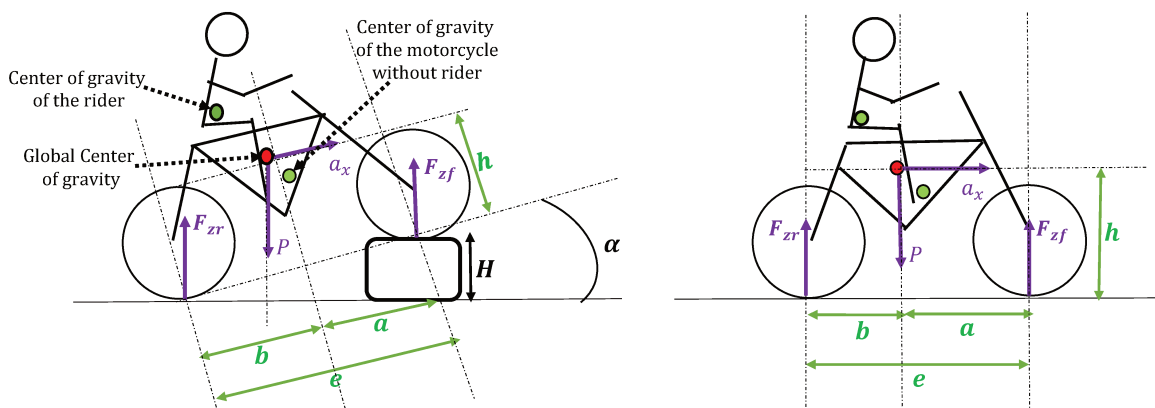


FIGURE 3.3: The position of the CoG o of the motorcycle and the rider.

## 3.2 Gradient Decent Algorithm

The gradient descent (GD) method is an iterative optimization algorithm for solving problems of the form  $\min_{\theta \in \mathbb{R}^n} f(\theta)$ , where  $f(\theta)$  is the parametric form model and  $\theta \in \mathbb{R}^n$  are model parameters. Starting from an initial value of the corresponding parameters vector, we take a first step downhill in the direction specified by the negative gradient, and this process is iterated until reaching a local minimum. The step rate  $\alpha$  determines the rate of the algorithm convergence.

In the present context, the objective is to derive the gradient-based iterative identification algorithm for the motorcycle rigid body model to estimate the moments of inertia  $\{I_x, I_y\}$ . Let consider the following one body motorcycle model:

$$\begin{cases} m(\dot{v}_y + \dot{\psi}v_x) = F_{yf} + F_{yr} \\ I_z \dot{\psi} = aF_{yf} - bF_{yr} \\ I_x \ddot{\phi} - mh(\dot{v}_y + \dot{\psi}v_x) = mgh\phi \end{cases} \quad (3.4)$$

Suppose that the set of the observed output data is  $y(t) = \{\ddot{\psi}, \ddot{\phi}\}$ , the identification process is schematized in figure (3.4). We define the following quadratic function:

$$C(t, \theta) = \frac{1}{2} \sum_k (y_m(t_k) - y(t_k, \theta))^2 \quad (3.5)$$

With  $\theta_1 = I_x$  and  $\theta_2 = I_z$  are the  $x$ -axis and  $y$ -axis moments of inertia.  $y_m$  is the measured outputs vector,  $y$  is the outputs vector of simulated model and  $t_k$  is the current sample time.

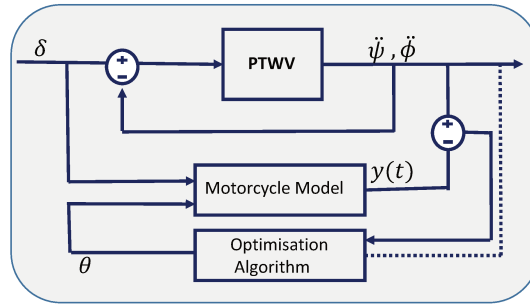


FIGURE 3.4: Functional diagram of Gradient Descent.

The optimization algorithm allows to find the parameter value of  $I_x$  and  $I_z$  by minimizing the criterion  $C(t, \theta)$  by computing the following gradient:

$$G(\theta) = \frac{\partial C(\theta)}{\partial \theta} = \sum (y_m(t_k) - y) S_y^\theta(t_k) \quad (3.6)$$

$S_y^\theta$  is the output sensitivity functions and is evaluated from equation (3.4) as following:

$$\frac{d\ddot{\psi}}{dI_z} = -\frac{aF_{yf} - bF_{yr}}{I_z^2} \quad (3.7)$$

$$\frac{d\ddot{\phi}}{dI_x} = -\frac{mgha_y + mh(\dot{v}_y + \dot{\psi}v_x)}{I_x^2} \phi \quad (3.8)$$

For a given initial value of  $\theta_1$  and  $\theta_2$ , the standard GD update equation is given by the following:

$$\theta_k = \theta_{k-1} - \alpha G_{k-1} \quad (3.9)$$

**Algorithm 1: Gradient Algorithm (GD):**( $\subseteq$ )**Require:**  $\theta_0 = \theta(t_0)$ ,  $epsGrad = 1e - 5$ ,  $epsCrit = 1e - 5$ , $K_{max} = 100$ ,  $\alpha = 1$ ,  $stop = 0$ ,  $K = 0$ .**while** ( $stop \neq 1$ ) **do**  **for** ( $t_{k-1} = t_0$  and  $\theta = \theta_0$ ) **do**     $C_{k-1} = 0.5 \sum (y_m(\theta_0) - y(t))^2$ ,     $G_{k-1} = - \sum (y_m(\theta_0) - y(t))S$      $\theta_k = \theta_0 - \alpha G_0$    $C_k = 0.5 \sum (y_m(\theta_k) - y(t))^2$    $G_k = - \sum (y_m(\theta_k) - y(t))S$   **if** ( $C_k < C_{k-1}$ ) **then**     $\theta_k = \theta_{k-1} - \alpha G_{k-1}$      $\alpha = \alpha \times 1.5$      $K = K + 1$   **else**     $\theta_k = \theta_{k-1} + \alpha G_{k-1}$      $\alpha = \alpha / 2$   **End**  **if**  $\|(\frac{C_{k-1} - C_k}{C_{k-1}})\| < epsCrit$  **then**     $stop = 1$   **else if**  $\|G_k\| < epsGrad$  **then**     $stop = 1$   **else if** ( $K > K_{max}$ ) **then**     $stop = 1$ **End**

After that the gradient algorithm is well defined, the results of this method are compared to algebraic identification approach. This is the subject of the next section 3.3.

### 3.3 Algebraic Identification Approach

Unlike gradient algorithm, algebraic approach do not require a parametric form modelling neither initial parameters guess. It allows the parameters identification of time invariant linear system represented as a rational transfer function from input signal  $u(t)$  to the output signal  $y(t)$  (Baronti et al., 2013, Fliess and Sira-Ramírez, 2003, Neves, 2005).

The algebraic approach is mainly based on the robust computation of the time-derivatives of signal by using a finite weighted combination of time-integration of this signal. We apply the basic principles of the method on the linear motorcycle model described by equations (3.4) to obtained the transfer function  $H(s)$  between the output  $\psi$  and the input  $\delta$  :

$$H(s) = \frac{Y(s)}{U(s)} = \frac{N_3 s^3 + N_2 s^2 + N_1 s + N_0}{s^4 + D_3 s^3 + D_2 s^2 + D_1 s + D_0} \quad (3.10)$$

where the coefficients  $N_0, \dots, N_3, D_0, \dots, D_3$  are functions of the unknown parameters  $I_x$  and  $I_z$ . If we can identify the coefficients of the transfer function, we can deduce the values of the system parameters by resolving a set of equations. We can rewrite the transfer function from equation (3.10) into the following form:

$$y^{(4)} + D_3 y^{(3)} + D_2 \ddot{y} + D_1 \dot{y} + D_0 y = N_3 u^{(3)} + N_2 \ddot{u} + N_1 \dot{u} + N_0 u \quad (3.11)$$

where the exponent ( $i$ ) indicates the time differentiation of order  $i$ . To compute the unknowns system parameters  $D_i$ ,  $N_i$ , we take the Laplace transform of the expression (3.11) and we multiply each side by  $s$ :

$$[s^5 y(s) - s^4 y(0) - s^3 y(0) - s^2 y(0) - s y(0)] + D_3 [s^4 y(s) - s^3 y(0) - s^2 y(0) - s y(0)] + \dots + D_0 s y(s) = \quad (3.12)$$

$$N_3 [s^4 u(s) - s^3 u(0) - s^2 u(0) - s u(0)] + \dots + N_0 s u \quad (3.13)$$

Since the initial conditions are unknown so we differentiate five times so that all constant terms leave, then :

$$\begin{aligned} \frac{\partial^5}{\partial s^5} [s^5 y] + D_3 \frac{\partial^5}{\partial s^5} [s^4 y] + D_2 \frac{\partial^5}{\partial s^5} [s^3 y] + D_1 \frac{\partial^5}{\partial s^5} [s^2 y] + D_0 \frac{\partial^5}{\partial s^5} [s y] = \\ N_3 \frac{\partial^5}{\partial s^5} [s^4 u] + N_2 \frac{\partial^5}{\partial s^5} [s^3 u] + N_1 \frac{\partial^5}{\partial s^5} [s^2 u] + N_0 \frac{\partial^5}{\partial s^5} [s u] \end{aligned} \quad (3.14)$$

Let's calculate  $\frac{\partial^5}{\partial s^5} [s^5 y]$  as:

$$\frac{\partial^5}{\partial s^5} [s^5 y] = 5! y + 5! \times C_5^1 \times s \frac{\partial y}{\partial s} + \frac{5!}{2!} \times C_5^2 \times s^2 \frac{\partial^2 y}{\partial s^2} + \frac{5!}{3!} \times C_5^3 \times s^3 \frac{\partial^3 y}{\partial s^3} + \quad (3.15)$$

$$\frac{5!}{4!} \times C_5^4 \times s^4 \frac{\partial^4 y}{\partial s^4} + \frac{5!}{5!} \times C_5^5 \times s^5 \frac{\partial^5 y}{\partial s^5} \quad (3.16)$$

with  $C_n^r = \frac{n!}{r!(n-r)!}$ . The remaining terms are also calculated using the same procedure.

Next, and to avoid numerical problem arising from differentiation, each side of the previous equation is multiplied by  $s^{-5}$  and so on for the other terms. Thus, in the time domain, the resulting equations can be written as :

$$D_3 p_{1\_1} + D_2 p_{1\_2} + D_1 p_{1\_3} + D_0 p_{1\_4} + N_3 p_{1\_5} + N_2 p_{1\_6} + N_1 p_{1\_7} + N_0 p_{1\_8} = -q_1 \quad (3.17)$$

where  $q_1$  represents the time form of  $s^{-5} \frac{\partial^5}{\partial s^5} [s^5 y]$  which can be calculated by the inverse Laplace transform of equation (3.15) as:

$$q_1 = -5! C_5^1 \int^5 t y + 5! C_5^2 \int^4 t^2 y - \frac{5!}{2!} C_5^3 \int^3 t^3 y + \frac{5!}{3!} C_5^4 \int^2 t^4 y - \frac{5!}{4!} C_7^5 \int^5 y + \frac{5!}{5!} C_5^5 \int^2 t^5 y - \frac{5!}{5!} C_5^5 \int t^7 y \quad (3.18)$$

The expressions of  $p_{1\_1}, p_{1\_2}, \dots, p_{1\_8}$  maybe written as a differential equation in the manner of  $q_1$  (3.18). With regard of estimating the coefficients of the transfer function, equation (3.17) must be invertible. To this end, equation (3.17) can be completed by integration to have a full rank matrix. Then, we conclude the following system:

$$\underbrace{\begin{pmatrix} p_{1\_1} & p_{1\_2} & \dots & p_{1\_8} \\ p_{2\_1} & p_{2\_2} & \dots & p_{2\_8} \\ \vdots & \vdots & \ddots & \vdots \\ p_{8\_1} & p_{10\_2} & \dots & p_{8\_8} \end{pmatrix}}_{\mathcal{P}} \begin{pmatrix} D_3 \\ \vdots \\ D_0 \\ N_3 \\ \vdots \\ N_0 \end{pmatrix} = - \underbrace{\begin{pmatrix} q_1 \\ q_2 \\ \vdots \\ q_8 \end{pmatrix}}_{\mathcal{Q}} \quad (3.19)$$

With  $p_{8\_i} = \int p_{7\_i} = \iint p_{6\_i} = \iiint p_{5\_i} = \dots = \int^7 p_{1\_i}$  for  $\forall i = \{1, 2, \dots, 8\}$   
 et  $q_8 = \int q_7 = \iint q_6 = \iiint q_6 = \dots = \int^7 q_1$  for  $\forall i = \{1, 2, \dots, 8\}$ . Now, let consider the following definition:

**Definition 3.1.** *The parameters vector  $\Theta = ( D_3 \ \dots \ D_0 \ N_3 \ \dots \ N_0 )$  is linearly identifiable if, and only if,*

$$\mathcal{P} \times \Theta^T = \mathcal{Q} \quad (3.20)$$

$$\det(\mathcal{P}) \neq 0 \quad (3.21)$$

where

- $\mathcal{P}$  and  $\mathcal{Q}$  are respectively  $(8 \times 8)$  and  $(8 \times 1)$  matrices.
- $\Theta$  is the set of parameters.

The coefficients  $D_i$  and  $N_i$  are identified by solving equation (3.19). For implementation issue, each component of the  $\mathcal{P}$  and  $\mathcal{Q}$  matrices can be written in a state space representation of a simple linear variant time filter.

## 3.4 Experimental Result

As part of the *VIROLO++* project, several PTWV are available to make experimental tests (figure 3.5). All the tests were carried-out at Gif-sur-Yvette within a collaboration framework between the IBISC laboratory, IFSTTAR and the UPSud IEF.



FIGURE 3.5: The instrumented Kawasaki ER6N PTWV.

### 3.4.1 Static Test

As previously seen, the center of mass of a motorcycle is defined by the values of the parameters  $a$ ,  $b$  and  $h$  for a one-body model. This CoG point can vary with the weight of the rider. Thus, we distinguished two different cases with and without rider (figure 3.3). To know accurately the slope angle, we used a hydraulic lifting equipment to lift the motorcycle to a desired inclination angle. These parameters are identified based on a wheelbase of  $1405 \text{ mm}$  obtained from the PTWV manufacturer datasheet, a slope angle of  $\alpha = 12.75^\circ$ , a motorcycle weight of  $208 \text{ kg}$  and a rider weight of  $97.5 \text{ kg}$ . The value of the wheelbase can also be easily calculated using a tape measure from the center of a front wheel, down the side of the motorcycle to the center of the rear wheel.



FIGURE 3.6: Measurement environment

Table 3.1 presents the recorded masses on the front and rear wheels as well as the identified values of the geometric parameters. First, we record the values of the vertical forces (masses) at the front and the rear wheels using two weighting machines. After that, the geometric parameters are concluded thanks to the basic principles of statics described in section 3.1.

TABLE 3.1: Weight measurements  $F_{zf}$  and  $F_{zr}$  for Kawasaki ERN6 and identification results.

<b>Case.1: Without Rider</b>	$F_{zf}$ [Kg]	$F_{zr}$ [Kg]	$a$ [m]	$b$ [m]	$h$ [m]
Test.1: flat	102	112.4	0.7366	0.6684	*
Test.2: flat	96	112	0.7565	0.6485	*
Test.3: slope 1 <sup>st</sup> configuration	$F_{zf_1} = 118$	$F_{zr_1} = 88$	0.7419	0.6631	0.2781
2 <sup>nd</sup> configuration	$F_{zf_2} = 108$	$F_{zr_2} = 101$			
Test.4: slope 1 <sup>st</sup> configuration	$F_{zf_1} = 118$	$F_{zr_1} = 89$	0.7399	0.6651	0.2695
2 <sup>nd</sup> configuration	$F_{zf_2} = 108$	$F_{zr_2} = 101$			
<b>Case.2: With Rider</b>					
Test.1: flat	130	179	0.8139	0.5911	*
Test.2: flat	130	177	0.8100	0.5950	*
Test.3: slope 1 <sup>st</sup> configuration	$F_{zf_1} = 192$	$F_{zr_1} = 113$	0.7968	0.6082	0.3873
2 <sup>nd</sup> configuration	$F_{zf_2} = 155$	$F_{zr_2} = 158$			
Test.4: slope 1 <sup>st</sup> configuration	$F_{zf_1} = 192$	$F_{zr_1} = 113$	0.7877	0.6173	0.4276
2 <sup>nd</sup> configuration	$F_{zf_2} = 155$	$F_{zr_2} = 150$			

To this end, we consider two static configurations, the first is a "flat configuration" to estimate the horizontal parameters  $a$ ,  $b$  and the total motorcycle mass. The second is the "inclined configurations", allow to determine the front and rear masses  $m_f$ ,  $m_r$ , the horizontal positions ( $a$ ,  $b$ ) and vertical position  $h$ .

1<sup>st</sup> configuration: Rear wheel lifted case.

2<sup>nd</sup> configuration: Front wheel lifted case.

The results of the repeated tests, presented in table 3.1, are averaged in table 3.2.

TABLE 3.2: Identification Result: Geometric parameters  $a, b, h(m), m(kg)$  for Kawasaki.

Without Rider	$a$ [m]	$b$ [m]	$h$ [m]	$m$ [Kg]
mean value	0.7437m	0.6613m	0.3738	209.3429
standard deviation	0.0088	0.0088	0.0061	2.9251
With Rider				
mean value	0.8021	0.6029	0.4074	307.80
standard deviation	0.0121	0.0121	0.0285	3.3466

The rider effect is obviously important in particular for the CoG height parameter  $h$ . The values of  $a$  and  $b$  share the wheelbase with a ratio of 53% and 47% for the case without rider and and 57% and 43% with rider. The standard deviation of the identified parameters is small, which means that the parameter values are well grouped around the average and tended to be close to the mean expected value of the set. Table 3.3 presents the same experimental tests carried out on the scooter of the laboratory presented in section 2.11.

TABLE 3.3: Geometric parameters  $a, b, h(m), m(kg)$  for Scooter

Geomtric parameters	$a$ [m]	$b$ [m]	$h$ [m]	$m$ [Kg]
without rider	0.7363	0.5637	0.3960	142
with rider	0.8015	0.4985	0.5194	221

The values of  $a$  and  $b$  share the wheelbase with a ratio of 56.64% and 43.36% without rider and, 61.65% and 38.35% with rider.

### 3.4.2 Dynamic Test

The test described in this section is carried-out on the *BikeSim* simulator. This later provides different datasets allowing construction and configuration a specific PTWV. Also, *BikeSim* includes several virtual sensors freely positioned which facilitate to measure several kinematics and dynamics variables at any location. For this, a chirp signal is used to excite the motorcycle dynamics as in figure 3.7. Recall that, this test aims to identify the roll and yaw inertia based on gradient descent optimization and algebraic methods.

The chirp signal is a flying sinus law whose instantaneous frequency is gradually increasing with time between two specified frequencies, for more details please refer to (Burgess, 1992, Venture, 2003). This wobbled signal is commonly used in sonar, radar, laser and spread-spectrum applications. It has a good excitation characteristics to excite both the low and the higher frequencies. Despite the importance of this signals to practical system identification, this signal appear less well known. This flying sinus required a quite short measurement time compared to the other signal such as impulse or sequential random excitation signals which may require repetitive measurements to reduce the effects of noise or to achieve statistical reliability. However, a real chirp test is in some way dangerous to produce in real life, in particular if the test included rider. In our case, we preferred to make use of motorcycle simulator rather than a real motorcycle/rider. Hence, a preliminary study was conducted in the well-known *BikeSim* simulator to choose the exciting signal and in the same time to be sure that PTWV is still keeping its balance.

$$\delta = 0.5 \sin(\pi t) + 0.5t + 0.5$$

with  $t$  is the measurement time.

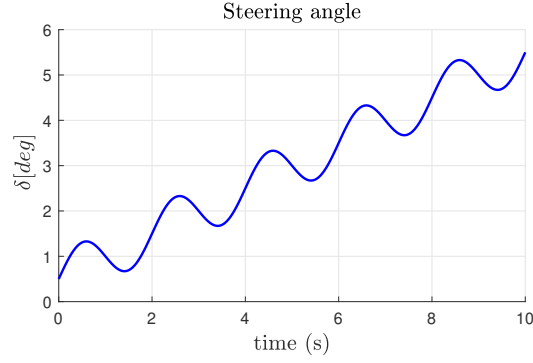


FIGURE 3.7: Steering angle, chirp flying input.

The conducted test involves the two-wheeled vehicle mainly in yaw and roll motions to excite the main inertia of the motorcycle body. Figure 3.8 shows the output data (roll angle, roll and yaw rate) recorded for a chirp signal. This last serves to excite the dynamics with a sinus-flying at 20 km/h.

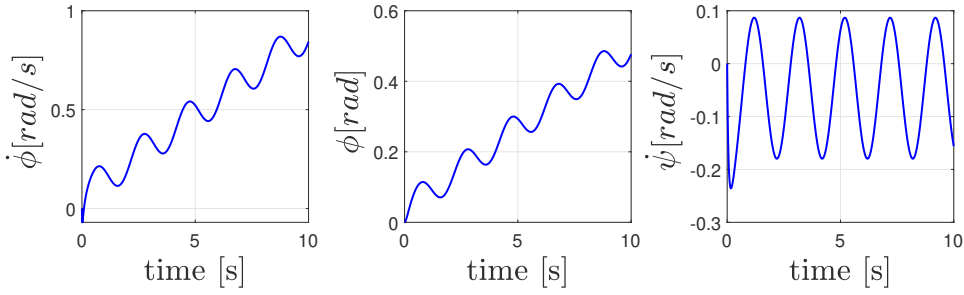


FIGURE 3.8: System outputs.

### 3.4.3 Algebraic Identification

The PTWV dynamics have been excited with a steering chirp signal for a constant longitudinal velocity  $v_x = 20$  km/h. Then, measurement data are used in the parametric identification method to estimate the following transfer function:

$$\begin{aligned}
 H_{id}(s) = \frac{\dot{\psi}}{\delta} &= \frac{503.9s^3 + 1.511 \times 10^4 s^2 - 9.22 \times 10^4 s - 1.317 \times 10^6}{s^4 + 158.5s^3 + 5749s^2 + 4.136 \times 10^4 s + 4.755 \times 10^4} \\
 &= \frac{N_3 s^3 + N_2 s^2 + N_1 s + N_0}{s^4 + D_3 s^3 + D_2 s^2 + D_1 s + D_0}
 \end{aligned} \tag{3.22}$$

On the other hand, from the state-space representation of the one-body lateral dynamics in section (2.9.3), we compute the theoretical transfer function between the  $\dot{\psi}$  output to the  $\delta$  input, this yaw rate dynamics can be written in the form of equation (3.10). The coefficients  $[D_i, N_i]$  of the transfer function depend on the unknown parameters  $I_x, I_z$ , their expressions are highly complex and non-linear, after simplification, we get the following denominator coefficients:

$$D_3 = \frac{3.5837 \times 10^3}{I_z} + \frac{528.1462}{I_x} + 13.1750 \tag{3.23}$$

$$D_2 = \frac{6.0275 \times 10^4}{I_z} + \frac{1.4796 \times 10^3}{I_x} + 2.0384 \times 10^6 \tag{3.24}$$

$$D_1 = \frac{2.3268 \times 10^7}{I_x \cdot I_z} - \frac{2.0230 \times 10^4}{I_z} \tag{3.25}$$

$$D_0 = \frac{2.6024 \times 10^7}{I_x \cdot I_z} \tag{3.26}$$

The parameters  $I_x$  and  $I_z$  can be identified from the  $D_3$  and  $D_2$  coefficients of the denominator, plotted in figure 3.9.

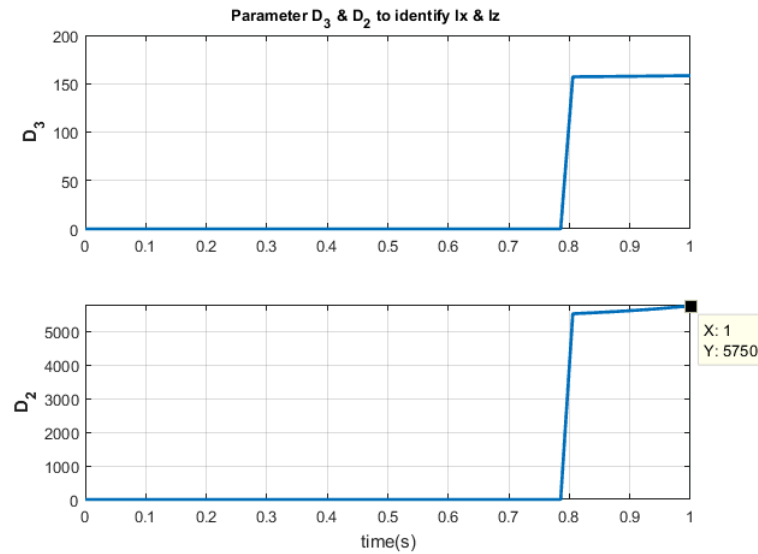


FIGURE 3.9: Parameters convergence.

It can be seen, from the above simulation that the method converges after 0.8s this time laps is due to the response time of the filters  $p_i$  and  $q_i$ . After estimation by the algebraic method, we computed the values of parameters  $I_x$  and  $I_z$  from the expressions of  $D_3$  and  $D_2$  and the identified function  $H_{id}(s)$  (equation 3.22). The result of the parameters  $I_x$  and  $I_z$  identification are compared with the gradient method in the next subsection 3.4.4 .

### 3.4.4 Gradient Method

The test described in section 3.4.2 is used also to identify the roll and yaw moment of inertia. The geometric parameters in equations (3.7) are captured from the static test allowing to apply the algorithm 1. The gradient decent results are therefore obtained in simulation with a chirp trajectory. The excitation input (figure 3.7) was selected in order to excite PTWV dynamics and also to ensure the motorcycle stability. Figure 3.10 shows the convergence parameters and the errors between the estimated responses and the actual ones.

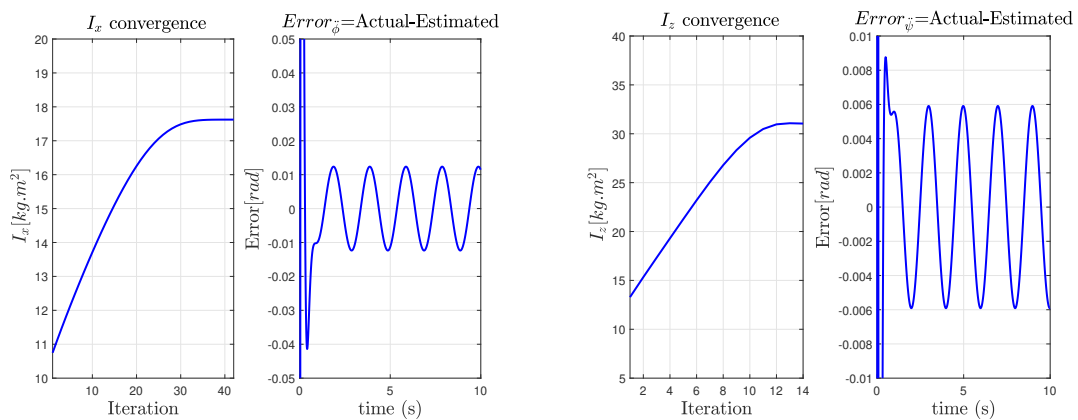


FIGURE 3.10: Parameters convergence

The identification results of the algebraic and the gradients methods are summarized in the following Table 3.4:

Parameters	Test #	$I_x$ [kg.m <sup>2</sup> ]	$I_z$ [kg.m <sup>2</sup> ]
Identification	<i>BikeSim</i>	17.623	31.058
	Algebraic method	17.609	31.073
	Gradient descent	17.6232	31.0279

TABLE 3.4: Inertial parameters identification result for one body PTWV model.

After the identification process, the result of geometric parameters (section 3.4.1) and the inertial parameters (section 3.4.2) are used to simulate the PTWV one-body model and to validate with respect to real data. As discussed, the main inertial parameters were identified from *BikeSim* using a motorcycle with approximately the same feature as the one used in static tests (section 3.4.1). For the sake of validation, a scenario was performed where the motorcycle was turning on a roundabout (see figures 3.11) to excite the lateral dynamics, the test is carried out at relatively high speeds of around 70 km/h.

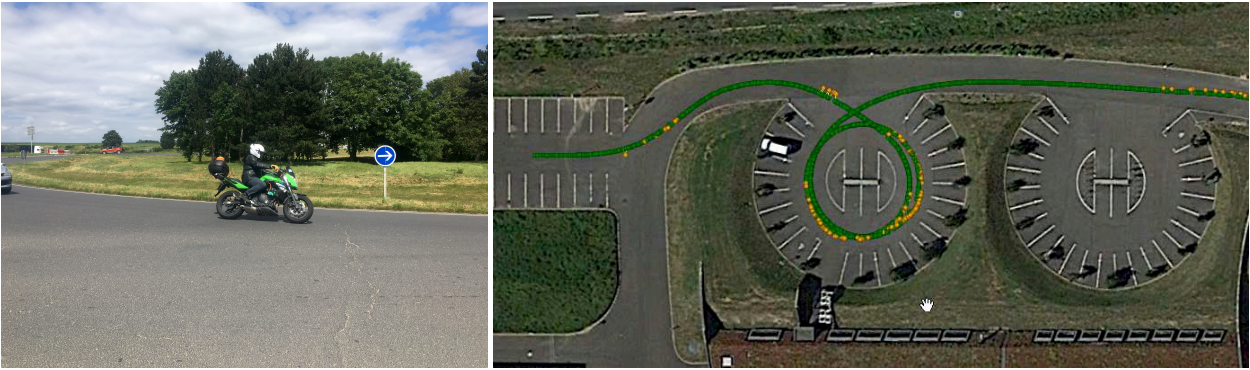


FIGURE 3.11: Turning at the roundabout.

The recorded steering angle from experiment test is used to excite the identified PTWV one-body model.

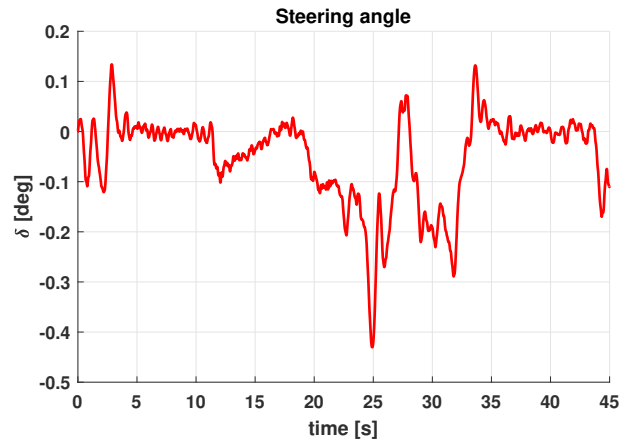


FIGURE 3.12: Steering angle input.

Then, the estimated roll angle is compared with the roll acquired from experiment using IMU sensor placed near to the center of gravity under the seat. Figure (3.13) shows that the roll angle from the model has a very close profile with the measured one. These simulation results converge well to the data measured by sensors embedded on the motorcycle which confirm the accuracy of the identified parameters.

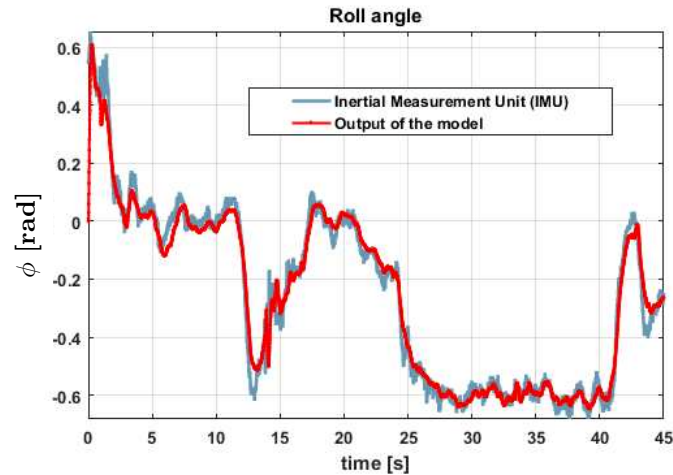


FIGURE 3.13: Validation of the model: turning at the roundabout.

### 3.5 Conclusions

This chapter considered the identification of a single rigid body motorcycle model. First, the motorcycle center of gravity was identified using static tests and basic principles of forces and moments, in which different configurations are considered. This operating mode makes it possible to estimate the geometric variables. Second, the inertial parameters are identified, using dynamic tests, based on two methods:

- The gradient descent (GD) algorithm designates a differentiable optimization to minimize the cost function. Note that this method does not require to compute the second-derivative (Hessian matrix) which make it simple for the implementation as well as it is computationally fast per iteration. However, the GD is slower when the step rate is very small and consequently the gradient direction is not well-scaled. Thus, the number of iterations largely depends on the scale of the problem.
- The algebraic method allows the identification of a transfer function from the output and the input signals. The algebraic approach uses the model of the system, that is almost known. Furthermore, the algorithm is computed on-line and in real time, the estimation does not require initial conditions. The method, however, is sensitive to the persistent input to excite the dynamics of the motorcycle.

# Chapter 4

## Identification of Two-bodies model

### Abstract

Recent assistive safety systems require good approximations of motorcycle inertial properties to obtain dynamic model that tightly adjusts to the real lateral behaviour of the motorcycle, in the way that it will lead to precise simulation and experimental results. This chapter deals with the identification problem for two-bodies motorcycle model.

In the first part of this chapter, a technique for cascade identification based on parametric model, input/output data and optimization algorithm is presented in section 4.1. This methodology makes profit of the possibility given by this type of algorithm for solving consecutively multiple objectives function. After the identification method is outlined, simulations results are presented in order to confirm the accuracy of the parameters estimation under the persistent condition of the inputs. The theoretical aspects and evaluation of this approach were published in Fouka et al., 2017a.

The second part of the chapter presents further research on parametric identification of two wheeler vehicles using a recursive Levenberg-Marquardt parameter identification formulation (section 4.2). This work was published in Fouka et al., 2018b.

### 4.1 Multi-Objective Optimization

A multi-objective optimization problem is characterized by a set of objective functions to be maximized or minimized (Piegay, 2015). Unlike the single-objective case for which a single well-defined function is to be optimized, multi-objective optimization consists in finding the set of parameters for different objective functions. The multi-optimization problems can be addressed with different approaches, either by reducing the multi-objective functions to a single-objective problem, or by sequentially optimizes objective functions, independently of the others, in a pre-established order or neither by treating all the goals simultaneously (Pareto methods in Jakob and Blume, 2014). While these techniques have many advantages, the convergence toward the global optimum is, on the other hand, strongly conditioned by the control parameters and by the initial conditions.

Indeed, regarding the PTWV two-bodies model and the physical characteristics of such a system, different inertial and geometric parameters need to be estimated from identification approaches. Unfortunately, when the number of the unknown parameters increases, or when the parameters excitation can not be achievable in the same time, the single-objective function algorithm maybe not well adapted to process all the desired parameters of the PTWV system. Due to this fact, addressing this problem from the standpoint of classical optimization could be insufficient which require to extend the problem of optimization to the multi-objective framework.

### 4.1.1 Identification Problem Formulation

Let reconsider the two-bodies PTWV model:

$$\begin{cases} e_{33}\dot{v}_y + e_{34}\ddot{\psi} + e_{35}\ddot{\phi} + e_{36}\ddot{\delta} = a_{34}\dot{\psi} + F_{yf} + F_{yr} \\ e_{34}\dot{v}_y + e_{44}\ddot{\psi} + e_{45}\ddot{\phi} + e_{46}\ddot{\delta} = a_{44}\dot{\psi} + a_{45}v_x\dot{\phi} + a_{46}v_x\dot{\delta} + a_{47}F_{yf} + a_{48}F_{yr} \\ e_{35}\dot{v}_y + e_{45}\ddot{\psi} + e_{55}\ddot{\phi} + e_{56}\ddot{\delta} = a_{54}v_x\dot{\psi} + a_{56}v_x\dot{\delta} + a_{51}\sin\phi + a_{52}\sin\delta \\ e_{36}\dot{v}_y + e_{46}\ddot{\psi} + e_{56}\ddot{\phi} + e_{66}\ddot{\delta} = a_{64}v_x\dot{\psi} + a_{65}\dot{\phi} + a_{66}\dot{\delta} + a_{61}\sin\phi + a_{62}\sin\epsilon\sin\delta + a_{67}F_{yf} + \tau \end{cases} \quad (4.1)$$

From the above dynamics equations, we can underline a set of 15 unknown parameters  $\theta_i$ . In this section, we aim to identify  $\theta = \{e_{34}, e_{36}, e_{44}, e_{45}, e_{46}, a_{45}, a_{46}, e_{55}, e_{56}, a_{54}, a_{56}, a_{52}, e_{66}, a_{64}, a_{66}\}$ . The two-bodies PTWV model is rewritten under a parametric form as following:

$$\begin{cases} m\dot{v}_y + \theta_1\ddot{\psi} + (m_f j + m_r h)\ddot{\phi} + \theta_2\ddot{\delta} + m v_x \dot{\psi} = F_{yf} + F_{yr} \\ \theta_1(\dot{v}_y + v_x \dot{\psi}) + \theta_4\ddot{\phi} + \theta_3\ddot{\psi} + \theta_5\ddot{\delta} - \theta_6 v_x \dot{\phi} - \theta_7 v_x \dot{\delta} = l_f F_{yf} - l_r F_{yr} \\ (m_f j + m_r h)\dot{v}_y + \theta_8\ddot{\phi} + \theta_4\ddot{\psi} + \theta_9\ddot{\delta} - \theta_{10}v_x\dot{\psi} - \theta_{11}v_x\dot{\delta} = (m_f j + m_r h)g \sin\phi + \theta_{12}\sin\delta \\ \theta_2\dot{v}_y + \theta_9\ddot{\phi} + \theta_5\ddot{\psi} + \theta_{13}\ddot{\delta} + \theta_{11}v_x\dot{\phi} - \theta_{14}v_x\dot{\psi} - \theta_{15}\dot{\delta} = \theta_{12}\sin\phi + \theta_{12}\sin\epsilon\sin\delta - \eta F_{yf} + \tau \end{cases} \quad (4.2)$$

Moreover, we have the following geometric constraints equations:

$$\begin{cases} k = (a + e)\cos\epsilon - f\sin\epsilon \\ j = (a + e)\sin\epsilon + f\cos\epsilon \\ a = \frac{l_f}{\cos\epsilon} - \eta \\ l = l_f + l_r \\ F_{zf} = -\frac{m}{l}l_r g \\ F_{zr} = -(m_f + m_r)g + F_{zf} \end{cases} \quad (4.3)$$

Beside these geometric constraints, we know that  $m = m_f + m_r$ . Also, to simplify the identification process, we assume that  $m_r \gg m_f$  and  $h \simeq j$ , then, a new dependence equations is formulated as  $mh = m_f j + m_r h$ . Under these constraints and hypothesis, it remains only nine unknown parameters vector  $\theta = [\theta_1, \dots, \theta_8, \theta_{15}]^T$ . Further, geometric and inertial parameters can be easily deduced as following:

$$\begin{cases} k = \frac{\theta_1}{M_f} \\ e = \frac{\theta_2}{M_f} \\ a = \frac{l_f}{\cos(\epsilon)} - \eta \\ f = \frac{a+e}{\tan(\epsilon)} - \frac{k}{\sin(\epsilon)} \\ j = (a + e)\sin(\epsilon) + f\cos(\epsilon) \\ I_{fz} = \frac{\theta_5 - M_f e k}{\cos(\epsilon)} \\ i_{fy} = \frac{\theta_7 \cdot R_f}{\sin(\epsilon)} \\ i_{ry} = \frac{\theta_6 - i_{fy}}{R_f} R_r \end{cases} \quad (4.4)$$

Afterwards, the other parameters  $[\theta_9, \dots, \theta_{14}]^T$  are directly deduced by:

$$\begin{cases} \theta_9 = M_f e j + I_{fz} \sin(\epsilon) \\ \theta_{10} = -M_f j + M_r h + \theta_6 \\ \theta_{11} = -\frac{-\theta_7}{\tan(\epsilon)} \\ \theta_{12} = M_f e g - \eta F_{zf} \theta_{13} = I_{fz} + M_f e^2 \\ \theta_{14} = -M_f \cdot e + \frac{i f y}{R_f} \cdot \sin(\epsilon) = -\theta_2 - \theta_7 \end{cases} \quad (4.5)$$

The next step is to define the vector of the measured outputs. From the system dynamics of equation (4.2), we can write the following expressions:

$$\begin{cases} y_1 = -\frac{(Mh\ddot{\phi} + Mv_x\dot{\psi} + M\dot{v}_y - Ma_y)}{\theta_1} \\ y_2 = -\frac{(Mh\ddot{\phi} + \theta_1\dot{\psi} + Mv_x\dot{\psi} + M\dot{v}_y - Ma_y)}{\theta_2} \\ y_3 = \frac{-\theta_1 d_v - \theta_1 v_x \dot{\psi} + l_f F_{yf} - l_r F_{yr}}{\theta_3} \\ y_4 = \frac{-\theta_1 d_v - \theta_3 \dot{\psi} - \theta_1 v_x \dot{\psi} + l_f F_{yf} - l_r F_{yr}}{\theta_4} \\ y_5 = \frac{-\theta_1 d_v - \theta_3 \dot{\psi} - \theta_4 \dot{\phi} + l_f F_{yf} - l_r F_{yr}}{\theta_5} \\ y_6 = \frac{-\theta_1 d_v - \theta_3 \dot{\psi} - \theta_4 \dot{\phi} - \theta_5 \dot{\delta} + l_f F_{yf} - l_r F_{yr}}{v_x \theta_6} \\ y_7 = \frac{-\theta_1 d_v - \theta_3 \dot{\psi} - \theta_4 \dot{\phi} - \theta_5 \dot{\delta} + \theta_6 v_x \dot{\phi} + l_f F_{yf} - l_r F_{yr}}{v_x \theta_7} \\ y_8 = \frac{-Mh\dot{v}_y + \theta_4 \dot{\psi} + \theta_9 \dot{\delta} - \theta_{10} v_x \dot{\psi} - \theta_{11} v_x \dot{\delta} + Mhg \sin(\phi) + \theta_{12} \sin(\delta)}{\theta_8} \\ y_9 = \frac{-(\theta_2 \dot{v}_y + \theta_9 \dot{\phi} + \theta_5 \dot{\psi} + \theta_{13} \dot{\delta} + \theta_{11} v_x \dot{\phi} - \theta_{14} v_x \dot{\psi} + \theta_{12} d_x - \eta F_{yf} + \tau)}{\theta_{15}} \end{cases} \quad (4.6)$$

where  $d_v = \dot{v}_y + v_x \dot{\psi}$  and  $d_x = \sin \phi + \sin \epsilon \sin \delta$ .

Therefore, the system of equations have the following form:

$$\begin{cases} y_1 = f(y, \bar{\theta}_0, \theta_1) \\ y_2 = f(y, \bar{\theta}_0, \theta_1, \theta_2) \\ y_3 = f(y, \bar{\theta}_0, \theta_1, \theta_2, \theta_3) \\ \vdots \\ y_i = f(y, \bar{\theta}_0, \theta_1, \theta_2, \dots, \theta_j) \end{cases} \quad (4.7)$$

Where  $y_i$  is measurement outputs vector and  $\bar{\theta}_0$  is the initial value of the unknown parameters with  $i = 1, \dots, 9$  and  $j = 1, \dots, 15$ .

### 4.1.2 Optimization Problem Formulation

After defining the set of the unknown parameters to be identified, the next step is to setup the optimization problem. Any multi-objective optimization problem can be stated as:

$$\min_{x \in R^n} \mathcal{C}(\theta) = [C_1(\theta), C_2(\theta), \dots, C_9(\theta)] \quad (4.8)$$

Generally, it is an arduous task to find a solution  $\theta$  for the above stated problem that satisfies all objectives. To deal with this issue, we choose test scenarios that allows to decouple objectives resulting in a cascade identification scheme. Let consider the following multi-objective cost with its associated sensitivity and gradient:

$$\begin{cases} \text{Criteria} \rightarrow C_i(t_k) = \frac{1}{2} \cdot \sum (y_{i_m}(t_k) - y_i(t_k))^2 \\ \text{Sensitivity} \rightarrow S_i(t_k) = \frac{dy_i}{d\theta_j} \\ \text{Gradient} \rightarrow G_i(t_k) = \sum (y_{i_m}(t_k) - y_i(t_k)) \cdot S_i \end{cases} \quad (4.9)$$

Where  $y_{i_m}$  are the measured outputs,  $y_i$  are model simulated output and  $t_k$  is the current simple time.

As an example, to identify the parameter  $\theta_1$ , one select a short manoeuvre for the lateral motion in which, the second derivative of the steering angle is neglected, i.e.  $\ddot{\delta} \approx 0$ . From equations (4.2) and knowing that  $ma_y = F_{yf} + F_{yr}$ , we get  $y_1 = \ddot{\psi}$  such that:

$$m\dot{v}_y + \theta_1 \ddot{\psi} + mh\ddot{\phi} + mv_x \dot{\psi} = ma_y \quad (4.10)$$

From the above equation, we can deduce the expression of  $y_1$  and compute then its sensitivity  $S_1 = \frac{d\ddot{\psi}}{d\theta_1}$  and its gradient  $G_1$ . Next, the gradient algorithm is applied to estimate the value of the first parameter  $\theta_1$ . Further, the algorithm is repeated for each parameter after selecting the corresponding scenario as described a follows:

1. From an initial starting point  $\theta_i(t_0)$ , we calculate the criterion  $C_i(t_0)$  and the gradient  $G_i(t_0)$ .
2. Compute the new value:  $\theta_i(t_k) = \theta_i(t_{k-1}) - \alpha G_i(t_{k-1})$
3. Compute a new value of  $C_i(t_k)$  and  $G_i(t_k)$  taking  $\theta_i(t_k)$ .
4. If the second criterion is smaller keep the new parameter value of the corresponding  $\theta_i(t_k)$ . Increase  $\alpha$  for efficiency and increment the counter  $k + 1$ .
5. Else, keep the old value of  $\theta_i(t_{k-1})$  and reduce  $\alpha$  to seek a nearest local minimum.
6. Evaluate the stopping criteria for exit loop: accuracy on the criteria, the gradient, maximum number of effective iteration, tolerance between the last two values of  $\theta$ . For more detail see Algorithm (1).

### 4.1.3 Simulation Results

The test described in this section is carried-out on the *BikeSim* simulator. The accessible parameters are captured from the motorcycle's datasheet. The algorithm is tested during a track test on handling road course. Figures 4.1 show the rider steering torque and the trajectory of the conducted manoeuvre. The

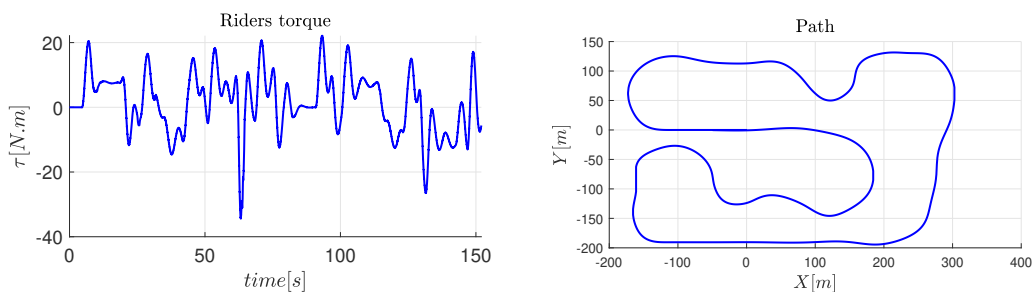


FIGURE 4.1: Riders torque and motorcycle path.

identification results of the multi-objective optimisation are summarized in the following Table 4.1. Where,  $\theta_i = [e_{34}, e_{36}, e_{44}, e_{45}, e_{46}, a_{45}, a_{46}, e_{55}, a_{66}]$  is the identified vector of interest which depends on the physical parameters of motorcycle. The other parameters are concluded from equation (4.5).

TABLE 4.1: Multi-Objective-Optimisation method.

	<i>Initial</i>	<i>Prior values</i>	<i>Identification</i>
Parameters	$\theta_0$	$\theta_r$	$\theta_i$
$e_{34}$	5	14.64	14.3073
$e_{36}$	0.1	0.1262	0.1519
$e_{44}$	20	24.7385	23.7342
$e_{45}$	2	5.0518	4.3416
$e_{46}$	0.1	0.2968	0.3141
$a_{46}$	0.1	0.8452	0.79503
$a_{45}$	4	4.304	4.1104
$e_{55}$	50	68.0442	68.1543
$a_{66}$	10	-11.45	-11.7332
$e_{56}$	*	0.1307	0.142
$a_{54}$	*	-96.69	-95.75
$a_{65}$	*	1.81264	1.77264
$a_{52}$	*	40.5384	38.0886
$e_{66}$	*	0.201	0.189
$a_{64}$	*	-0.9714	-0.9469

The objective is to validate the result of the identification method on the two-bodies motorcycle model. After the identification process, the estimated parameters are used to simulate the PTWV lateral dynamics and hence to validate the dynamics behaviour with respect to *BikeSim* data. To assess the performance of the algorithm, we report the track test generated by the input in figure 4.1. With the kind of this trajectory, the motorcycle lateral dynamics is largely excited. The following simulation results introduce the states of the PTWV lateral two-bodies dynamics in dashed red and the actual ones from *BikeSim* in blue.

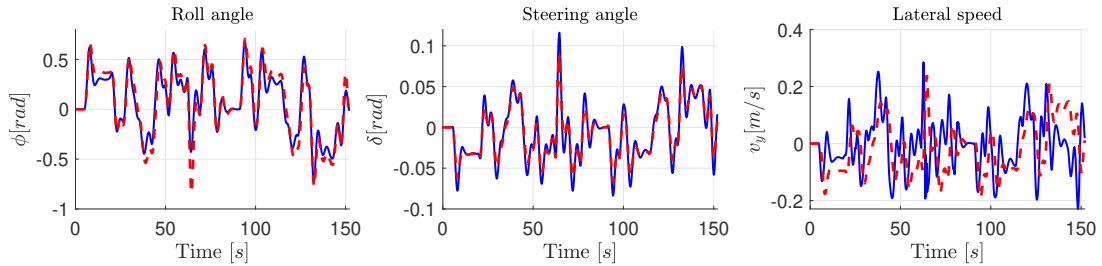


FIGURE 4.2: Comparison between the roll, steer angles and lateral speed of the identified model and the *BikeSim* motorcycle data.

Figures 4.2 illustrate the time variation of the roll angle, steering angle and the lateral speed that characterize the lateral dynamics recorded from *BikeSim*. These variables are compared to their corresponding states computed from the identified parameters. We can note that the errors between the identified states (dashed red) and the actuals data are practically acceptable except the lateral speed. Even if the considered scenario seems to be aggressive, the lateral velocity is a dynamic state that is not very excited in the PTWV dynamics. Indeed, figures 4.3 depict the comparison of the actual roll, yaw and steer rates with the estimated ones.

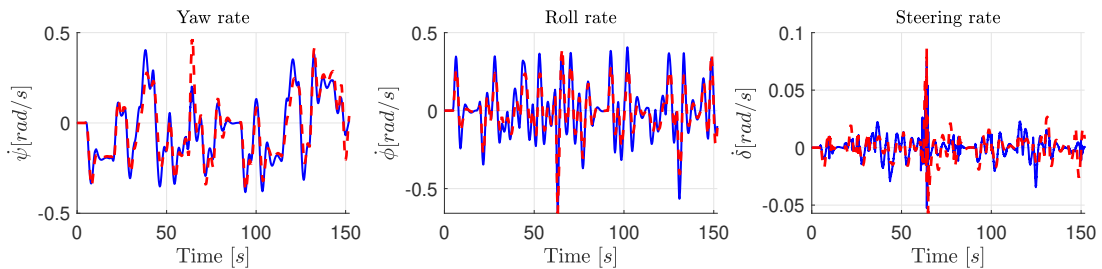


FIGURE 4.3: Comparison between the identified model and the *BikeSim* motorcycle data.

In the same way, figures 4.4 show the cornering front and rear forces as well as the lateral acceleration, these identified states are closely similar to the actual data. The results show that the model perfectly reconstructs the most of the dynamic states, hence the cornering behaviour of the motorcycle is well identified.

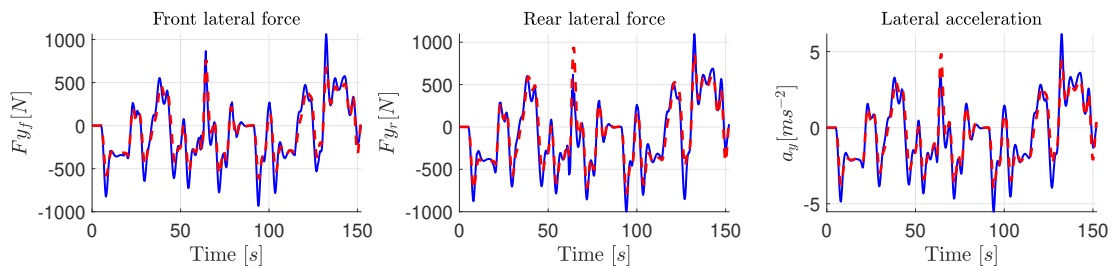


FIGURE 4.4: Comparison between the identified model and the *BikeSim* motorcycle data.

One can notice some differences between the identified model and the actual data. These identification errors come from the PTWV two-bodies modelling assumptions whereas *BikeSim* uses a non-linear eight-body model. Also, the accuracy of the identified parameters of the model depends on the initial parameter value and the step rate  $\alpha$  in each iteration of the algorithm. Further, we can notice also a large amplitude of the roll angle (about 35 deg). However, it will be recalled that the two-bodies model is theoretically valid only for small variations around the equilibrium position in a straight line ( $\phi = 0$ ). This extreme scenario shows that, we are reaching the limits of the model.

This section ends with a study of the identification errors. The errors between the identified model and the *BikeSim* states are quantified by mean of the Theil Inequality Coefficient (TIC), is the standardized root mean-squared error, used in the sensitivity analysis to measure the model predictive accuracy and to facilitate comparison between the actual and identified model (Woschnagg and Cipan, 2004). Note that, the identification errors are quantified also in terms of errors variation percentage, this coefficient is denoted "FIT", to compare the performance of the models that we have estimated.

$$TIC_i = \frac{\sqrt{\frac{1}{n} \sum (y_{im}(t_k) - y_i(t_k))^2}}{\sqrt{\frac{1}{n} \sum (y_{im}(t_k))^2 + \frac{1}{n} \sum (y_i(t_k))^2}} \quad (4.11)$$

$$FIT_i = 100 \frac{(1 - \|(y_i - y_{im})\|)}{\|(y_{im} - \text{mean}(y_{im}))\|}$$

where  $y_{im}$  are the actual observations containing  $n$  samples and  $y_i$  are the corresponding predictions, resulting from estimated parameters.

Table 4.2 quantifies the identification errors between the *BikeSim* variables and the identified states of the two-bodies model, confirms the efficiency with acceptable errors. The TIC is bounded by 0 and 1, the lower boundary is the ideal case of perfect identification. The small values of TIC and the percentage of the fit values, show a good forecast accuracy and prove the reliability of the model.

#	States			
	$\phi$	$\delta$	$v_y$	$\psi$
TIC	0.0974	0.1172	0.2924	0.0565
FIT%	79.9940	77.7522	66.2456	79.9202
#	$\dot{\phi}$	$\dot{\delta}$	$F_{yf}$	$F_{yr}$
TIC	0.1199	0.1962	0.1372	0.1113
FIT%	77.3422	62.7593	74.4299	78.6061

TABLE 4.2: Analysis of the estimated states for the tests conducted.

The results, from the identification process, are very promising. The comparison with *BikeSim* data demonstrates the potential of the identification procedure.

## 4.2 Levenberg-Marquardt (LM) Algorithm

This section describes another identification algorithm based on Levenberg-Marquardt (LM) estimation (Yu and Wilamowski, 2011, Hammar, 2015). The LM method combines the steepest descent and the Gauss-Newton algorithms. In our context, it is used to identify the front and rear body moment of inertia. Classically, in this estimation scheme, the objective function is usually defined as the difference between the model and the experimental responses, expressed through some kind of metric.

Let us assume that  $f(y, \dot{y}(\theta), \ddot{y}(\theta))$  is a generic response function which depends on a set of unknown parameters  $\theta$ , measurement output  $y$  and its times derivatives  $\dot{y}$ ,  $\ddot{y}$

$$f = \begin{Bmatrix} f_1 \\ f_2 \\ f_3 \end{Bmatrix} = \begin{Bmatrix} \dot{\psi}(y, \dot{y}(\theta), \ddot{y}(\theta)) \\ \ddot{\phi}(y, \dot{y}(\theta), \ddot{y}(\theta)) \\ \ddot{\delta}(y, \dot{y}(\theta), \ddot{y}(\theta)) \end{Bmatrix} \quad (4.12)$$

The sensitivities of the generic functions is described as as follow :

$$f_{\theta} = \frac{df}{d\theta} = \frac{\partial f}{\partial y} \frac{dy}{d\theta} + \frac{\partial f}{\partial \dot{y}} \frac{d\dot{y}}{d\theta} + \frac{\partial f}{\partial \ddot{y}} \frac{d\ddot{y}}{d\theta} \rightarrow \frac{\partial f}{\partial y} y_{\theta} + \frac{\partial f}{\partial \dot{y}} \dot{y}_{\theta} + \frac{\partial f}{\partial \ddot{y}} \ddot{y}_{\theta}$$

Where, the operator  $\frac{d(\cdot)}{d(\cdot)}$  denotes total derivatives, and the operator  $\frac{\partial(\cdot)}{\partial(\cdot)}$  denotes partial derivatives.  $y_{\theta}$ ,  $\dot{y}_{\theta}$  and  $\ddot{y}_{\theta}$  are state sensitivities.

### 4.2.1 Problem Statement

Identification methods are generally based on minimizing the difference between the measured outputs and the estimated outputs.

Let consider the following quadratic criterion  $J$  to be minimized:

$$\min J(t) = \frac{1}{2} \varepsilon^2(t) \quad (4.13)$$

where  $\varepsilon(t) = f(t) - \hat{f}(t)$  is the prediction error which represents the quadratic deviation between the generic responses function defined in equation (4.12) and the their real measurement from sensor. The LM algorithm requires the computation of the Jacobian matrix of the vector  $f$  with respect to the unknown parameter, such that:

$$J_{\theta} = \begin{bmatrix} \frac{\partial J}{\partial \theta_1} \\ \vdots \\ \frac{\partial J}{\partial \theta_j} \end{bmatrix} = \frac{\partial J}{\partial \theta} = \frac{\partial J}{\partial \varepsilon} \frac{\partial \varepsilon}{\partial \theta} \Rightarrow J_{\theta} = -\varepsilon \frac{\partial f}{\partial \theta} = -\varepsilon f_{\theta} \quad (4.14)$$

From equation (4.14), we define the following Hessian matrix:

$$J_{\theta\theta} = \frac{\partial(\varepsilon f_{\theta_i})}{\partial \theta_j} \rightarrow J_{\theta\theta} = f_{\theta_j}^T f_{\theta_i} \quad (4.15)$$

In order to make sure that the Hessian matrix  $J_{\theta\theta}$  is invertible, Levenberg-Marquardt algorithm introduces an approximation to the Hessian matrix such that  $H \simeq J_{\theta\theta} + \lambda I$  where,  $\lambda > 0$  is called combination coefficient and  $I$  is the identity matrix.

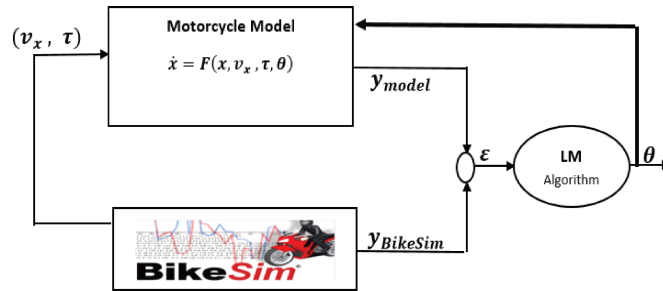


FIGURE 4.5: Block diagram of the LM method.

Figure 4.5 shows a practical implementation of the LM method where the the update rule can be expressed by the following:

$$\hat{\theta}^{(i+1)} = \hat{\theta}^{(i)} - H^{-1} J_{\hat{\theta}^{(i)}} \quad (4.16)$$

Finally, by defining the matrix  $Q_i$  as bellow, the standard LM process can be summarized by the following algorithm:

$$Q_i = \left\{ \begin{array}{cccc} \epsilon^T \epsilon & \epsilon^T \frac{\partial f_i}{\partial \theta_1} & \dots & \epsilon^T \frac{\partial f_i}{\partial \theta_n} \\ \left( \frac{\partial f_i}{\partial \theta_1} \right)^T \epsilon & \left( \frac{\partial f_i}{\partial \theta_1} \right)^T \frac{\partial f_i}{\partial \theta_1} & \dots & \left( \frac{\partial f_i}{\partial \theta_1} \right)^T \frac{\partial f_i}{\partial \theta_n} \\ \dots & \dots & \dots & \dots \\ \left( \frac{\partial f_i}{\partial \theta_n} \right)^T \epsilon & \left( \frac{\partial f_i}{\partial \theta_n} \right)^T \frac{\partial f_i}{\partial \theta_1} & \dots & \left( \frac{\partial f_i}{\partial \theta_n} \right)^T \frac{\partial f_i}{\partial \theta_n} \end{array} \right\} \quad (4.17)$$

---

**Algorithm 2: Levenberg-Marquardt (LM) : ( $\subseteq$ )**


---

**Require:**  $\theta_0(t_0)$ ,  $\lambda = 1$ ,  $stop = 0$ ,  $epsCrit = 10^{-5}$

```

1- if stop  $\neq$  1 then
  for( $t_{k-1} = t_0$ )  $\Rightarrow$ 
    Calculate  $J_0(\theta_0)$ ,  $G_0(\theta_0)$ ,  $H_0(\theta_0)$ , then :  $f_{i\theta}$  = the sensitivities function
     $S_i = [\epsilon_i f_{i\theta_j}]$ ,  $i=(1,2,3)$ ,  $j=(1,\dots,10)$ 
     $Q_i = S_i^T \times S_i$ ,
     $J_i = Q_i(1,1)$ ,  $G_i = Q_i(2:end,1)$ ,  $H_i = Q_i(2:end,2:end)$ 
     $J(\theta_0) = \sum_1^3 J_i$ ,  $G(\theta_0) = \sum_1^3 G_i$ ,  $H(\theta_0) = \sum_1^3 H_i$ 
2- then  $\hat{\theta}_1 = \theta_0(t) + (H(\theta_0) + \lambda I)^{-1} G(\theta_0)$ 
3- for( $\hat{\theta}_1$ )  $\Rightarrow$  Calculate  $J(\theta_1)$ ,  $G(\theta_1)$ ,  $H(\theta_1)$ , then :
4- if  $J(\theta_1) < J(\theta_0)$  then
   $\theta_1 = \theta_0$  and  $\lambda = \lambda/10$ 
5- else
   $\lambda = \lambda \times 10$  return to step 2
6- if  $(|J(\theta_1) - J(\theta_0)| < epsCrit)$  then
  return stop = 1;

```

---

## 4.2.2 Simulation Results

The LM estimation algorithm is evaluated using data from *BikeSim* simulator. We select a 8 bodies Sport Touring PTWV from the *BikeSim* datasets. The algorithm is evaluated on two different scenarios. The first test is a double lane change manoeuvre at a high speed of 100 km/h involving both accelerating and braking in a turn on flat curved road with a curvature radius 152.4 m and a high friction  $\mu = 0.85$ . This scenario aims to simulate an extreme riding behaviour since it highly excites the motorcycle in lateral dynamics.

Figures 4.6 and 4.11 introduce the steering torque  $\tau$ , the forward speed  $v_x$ , and the PTWV trajectory during the double lane change manoeuvre.

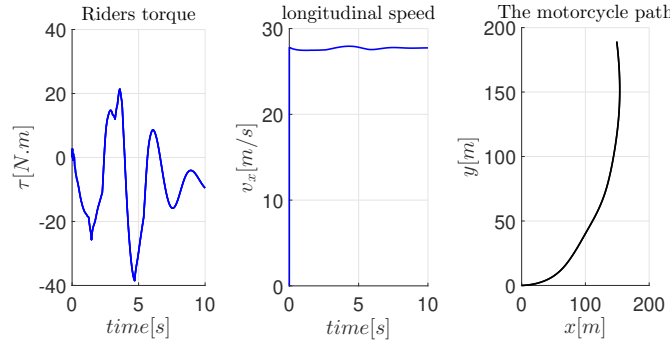


FIGURE 4.6: Test manoeuvre : double line change,  $v_x = 100$  km/h in circle road, on high-friction surface  $\mu = 0.85$  : Rider torque  $\tau$  - Longitudinal velocity - Path.

As mentioned in the previous sections, the generic response function  $f$  converges to true state when the unknown parameters are updated with the estimated values of the inertial parameters. Moreover, figures 4.7 show the generic response function  $f = \{\ddot{\psi}, \ddot{\psi}, \ddot{\delta}\}$  for the initial parameters. Then in Figures (4.8) after updating the inertial parameters convergence. Note that, the algorithm initialisation were willingly chosen different from the prior knowledge on the parameters to prove the ability to identify the true values and converge toward the actual generic response.

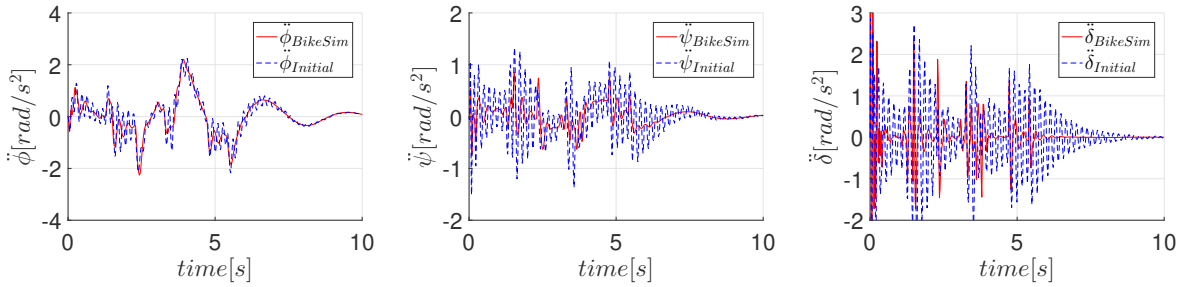


FIGURE 4.7: Generic responses (acceleration angles) estimation in initial parameters value  $\theta_0$  compared to actual responses.

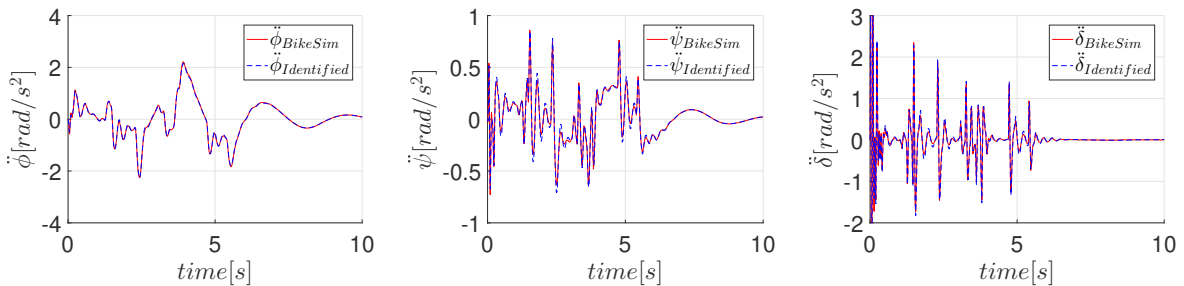


FIGURE 4.8: Generic responses (acceleration angles) estimation after updating parameters estimates value  $\theta_i$ , compared to actual responses

One can notice the significant mismatched between the actual response and the generic functions calculated from the initialisation. The results show that at the beginning when applying the initial value of parameters the model didn't match the actual generic responses, however, by updating the values of the identified parameters by LM method, the generic responses estimation closely match the simulated generic functions.

Table 4.3 summarizes the values of the identifiable inertial parameters. The lateral two-bodies model is a parameters varying system which depend on the forward speed  $v_x$ , hence, some parameters of this model depend on  $v_x$ . For this test, the forward speed is constant, one can easily deduce the value of the physical parameters by omitting the speed. These varying parameters are plotted in figure 4.9.

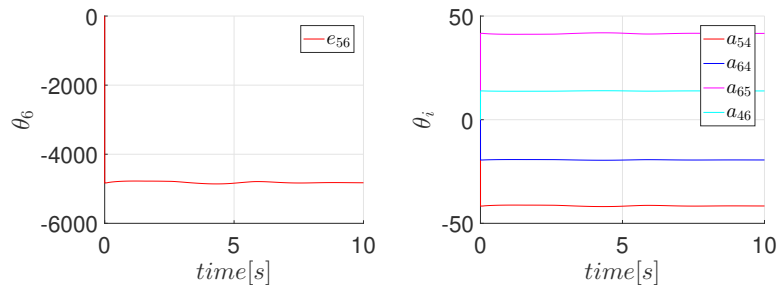


FIGURE 4.9: Combined inertial parameters estimates  $\hat{\theta}_i$ ,  $\hat{\theta}_6$ .

Furthermore, to test the effect of noises on the output vector, a Gaussian noise is added to outputs vector to realistically recreate real application scenarios. The variances for Gaussian noise is  $0.05rad/s^2$ . For a good identification, these residuals should be white, which statistically means that we have insignificant correlations for non-zero lags. Figures 4.10 plot the autocorrelation of the residuals error compared to that of a white noise. From the autocorrelation graphs and except at zero lag, the autocorrelation values of the residual errors lie within the autocorrelation of a white noise signal. From this, we conclude that the prediction errors are white Gaussian noise.

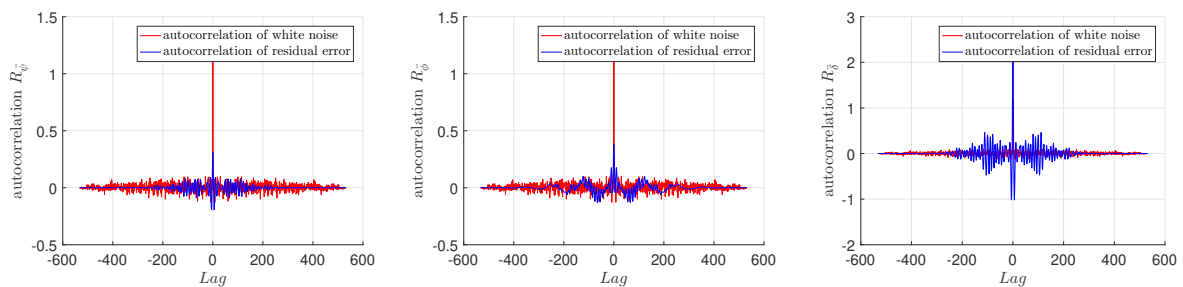


FIGURE 4.10: Correlation graph for white noise and residual error.

The second test deals with an oncoming traffic with rapid variable speed between 12 and 35  $m/s$  on handling road course including straight lines, large and narrow turns. This test is a very common scenario on real life riding situation. Figures 4.11 present the steering torque  $\tau$ , the forward speed  $v_x$ , and the PTWV trajectory of the track test.

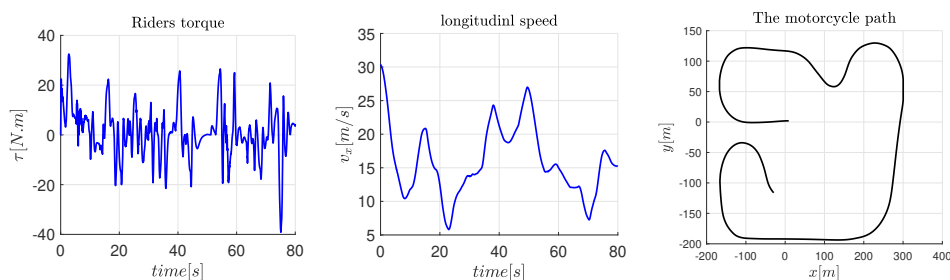


FIGURE 4.11: Test manoeuvre 2: oncoming variable speed, in road course with  $\mu = 0.85$  : Rider torque  $\tau$  - Longitudinal velocity - Path.

Whereas, figures (4.12) and (4.13) plot the generic response function  $f = \{\ddot{\psi}, \ddot{\psi}, \ddot{\delta}\}$ , first as function of the initial parameters, and then after the convergence of the algorithm by updating with the identified inertial parameters.

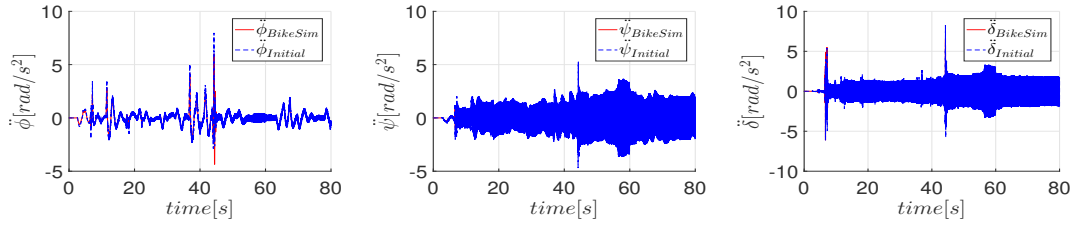


FIGURE 4.12: Generic responses (acceleration angles) estimation in initial parameters value  $\theta_0$  compared to actual responses.

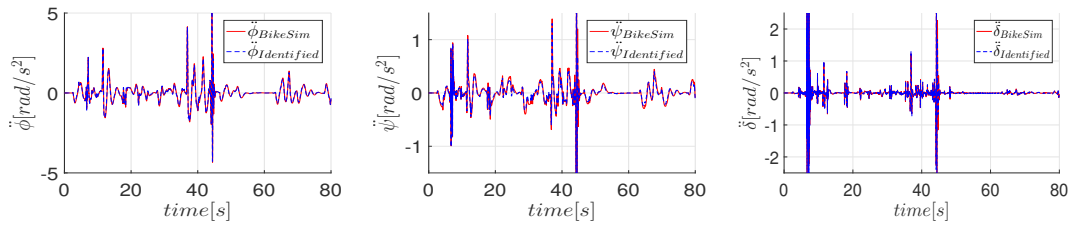


FIGURE 4.13: Generic responses (acceleration angles) estimation after updating parameters estimates value  $\theta_i$ , compared to actual responses.

As for the first test, the parameters which depend on the forward speed are plotted in figures 4.14.

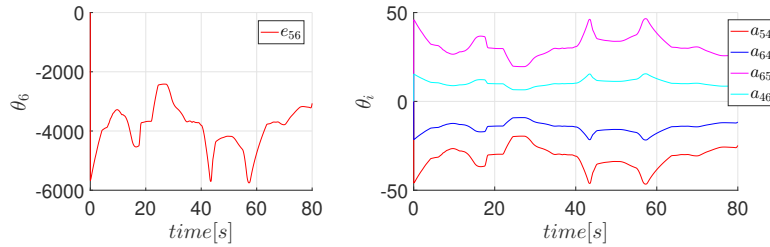


FIGURE 4.14: Combined inertial parameters estimates.

The final step is to analyse the residuals generated by LM method. The result on the autocorrelation of the residuals error compared to that of the white noise are given in figures 4.15. One can remark some small difference on the autocorrelation of the residuals error in the zero lag, specially on the generic response of the roll acceleration  $R_{\ddot{\phi}}$ . However, in general the autocorrelation sequence of the residuals looks like that of the white noise process which means that the generic response are well fitted. Hence, we conclude that the prediction errors have almost the same characteristics as a white Gaussian noise.

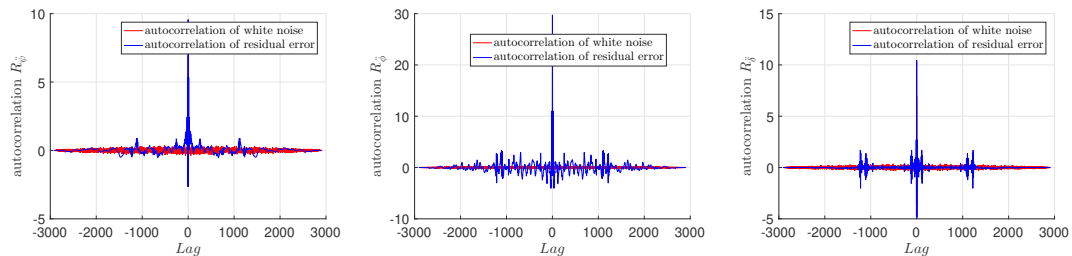


FIGURE 4.15: Correlation graph for white noise and residual error.

Table 4.3 presents parameters values estimates. For (\*) parameters, the estimated convergence is shown in figures (4.9) and (4.14). Where,  $\theta = [e_{44}, e_{45}, e_{46}, e_{55}, e_{56}, a_{54}, a_{56}, a_{64}, a_{65}, a_{46}]$  is the unknown vector of interest which represent the combined inertial parameters of motorcycle of the front and rear wheels, depending on :  $I_{f_{x,y,z}} = \{I_{f_x}, I_{f_y}, I_{f_z}\}$ ,  $I_{r_{x,y,z}} = \{I_{r_x}, I_{r_y}, I_{r_z}\}$ ,  $C_{rxz}$  and  $i_{y_{f,x}} = \{i_{r_y}, i_{f_y}\}$ .

TABLE 4.3: LM identification results

	<i>Initial</i>	<i>True values</i>	<i>Scenario1</i>	<i>Scenario2</i>
Parameters	$\theta_0$	$\theta_r$	$\theta_i$	$\theta_i$
$e_{44}$	1	34.7228	31.7914	28.2429
$e_{45}$	2	1.9632	0.968	-4.0424
$e_{46}$	0.1	0.6584	0.5	0.5
$e_{55}$	113	118.0202	119.78	119.9828
$a_{54}$	$-170 \times v_x$	$-175.0479 \times v_x$	*	*
$e_{56}$	$-1 \times v_x$	$-1.4622 \times v_x$	*	*
$a_{56}$	0.1	0.3827	0.5	0.5
$a_{64}$	$-1 \times v_x$	$-0.8685 \times v_x$	*	*
$a_{65}$	$1 \times v_x$	$1.4622 \times v_x$	*	*
$a_{46}$	$0.2 \times v_x$	$0.6818 \times v_x$	*	*

### 4.3 Final Remarks

This chapter deals with the identification of PTWV two bodies model. First, a methodology for iterative, cascade identification has been proposed for the estimation of unknown parameters. Equations that describe the lateral dynamic are used to form the resulting problem that is solved using a multiple-objective optimization algorithm adapted to the complexity of our model. In order to find the lateral dynamics we had to solve a linear gray-box problem by gradient method. The method has been successfully evaluated by simulation.

Second, we have described the design process of Levenberg-Marquardt (LM) identifier to estimate motorcycle combined inertial parameters, this approach uses sensitivity functions of generic responses developed using the Sharp motorcycle model to optimal estimation. The LM estimation improved convergence characteristics for state by updating inertial parameters, which are most apparent in the estimation of the generic responses: yaw, roll and the steering acceleration. The designed LM method, identified combined expression of inertial parameters and predicted the objective functions. The simulation results were very promising, the LM formulation is a good method to predict the response with very high accuracy. The main difficulty lies in the number of important parameters to estimate, which results in unrealized scenarios capable to excite the target modes for the identification.

### 4.4 Comparison and analysis

From the analysis of the identification results presented in chapters 3 and 4, we draw up the most important feature of each method. The simulation results were quite promising to prove that the identification approaches provide an interesting solution. However, as one may expects none of these identification strategies may behave perfectly for all the considerations, conditions and requirements. These explains our choice to consider different methods related to a specified motorcycle model. For the sake of comparison, we summarize all the presented design procedures in Table 4.4. Overall, the analysis of this table reveals the advantages and the drawbacks of each identification strategy from the required specifications. One of the main common contributions is that these methods take into account the motorcycle behavior rather than the black-box identification techniques. Besides, these identification procedures were validated by comparing with *BikeSim* data or real measurements. Obviously, the difficulties encountered concern mostly the choice of the persistent input to excite the dynamics of the motorcycle.

Approach	Considerations	Parameters and Advantages	Disadvantages
<i>Static Tests</i> <i>Practical method</i>	Datasheet No sensors Technical Tools for data collection Rigid body model	CoG position: $a, b, h$ Wheelbase $e$ Mass $m$ Wheel Radius: $R_f, R_r$ Caster $\epsilon$	No convergence Need physical efforts
<i>Gradient</i> <i>Descent</i>	<i>BikeSim</i> data Rigid body model Iterative procedure	Inertial parameters: $I_x, I_z$ No second derivative	Prior values Step rate $\alpha$ Need observer Input excitation
<i>Algebraic</i> <i>Method</i>	<i>BikeSim</i> data Rigid body model	Inertial parameters: $I_x, I_z$ Without initial conditions On-line and real time	No convergence proof Requires Input excitation Bad conditioning Computation complex
<i>Multi-</i> <i>Optimization</i> <i>Algorithm</i>	<i>BikeSim</i> data Two-bodies model Recursive Cascade	Combination's of geometric and inertial parameters $\theta_i, i = \{1, \dots, 15\}$ No need to second derivative	Prior values Time consuming Need observer
<i>Levenberg-</i> <i>Marquardt</i> <i>Algorithm (LM)</i>	<i>BikeSim</i> data Two-bodies model Recursive	Combined inertial parameters $\theta_i, i = \{1, \dots, 10\}$ depend on $\{I_{f_x}, I_{f_y}, I_{f_z}\}$ , $\{I_{r_x}, I_{r_y}, I_{r_z}\}, C_{r_{xz}}$ $\{i_{r_y}, i_{f_y}\}$ .	Prior values Need differentiator for second derivatives Need observer

TABLE 4.4: Comparison table: Advantages/disadvantages of the presented parametric identification for PTWV.

## Conclusions

This section concludes all the presented identification design procedures. We have described five estimation strategies to achieve the identification of the most important unknown parameters of the two motorcycle models.

For the first single rigid model, three design methods were considered in chapter 3 to identify the center of gravity (CoG) position and to estimate motorcycle inertial and geometric parameters using static test, an algebraic identification approach compared to an iterative gradient decent algorithm. Concerning the Sharp two-bodies model, two methods were proposed to identify parameters of the motorcycle model in chapter 4. The first method was a cascade recursive optimization, in which, equations that describe the lateral dynamics are used to form the resulting problem that is solved using a multiple-objective optimization algorithm adapted to the complexity of our model. The second design process was a Levenberg-Marquardt (LM), in which, the parametric identification is modeled based on minimizing the difference between measured responses and calculated responses from a mathematical model. The LM estimation improved convergence characteristics for state by updating inertial parameters, which are most apparent in the estimation of the generic responses.

Despite the fact that the motorcycle identification state-of-the-art was very limited in literature, the proposed approaches were inspired from other existing application and revisited in order to adapt the methods to our requirements. Note that the identification methods does not offer the possibility to take into account the uncertainties of modeling, because, they are designed from algebraic manipulations. In this case, it would be interesting to search for a more robust methods to get a good performance in the presence of uncertain parameters or noisy measurements. In this context, we have initiated several works on the parametric identification with more robust methods. To go even further, we have proposed observers based identifiers able to simultaneously estimate the dynamic states and identify the parameters of the model. These new estimation methods will be presented in the next chapters.

## Part III

# Model-based Observers for PTWV Estimation and Identification



## Introduction

THE growing need of safety for powered two wheeled vehicles (PTWV) has given rise to serious open questions related to estimation problem. Yet, the elaboration of advanced rider assistance systems (ARAS) to enhance safety issue, depends basically on motorcycle motion states such as steering behavior, roll angle and tire/road interaction. The evolution of these states depends strongly on the riders' steering torque and steer angle applied on the motorcycle handlebar, vehicle's parameters such that tire cornering stiffness, PTWV mass and inertia moment and the infrastructure geometry like the road bank angle which is very useful to detect the rollover and sideslip angles and thus detect a skidding motorcycle. While some states are readily measured with inexpensive sensors as the yaw rate, others states must be estimated by more sophisticated means for instance the tire cornering forces. Safety systems nowadays available collect some states from integration of inertial sensors, but this estimation method is subject to errors accumulation and uncertainties from road geometry, slope and bank angles. Therefore, building up an ARAS requires a precise knowledge, at every instant, of the vehicle's dynamics throughout physical or virtual sensors. This topic is one of our research interest which intends to develop ARAS systems starting from a minimum set of vehicle self-integrated sensors to acquire measured states. In this scope, model-based estimators are interesting to overcome previous shortcomings in order to provide estimates of unmeasured states and relevant parameters.

Throughout the last half century, observation theory has continuously evolved from the Luenberger observer for linear systems (Luenberger, 1966), to the more recent state and unknown input observers for nonlinear systems (Koenig, 2006). Various versions of unknown input observers were studied (Darouach and Boutat-Baddas, 2008), such as reduced-order, minimal-order and full-order observers. In which, the necessary and sufficient conditions for the existence of the observer are established. Further, new reformulation of this observer, by introducing high order sliding mode, is also exposed in (Fridman, Levant, and Davila, 2007). Under which, the sufficient and necessary conditions of strong observability and detectability are formulated in the terms of the system relative degrees with respect to unknown inputs. On the other hand, an extensive use of polytopic and Takagi-Sugeno representation is also undertaken, which giving rise to an ease transposition of the over-mentioned observation techniques for nonlinear systems (Ichalal and Mammar, 2015). In (Lam, Li, and Liu, 2013), a new category of fuzzy-observer-based controllers is proposed to stabilise non-linear plants. Moreover, the problem of the simultaneous state and parameters estimation, in the case of nonlinear continuous-time systems, is also studied. In (Chong et al., 2015), an hybrid scheme is considered, in which state observers are achieved for some nominal parameter values and, at every time instant, a criterion is designed to select one of the pre-designated observers providing state and parameter estimates updates. Although providing good estimation accuracy, this approach yields to an over-dimension problem even for the linear systems case. Withal these approaches, several open topics in estimation methods need more thorough investigations as for structural constraints and rank condition (Bolandhemmat, Clark, and Golnaraghi, 2012).

Concerning PTWV estimation research, there is a growing body of literature for observer design, one can cite (Gasbarro et al., 2004b; Corno, Savaresi, and Balas, 2009; Boniolo, Savaresi, and Tanelli, 2009a; Teerhuis and Jansen, 2012b; Boniolo, Savaresi, and Tanelli, 2012; Teerhuis and Jansen, 2012b; De Filippi et al., 2012; Boniolo, Savaresi, and Tanelli, 2012; Corno, Panzani, and Savaresi, 2013; Dabladji et al., 2016).

Almost references, the estimation of the PTWV dynamics is done by considering restrictive assumptions regarding riding motorcycle practices, decoupling motion or independent behavior, known tire friction or under a constant speed assumption, road geometry and tire-road contact has often been neglected (Chabane et al., 2012; Dabladji et al., 2015). These assumptions simplify the estimation problem but, it may lead to an inaccurate reconstruction with respect to the real dynamics. In fact, motorcycle characteristics and road conditions may change for different riding situations. Indeed, the road banking for instance, has a direct influence on motorcycle lateral motions to achieve safety speeds and desired control on difficult road conditions. The estimating of the road bank angle is a challenging task to evaluate the infrastructure impact and to improve the estimation of the side slip angle on tilted road surfaces. In addition, hard acceleration or braking is an unsafe riding which often caused motorcycles crashes. Thereby, the estimation of rectilinear motion highlights certain dynamic aspects that also affect PTWV safety, such as, overturning during braking or wheeling in acceleration (Evangelou, 2004).

To the authors' best knowledge, the simultaneous estimation of the lateral dynamics and the road geometry was treated on vehicles and those methods developed for four-wheeled vehicles are not necessarily adequate for motorcycle Dahmani et al., 2011. Also, the coupling motion of the lateral and longitudinal dynamics of two wheeled vehicle have not received much attention in the literature. Besides, as discussed in the previous

chapter a very few works deal with the PTWV parameters identification. Thereby, the convergence of state estimation approach jointly with parametric identification algorithm needs more deep exploration (Chong et al., 2015). Alternative approaches suggest the use of observer-based identification. In this scope, adaptive observers present a convenient approach to deal with both dynamics states and parameters estimation (Dixit and Suryanarayanan, 2008; Garimella and Yao, 2003). Moreover, the matching constraint in unknown input observer design is also a challenging issue for motorcycle state and parameters identification. Moreover, designing unknown input observer for PTWV, which meets some requirements, as the matching constraint and the relative degree with respect to unknown part, constitutes a complementary challenge. As matter of fact, many challenges are still open with respect to the estimation unknown states and the identification of a set of optimal system's parameters from the available input-output data and a prior knowledge about the PTWV's behavior.

Regarding these requirements, our work deals with the previous challenges in estimation PTWV dynamics. To do this, we propose two observers for states estimation, first, an Unknown Input Observer (UIO) is designed for road and steering dynamics reconstruction. Then, we were interested in both lateral and longitudinal dynamics estimation, in this scope, an Interconnected Fuzzy Observer (IFO) for PTWV was designed. Further, the convergence of state estimation approach jointly with parametric identification algorithm is one of our keen of interest. To fit some needs, we suggest two observers-based identifier to estimate simultaneously the model parameters and the unknown states. The first one is an LPV Luenberger-adaptive observer (LAO) synthesized for motorcycle state estimation and tire cornering stiffness identification, and the second one is a Delayed Unknown Input Observer (DUIO) for nonlinear system concerned the states and model parameters when the mismatched condition is not fulfilled.

The outlined observers are designed considering linear parameter-varying (LPV) motorcycle model and a certain number of valid measurements, taking into account real constraints such as the variations in the longitudinal speed during the synthesis of the observers. The result is formalized using Lyapunov theory where the observer's gains are computed by resolving an optimization problem in form of a set of a Linear Matrix Inequality (LMI) aiming to minimize the estimation error. In addition, these observers require realistic instrumentation with sensors or a high-end simulator. It requires an encoder installed on the steering mechanism, a gyroscope and an accelerometer (IMU), which are assumed to be placed near the Gravity Center (CoG) of the motorcycle. In this part, it will be assumed that these measurements are directly available in the reference frame used for the dynamic modeling of the PTWV. It will be recalled that the sensors provide the measurements in the sensor reference frame attached to the vehicle that is different from the body reference frame. Indeed, it is affected in particular with the roll and pitch motions. Nevertheless, under some hypothesis, there are simple algebraic relations that allow reconstructing the measurements in the body reference frame. For additional information, the reader may refer to section 2.11 for calibration algorithm which explains a practical procedure to align the measurement data. It will be recalled that these estimators have been designed to answer real technical issues taking into account the physical behavior of PTWV riding. For this end, the validation for each observer is performed either with the *BikeSim* simulator or with experimental data. In a first step, the observers are validated under ideal conditions, without noise consideration or parametric uncertainties. The purpose of this latter is to confirm the observer's design and to prove convergence from a theoretical point of view. To go even further, we also studied the robustness of the observers with respect to the measurement noises or parameters uncertainties based on the acquired data. In a second step, a much more advanced validation is proposed based on real data acquired on the scooter of the laboratory. Note that many observers for the PTWV dynamic in the literature have significant gaps in experimental validation. Indeed, many contributions focused at the validation on the synthesis dynamic model of PTWV. But the latter is often based on a set of nominal parameters exactly known and in the presence of ideal sensors (no-noise). Even if the results of such a validation are very promising, they are often disappointing in practice. Finally, this part ends with a conclusion that takes up important notions about the developed observers. Each of these chapters is constructed in a nearly identical frame. A first section introduces the theoretical prerequisites and the motorcycle LPV model, a second addresses the formulation of the problem and the necessary consideration to rewrite a state space representation for the synthesis of the observer. A last section presents the validation results, discussed either on *BikeSim* or on a much more realistic tests. Finally, a few general remarks conclude each chapter.

# Chapter 5

## Road and Steering Dynamics Reconstruction

### Abstract

This chapter deals with the estimation of both motorcycle lateral dynamics and road geometry reconstruction. It discusses the synthesis of a linear parameter varying (LPV) unknown input observer (UIO) for the estimation of the whole motorcycle dynamic states. These last include road banking angle and the rider's steering torque taking into account the variation of the forward velocity. As discussed, some dynamic states are not directly measurable or the sensors to acquire data are too expensive. Even without prior information on these states, the unknown input observers allow the estimation of the unmeasured dynamics under certain conditions. In addition, using automatic tools such as differentiation techniques, makes it possible to reconstruct the Unknown Inputs (UI) from the estimated states and the derivative of the output vector. The theoretical aspects and the practical validation of this idea were published in Fouka et al., 2018c.

The major contribution of the proposed observer is the adaptation of the UIO concept to the case of the PTWV with road bank angle consideration. Henceforth, the observer is studied to satisfy the asymptotic convergence of the estimation error based on Lyapunov theory. The main idea consists in getting a set of conditions expressed in linear matrix inequalities (LMIs) formalism to design an observer transformed into a polytopic form, which estimate a part of the motorcycle dynamics independently of the ridersteering torque and/or roll angle taken into account the variation of the longitudinal velocity. This chapter is organized as follows. First, we present very briefly a modified observable version of the Linear Parameter-Varying (LPV) motorcycle out-of-plane model considering the road bank. In the same section 5.1, we will illustrate the observer design and present the convergence analysis applied to the estimation of the lateral dynamics of the PTWV. In section 5.3, the UIO will be tested off-line on experimental data obtained during a test setup on the Scooter of the laboratory. Simulation results of experimental test are provided to confirm the efficiency of the proposed design method.

### 5.1 LPV Observer Design

The PTWV dynamics model can be written in a LPV form as following:

$$\begin{cases} \dot{x}(t) &= A(\zeta)x(t) + G(\zeta)\nu(t) \\ y(t) &= Cx(t) \end{cases} \quad (5.1)$$

where  $x(t) \in \mathbb{R}^n$  denotes the state vector and  $x = [\delta, v_y, \psi, \phi, \dot{\delta}, F_{yf}, F_{yr}]^T$ .  $y(t) \in \mathbb{R}^{n_y}$  is the measured output vector.  $\nu(t) = [\phi, \phi_r, \tau]^T \in \mathbb{R}^p$  is the vector of the unknown inputs including roll angle  $\phi$ , road

bank angle  $\phi_r$  and the rider steering torque  $\tau$ . The matrices  $A(\zeta)$  and  $G(\zeta)$  are parameter varying with appropriate dimensions. We assume that  $\dim(y(t)) > \dim(\nu(t))$ .

The PTWV dynamic model (5.1) is transformed to a set of LTI interconnected model by using Takagi-Sugeno (TS) fuzzy structure. An effective choice is the use of sector nonlinearity approach as described in Tanaka and Wang, 2004. We consider one varying parameter  $\zeta(t)$  as the forward speed of the PTWV  $v_x(t)$  assumed to be accessible in realtime with its first time derivative. With one nonlinearity, the model (5.1) is described with 2 LTI sub-models as:

$$\begin{cases} \dot{x}(t) &= \sum_{i=1}^2 \eta_i(\zeta) (A_i x(t) + G_i \nu(t)) \\ y(t) &= Cx(t) \end{cases} \quad (5.2)$$

where  $\eta_i(\zeta)$  are the nonlinear weighting functions satisfying the following convex sum property:

$$\begin{cases} \sum_{i=1}^r \eta_i(\zeta) = 1 \\ 0 \leq \eta_i(\zeta) \leq 1 \end{cases} \quad \text{with} \quad \begin{cases} \eta_1 = \frac{v_{x_{\max}} - v_x}{v_{x_{\max}} - v_{x_{\min}}} \\ \eta_2 = \frac{v_x - v_{x_{\min}}}{v_{x_{\max}} - v_{x_{\min}}} \end{cases} \quad (5.3)$$

where  $r = 2^{n_\zeta}$  represents the number of local sub-models defines and  $n_\zeta$  is the number of nonlinearities ( $r = 2$ ).

We aim to design an unknown input observer for the PTWV TS model (5.2) to estimate the state vector  $x(t)$  and the unknown inputs vector  $\nu(t)$ . For this, let consider the following UIO (Fouka et al., 2018c:

$$\begin{cases} \dot{z}(t) &= N(\zeta, \dot{\zeta})z(t) + L(\zeta, \dot{\zeta})y(t) \\ \hat{x}(t) &= z(t) - H(\zeta)y(t) \end{cases} \quad (5.4)$$

where  $\hat{x}(t)$  and  $\hat{y}(t)$  denote the estimated state and output vectors respectively.  $N(\zeta, \dot{\zeta})$ ,  $L(\zeta, \dot{\zeta})$  and  $H(\zeta)$  are the observer's matrices to be determined to ensure asymptotic convergence of the error even in the presence of unknown inputs.

**Assumption 5.1.** *To design a stable unknown input observer, the well-known conditions for the existence of the UIO are given by the following assumption (Darouach, Zasadzinski, and Xu, 1994):*

1. The pair  $(A(\zeta), C)$  is detectable  $\forall \zeta(t) \in \Delta$ , where  $\Delta$  defines the following set:

$$\Delta = \left\{ \zeta \in \mathbb{R} \mid \zeta_{\min} \leq \zeta \leq \zeta_{\max}, \dot{\zeta}_{\min} \leq \dot{\zeta} \leq \dot{\zeta}_{\max} \right\} \quad (5.5)$$

2.  $\text{rank}(CG(\zeta)) = \text{rank}(G(\zeta))$ ,  $\forall \zeta(t) \in \Delta$ , is satisfied.

According to equations (5.2) and (5.4), the state estimation error is given by:

$$e(t) = x(t) - \hat{x}(t) = (I + H(\zeta)C)x(t) - z(t) = P(\zeta(t))x(t) - z(t) \quad (5.6)$$

By differentiating the previous equation, and knowing that  $z(t) = P(\zeta)x(t) - e(t)$ , the error dynamics is:

$$\begin{aligned}\dot{e}(t) &= \dot{P}(\zeta, \dot{\zeta})x + P(\zeta)\dot{x} - \dot{z} \\ &= N(\zeta, \dot{\zeta})e + (\dot{P}(\zeta, \dot{\zeta}) + P(\zeta)A(\zeta) - N(\zeta, \dot{\zeta})P(\zeta) - L(\zeta, \dot{\zeta})C)x(t) + P(\zeta)G(\zeta)\nu(t)\end{aligned}\quad (5.7)$$

If the following conditions hold:

$$\dot{P}(\zeta, \dot{\zeta}) + P(\zeta)A(\zeta) - N(\zeta, \dot{\zeta})P(\zeta) - L(\zeta, \dot{\zeta})C = 0 \quad (5.8)$$

$$P(\zeta)G(\zeta) = 0 \quad (5.9)$$

The estimation error dynamics will be reduced to:

$$\dot{e}(t) = N(\zeta, \dot{\zeta})e(t) \quad (5.10)$$

In which,  $N(\zeta, \dot{\zeta})$  must be Hurwitz.

The convergence of the estimation error in equation (5.7) is studied by introducing a quadratic Lyapunov function  $V(e(t))$ . This analysis allows to find the observer gains under optimization conditions. Let consider the following quadratic Lyapunov function :

$$V(e(t)) = e(t)^T Q e(t), \quad Q = Q^T > 0 \quad (5.11)$$

By using the error dynamics in equation (5.10), the time derivative of the Lyapunov function can be written as:

$$\dot{V}(t) = e(t)^T \left( N(\zeta, \dot{\zeta})^T Q + Q N(\zeta, \dot{\zeta}) \right) e(t) \quad (5.12)$$

Next we replace  $P(\zeta) = I + H(\zeta)C$  in the first equality constraints equation (5.8), we get:

$$N(\zeta, \dot{\zeta}) = \Gamma(\zeta, \dot{\zeta}) - K(\zeta, \dot{\zeta})C$$

where  $\Gamma(\zeta, \dot{\zeta}) = \dot{P}(\zeta, \dot{\zeta}) + P(\zeta)A(\zeta)$  and  $K(\zeta, \dot{\zeta}) = N(\zeta, \dot{\zeta})H(\zeta) + L(\zeta, \dot{\zeta})$ . By using the previous equation of  $N(\zeta, \dot{\zeta})$ , the error dynamics becomes:

$$\dot{e}(t) = (\Gamma(\zeta, \dot{\zeta}) - K(\zeta, \dot{\zeta})C)e(t) \quad (5.13)$$

and the time derivative of the Lyapunov function in equation (6.23) is transformed to:

$$\dot{V} = e^T \left( \Gamma(\zeta, \dot{\zeta})^T Q - C^T R(\zeta, \dot{\zeta})^T + Q \Gamma(\zeta, \dot{\zeta}) - R(\zeta, \dot{\zeta})C \right) e \quad (5.14)$$

where  $R(\zeta, \dot{\zeta}) = QK(\zeta, \dot{\zeta})$

**Theorem 5.1.** *The state estimation error converges asymptotically toward zero if there exist a symmetric positive definite matrix  $Q \in \mathbb{R}^{n \times n}$  and a matrix  $R \in \mathbb{R}^{n \times ny}$  satisfying the Lyapunov inequality below:*

$$\Gamma(\zeta, \dot{\zeta})^T Q + Q\Gamma(\zeta, \dot{\zeta}) - R(\zeta, \dot{\zeta})C - C^T R(\zeta, \dot{\zeta})^T < 0 \quad (5.15)$$

It follows that  $V(e) = e^T Q e > 0$  defines a common quadratic Lyapunov function for the observer.

Note that the Lyapunov inequality (5.15) depends on the varying parameters  $\zeta$  and its derivative  $\dot{\zeta}$ . In order to derive LMI conditions that ensure the asymptotic convergence of the state estimation error, the polytopic approach is used.

To solve this problem, a TS sector nonlinearity approach is considered once again :

$$\begin{aligned} \Gamma(\zeta, \dot{\zeta}) &= \sum_{i=1}^r \eta_i(\zeta, \dot{\zeta}) \Gamma_i \\ K(\zeta, \dot{\zeta}) &= \sum_{i=1}^r \eta_i(\zeta, \dot{\zeta}) K_i \end{aligned} \quad (5.16)$$

and the observer matrices  $N$  and  $L$  can be expressed by:

$$\begin{cases} L(\zeta, \dot{\zeta}) &= \sum_{i=1}^r \eta_i(\zeta, \dot{\zeta}) L_i \\ N(\zeta, \dot{\zeta}) &= \sum_{i=1}^r \eta_i(\zeta, \dot{\zeta}) N_i \\ H(\zeta) &= \sum_{i=1}^r \eta_i(\zeta) H_i \end{cases} \quad (5.17)$$

Moreover, the performances of the observer can be improved by pole assignment in an LMI region to ensure an acceptable transient response. The poles of the estimator are considered in the complex plane region, this region can be represented as an LMI region given by the stability margin  $\alpha > 0$  in a subset  $\Theta$  of the complex plane such that the matrix  $\Gamma_i$  is said  $\Theta_i$ -Stable when its spectrum  $\lambda(\Gamma_i)$  belongs to region  $\Theta_i$  (Patton, Chen, and Lopez-Toribio, 1998).

$$\Theta_i = \{z = x_z + i.y_z \in \mathbb{C} \mid \text{Re}(z) \leq -\alpha \Leftrightarrow z + \bar{z} + 2\alpha < 0\} \quad (5.18)$$

where  $\mathbb{C}$  is the set of complex numbers, and  $\bar{z}$  denotes the complex conjugate of  $z$ .

Using the convex sum property of the weighting functions, sufficient LMI conditions ensuring asymptotic stability in LMI region are obtained as follows :

$$\Gamma_i^T Q + Q\Gamma_i - C^T R^T - RC + 2\alpha Q < 0, \quad i \in (1, \dots, r) \quad (5.19)$$

Where,  $R_i = QK_i$  and  $Q = Q^T > 0$ . The equations provide a way of ensuring the eigenvalues within a specific region.

Based on the stability analysis of the lyapunov quadratic function, sufficient observer conditions are derived in order to determine the observer gains which stabilize the error dynamics. Hence, if the LMI constraints (5.19) are verified, the state estimation error in equation (5.13) converges asymptotically towards zero. The gain of the observer are computed as follow:

1. The LMI problem includes the following condition to compute the matrices  $H(\zeta)$  as follows:

$$\begin{cases} P(\zeta)G(\zeta) = 0 \\ P(\zeta) = I + H(\zeta)C \end{cases} \quad (5.20)$$

$$H(\zeta) = -G(\zeta)(CG(\zeta))^\dagger$$

The solution of this equation depends on the rank of matrix  $CG(\zeta)$  and  $H(\zeta)$  exists if  $\text{rank}(CG(\zeta)) = \text{rank}(G(\zeta))$ . Since  $CG(\zeta)$  is of full column rank,  $(CG(\zeta))^\dagger = \left[ (CG(\zeta))^T (CG(\zeta)) \right]^{-1} (CG(\zeta))^T$  is the left pseudo-inverse of the matrix  $(CG(\zeta))$ . Whereas  $H_i = H(\zeta_i)$ ,  $\zeta_i = (\zeta_{min}, \zeta_{max})$

2. The gains of the observer are computed as follows:

$$\begin{aligned} K_i &= Q^{-1}R_i \\ N_i &= \Gamma_i - K_iC \\ L_i &= K_i - N_iH_i \end{aligned} \quad (5.21)$$

Note that the matrices  $N(v_x, \dot{v}_x)$ ,  $L(v_x, \dot{v}_x)$  and  $H(v_x)$  depend on the longitudinal velocity  $\zeta = v_x$  and its derivative  $\dot{\zeta} = \dot{v}_x$ . These varying parameters are bounded. Henceforth, the gain matrices can be expressed in TS form using the non-linear polytopic sectors. Finally, the goal is to find a stable gain matrix  $N(v_x, \dot{v}_x)$  (Hurwitz) and ensures the asymptotic convergence of the estimation error to zero. To do this, Lyapunov's theory is used to address the error stability. To sum up, the design of the UIO comes down to find the matrix  $H_i$  satisfying the convergence conditions (5.19) and the two conditions of existence (5.8 and 5.9), then computing a vector  $K_i$  so that the matrix  $N_i = \Gamma_i - K_iC$  is a Hurwitz matrix. In other words,  $H_i$  exists if  $\text{rank}(CG(\zeta)) = \text{rank}(G(\zeta))$  and if the system (5.1) is detectable. Once the LMIs are solved, the gain matrices of the observer  $K_i$ ,  $N_i$  and  $L_i$  are reconstructed. Moreover, in the observer model (5.4) there is no term related to the input vector since the latter is included in the vector of the unknown part. In the next section 5.2, the estimation of the unknown inputs is discussed.

## 5.2 Unknown Input Estimation

After estimating the states of the system, the unknown inputs can be estimated by a simple dynamic inversion. From the output equation  $y = Cx$ , one can write:

$$\dot{y}(t) = CA(\zeta)x(t) + CG(\zeta)\nu(t)$$

Since the condition  $\text{rank}(CG(\zeta)) = \text{rank}(G(\zeta))$  is satisfied, it follows:

$$\nu(t) = \begin{bmatrix} \phi(t) \\ \phi_r(t) \\ \tau(t) \end{bmatrix} = (CG(\zeta))^\dagger (\dot{y}(t) - CA(\zeta)x(t)) \quad (5.22)$$

When the state estimation error  $e(t)$  converges to zero, we have  $\hat{x}(t) \rightarrow x(t)$ , then the following UI estimation  $\hat{\nu}(t)$  is obtained by the following equation :

$$\hat{\nu}(t) = (CG)^\dagger (\dot{y}(t) - CA(\zeta)\hat{x}(t))$$

In which, the convergence of  $\hat{\nu}$  toward  $\nu$  can be analyzed by defining the unknown input estimation error

$$e_\nu(t) = \nu(t) - \hat{\nu}(t) = -(CG)^\dagger CA(\zeta)e(t), \quad \forall \zeta(t) \in \Delta$$

knowing that  $e(t)$  converges asymptotically to zero, then  $e_\nu(t)$  also converges asymptotically to zero. According to Lyapunov formulation, the state and unknown input errors converge asymptotically to zero in order to achieve an accurate estimation of the states of the motorcycle and the torque applied on the handlebar.

### 5.3 Experimental Results

This section aims to present the experimental results of the proposed UIO. The test scenario is carried out by using the Scooter on urban road within normal riding conditions. Recall that, the UIO observer estimates the lateral dynamics using the measured states  $\phi$ ,  $\psi$ ,  $a_y$  and  $\delta$  with respect to the vehicle's forward speed  $v_x$  varying from  $7m/s$  on  $18m/s$  as depicted in figure 5.1. Applicability conditions of the UIO are expressed by a set of LMIs (5.19) which are solved by using a free optimization toolbox (Yalmip or Sedumi).

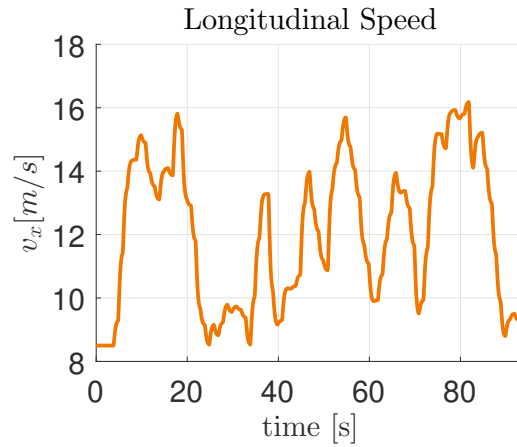
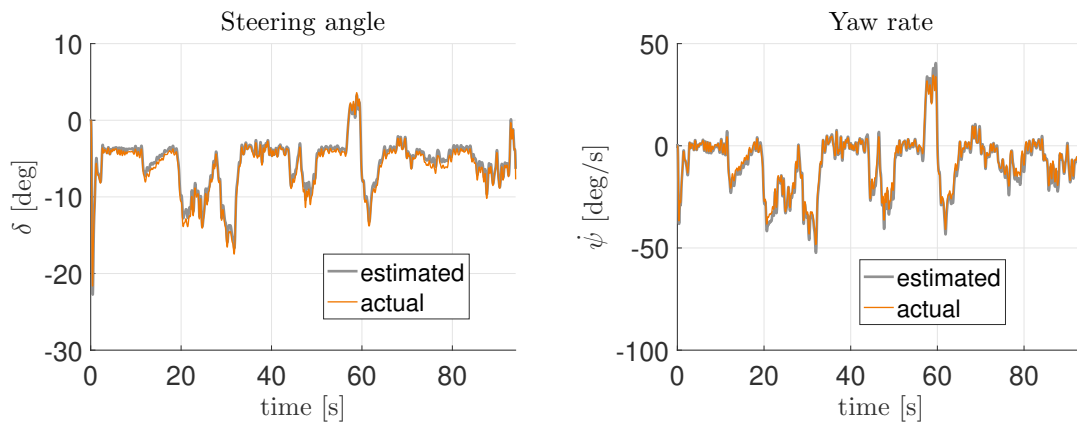


FIGURE 5.1: Longitudinal velocity

The actual steering angle  $\delta$  and its derivative  $\dot{\delta}$  are depicted in figure 5.2 with their corresponding estimates. Also, this figure shows a comparison between the estimation of the yaw and the roll rates with respect to their measurements.



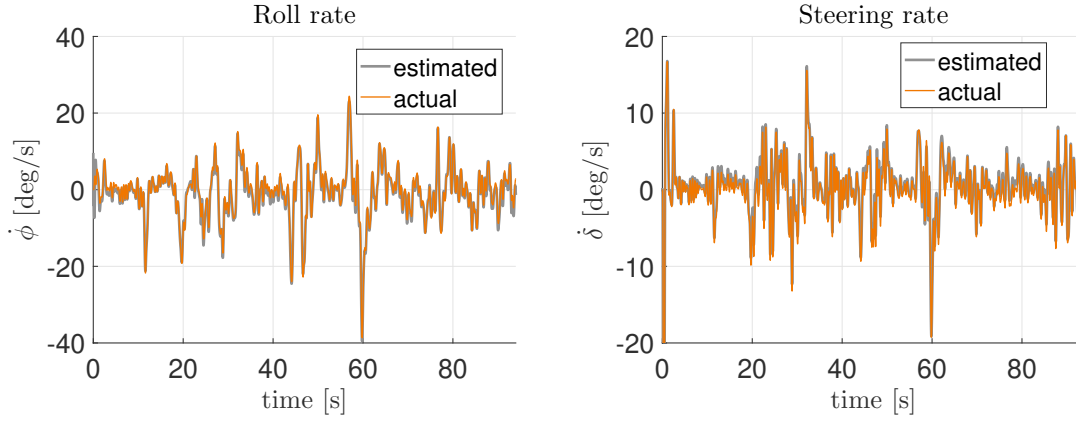


FIGURE 5.2: States estimation (gray) compared to actual measurement (orange).

According to the above simulation results, it can be seen that the observer has a fast transient phase and an acceptable convergence rate to the estimated values, which gives a good representation of the actual states. To assess the performances of the observer, the estimated states are compared with their corresponding measurement by means of the root mean square percentage ( $RMSE_{\%}$ ), and the average of the state estimation error (RMS). Considering that the ( $RMSE_{\%}$  and RMS) are proportional to the square of the estimation error, the lower these indexes are, the better the estimation performances are. Let us remind that their formulas are defined by:

$$RMSE_{\%} = \frac{\sqrt{\frac{1}{n} \sum_{i=1}^n (y_{j_{mes}}(i) - y_{j_{est}}(i))^2}}{\sqrt{\frac{1}{n} \sum_{i=1}^n y_{j_{mes}}(i)^2}} 100, \quad RMS = \sqrt{\frac{\sum_{i=1}^n (y_{j_{mes}}(i) - y_{j_{est}}(i))^2}{n}} \quad (5.23)$$

where  $y_{j_{mes}}$  is the measurement of  $y_j$  containing  $n$  data points and  $y_{j_{est}}$  is its estimate provided by the observer.

State #	RMS	$RMSE_{\%}$
$\delta [rad]$	0.0016	8.56
$\dot{\phi} [rad/s]$	0.0309	10.73
$\dot{\psi} [rad/s]$	0.0197	12.90
$\dot{\delta} [rad/s]$	0.0103	12.48
$a_y [m/s^2]$	0.1603	12.42

TABLE 5.1: Analysis of the estimated state.

Table 5.1 reports the resulting RMS and RMSE, to evaluate the performance of the LPV unknown input observer for the track scenario conducted by the scooter. The RMS index presents small values of the estimation errors between the estimated states and output measurements. Indeed, small values of the RMSE index are observed for the yaw rate and especially for the steering angle estimation which has a low sensitivity to the modeling errors. Nevertheless, the roll and steer rates as well as the lateral acceleration highlight the greater RMSE values. But, these values are still acceptable and ( $RMSE_{\%}$ ) does not exceed 12.9% between the proposed method and sensor measurement. The modeling assumptions are responsible for estimation error, especially the linear approximation of the motorcycle and the tire models. Let us remind that the observer is derived from a two-body model, whereas the real motorcycle is a highly nonlinear multi-body system. Hence, the modeling approximations contribute to these errors. In addition, during the observer design, the lateral tire forces were approximated by their linear expressions. Whereas, cornering forces have a nonlinear behavior. Results, summarized in Table 5.1, show the potential of our observer and prove the reliability of the estimated model for the track scenario.

Now, figures 5.3 show the estimation of the unmeasurable states from the lateral dynamic model ( $v_y, F_{yf}, F_{yr}, F_{\phi_r}$ ), whereas figures 5.4 illustrate the estimation of the unknown inputs from the model inversion.

This UIO observer copes in particular with road bank angle estimation and the roll angle in the motorcycle lateral dynamics model and addresses the estimation of the torque applied on the handlebar.

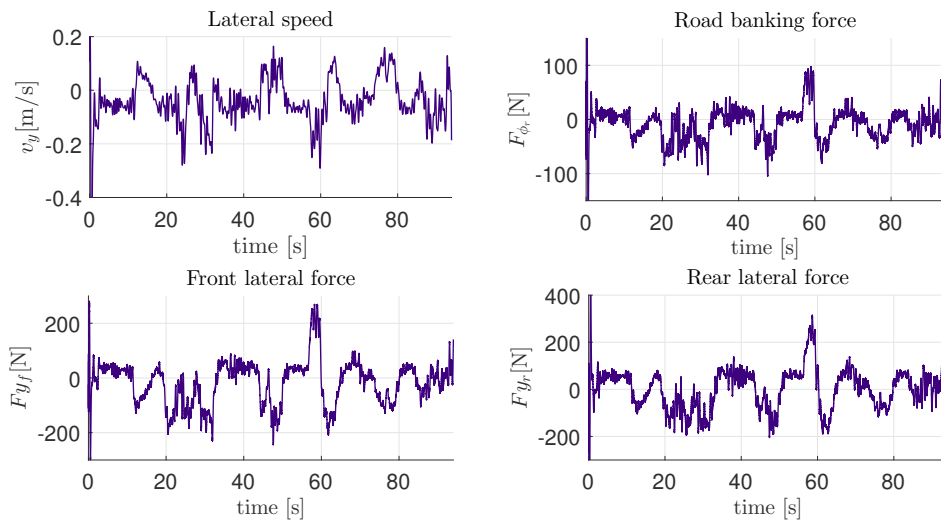


FIGURE 5.3: Unmeasurable states estimation of Scooter.

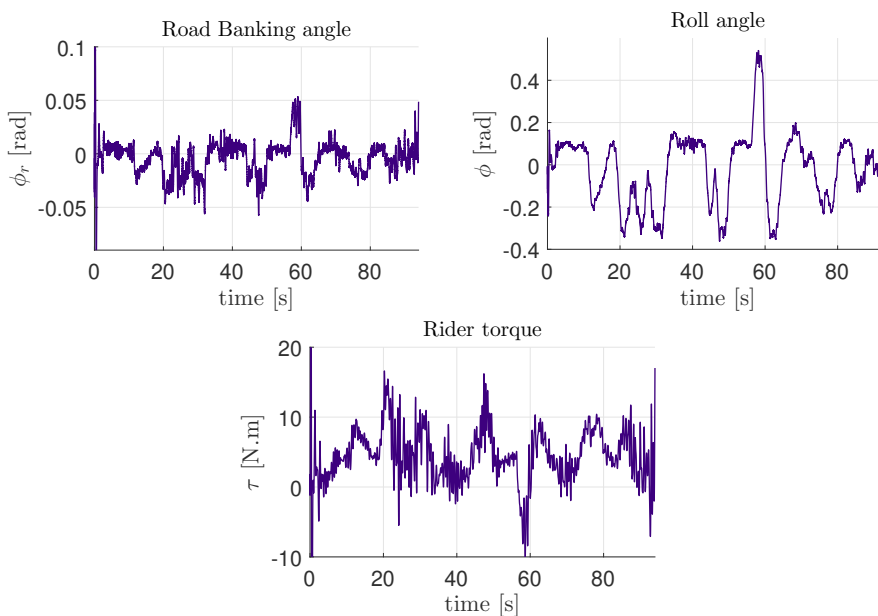


FIGURE 5.4: Unknown inputs estimation.

As a mean of validation, the lateral acceleration  $a_y$  is reconstructed from the estimated state and unknown input vectors. This reconstruction allows to validate the unmeasurable states  $F_{yf}$ ,  $F_{yr}$ ,  $F_{\phi_r}$  and  $v_y$ . We know that:

$$m\hat{a}_y = \hat{F}_{yf} + \hat{F}_{yr} - \hat{F}_{\phi_r} \quad (5.24)$$

$$\hat{a}_y = \hat{v}_y + v_x\dot{\psi} \quad (5.25)$$

$$\phi_{IMU} = \hat{\phi} + \hat{\phi}_r \quad (5.26)$$

Figure 5.5 depicts the actual lateral acceleration compared to that reconstructed from equation (5.24) while Figure 5.6 shows the same comparison in which equation (5.25) is used. Finally, figure 5.7 presents the comparison between the measured roll angle and those estimated in the sense of equation (5.26). The LMI

region performance is verified through the observer transient phase showing the good estimate ability of the proposed observer in spite of the presence of unknown inputs.

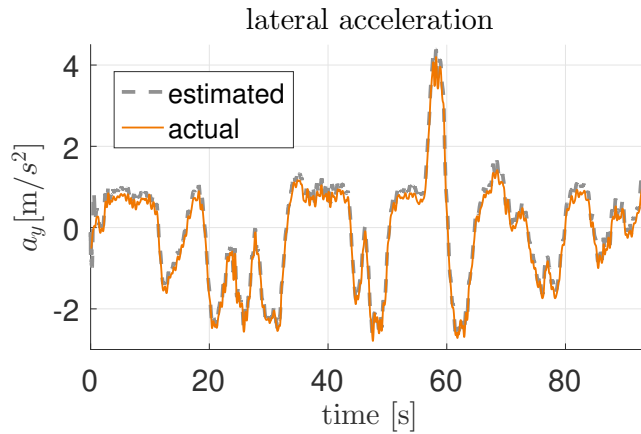


FIGURE 5.5: State estimation validation:  $F_{yf}$ ,  $F_{yr}$ ,  $F_{\phi_r}$  from the estimated lateral acceleration (dashed gray) compared to the IMU lateral acceleration (orange).

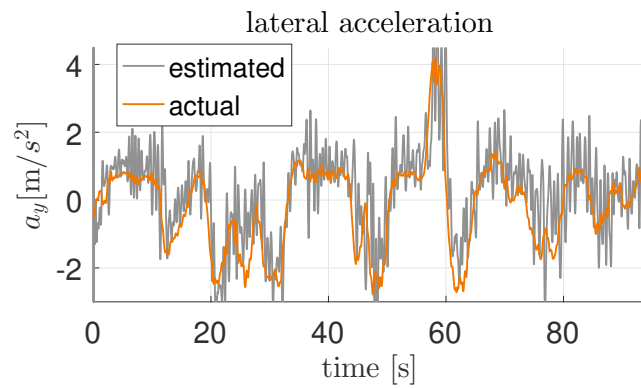


FIGURE 5.6: State estimation validation:  $\hat{v}_y$  from the lateral acceleration (dashed gray) compared to the IMU lateral acceleration (orange).

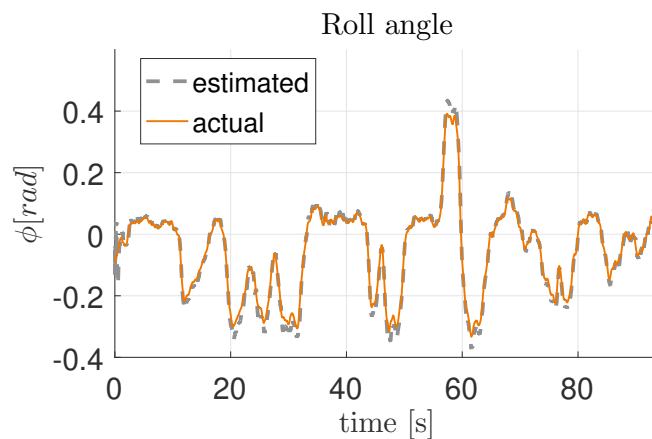


FIGURE 5.7: State estimation validation:  $\phi$ ,  $\phi_r$  estimated (gray) from the IMU roll angle measurement (orange).

One can note that all the state and variables are well estimated except the lateral velocity which has error estimation (from validation figure 5.6), but it is still acceptable. The lateral velocity is difficult to estimate

accurately, however, because of its low value compared to longitudinal velocity this error does not affect the performances of the roll angle estimation. The roll and steer angles ( $\phi + \phi_r$ ,  $\delta$ ) and also the lateral forces are well estimated. There are some differences at the peak due to modeling uncertainties, between the Scooter and the estimated model. The model used for the observer design does not take into account large roll angles but the observer still gives acceptable results. Finally, simulation results show the performance and the ability of the designed observer to well recover simultaneously the motorcycle dynamics, unknown inputs and the road banking angle on a real driving scenario realized with normal riding behavior.

From the states and unknown vectors estimation, we can also recover the side-slip angle  $\alpha_i$  of the front and rear tires. The angles are very important to deal with stability region of the PTWV. Recall that, the lateral forces are modelled by the following set of equations:

$$\begin{cases} \frac{\sigma_f}{v_x} \dot{F}_{yf} = -F_{yf} - C_{f1}\alpha_f + C_{f2}(\phi + \phi_r + \delta \sin(\varepsilon)) \\ \frac{\sigma_r}{v_x} \dot{F}_{yr} = -F_{yr} - C_{r1}\alpha_r + C_{r2}(\phi + \phi_r) \end{cases} \quad (5.27)$$

where  $C_{fi}$  and  $C_{ri}$  are the front and rear tire cornering stiffness supposed to be known. The front and rear side-slip angles can be estimated from the following equations:

$$\begin{cases} \hat{\alpha}_f = \left( \frac{\hat{v}_y + l_f \hat{\psi} - \eta \hat{\delta}}{v_x} \right) - \hat{\delta} \cos(\varepsilon) \\ \hat{\alpha}_r = \left( \frac{\hat{v}_y - l_r \hat{\psi}}{v_x} \right) \end{cases} \quad (5.28)$$

Using the estimation states previously discussed, the front and rear sideslip angles are obtained from equations (5.28). Figure 5.8 shows the reconstruction of the sideslip dynamics. This estimation is very important to evaluate the behavior and the stability of the motorcycle. In fact, the PTWV stability region is directly correlated to the sideslip dynamics defined from the phase-plane ( $\alpha_i - \dot{\alpha}_i$ ).

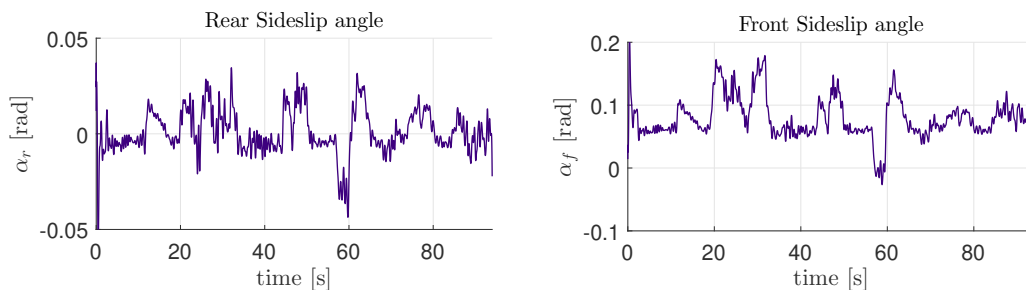


FIGURE 5.8: Front and Rear Sidelip angles.

## 5.4 Conclusions

In this chapter, an estimation of out of plane motorcycle model states, road feature and unknown inputs have been proposed using an unknown input observer associated with model inversion. The design method takes into account the forward speed as a linear parameter varying. Sufficient conditions for the existence of the estimator are given in terms of linear matrix inequalities (LMIs). The performance of the resulting observer has been evaluated by experimental validation using a real riding scenario. Simulation results are provided which illustrate the effectiveness of the proposed observer in estimating the states, unknown input and road geometry, the observer results demonstrate that it gives reliable estimations. Furthermore, we are also concerned with the case when the decoupling condition on the observer design is not fulfilled ( $CG(\zeta) \neq G(\zeta)$ ), in such a case the observer is not valide to estimate the unknown inputs. The next chapter (6) is dedicated to study the mismatched constraint in the UIO design.

# Chapter 6

## Delayed Unknown Input Observer

### Abstract

This chapter proposes an observer based identifier to address the problem of state estimation and parameters identification for system when the so-called matching condition is not fulfilled. Thereby, we suggest a new approach to how a failed matching condition for a unknown input observer (UIO) can be recovered by using time delayed measurements.

In the first part of this chapter, we present the general concept of the full order delayed unknown inputs observer (DUIO) with unmatched unknown parts, in which, the time delay concept is investigated to define a new augmented dynamic system, which satisfies the decoupling constraint. Based on these last, the unknown parameters of the model and the unmeasured system states can be simultaneously estimated. The resulting observer has been improved, from the restrictive decoupling condition point of view to guarantee the estimation of state and parameters with asymptotic convergence. The theoretical aspects and the validation of this work were published in Fouka et al., 2018e and Fouka et al., 2019a. In the second part, the concept is adapted to the LPV two-wheelers vehicle model in order to reconstruct the unknown states and identify the unknown parameters. In this context, the augmented observer clearly enlarges the applicability of this design method for real systems.

### 6.1 Problem Statement

Almost real systems and process subjected to unknown inputs, parameters and/or disturbances, the matching condition does not hold (Yanhua and Zhibin, 2015 and Yang et al., 2011). Overall, research on the problems of mismatched rank condition can primarily be decomposed into two categories. The first one deals with the compensation of the effects of unknown model uncertainties and external disturbances, based on motion control systems (Yang et al., 2014). Alternative methods are proposed in the case of perturbation attenuation for system with unsatisfied matching condition (She, Xin, and Pan, 2011). Another set of research is devoted to fulfill the observer matching condition considering auxiliary outputs and augmented models, derived from high-order differentiators (Park and Kim, 2014 and Kalsi et al., 2010).

In this section, we are concerned with a class of systems which can be represented in a linear parametric affine form as following:

$$\begin{cases} \dot{\bar{x}}(t) &= \bar{A}\bar{x}(t) + \bar{B}\bar{u}(t) + \bar{D}_{\bar{y}}\theta \\ \bar{y} &= \bar{C}\bar{x}(t) \end{cases} \quad (6.1)$$

where  $\bar{x}(t) \in \mathbb{R}^n$  is the state vector,  $\bar{u}(t) \in \mathbb{R}^{n_{\bar{u}}}$  is the input vector,  $\bar{y}(t) \in \mathbb{R}^{n_{\bar{y}}}$  is the measured output

vector, and  $\theta \in \mathbb{R}^{n_\theta}$  represents the vector of unknown constant parameters. The matrices  $\bar{D}_{\bar{y}}$ ,  $\bar{A}$ ,  $\bar{C}$  and  $\bar{B}$  are of appropriate dimensions and time invariant except  $\bar{D}_{\bar{y}}$ . Without loss of generality, we consider that:

$$\begin{aligned} \text{rank}(\bar{C}) &= n_{\bar{y}} \\ \text{rank}(\bar{D}_{\bar{y}}) &= n_\theta \end{aligned} \quad (6.2)$$

for all  $\bar{y} \in \Delta$ , where  $\Delta$  defines an hyper-rectangles:

$$\Delta = \{ \bar{y}, \dot{\bar{y}} \in \mathbb{R}^{n_{\bar{y}}} \mid \bar{y}_{i_{min}} \leq \bar{y}_i \leq \bar{y}_{i_{max}}, \dot{\bar{y}}_{i_{min}} \leq \dot{\bar{y}}_i \leq \dot{\bar{y}}_{i_{max}} \} \quad (6.3)$$

where  $(\bar{y}_{i_{min}}, \bar{y}_{i_{max}})$  and  $(\dot{\bar{y}}_{i_{min}}, \dot{\bar{y}}_{i_{max}})$  are the lower and upper bounds of the measured signal and its derivative respectively.

The observer design approach is based on the existence of the left inverse matrix, called decoupling matrix, to make possible the reconstruction of the unknown parameters vector (Bejarano, Poznyak, and Fridman, 2006). In other words, this condition imposes that the number of unknown parameters must be less than the number of system's outputs, so, the rank condition is given as following:

$$\text{rank}(\bar{C}\bar{D}_{\bar{y}}) = \text{rank}(\bar{D}_{\bar{y}}) \quad (6.4)$$

Also, we have  $(\bar{C}\bar{D}_{\bar{y}}) \in \mathbb{R}^{n_{\bar{y}} \times n_\theta}$  and  $\bar{D}_{\bar{y}} \in \mathbb{R}^{n_\theta \times n_\theta}$ . By computing the rank of each part we have:

$$\text{rank}(\bar{D}_{\bar{y}}) = n_\theta \quad (6.5)$$

$$\text{rank}(\bar{C}\bar{D}_{\bar{y}}) = n_{\bar{y}} \quad (6.6)$$

If  $n_\theta > n_{\bar{y}}$  then the rank condition is not fulfilled, which is the case of the original system:  $\text{rank}(\bar{C}\bar{D}_{\bar{y}}) \neq \text{rank}(\bar{D}_{\bar{y}})$ .

To overcome this restriction, the original system must be rearranged in an augmented form by introducing auxiliary outputs. Almost methods use differentiators to get a successive time-derivatives of the original system's outputs. In our method, a more relaxed approach is proposed by taking the time-delayed outputs of the original system's to fulfill the previous rank condition.

Let us adopt the matrices notation  $*_{\bar{y}} = *(\bar{y}(t))$ ,  $*_{\bar{y}, \dot{\bar{y}}} = *(\bar{y}(t), \dot{\bar{y}}(t))$ , and  $*_{\tau_i} = *(t - \tau_i)$ ,  $*_{\bar{y}_{\tau_i}} = *(\bar{y}(t - \tau_i))$ , where  $\tau_i$  is a constant time delay.

## 6.2 Augmented State Space

In this section, a transformation to break out with the rank condition related to mismatched unknown part is developed. Augmented models are constructed by adding exogenous dynamics to an already existing system's model. In this scope, an augmented system is considered by including delayed states and outputs dynamics.

Consider  $m$  delays  $\tau_i$ , where  $1 \leq i \leq m$  and  $\bar{y}_\tau$ , the delayed output vector, an augmented model is constructed with a new state  $x(t)$ , input  $u(t)$  and output vectors  $y(t)$  as following:

$$\begin{aligned} x &= [ \bar{x}^T \quad \bar{x}_{\tau_1}^T \quad \bar{x}_{\tau_i}^T \quad \dots \quad \bar{x}_{\tau_m}^T ]^T \\ y &= [ \bar{y}^T \quad \bar{y}_{\tau_1}^T \quad \bar{y}_{\tau_i}^T \quad \dots \quad \bar{y}_{\tau_m}^T ]^T \\ u &= [ \bar{u}^T \quad \bar{u}_{\tau_1}^T \quad \bar{u}_{\tau_i}^T \quad \dots \quad \bar{u}_{\tau_m}^T ]^T \end{aligned} \quad (6.7)$$

where  $m$  represents the number of set of auxiliary outputs such that:

$$\frac{n_\theta}{n_{\bar{y}}} - 1 \leq m < \frac{n_\theta}{n_{\bar{y}}} \quad (6.8)$$

The augmented state-space system is given by:

$$\begin{cases} \dot{x}(t) &= Ax(t) + Bu(t) + D_y\theta \\ y &= Cx(t) \end{cases} \quad (6.9)$$

where,

$$A = \begin{bmatrix} \bar{A} & 0_n & \cdots & 0_n \\ 0_n & \bar{A} & \cdots & 0_n \\ \vdots & \vdots & \ddots & \vdots \\ 0_n & 0_n & \cdots & \bar{A} \end{bmatrix} \quad B = \begin{bmatrix} \bar{B} & 0_{n \times n_{\bar{u}}} & \cdots & 0_{n \times n_{\bar{u}}} \\ 0_{n \times n_{\bar{u}}} & \bar{B} & \cdots & 0_{n \times n_{\bar{u}}} \\ \vdots & \vdots & \ddots & \vdots \\ 0_{n \times n_{\bar{u}}} & 0_{n \times n_{\bar{u}}} & \cdots & \bar{B} \end{bmatrix}$$

$$D_y = \begin{bmatrix} \bar{D}_{\bar{y}} \\ \bar{D}_{\bar{y}\tau_1} \\ \vdots \\ \bar{D}_{\bar{y}\tau_m} \end{bmatrix} \quad C = \begin{bmatrix} \bar{C} & 0_{n_{\bar{y}} \times n} & \cdots & 0_{n_{\bar{y}} \times n} \\ 0_{n_{\bar{y}} \times n} & \bar{C} & \cdots & 0_{n_{\bar{y}} \times n} \\ \vdots & \vdots & \ddots & \vdots \\ 0_{n_{\bar{y}} \times n} & 0_{n_{\bar{y}} \times n} & \cdots & \bar{C} \end{bmatrix}$$

where,  $\bar{D}_{\bar{y}\tau_i}$  are the delayed matrices,  $A \in \mathbb{R}^{((m+1)n) \times ((m+1)n)}$ ,  $B \in \mathbb{R}^{((m+1)n) \times ((m+1)n_{\bar{u}})}$ ,  $D_y \in \mathbb{R}^{((m+1)n) \times n_\theta}$  and  $C \in \mathbb{R}^{((m+1)n_{\bar{y}}) \times ((m+1)n)}$ .

The system's dimension, with respect to equation (6.8), is as follow:

$$\begin{cases} \text{rank}(C) = (m+1)n_{\bar{y}} \\ n_\theta \leq (m+1)n_{\bar{y}} < (m+1)n \\ \text{rank}(D_y) = \min((m+1)n, n_\theta) = n_\theta \end{cases} \quad (6.10)$$

Also:

$$\text{rank}(CD_y) \leq \min(\text{rank}(C), \text{rank}(D_y)) = \min((m+1)n_{\bar{y}}, n_\theta) \Rightarrow \text{rank}(CD_y) \leq n_\theta \quad (6.11)$$

One can notice that  $\text{rank}(D_y) = \text{rank}(\bar{D}_{\bar{y}}) = n_\theta$  keeps the same number of column because  $\dim(\theta) = n_\theta$  is constant on the original and augmented models. Knowing that the decoupling matrix  $CD_y$  has non collinear rows, such that  $n_\theta \leq (m+1)n_{\bar{y}}$ . The idea is to enhance the rank of the decoupling matrix in the augmented model such that  $n_\theta \leq (m+1)n_{\bar{y}}$ , to fulfill the matching condition imposed by the observer, it implies:

$$\text{rank}(CD_y) = \min((m+1)n_{\bar{y}}, n_\theta) = \text{rank}(D_y) = n_\theta \quad (6.12)$$

### 6.3 Observer Design

Let us consider the following full order Delayed Unknown Input Observer (DUIO) :

$$\begin{cases} \dot{z}(t) &= N_{y,\dot{y}}z(t) + L_{y,\dot{y}}y(t) + G_y u(t) \\ \hat{x}(t) &= z(t) - H_y y(t) \end{cases} \quad (6.13)$$

where,  $\hat{x}$  and  $\hat{y}$  are respectively the estimated state and output vectors.  $N_{y,\dot{y}}$ ,  $L_{y,\dot{y}}$ ,  $H_y$  and  $G_y$  are parameter varying matrices with appropriate dimension. The problem of DUIO design can be stated as finding these matrices in order to satisfy a stable asymptotic convergence of the estimation error dynamics. The proposed estimation approach is taken under the matching condition fulfilled for the augmented model.

**Definition 6.1.** *The DUIO observer is called to be asymptotically stable if :*

- $\tilde{x}(t) = 0$  when  $t \rightarrow \infty$ , where  $\tilde{x}(t) = x(t) - \hat{x}(t)$  is the observer error.
- the matrix  $N_{y,\dot{y}}$  is Hurwitz.

Assume that there exists a square matrix  $P_y \in \mathbb{R}^{(m+1) \times n}$  defined as  $P_y = I + H_y C$ . From the augmented model (6.9) and DUIO equation (6.13), one can easily prove that the estimation error  $\tilde{x}$  can be expressed as:

$$\tilde{x} = P_y x - z \quad (6.14)$$

By time differentiating, we get the error dynamics:

$$\dot{\tilde{x}} = N_{y,\dot{y}}\tilde{x} + (\dot{P}_{y,\dot{y}} + P_y A - N_{y,\dot{y}}P_y - L_{y,\dot{y}}C)x + P_y D_y \theta + (P_y B - G_y)u \quad (6.15)$$

Obviously, if the following matrix equalities are verified:

- (i)  $N_{y,\dot{y}} = \Gamma_{y,\dot{y}} - K_{y,\dot{y}}C$ , where,  $\Gamma_{y,\dot{y}} = \dot{P}_{y,\dot{y}} + P_y A$  and  $K_{y,\dot{y}} = N_{y,\dot{y}}H_y + L_{y,\dot{y}}$ .
- (ii)  $P_y D_y = 0$ , where  $P_y = I + H_y C$ .
- (iii)  $P_y B - G_y = 0$ .

then, the error dynamics in equation (6.15) can be reduced to :

$$\dot{\tilde{x}}(t) = N_{y,\dot{y}}\tilde{x}(t) \quad (6.16)$$

Consequently, the error dynamics asymptotic convergence is ensured if  $N_{y,\dot{y}}$  is Hurwitz.

However, the three previous equalities are time variant since they depend on the output vector  $y(t)$  and its time derivative  $\dot{y}(t)$ . To be able to solve this optimization problem with LMI, the TS transformation is applied as in the previous chapter. It will be assumed that, the premise variables  $y, \dot{y} \in \mathbf{\Delta}$  are real-time accessible. The non-linearities related to  $y, \dot{y} \in \mathbf{\Delta}$  are captured via membership functions  $\eta_i(\cdot)$ , which have the convex-sum property in the compact set of the state space:

$$\sum_{i=1}^r \eta_i(y, \dot{y}) = 1, \quad 0 \leq \eta_i(y, \dot{y}) \leq 1 \quad (6.17)$$

where  $r$  is the number of the sub-models. Then, a polytopic exact forms is obtained as following:

$$\begin{aligned}\Gamma_{y,\dot{y}} &= \sum_{i=1}^r \eta_i(y, \dot{y}) \Gamma_i \\ K_{y,\dot{y}} &= \sum_{i=1}^r \eta_i(y, \dot{y}) K_i\end{aligned}\quad (6.18)$$

where,  $\Gamma_i$  and  $K_i$  are constant matrices. From this, the DUIO gain matrices  $L_{y,\dot{y}}$  and  $N_{y,\dot{y}}$  can be defined as:

$$\begin{cases} N_{y,\dot{y}} = \sum_{i=1}^r \eta_i(y, \dot{y}) N_i, & N_i = \Gamma_i - K_i C \\ L_{y,\dot{y}} = \sum_{i=1}^r \eta_i(y, \dot{y}) L_i, & L_i = K_i - N_i H_i \end{cases}\quad (6.19)$$

and, the estimation error dynamics is written under the following :

$$\dot{\tilde{x}}(t) = \sum_{i=1}^r \eta_i(y, \dot{y}) (\Gamma_i - K_i C) \tilde{x}(t), \quad i \in \{1, 2, \dots, 2^{2n_{\dot{y}}}\} \quad (6.20)$$

The following theorem provides the LMI conditions of the existence of the observer.

**Theorem 6.1.** *The full order DUIO (6.13) for the augmented model (6.9), guaranties the state estimation convergence, if there exists a symmetric positive definite matrix  $Q \in \mathbb{R}^{(m+1)n \times (m+1)n}$  defining a Lyapunov function  $V(\tilde{x}) > 0$ , such that  $\dot{V}(\tilde{x}) < 0, \forall \tilde{x}(t) \neq 0$ . Hence, the following linear matrix inequality holds:*

$$\begin{pmatrix} -Q & 0 \\ 0 & \Gamma_i^T Q + Q \Gamma_i - C^T R_i^T - R_i C \end{pmatrix} < 0 \quad (6.21)$$

**Proof 6.1.** *The observer gains are selected so that  $N_i$  is a Hurwitz matrix, based on the stability analysis of the Lyapunov theory. Now, consider that there exists a positive definite matrix function  $Q$  such that a quadratic Lyapunov function is defined to analyze the asymptotic convergence of the dynamical error, as follow:*

$$V(\tilde{x}) = \tilde{x}^T Q \tilde{x} \quad (6.22)$$

Taking the time derivative of  $V(\tilde{x})$  along the error dynamics yields:

$$\dot{V} = \tilde{x}^T \left( \sum_{i=1}^r \eta_i(y, \dot{y}) (\Gamma_i^T Q + Q \Gamma_i - C^T K_i^T Q - Q K_i C) \right) \tilde{x} \quad (6.23)$$

Note that  $\dot{V} < 0$  implies that the estimation error  $\tilde{x}(t)$  tends towards zero asymptotically for any initial value  $\tilde{x}(0)$  if the following BMI holds:

$$\Gamma_i^T Q + Q \Gamma_i - C^T K_i^T Q - Q K_i C < 0, \quad Q = Q^T > 0 \quad (6.24)$$

One note that the inequality (6.24) is bilinear with respect to the unknown matrices  $Q$  and  $K_i$ . To solve this BMI problem, a variable change  $R_i = Q K_i$  is introduced allowing to get LMI problem as following:

$$\Gamma_i^T Q + Q \Gamma_i - C^T R_i^T - R_i C < 0 \quad (6.25)$$

Thus, from the Lyapunov stability theory, if the LMI condition (6.21) is satisfied, the system (6.13) is exponentially asymptotically stable. This completes the proof of Theorem 6.1.

Once, the state vector is estimated, finding the unknown parameters is straightforward by using an algebraic inversion as following:

$$\hat{\theta} = (CD_y)^\dagger (\hat{y} - CA\hat{x} - CBu) \quad (6.26)$$

where  $(CD_y)^\dagger = \left[ (CD_y)^T (CD_y) \right]^{-1} (CD_y)^T$ . However, the feasibility of this inversion is conditioned by a convenient selection of the time delay to fulfill the rank condition. By substituting the output derivative in the inversion model (6.26), the parameter estimation error is defined as:

$$e_\theta = \theta - \hat{\theta} = -(CD_y)^\dagger CA\tilde{x} \quad (6.27)$$

It is easy, from this equation, to show that the convergence of  $\hat{\theta}$  towards  $\theta$  is ensured from the asymptotic stability of the state estimation errors  $\tilde{x}(t)$  under suitable persistence excitation described in the following definition.

**Definition 6.2.** *The Persistent Excitation Condition is fulfilled if there exist  $c_{1ij}$ ,  $c_{2ij}$  and  $c_{3ij}$  positive for  $i, j = 1, \dots, q$ , such that for all  $t$  the following inequality holds (Ioannou and Sun, 1996):*

$$c_{1ij} I \leq \int_{t_0}^{t_0+c_{3ij}} \bar{D}_{\bar{y}_{\tau_i}} \bar{D}_{\bar{y}_{\tau_j}}^T dt \leq c_{2ij} I \quad \forall i, j = 1, \dots, q$$

Finally, the design procedure of the full order DUIO observer is summarized in the following Algorithm 3. An example is proposed in the appendix B to illustrate the estimation performance of DUIO observer.

---

### Algorithm 3: Observer design procedure DUIO

---

#### Require:

- 1: Check if system  $(A, D_y, C)$  is observable or detectable. If so, go to Step 2; Otherwise, stop.
  - 2: Check the decoupling conditions :
  - 3: **if**  $\text{rank}(CD_y) = \text{rank}(D_y) \quad \forall y \in \Delta$  **holds then**  
 $\lfloor m = 0$ , go to step 10.
  - 4: **else**  
 $\lfloor$  Find the minimum integer ( $m$ )  $\leftarrow$  according to (6.8).  
 $\lfloor$  Reconstruct the augmented matrices  $A, B, C, D$  in (6.9).
  - 5: Compute matrices  $H_y, P_y$  and deduce the matrix  $G_y$ .
  - 6: Compute the matrix  $\dot{P}_{y,\dot{y}}$  and deduce  $\Gamma = P_y A_y + \dot{P}_{y,\dot{y}}$ .
  - 7: Solve the LMIs (6.21).
  - 8: Compute  $K_i = Q^{-1} R_i$ .
  - 9: Deduce  $N_{y,\dot{y}} = \Gamma - K_{y,\dot{y}} C$  and  $L_{y,\dot{y}} = K_{y,\dot{y}} - N_{y,\dot{y}} H_y$ .
  - 10: Estimate the parameters  $\hat{\theta}$ .
  - 11: End
- 

## 6.4 Extension to the PTWV case

### 6.4.1 Problem Statement

In the state space representation described in equation (6.1), the matrices  $\bar{A}$ ,  $\bar{C}$  and  $\bar{B}$  are supposed to be time invariant. However, we have seen in section 5.1 that matrix  $A$  in the PTWV dynamics model of equation

(5.1) is parameter varying with respect to  $\zeta$ . So, in this section we aim to extend the full order DUIO design procedure to the case of the following LPV class :

$$\begin{cases} \dot{x}(t) &= \tilde{A}(\zeta)x(t) + \tilde{B}u(t) + \tilde{D}(\zeta)F(y, \dot{y}, \dots, y^{(n)}, \theta) \\ y &= \tilde{C}x(t) \end{cases} \quad (6.28)$$

where  $x(t) \in \mathbb{R}^n$  is the state vector,  $u(t) \in \mathbb{R}^m$  is the input vector and  $y(t) \in \mathbb{R}^{n_y}$  denotes the output vector. The vector  $F(y, \dot{y}, \dots, y^{(n)}, \theta) \in \mathbb{R}^p$  incloses all non-linear terms which depend on the known time varying parameter  $\zeta$  and the unknown constant parameter  $\theta$ . The matrices  $\tilde{A}(\zeta)$  and  $\tilde{D}(\zeta)$  are parameter varying matrices of appropriate dimensions while we suppose that the matrices  $\tilde{C}$  and  $\tilde{B}$  are constant.

Without loss of generality, here we assume that  $\text{rank}(\tilde{D}(\zeta)) = p$  and  $\text{rank}(\tilde{C}) = n_y$  where  $n_y < p$ . Also, we assume that the vector  $\zeta$  and  $\dot{\zeta}$  are respectively defined on the hyperplanes  $\Delta$  and  $\tilde{\Delta}$  defined by:

$$\begin{cases} \Delta = \{ \zeta \in \mathbb{R}^{n_\zeta} \mid \zeta_{i_{min}} \leq \zeta_i \leq \zeta_{i_{max}} \} \\ \tilde{\Delta} = \{ \dot{\zeta} \in \mathbb{R}^{n_{\dot{\zeta}}} \mid \dot{\zeta}_{i_{min}} \leq \dot{\zeta}_i \leq \dot{\zeta}_{i_{max}} \} \end{cases} \quad (6.29)$$

where  $(\zeta_{i_{min}}, \zeta_{i_{max}})$  and  $(\dot{\zeta}_{i_{min}}, \dot{\zeta}_{i_{max}})$  are the lower and upper bounds of the forward speed and its derivative respectively.

**Assumption 6.1.** *In the following, assume that  $F$  can be written in an affine linear form with respect to unknown parameters such that:*

$$F(y, \dot{y}, \dots, y^{(n)}, \theta) = D(y, \dot{y}, \dots, y^{(n)})f(\theta) \quad (6.30)$$

where the matrix  $D_y = D(y, \dot{y}, \dots, y^{(n)}) \in \mathbb{R}^{p \times p}$  is full column rank, i.e.  $\text{rank}(D_y) = p$ .

From the aforementioned assumption, and for simple readability, the system in equation (6.28) is rewritten as:

$$\begin{cases} \dot{x}(t) &= \tilde{A}_\zeta x(t) + \tilde{B}u(t) + \tilde{D}_\zeta D_y f(\theta) \\ y &= \tilde{C}x(t) \end{cases} \quad (6.31)$$

**Theorem 6.2.** *The well-known rank condition for the existence of the UIO is given by the following statements (Darouach and Boutat-Baddas, 2008 and Trentelman, Stoorvogel, and Hautus, 2012):*

1. *The state  $x$  is bounded (stable or stabilized),*
2. *The system  $(\tilde{A}_\zeta, \tilde{D}_\zeta, \tilde{C})$  is observable or detectable,*
3. *The relative degree  $r$  of the system with respect to the unknown part  $F = D_y f(\theta)$  exists.*

Usually, this theorem can be summarized into two well-known conditions for the existence of the UIO, the observability condition of the pair  $(\tilde{A}_\zeta, \tilde{C})$  and the matching condition  $\text{rank}(\tilde{C}\tilde{D}_\zeta) = \text{rank}(\tilde{D}_\zeta)$  on the system matrices. Based on system defined by (6.31), one considers the case when  $\text{rank}(\tilde{C}\tilde{D}_\zeta) \neq \text{rank}(\tilde{D}_\zeta)$ ,  $\forall \zeta \in \Delta$  and  $\dot{\zeta} \in \tilde{\Delta}$ . In this case, the matching condition is not satisfied since  $p > n_y$  and an augmented model is reconstructed from delayed outputs as described in section 6.1.

### 6.4.2 Augmented Model

Considering a constant time delay  $\tau$  and the output vector  $y(t)$ , its delayed version is  $y(t - \tau)$ . The augmented model can be reconstructed with a new state  $x_a(t)$  and output  $y_a(t)$  vectors:

$$\begin{aligned} x_a &= [ (x(t))^T, (x(t - \tau_1))^T, (x(t - \tau_2))^T, \dots, (x(t - \tau_m))^T ]^T \\ y_a &= [ (y(t))^T, (y(t - \tau_1))^T, (y(t - \tau_2))^T, \dots, (y(t - \tau_m))^T ]^T \end{aligned}$$

where  $\tau_m$  is the  $m^{\text{th}}$  time delay, and  $m$  represents the number of delayed outputs to recover the matching condition. The parameter  $m$  can be easily computed from  $p = \vartheta \times n + \beta$ , where,

$$|\beta| < n \text{ and } m = \begin{cases} \vartheta & \text{if } \beta \leq 0 \\ \vartheta + 1 & \text{Otherwise} \end{cases} \quad (6.32)$$

The augmented state-space representation of the system is as follow:

$$\begin{aligned} \begin{bmatrix} \dot{x}(t) \\ \dot{x}(t - \tau_1) \\ \vdots \\ \dot{x}(t - \tau_m) \end{bmatrix} &= \begin{bmatrix} \tilde{A}_\zeta(t) & 0_{n \times n} & 0_{n \times n} & \cdots & 0_{n \times n} \\ 0_{n \times n} & \tilde{A}_\zeta(t - \tau_1) & 0_{n \times n} & \cdots & 0_{n \times n} \\ \vdots & \vdots & \vdots & \cdots & \vdots \\ 0_{n \times n} & 0_{n \times n} & 0_{n \times n} & \cdots & \tilde{A}_\zeta(t - \tau_m) \end{bmatrix} \begin{bmatrix} x(t) \\ x(t - \tau_1) \\ \vdots \\ x(t - \tau_m) \end{bmatrix} + \\ & \begin{bmatrix} \tilde{B} & 0 & 0 & \cdots & 0 \\ 0 & \tilde{B} & 0 & \cdots & 0 \\ \vdots & \vdots & \vdots & \cdots & \vdots \\ 0 & 0 & 0 & \cdots & \tilde{B} \end{bmatrix} \begin{bmatrix} u(t) \\ u(t - \tau_1) \\ \vdots \\ u(t - \tau_m) \end{bmatrix} + \begin{bmatrix} \tilde{D}_\zeta(t) D_{y(t)} \\ \tilde{D}_\zeta(t - \tau_1) D_{y(t - \tau_1)} \\ \vdots \\ \tilde{D}_\zeta(t - \tau_m) D_{y(t - \tau_m)} \end{bmatrix} f(\theta) \\ \begin{bmatrix} y(t) \\ y(t - \tau_1) \\ \vdots \\ y(t - \tau_m) \end{bmatrix} &= \begin{bmatrix} \tilde{C} & 0_{n_y \times n} & \cdots & 0_{n_y \times n} \\ 0_{n_y \times n} & \tilde{C} & \cdots & 0_{n_y \times n} \\ \vdots & \vdots & \cdots & \vdots \\ 0_{n_y \times n} & 0_{n_y \times n} & \cdots & \tilde{C} \end{bmatrix} x_a(t) \end{aligned} \quad (6.33)$$

In a simple form, the augmented system takes the following structure :

$$\begin{cases} \dot{x}_a(t) = A_\zeta x_a(t) + B_\zeta u_a(t) + D_{\zeta,y} f(\theta) \\ y_a = C_\zeta x_a(t) \end{cases} \quad (6.34)$$

whereas,  $A_\zeta \in \mathbb{R}^{((m+1) \times n) \times ((m+1) \times n)}$ ,  $B_\zeta \in \mathbb{R}^{((m+1) \times n) \times ((m+1) \times m)}$ ,  $D_{\zeta,y} \in \mathbb{R}^{((m+1) \times n) \times p}$  and  $C_\zeta \in \mathbb{R}^{((m+1) \times n_y) \times ((m+1) \times n)}$ .

**Remark 6.1.** The matching condition for the augmented model holds i.e.,  $\text{rank}(C_\zeta D_{\zeta,y}) = \text{rank}(D_{\zeta,y})$  and  $\text{rank}(C_\zeta D_\zeta) = \text{rank}(D_\zeta)$ .

### 6.4.3 Observer Design

For the augmented system (6.33) we propose the LPV unknown input observer of the form:

$$\begin{cases} \dot{z}(t) &= N_{\zeta,\dot{\zeta}}z + L_{\zeta,\dot{\zeta}}y_a + G_{\zeta}u_a \\ \hat{x}_a(t) &= z(t) - H_{\zeta}y_a(t) \end{cases} \quad (6.35)$$

where,  $\hat{x}_a$  and  $\hat{y}_a$  are respectively the estimated state and the output vector. The matrices  $N_{\zeta,\dot{\zeta}}$ ,  $L_{\zeta,\dot{\zeta}}$ ,  $G_{\zeta}$  and  $H_{\zeta}$  are parameter varying. The gains design is addressed in the same manner as in section 6.3. Therefore, if  $e = x_a - \hat{x}_a$  is the estimation error and  $\forall \zeta \in \Delta$  and  $\forall \dot{\zeta} \in \bar{\Delta}$ , if the following conditions hold, the estimation error tends asymptotically towards zero.

(1)  $\dot{e} = N_{\zeta,\dot{\zeta}}e$ , must be asymptotically stable i.e.,  $N_{\zeta,\dot{\zeta}}$  is Hurwitz,

(2)  $\dot{P}_{\zeta,\dot{\zeta}} + P_{\zeta}A_{\zeta} - N_{\zeta,\dot{\zeta}}P_{\zeta} - L_{\zeta,\dot{\zeta}}C_{\zeta} = 0$ .

(3)  $P_{\zeta}D_{\zeta,y} = 0$

(4)  $P_{\zeta}B_{\zeta} - G_{\zeta} = 0$

From these conditions, we can state the set of LMIs to be solved in order to design the DUIO gains as follows:

$$N_{\zeta,\dot{\zeta}} = \Gamma_{\zeta,\dot{\zeta}} - K_{\zeta,\dot{\zeta}}C_{\zeta} \quad (6.36)$$

$$H_{\zeta} = -D_{\zeta,y}(C_{\zeta}D_{\zeta,y})^{\dagger} \quad (6.37)$$

$$P_{\zeta} = I_{2n} + H_{\zeta}C_{\zeta} \quad (6.38)$$

$$G_{\zeta} = P_{\zeta}B_{\zeta} \quad (6.39)$$

where  $\Gamma_{\zeta,\dot{\zeta}} = \dot{P}_{\zeta,\dot{\zeta}} + P_{\zeta}\bar{A}_{\zeta}$  and  $K_{\zeta,\dot{\zeta}} = N_{\zeta,\dot{\zeta}}H_{\zeta} + L_{\zeta,\dot{\zeta}}$ .

Since the matching condition  $rank(CD_{\zeta,y}) = rank(D_{\zeta,y})$  is satisfied, the unknown parameters can be recovered by a simple algebraic inversion as following :

$$\hat{f} = (C_{\zeta}D_{\zeta,y})^{\dagger} (\dot{y}_a(t) - C_{\zeta}A_{\zeta}\hat{x}_a - C_{\zeta}B_{\zeta}u_a(t)) \quad (6.40)$$

In which, the convergence of  $\hat{f}$  towards  $f$  can be analyzed by defining the unknown part estimation error

$$e_f = f - \hat{f} = -(C_{\zeta}D_{\zeta,y})^{\dagger} C_{\zeta}A_{\zeta}e$$

Knowing that  $e$  converges asymptotically towards zero, then  $e_f$  also converges asymptotically towards zero. The stability analysis of the system is studied in the same way as in section (6.3) and yields to the following BMI conditions ensuring asymptotic stability:

$$\Gamma_i^T Q + Q\Gamma_i - C_i^T K_i^T Q - QK_i C_i < 0, \quad i = 1, \dots, r.$$

Finally, the performances of the DUIO can be improved by pole assignment in an LMI region to ensure an acceptable transient response. The poles of the estimator are considered in the complex plane region, and can be represented as an LMI region given by the stability margin  $\varsigma > 0$  in a subset  $\Theta$  of the complex plane. In this case, the matrix  $\Gamma_i$  is said  $\Theta_i$ -stable when its spectrum  $\lambda(\Gamma_i)$  belongs to region  $\Theta_i$ .

$$\Theta_i = \{z = (x_z + i.y_z) \in \mathbf{C} \mid Re(z) \leq -\varsigma \Leftrightarrow z + \bar{z} + 2\varsigma < 0 \} \quad (6.41)$$

where  $\mathbb{C}$  is the set of complex numbers, and  $\bar{z}$  denotes the complex conjugate of  $z$ .

**Theorem 6.3.** *The delayed unknown input observer (6.35) for the model (6.33), satisfying the pole clustering in  $\Theta_i(\zeta)$  (6.41), allows an asymptotically convergence of the state estimation error towards zero in the LMI region, if there exist a symmetric positive definite matrix  $Q \in \mathbb{R}^{2n \times 2n}$  and a matrix  $R_i \in \mathbb{R}^{2n \times 2n_y}$  such that the following LMI holds:*

$$\Gamma_i^T Q + Q \Gamma_i - C_i^T R_i^T - R C_i + 2\zeta Q < 0, \quad i \in (1, \dots, r) \quad (6.42)$$

where,  $R_i = Q K_i$ .

In the following section, an application of the described DUIO design procedure in the PTWV parameter identification framework is proposed.

## 6.5 Application for PTWV Estimation

The main focus of this work is to extend the estimation problematic of the PTWV lateral dynamics by including the parameter identification. Thereby, the reasons that motivate our choice to apply the delayed unknown input observer to the PTWV vehicle, is that the unknown part of the PTWV model do not satisfy the matching condition that are normally required in the unknown part reconstruction. The other reason is that most of the existing methods on parametric identification are designed under some assumptions taking into account a restricted parameters space to be identified and they do not deal with a great number of unknown parameters estimation (Cossalter et al., 2006a; Tanelli et al., 2009b; Schwab, De Lange, and Moore, 2012; Cabrera et al., 2014). Our contribution focuses on giving a solution of the unknown input observer for PTWV with large constant parametric space and also, with an arbitrary relative degree with respect to the unknown inputs. Henceforth, we will explore the ability of the delayed unknown input observer concept to estimate the dynamic states and the unknown parameters for PTWV model with mismatched condition.

In this section, we consider a four DoF model (Sharp, 1971), describing the lateral motion of the PTWV as following:

$$\bar{E}\dot{x} = \bar{A}x + \bar{B}u \quad (6.43)$$

where  $\bar{E} = [e_{ij}] \in \mathbb{R}^{8 \times 8}$ ,  $\bar{A} = [a_{ij}] \in \mathbb{R}^{8 \times 8}$  and  $\bar{B} \in \mathbb{R}^{8 \times 1}$ . The state vector is  $x \in \mathbb{R}^{8 \times 1}$  and includes  $[\phi, \delta, v_y, \dot{\psi}, \dot{\phi}, \delta, F_{yf}, F_{yr}]^T$ . Details of  $e_{ij}$  and  $a_{ij}$  are given in the appendix.

The model of equation (6.43) is written in a LPV structure with one varying parameter  $\zeta = v_x$  :

$$\begin{cases} \dot{x}(t) = \tilde{A}_\zeta x(t) + \tilde{B}u(t) + \tilde{D}_\zeta F(y, \theta) \\ y = \tilde{C}x(t) \end{cases} \quad (6.44)$$

whereas the matrix  $\tilde{A}_\zeta \in \mathbb{R}^{8 \times 8}$ ,  $\tilde{B} \in \mathbb{R}^{8 \times 1}$ ,  $\tilde{D}_\zeta \in \mathbb{R}^{8 \times 26}$  and  $\tilde{C} \in \mathbb{R}^{5 \times 8}$ .

For the PTWV, we can measure different state variables from the embedded sensors. We consider the output measured vector as  $y = [\delta, \psi, \dot{\phi}, \dot{\delta}, a_y]^T$ . By rearranging equation (6.43), the unknown parameter dependent part can be expressed in a linear affine form:

$$D_\zeta \hat{F} = \begin{cases} a_{34}\zeta y_2 \\ a_{44}\zeta y_2 + a_{45}y_3 + a_{46}\zeta y_4 + a_{47}\hat{x}_7 + a_{48}\hat{x}_8 \\ a_{51}\hat{x}_1 + a_{52}y_1 + a_{54}\zeta y_2 + a_{56}\zeta y_4 \\ a_{61}\hat{x}_1 + a_{62}y_1 + a_{64}\zeta y_2 + a_{65}\zeta y_3 + a_{66}y_4 + a_{67}\hat{x}_7 \\ a_{71}\zeta \hat{x}_1 + a_{72}\zeta y_1 + a_{73}\hat{x}_3 + a_{74}y_2 + a_{76}y_4 + a_{77}\zeta \hat{x}_7 \\ a_{81}\zeta \hat{x}_1 + a_{83}\hat{x}_3 + a_{84}y_2 + a_{88}\zeta \hat{x}_8 \end{cases} \quad (6.45)$$

where,  $a_{ij}$  are the unknown parameters of the model. One can remark that the matching condition is not satisfied for the LPV model defined above since  $n_y = 5$  and  $p = 26$ . Therefore, we need at least  $m = 4$  delayed outputs to reconstruct an augmented model.

**Remark 6.2.** *In practice, every system has physical limitations in the Persistent Excitation (PE) signals. Such a limitation could be the response time, maximum capacity, an operating limits, saturation. The convergence of parameters estimation are closely related to PE. Since this is not always fixed. These PE conditions are translated into sufficiently rich conditions on the inputs, which guarantee convergence rates of parameters estimation errors. In this context, an excitation with oscillations of sufficiently high frequency generally is used to excite the dynamics and to maximize the information content in the model parameters to ensure convergence. The reference excitation signal during the identification phase is a pseudo-random binary sequence (PRBS). However, this can only be achieved in simulation and unrealisable in case of real riding scenario. Indeed, the main input of the PTWV models is the steering torque at the front wheel, but the rider is unable to carry out this type of control. In our case, the PRBS input can be replaced by a chirp signal.*

## 6.6 Simulations Results

The DUIO is evaluated in co-simulation by using data from *BikeSim* simulator (Sharp, Evangelou, and Limebeer, 2004). The PTWV type Scooter Big Baseline with 8 bodies is selected with on a handling flat road and a high road friction coefficient  $\mu = 0.9$ . The forward speed is around 40 km/h. A chirp signal is applied as a steering torque (figure 6.1)

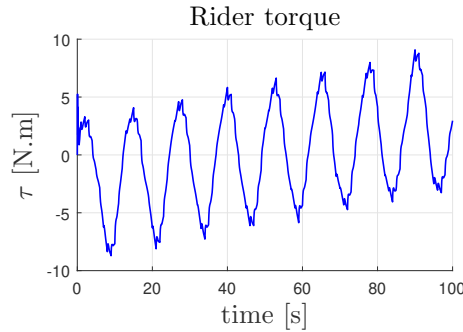


FIGURE 6.1: Steering torque input (chirp signal).

This maneuver is a well-known reference aiming to generate complicated lateral dynamics allowing the excitation of the pertinent parameters. The figure 6.2 depicts the measured states and their estimation along the track. One can remark a small error in the states estimation peaks, this can be explained by modeling errors. The estimated roll angle is also validated with measured roll angle as shown in figure 6.3.

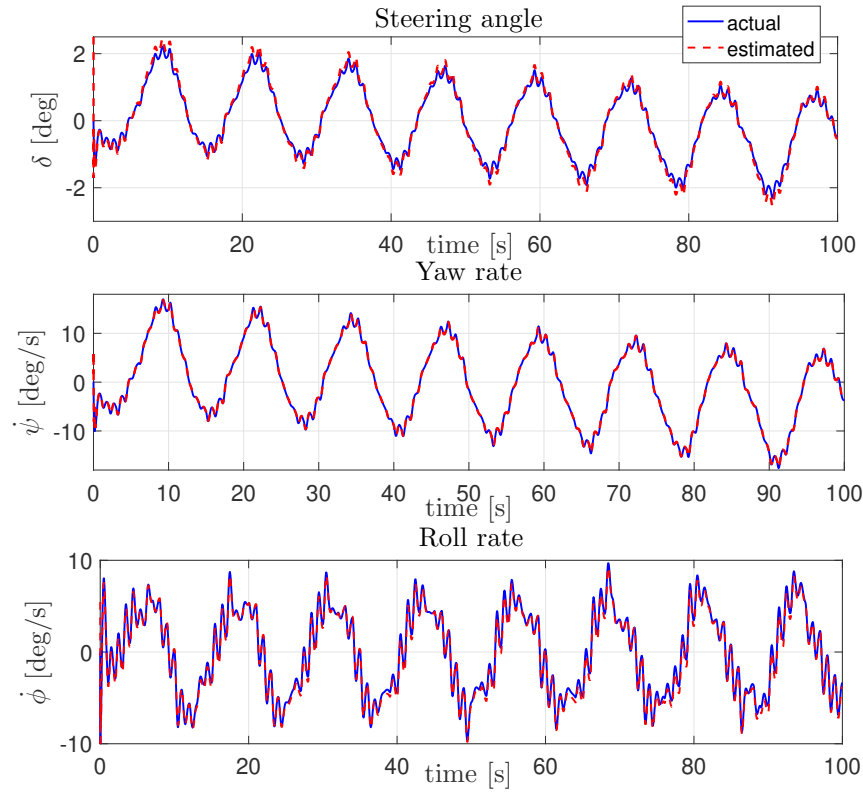


FIGURE 6.2: Actual measures (blue) and their estimation (dashed red).

To verify the unmeasurable states estimation  $v_y$ ,  $F_{yf}$  and  $F_{yr}$ , the lateral acceleration  $a_y$  is reconstructed from equations (5.24) and (5.25) and compared to the one measured by the IMU as shown in figure 6.3.

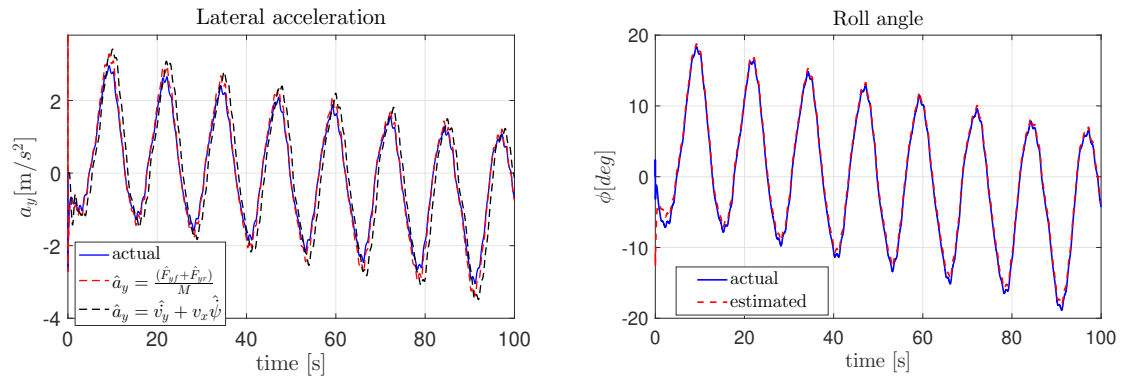


FIGURE 6.3: Observer validation.

Figure 6.4 depicts the estimation of unknown parameters vector with respect to their nominal values. It can be appreciated that the proposed observer shows a good estimation accuracy and proves the reliability of the approach to estimate simultaneously the dynamic states and the unknown parameters of the model. However, the singularities in figure 6.4 are mainly due to the observer transient state and the conditioning of the inverse matrix. Also, when we use a relatively poor excitation, the vector parameters is sensitive to outputs variations. Further, given the number of parameters to be estimated, it is a complex task to excite perfectly all the parameters simultaneously.

To validate the estimated parameters, one can extract the value of each parameter after the transient phase. Afterwards, once the unknown parameters vector is identified, these parameters are inserted into the motorcycle two-body model and used to simulate and validate the PTWV lateral dynamics. The resulting

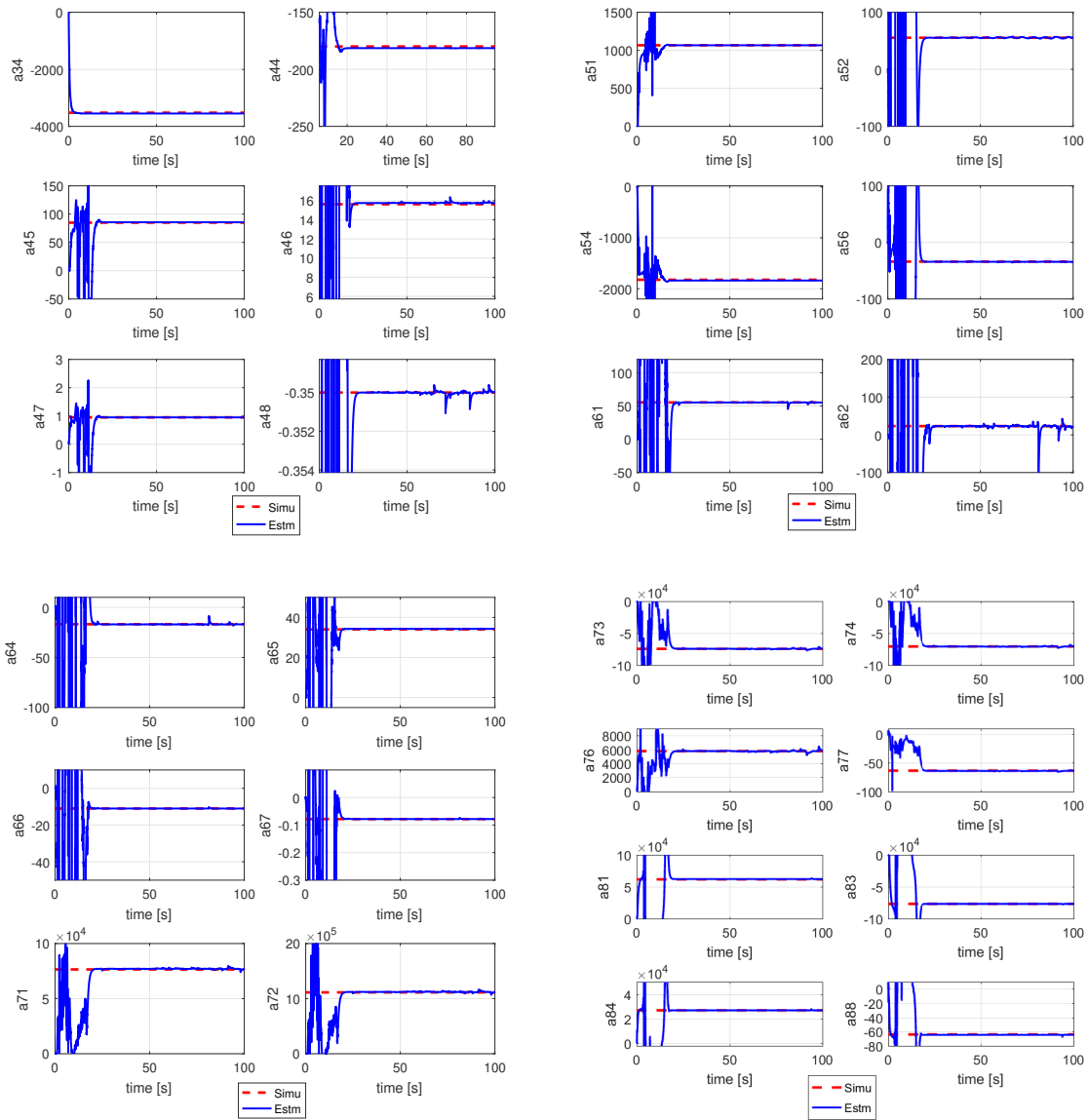


FIGURE 6.4: Actual parameters (dashed red) and estimated parameters (blue).

model is compared with respect to the corresponding *BikeSim* data in two others track tests. The first test consists on a slalom maneuver on a flat road surface with high friction coefficient  $\mu = 0.9$  and a forward speed of 40 km/h as depicted in figure 6.5. The second test is an oncoming traffic with variable speed on handling road as in figure 6.7.

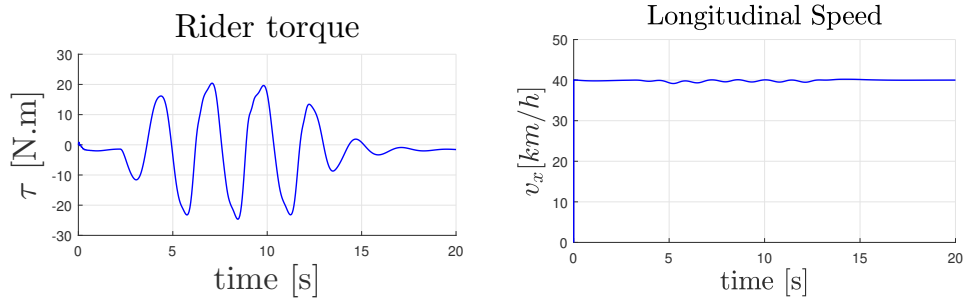


FIGURE 6.5: Slalom maneuver at constant speed 40 km/h.

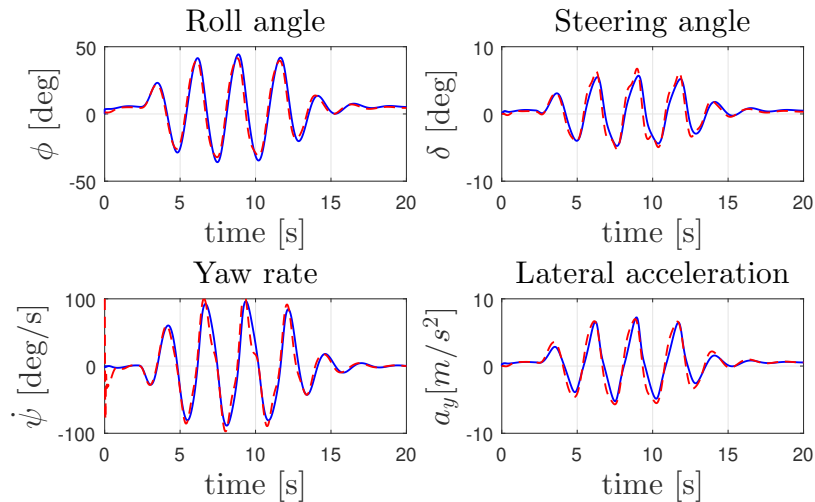


FIGURE 6.6: Test 1: Updated state (dashed red) compared to actual measurement (blue).

First, the performance of the identified model is evaluated in simulation by comparing with the actual output (see figures 6.6 and 6.8). These figures plot the most important states of the lateral dynamic model (roll and steering angles, yaw rate, the lateral acceleration). Second, this evaluation is quantified with two metrics by means of the root mean square error (RMS) and (MSE), summarized in table 6.1 to check the similarity between the actual and simulated outputs. Results, summarized in Table 6.1, show that the estimation error between the proposed method and actual states is generally small. The values of index, show a good forecast accuracy and prove the reliability of the estimated parameters in reconstructing the motorcycle behavior.

State #	Test	RMS	MSE
$\phi$	$Sc_1$	0.0331	0.0011
	$Sc_2$	0.0555	0.0031
$\delta$	$Sc_1$	0.0078	$6.0184 \cdot 10^{-3}$
	$Sc_2$	0.0042	$1.7881 \cdot 10^{-3}$
$\dot{\psi}$	$Sc_1$	0.0425	0.0018
	$Sc_2$	0.0288	$8.2925 \cdot 10^{-3}$
$\dot{\phi}$	$Sc_1$	0.0774	0.0060
	$Sc_2$	0.02131	$4.5511 \cdot 10^{-2}$
$a_y$	$Sc_1$	0.1803	0.0785
	$Sc_2$	0.3857	0.1359

TABLE 6.1: Analysis of the estimation method for the new tests conducted.

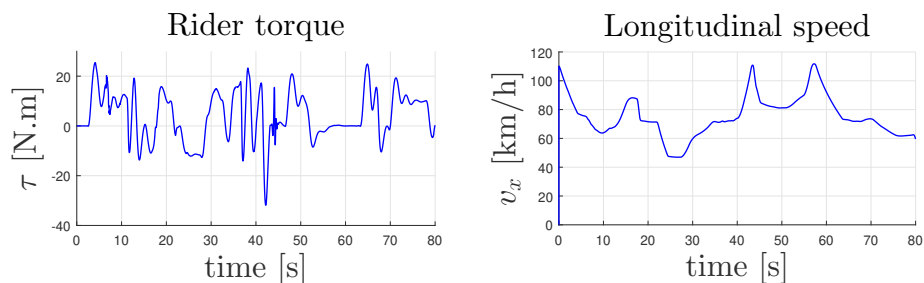


FIGURE 6.7: An oncoming traffic with variable speed.

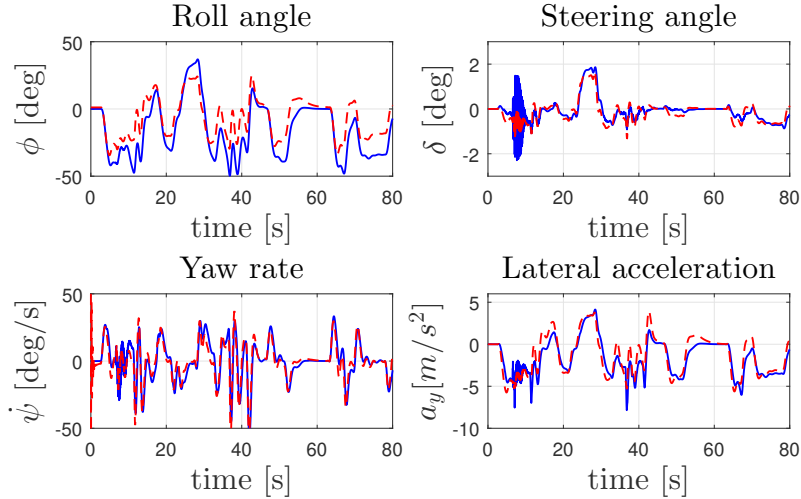


FIGURE 6.8: Test 2: Updated state (dashed red) compared to actual measurement (blue).

The simulated response with the synthesis model shown in dashed red is overlaid on the actual *BikeSim* data. The results of the slalom test with constant velocity are better than the track test with variable speed. This is because of the sharp two body model is developed assuming constant forward velocity or slowly varying speed to neglect the coupling between the longitudinal and lateral motions. But, even in the presence of forward speed in the second test, good representation of the lateral dynamics still be ensured. In the two scenarios, even if there are some errors at the peak of the reconstructed model states but the results remain acceptable. These differences between the simulated and measured data is due to modeling errors, the simulated model is a 2 bodies model while the data is collected using a high-fidelity 8 bodies model motorcycle. The validation plots show that our estimation scheme was successfully evaluated. These results confirm the performance of the observer in identifying the unknown parameters and show that the estimated parameters are robust enough to handle a variety of riding tests.

## 6.7 Conclusions

The chapter shows some significant features, to discuss how a failed decoupling condition, can be recovered using augmented model and time delay concept, with a specific characterization of the system matrices. Based on these last, a step by step algorithm is developed to design the DUIO observer.

Our main contribution concerns the modeling transformation to break out with the rank condition related to mismatched unknown part. An augmented system is considered by including delayed outputs. Different from existing methods, the proposed observer gives a general framework for observer-based parameters identification. It is shown that, by introducing delayed outputs, the rank condition is fulfilled, allowing to parameters identification in two steps. In the first step, the state vector and unknown inputs are estimated while, the parameter vector is identified in the next step. Afterwards, sufficient conditions for the existence of estimator are given in terms of LMIs to ensure the asymptotic state and parameters estimation error convergence. The effectiveness of the proposed approach is demonstrated throughout co-simulation with a high-end motorcycle simulator. In the LPV model, we take into account the forward speed as a linear varying parameter. Despite unknown inputs, the vehicle's intrinsic parameters are almost accurately identified and also, the rate convergence can be improved by convenient poles assignment in LMI region. The simulation results are quite promising to prove that the estimation approach provides an interesting solution for state reconstruction and parameters identification.

In future works, the observer robustness can be improved by considering uncertainties such as the neglected dynamics, the parametric uncertainties of the model, the sensor biases and the measurement noises. Thereby, the synthesis of robust observer regarding uncertainties requires adding terms containing perturbations in the observation equation. This leads to an adaptation of the model-based observers to the case of uncertain matrices of the state space model.

# Chapter 7

## Adaptive Observer for PTWV

### Abstract

Safety systems for powered two-wheelers, claim a thorough investigation of motorcycle motion and tires/road interaction, to help the rider to stay out of harm's way. This chapter deals with the problem of estimation of two wheelers lateral motion with consideration of cornering and camber stiffness unknown coefficients. It consists of the design of linear parameter varying (LPV) observer associated with an adaptive law to ensure convergence stability based on a general Lipschitz condition, Lyapunov theory and subjected to persistence excitation conditions. The LPV observer is transformed into Takagi-Sugeno (T-S) fuzzy observer and sufficient conditions, for the existence of the estimator, are given in terms of linear matrix inequalities (LMIs). The forward speed is treated as an online measured time-varying parameter and the cornering stiffness at the front and rear tires are assumed to be unknown with *a priori* known nominal values, evaluated from the Pacejka's formula tire model.

In this work, an evaluation framework is proposed to provide a critical overview and analyze the stiffness parameters estimation performance and accuracy. The proposed adaptive law is compared to a direct estimation method and a dynamic inversion estimation scheme adapted to our problem. Finally, several simulation cases are provided to highlight the feasibility and the effectiveness of the suggested methods, through test scenarios performed with the well-known motorcycle simulator *BikeSim* and by field test acquired using an instrumented motorcycle. The theoretical aspects and the validation of this idea were published in Fouka et al., 2018a.

### 7.1 Model Description

In this work, the well-known Sharp model is used to describe the PTWV lateral dynamics which can be written by the following state space representation:

$$E\dot{x} = \bar{A}(v_x(t))x(t) + \bar{B}\tau(t) \quad (7.1)$$

where  $x(t) \in \mathbb{R}^{n_x}$  is the state vector such that  $x = [\phi, \delta, v_y, \psi, \dot{\phi}, \dot{\delta}, F_{y_f}, F_{y_r}]^T$ . The input vector is denoted by  $\tau(t) \in \mathbb{R}$  refers to the rider's torque. The vehicle's forward speed  $v_x(t)$  is considered as a measured time-varying parameter.  $E = [e_{ij}]$  is an invertible matrix,  $\bar{A}(v_x(t)) = [\bar{a}_{ij}]$  is the state matrix and  $\bar{B}$  is a vector with their associated dimensions.

The lateral front and rear forces  $F_{y_f}$  and  $F_{y_r}$  are considered to be linear with respect to the tire's side-slip angle  $\alpha_k$  and camber angle  $\gamma_k$ , then:

$$F_{y_k,0} = C_{\alpha_k} \alpha_k + C_{\gamma_k} \gamma_k \quad k = f, r \quad (7.2)$$

Also, we introduce tire relaxation to characterize the transient behavior by means of a first order system as following:

$$\frac{\sigma}{v_x} \dot{F}_{y_k} = -F_{y_k} + F_{y_k,0} \quad (7.3)$$

The use of a linear tire representation is justified as is discussed in the introduction section. ADAS are dedicated to perform safety tasks before the vehicle reaches the limits of its stability region. Beyond the stability region, almost ADAS fails to recover the vehicle handling, particularly, in turn situations.

### 7.1.1 Parameter-Dependent Model

Let consider  $\zeta(t) = v_x(t)$  a varying measured parameter and  $\Theta \in \mathbb{R}^{n_\Theta}$  is the unknown parameters vector. The PTWV model of equation (7.1) can be reformulated in the following LPV form:

$$\begin{cases} \dot{x} = A_\zeta x + Bu + \Lambda(x, \zeta, \Theta) \\ y = Cx \end{cases} \quad (7.4)$$

where  $y \in \mathbb{R}^{n_y}$  is the output measured vector and  $\Lambda(x, \zeta, \Theta) \in \mathbb{R}^{n_x}$  represents the parameters dependent terms of the PTWV dynamics. The matrices  $A_\zeta$  and  $B$  are defined from (7.1) as  $A_\zeta = E^{-1} \bar{A}(\zeta(t)) - \Lambda(x, \zeta, \Theta)$ ,  $B = E^{-1} \bar{B}$  and  $u = \tau(t)$ .

An inertial measurement unit (IMU) is embedded to the PTWV and mounted under the vehicle's seat at approximately the vehicle's center of mass. The available measurements are three accelerations and three angular velocities expressed in the IMU body reference frame. These measurements are used to derive the roll angle rate  $\dot{\phi}$ , yaw angle rate  $\dot{\psi}$  and the lateral acceleration  $a_y$  expressed in the PTWV modeling reference frame. In addition to the IMU measurement, an optical encoder is fixed on the steering body providing the steering angle  $\delta$  and its time-derivative  $\dot{\delta}$ . The minimum set of sensor measurements are the following:

$$y = \left[ \delta \quad \dot{\psi} \quad \dot{\phi} \quad \dot{\delta} \quad a_y \right]^T \quad (7.5)$$

By using equations (7.2) and (7.3), the vector of the unknown varying parameters  $\Lambda(x, \zeta, \Theta)$  is written in a linear form with respect to the unknown parameters vector  $\Theta$  as following :

$$\Lambda(x, \zeta, \Theta) = D\chi(x, \zeta)\Theta \quad (7.6)$$

in which:

$$\chi(x, \zeta) = \begin{bmatrix} -\frac{v_x \alpha_f}{\sigma_f} & \frac{v_x \gamma_f}{\sigma_f} & 0 & 0 \\ 0 & 0 & -\frac{v_x \alpha_r}{\sigma_r} & \frac{v_x \gamma_r}{\sigma_r} \end{bmatrix} \quad (7.7)$$

and:

$$\Theta = \begin{bmatrix} C_{\alpha_f} - C_{\alpha_f,0} \\ C_{\gamma_f} - C_{\gamma_f,0} \\ C_{\alpha_r} - C_{\alpha_r,0} \\ C_{\gamma_r} - C_{\gamma_r,0} \end{bmatrix} \quad (7.8)$$

where,  $C_{s_k}$  is the tires' cornering stiffness,  $s = \alpha, \gamma$  designates lateral slip or camber angles,  $k = f, r$  denotes the front and rear tires,  $C_{s_k,0}$  are the corresponding nominal values of the tires' cornering stiffness and  $\sigma_k$  is the tire's relaxation. The cornering stiffness at the front and rear tires are assumed to be unknown and vary with respect to their nominal values.

### 7.1.2 Problem Statement

From PTWV dynamics equation, it is straightforward to find an approximate estimation of the tires' cornering stiffness using a direct method or a dynamics inversion approach. With the direct method (Sierra et al., 2006), the PTWV can be reduced to an equivalent one-body dynamics expressed by the following equations:

$$\begin{cases} ma_y = F_{yf} + F_{yr} \\ I_z \ddot{\psi} = l_f F_{yf} - l_r F_{yr} \end{cases} \quad (7.9)$$

where  $m$  and  $I_z$  are the equivalent body mass and  $z$ -inertia. By combining equations (7.2), (7.3) and (7.9), we get:

$$\begin{bmatrix} -\alpha_f & \gamma_f & -\alpha_r & \gamma_r \\ -l_f \alpha_f & l_f \gamma_f & l_r \alpha_r & -l_r \gamma_r \\ -\alpha_f & \gamma_f & 0 & 0 \\ 0 & 0 & -\alpha_r & \gamma_r \end{bmatrix} \begin{bmatrix} C_{\alpha_f} \\ C_{\gamma_f} \\ C_{\alpha_r} \\ C_{\gamma_r} \end{bmatrix} = \begin{bmatrix} ma_y \\ I_z \ddot{\psi} \\ \frac{\sigma_f}{v_x} \dot{F}_{yf} + F_{yf} \\ \frac{\sigma_r}{v_x} \dot{F}_{yr} + F_{yr} \end{bmatrix} \quad (7.10)$$

The dynamics inversion in equation (7.10) gives more insight in parameters estimation by avoiding state differentiation. This last method is based on classical unknown input observers and output differentiation as reported in (Zhang et al., 2017; Weiss et al., 2000). From equations (7.4), (7.5) and (7.6), we get:

$$\hat{y} = CA_\zeta \hat{x} + CBu + CD\chi(\hat{x}, \zeta) \hat{\Theta} \quad (7.11)$$

By an algebraic inversion of the previous equation, the unknown parameters vector  $\Theta$  can be reconstructed from the estimated state vector and output derivatives. However, the feasibility of this inversion is conditioned by a convenient selection of the excitation signal to fulfill rank condition  $\text{rank}(CD) = \text{rank}(D)$ .

In this section, we address the problem of state estimation and unknown parameters identification of the PTWV dynamics expressed by equation (7.4). We focus our interest on the identification of the front and rear tires' cornering stiffness since they play a key role to guarantee the motorcycle stability in turns maneuvers. Moreover, it is known among all vehicle dynamics literature that tires' cornering stiffness are combined with the available road friction  $\mu$ , then, solving the estimation problem for the unknown parameters vector  $\Theta$  is equivalent to finding the combined vector  $\Theta = \mu\Theta_0$ , where  $\Theta_0$  is the tires' nominal stiffness. Without loss of generality, we consider in this section that tires' cornering stiffness with their associated road friction are embedded in one variable. For some very spatial cases such a puddle and dead leaf causing an abrupt variation of road friction, the problem of friction estimation can be more efficiently solved by using other techniques such as vision-based classification (Roychowdhury et al., 2018; Liu et al., 2011).

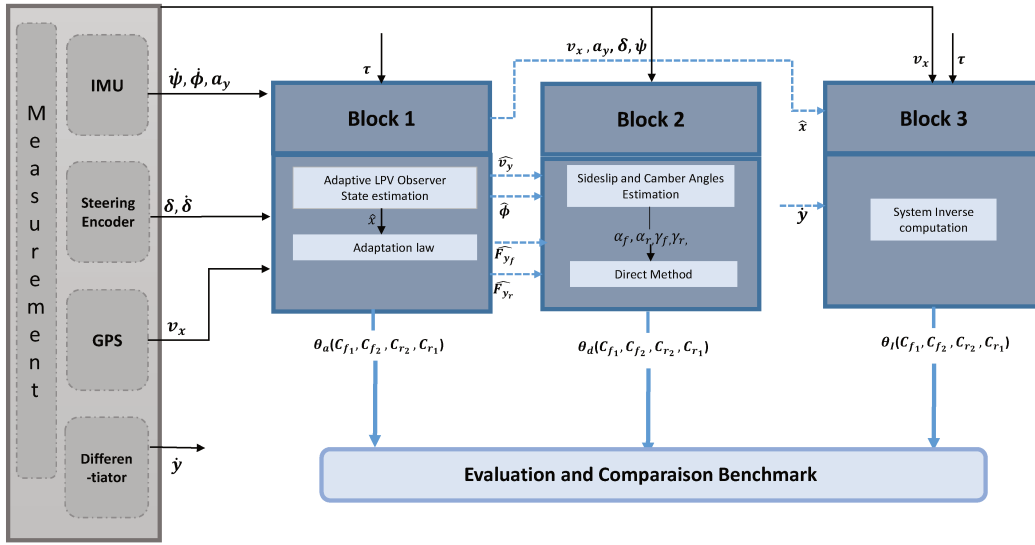


FIGURE 7.1: Schematic overview of estimation methodology.

## 7.2 Observer Design

In this section, the design of the adaptive observer is described based on the PTWV model of equation (7.4). Next, asymptotic convergence is proved by using Lyapunov theory associated with the Lipschitz property, giving rise to an optimization problem expressed by a set of LMI to be solved.

### 7.2.1 Observability Analysis

The PTWV model referenced by equation (7.4) with its associated output measurements vector does not satisfy the observability/detectability condition. One solution is to use the flatness properties (Sanchez et al., 2018) to define additional virtual measurements (Levant, 2003). From equations (7.1), we consider the lateral and yaw dynamics given by:

$$\begin{bmatrix} E_{3,:} \\ E_{4,:} \end{bmatrix} \dot{x} = \begin{bmatrix} \bar{A}_{3,:} \\ \bar{A}_{4,:} \end{bmatrix} x \quad (7.12)$$

where the notation  $E_{i,:}$  denotes the  $i^{\text{th}}$  line of matrix  $E$ . After some algebraic manipulations, the output measurements vector  $y$ , equation (7.4), can be augmented with an auxiliary virtual sensor output,  $y_a$ , expressed by:

$$y_a = (m_{fk} - ml_f)F_{yf} + (m_{fk} + ml_r)F_{yr} \quad (7.13)$$

### 7.2.2 Adaptive Observer

Throughout the observer design, the following nonrestrictive assumptions are considered:

**Assumption 7.1.** assume that  $\zeta \in \Delta$  be a set of vectors defined on an hyper-rectangles  $\Delta$  given by:

$$\Delta = \{ \zeta \in \mathbb{R}^{n_\zeta} \mid \zeta_{i_{min}} \leq \zeta_i \leq \zeta_{i_{max}} \} \quad (7.14)$$

**Assumption 7.2.**

- The system's input  $u(t)$  is known and sufficiently persistent, i.e, its exists constants  $c_1$ ,  $c_2$  and  $c_3$  such that for all  $t$  the following inequality holds (Belov et al., 2018) :

$$c_1 I \leq \int_{t_0}^{t_0+c_3} D\chi(\hat{x}, v_x)\chi^T(\hat{x}, v_x)D^T dt \leq c_2 I$$

- The state vector  $x(t)$  and the input vector  $u(t)$  are bounded. This assumption will fit the general practical case, e.g. a stable motion of a PTWV.

**Theorem 7.1.** given the PTWV dynamics of equation (7.1) satisfying assumptions (7.1-7.2), the following LPV-adaptive observer:

$$\begin{cases} \dot{\hat{x}} = A_\zeta \hat{x} + Bu + \Lambda(\hat{x}, \zeta, \hat{\Theta}) + L_\zeta (y - \hat{y}) \\ \hat{y} = C\hat{x} \end{cases} \quad (7.15)$$

with the adaptation law:

$$\dot{\hat{\Theta}} = \Gamma \chi^T(\hat{x}, \zeta) TC \tilde{x} \quad \text{and} \quad \Gamma = \Gamma^T > 0 \quad (7.16)$$

ensures an asymptotic convergence error for the simultaneous state and parameters vector estimation, towards zero if there exist a symmetric positive definite matrix  $P$  and matrices  $K_\zeta$  and  $R$  satisfying the following inequalities :

$$PA_\zeta + A_\zeta^T P - K_\zeta C - C^T K_\zeta^T + PQ^{-1}P^T + R < 0 \quad (7.17)$$

$$D^T P = TC \quad (7.18)$$

where  $\tilde{x}$  is the state estimation error vector and  $L_\zeta$  is the observer gain matrix .

**Proof 7.1.**

lets consider the following class of Luenberger-adaptive observer:

$$\begin{cases} \dot{\hat{x}} = A_\zeta \hat{x} + Bu + \Lambda(\hat{x}, \zeta, \hat{\Theta}) + L_\zeta (y - \hat{y}) \\ \hat{y} = C\hat{x} \end{cases} \quad (7.19)$$

where  $\hat{x}$ ,  $\hat{y}$  and  $\hat{\Theta}$  are respectively the estimated state, output and parameters vector.  $L_\zeta$  is the observer gain matrix such that  $\Phi_\zeta = A_\zeta - L_\zeta C$  is Hurwitz. Lets  $\tilde{x} = x - \hat{x}$  and  $\tilde{\Theta} = \Theta - \hat{\Theta}$  be respectively the state and the parameters estimation error vector. The error dynamics can be computed as following:

$$\dot{\tilde{x}} = \Phi_\zeta \tilde{x} + \tilde{\Lambda} + D\chi(\hat{x}, \zeta)\tilde{\Theta} \quad (7.20)$$

in which  $\tilde{\Lambda} = \Lambda(x, \zeta, \Theta) - \hat{\Lambda}(\hat{x}, \zeta, \Theta)$ .

The stability analysis can be performed by considering the following quadratic Lyapunov function :

$$V(\tilde{x}) = \tilde{x}^T P \tilde{x} + \tilde{\Theta}^T \Gamma^{-1} \tilde{\Theta} \quad (7.21)$$

where  $P$  and  $\Gamma$  are symmetric positive definite matrices.

By taking the time derivative of the Lyapunov function (7.21), and replacing the state estimation error dynamics by its equation (7.20), we obtain:

$$\begin{aligned} \dot{V} = & \tilde{x}^T \Psi_{\zeta} \tilde{x} + \tilde{\Lambda}^T P^T \tilde{x} + \tilde{x}^T P \tilde{\Lambda} + \tilde{\Theta}^T \Gamma^{-1} \dot{\tilde{\Theta}} + \dot{\tilde{\Theta}}^T \Gamma^{-1} \tilde{\Theta} \\ & + \tilde{\Theta}^T \chi^T(\hat{x}, \zeta) D^T P \tilde{x} + \tilde{x}^T P D \chi(\hat{x}, \zeta) \tilde{\Theta} \end{aligned} \quad (7.22)$$

where  $\Psi_{\zeta} = \Phi_{\zeta}^T P^T + P \Phi_{\zeta}$ .

Let consider the following lemmas:

**Lemma 7.1.** *the continuous function  $\Lambda(x, \zeta, \Theta)$  is said to be Lipschitz with respect to  $x$ , if for all  $x$ , the function  $\Lambda(x, \zeta, \Theta)$  can be rewritten under the following generalized Lipschitz condition (Pertew, Marquez, and Zhao, 2005):*

$$\Lambda^T Q \Lambda \leq x^T R x \quad (7.23)$$

where  $Q$  and  $R$  are respectively symmetric positive and semi-positive definite matrices. Thus, any system in the form of equation (7.4), can be reformulated in a generalized Lipschitz condition, as long as  $\Lambda(x, \zeta, \Theta)$  is continuously differentiable with respect to  $x$ .

**Lemma 7.2.** *for every matrix  $G$ , symmetric positive definite, the following property holds (Xie, 1996):*

$$X^T Y + Y^T X \leq X^T G X + Y^T G^{-1} Y$$

By using the Lipschitz condition in lemma (7.1) and the property in lemma (7.2), we get the following inequality:

$$\tilde{\Lambda}^T P^T \tilde{x} + \tilde{x}^T P \tilde{\Lambda} \leq \tilde{x}^T P Q^{-1} P^T \tilde{x} + \tilde{\Lambda}^T Q \tilde{\Lambda} \quad (7.24)$$

Now, we can prove exponential stability convergence:

$$\begin{aligned} \dot{V}(t) \leq & \tilde{x}^T \left( \Psi_{\zeta} + P Q^{-1} P^T + R \right) \tilde{x} + \tilde{\Theta}^T \chi^T(\hat{x}, \zeta) D^T P \tilde{x} + \\ & \tilde{x}^T P D \chi(\hat{x}, \zeta) \tilde{\Theta} + \tilde{\Theta}^T \Gamma^{-1} \dot{\tilde{\Theta}} + \dot{\tilde{\Theta}}^T \Gamma^{-1} \tilde{\Theta} \end{aligned} \quad (7.25)$$

Following assumption (7.2), in the case of a stable PTWV dynamics with a bounded states, the estimated term  $\chi(\hat{x}, \zeta)$  will be bounded by an upper singular values, e.g.,  $\|\chi(\hat{x}, \zeta)\|_2 < \sigma_{\max}$ . Consequently:

$$\dot{V}(t) \leq \tilde{x}^T \left( \Psi + P Q^{-1} P^T + R \right) \tilde{x} + 2 \tilde{\Theta}^T \Gamma^{-1} \dot{\tilde{\Theta}} + 2 \sigma_{\max} \tilde{\Theta}^T D^T P \tilde{x} \quad (7.26)$$

At this level, we can derive the observer's adaptive law from equation (7.26) as following:

$$\tilde{\Theta}^T \Gamma^{-1} \dot{\tilde{\Theta}} + \sigma_{\max} \tilde{\Theta}^T D^T P \tilde{x} < 0 \quad (7.27)$$

According to the tire's relaxation formula (7.3), the unknown parameters rate is practically slow, *e.g.*  $\dot{\Theta} = 0$  and hence,  $\dot{\Theta} = -\dot{\Theta}$ . Furthermore, it is possible to find a matrix  $T$ , such that  $D^T P = TC$  (Corless and Tu, 1998). By this transformation, the adaptive law can be stated as:

$$\dot{\Theta} = \Gamma \chi^T(\hat{x}, \zeta) TC \tilde{x} \quad \text{and} \quad \Gamma = \Gamma^T > 0 \quad (7.28)$$

With this law, the time derivative  $\dot{V}(t)$  becomes :

$$\dot{V}(t) \leq \tilde{x}^T (A_\zeta^T P^T + P A_\zeta - C^T K_\zeta^T - K_\zeta C + P Q^{-1} P^T + R) \tilde{x} \quad (7.29)$$

where  $K_\zeta = P L_\zeta$ .

### 7.2.3 Polytopic Form

Theorem (7.1) in section (7.2.2) introduces a theoretical framework for the states and parameters estimation. The resulting optimization problem, given by the inequality of equation (7.17), is parameter dependent, thus, we must revisit our observer.

**Theorem 7.2.** *the following adaptive observer :*

$$\begin{cases} \dot{\hat{x}} = A_\zeta \hat{x} + Bu + \Lambda(\hat{x}, \zeta, \hat{\Theta}) + L_\zeta (y - C\hat{x}) \\ \dot{\hat{\Theta}} = \sigma_{\max} \hat{\Theta}^T D^T P \tilde{x} \end{cases} \quad (7.30)$$

*ensures an asymptotic convergence of the state estimation error for system class of equation 7.1, if and only if there exist a matrix  $P$  symmetric positive definite, a matrix  $K_\zeta$ , and a matrix  $R$  satisfying the Liptchiz condition. Thus, if the condition  $\text{rank}(CD) = \text{rank}(D)$  is fulfilled, a matrix  $\Gamma$  symmetric positive definite can be found such that the following LMI holds:*

$$\min_{i=1, \dots, r} \varsigma \quad \text{s.t.}$$

$$\begin{bmatrix} \varsigma I & D^T P - TC \\ (D^T P - TC)^T & \varsigma I \end{bmatrix} > 0 \quad (7.31)$$

$$\begin{bmatrix} A_i^T P + P A_i - C^T K_i^T - K_i C + R & P \\ P & -Q \end{bmatrix} < 0 \quad (7.32)$$

#### Proof 7.2.

the PTWV model in equation (7.1) is dependent on the measured vehicle's speed, *e.g.*,  $\zeta = v_x$ . According to assumption (7.1), and knowing that  $\zeta$  satisfies the following convex property:

$$\sum_{i=1}^r \eta_i(\zeta) = 1, \quad 0 \leq \eta_i(\zeta) \leq 1 \quad (7.33)$$

where  $\eta_i$  are weighting functions. By using the so-called Takagi-Sugeno (TS) structure (Tanaka and Wang, 2004), the PTWV model in equation (7.1) can be reformulated as a set of interconnected linear time invariant models. Since we have one non-linearity  $\zeta \in \Delta$ , supposed to be accessible at real-time, the resulting LPV model (7.4) in TS structure is described by 2 sub-models as following:

$$\begin{cases} \dot{x} = \sum_{i=1}^r \eta_i(\zeta) A_i x + Bu + \Lambda(x, \zeta, \Theta) \\ y = Cx \end{cases} \quad (7.34)$$

where  $r = 2^{n_\zeta}$  is the number of the sub-models corresponding to  $n_\zeta$  non-linearities ( $n_\zeta = 1$  in our case). Then,  $A_\zeta$  in equation (7.1) becomes  $\sum_{i=1}^r \eta_i(\zeta) A_i$  and  $A_i$  are constant matrices.

From theorem (7.1) and using the convex sum property of the weighting functions, sufficient conditions ensuring  $\dot{V}(t) < 0$  are established by the following LMIs:

$$A_i^T P + P A_i - C^T K_i^T - K_i C + P Q^{-1} P^T + R < 0 \quad (7.35)$$

By applying Schur lemma, inequality (7.17) can be transformed to the second LMI of equation (7.31). The observer gain matrix  $L$  in theorem (7.2) is also defined by using the polytopic exact form:

$$\begin{cases} K_\zeta = \sum_{i=1}^r \eta_i(\zeta) K_i, \\ L_\zeta = \sum_{i=1}^r \eta_i(\zeta) L_i, \\ L_i = P^{-1} K_i \end{cases} \quad (7.36)$$

Finally, the equality constraint  $D^T P = TC$  can be formulated by the an optimization problem described by the first LMI of equation (7.31).

### 7.3 Simulation Results

In this section, the effectiveness of the proposed estimation framework is investigated by co-simulation with *BikeSim* software. The PTWV model *Scooter Big Baseline* is chosen from the software dataset, in which, the nominal values  $C_{j_i,0}$  of the side-slip and camber stiffness are available.

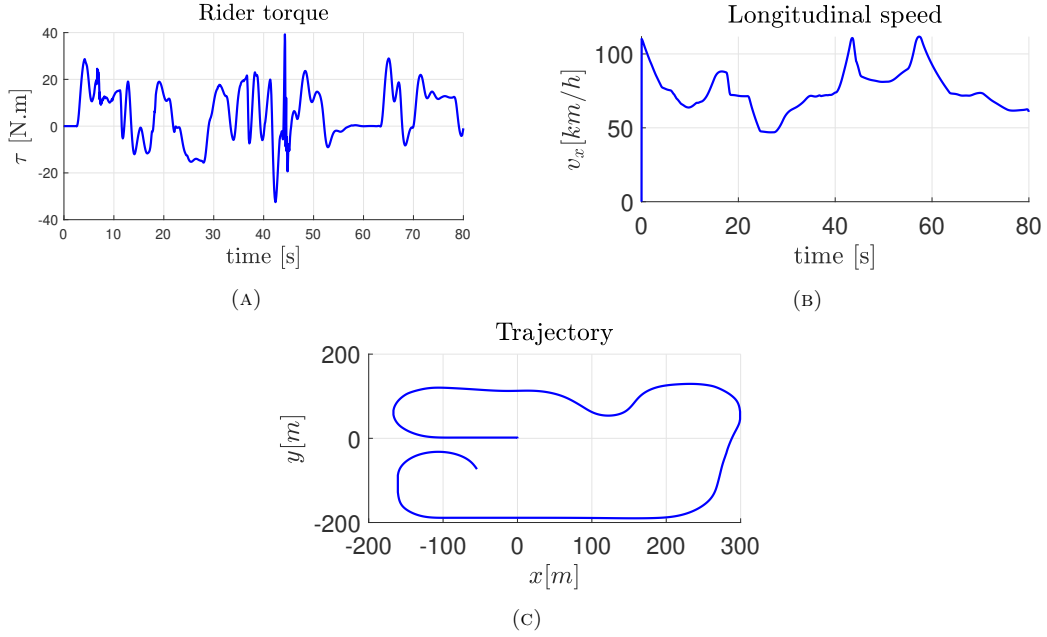


FIGURE 7.2: *BikeSim* scenario: the rider's steering torque input  $\tau$ , the forward speed  $v_x$ , and the vehicle's trajectory.

The test scenario is carried out by considering a handling maneuver depicted in figure 7.2c and involving a medium hard rider torque represented in figure 7.2a. The forward speed is a measured varying parameter ranging from 40 km/h to 120 km/h as shown in figure 7.2b. For this first setup, the road friction coefficient is fixed to a constant value  $\mu = 0.9$ . The observer gains  $L_i$  are computed using theorem 7.2. The test scenario is in accordance with a real regular riding condition. It also allows to highlight the observer performance by covering a broad spectrum of the PTWV dynamics within and beyond its linearization domain. Further, we test the adaptive law with a constant gain matrix  $\Gamma$  and with zero initial condition.

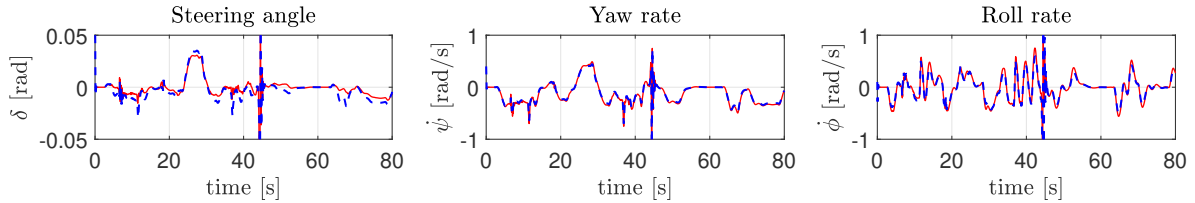


FIGURE 7.3: *BikeSim* sensor (red) and observer estimation (dashed blue).

Figures 7.3 show the state estimation performance with respect to their measured values from *BikeSim* and also demonstrate a finite-time asymptotic estimation. Furthermore, since the lateral velocity  $v_y$ , the roll angle  $\phi$  and tire forces  $F_{yf}$ ,  $F_{yr}$  are unmeasurable (figures 7.4), their estimations are used to reconstruct the lateral acceleration  $a_y$  at the center of mass of the rear body  $G_r$  by using the two equations in (7.37).

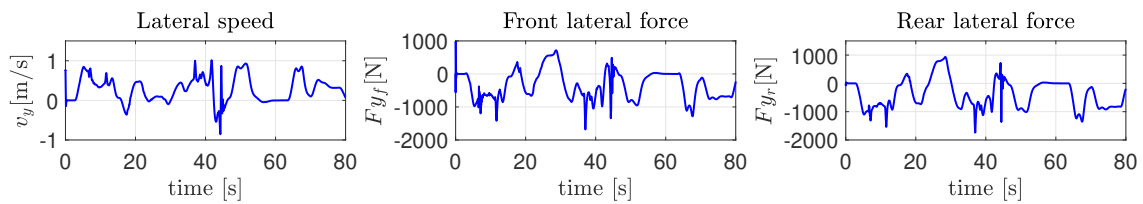


FIGURE 7.4: Unmeasurable states estimation.

Figures 7.5 represent the estimated lateral acceleration and the corresponding one given by *BikeSim*. It is obvious that these figures show finite-time asymptotic estimation where exact estimation can't be achieved since the PTWV dynamics linearization is carried out considering small roll perturbations from straight line running.

$$\begin{aligned}\hat{a}_y &= \frac{(\hat{F}_{yf} + \hat{F}_{yr})}{M} \\ \hat{a}_y &= \hat{v}_y + v_x \dot{\psi} - h \ddot{\phi}\end{aligned}\quad (7.37)$$

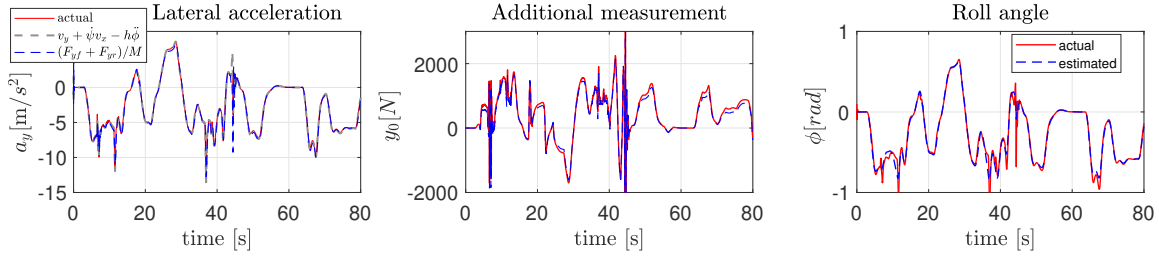


FIGURE 7.5: *BikeSim* sensor (red) and observer estimation (dashed blue).

Figure 7.6 shows the estimated tires stiffness deviations from their nominal values. Once again, finite-time asymptotic estimation is achieved with high accuracy and the observer effectiveness is guaranteed for simultaneous states and tires' stiffness estimation. For example, for the first parameter  $\Theta_1$ , the estimated deviation is used to recover the real front slip stiffness as following  $C_{\alpha_f} = C_{\alpha_f,0} + \Theta_1$ .

In order to make the analysis compacted, for each estimated parameters and for each method, the *Mean* is averaged among the track test. Results, summarized in Table 7.1, show that the computed generally close. It is important to remark that the parameters computed using the adaptive law are very close to nominal values, thanks to the the adaptive law used in the observer estimation. Comparing the three methods, the adaptive law has the best estimation.

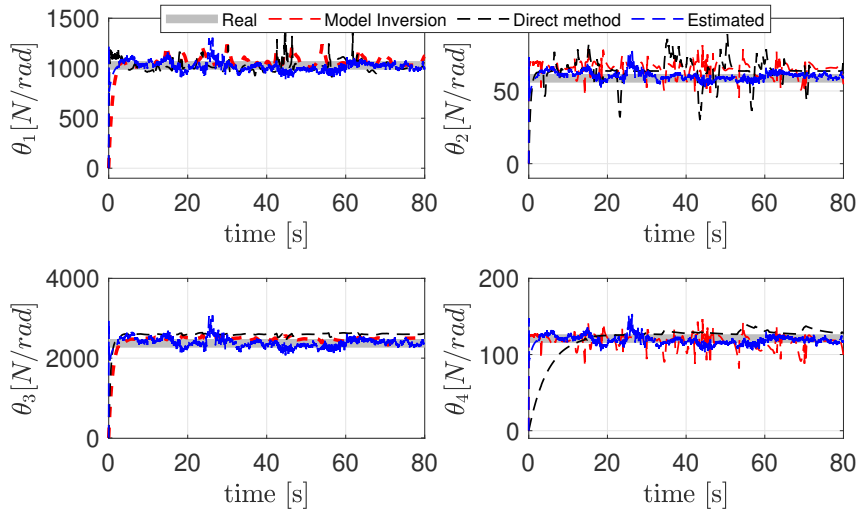


FIGURE 7.6: Estimation performance of tire cornering stiffness.

Parameters	Nominal	Estimated	Inversion	Direct
$\Theta_1$	1028	1022.6	1055.2	1015.7
$\Theta_2$	58.7	60.4638	45.7477	64.2932
$\Theta_3$	2371	2387.1	2485.3	2595.4
$\Theta_4$	121	119.918	117.9743	124.4637

TABLE 7.1: Parameters Mean values comparison

## 7.4 Observer Sensitivity and Robustness

This section aims to test the robustness and sensitivity of the observer with respect to the measurements' noise and regarding parameters uncertainties. To do that, the same test scenario previously described is considered. Remind that the observer was designed considering the nominal tires' cornering stiffness. Consequently, there are two objectives in this section, the first is to test the observer measurement noise sensibility. The second aims to demonstrate the observer robustness to parameters variation.

### 7.4.1 Observer Sensitivity against Sensors' Noise

In practice, the IMU measurements are highly affected by noises. In order to test the observer robustness in the presence of measurements noise, we consider a 5 – 10% random perturbation on the IMU measurements. An overview of the resulting observer performances is depicted in figure 7.7.

It can be noted that the effect of the noise on the states estimation is limited, however, it remains slightly visible. Also, we note that the steering angle and the front tire force are most affected by noise measurements. It reveals also that the rear tire force and the roll angle are less sensitive to measurement noises.

The different noise sensitivities between the front and rear tire forces is explained by the fact that the steering dynamics mostly affects the front tire dynamics. For better performances, the estimated signals can be denoised to remove the noise effect. To that end, a simple second-order Butterworth filter can be used. Simulation result, shows that the adaptive observer is robust enough to handle the noisy case.

### 7.4.2 Observer Robustness against Modeling Uncertainties

In this section, the robustness of the state observer with its associated adaptive law against modeling uncertainties is studied. This observer is designed by considering the nominal values of the tires' stiffness, hence, it is hopeful to quantify the effect of parameters variation on the observer performance. To this end, we consider a variation of  $\pm 50\%$  on the real values of the front and rear tire stiffness. Next, the robustness of the observer to the parameters uncertainties is also evaluated by considering  $\pm 16.5\%$  on the design value of the front and rear mass which is equivalent to an over or an underweight of 50 Kg.

The estimated states are compared with their counterparts by means of the root mean square percentage (RMSE%). The metric quantifies the amount of error to show how close the estimated values are to the true data, RMSE% is defined as:

$$\text{RMSE}_{\%} = \sqrt{\frac{1}{N_{\text{dataset}}} \sum_{i=1}^{N_{\text{dataset}}} (y_{\text{mes}} - y_{\text{est}})^2} \quad (7.38)$$

where  $y_{\text{mes}}$  is the measurement of  $y$  including  $N_{\text{dataset}}$  data points and  $y_{\text{est}}$  is its estimate provided by the observer. The resulting (RMSE%) for the the present scenario are shown in tables 7.2.

From table 7.2, one can states that the  $RMSE$  for  $(\dot{\phi}, \psi, \delta, \phi, a_y)$  raise with parameters variation. Otherwise, it can be seen that the  $RMSE$  for tires' stiffness parameters remain approximately constant, so, the observer

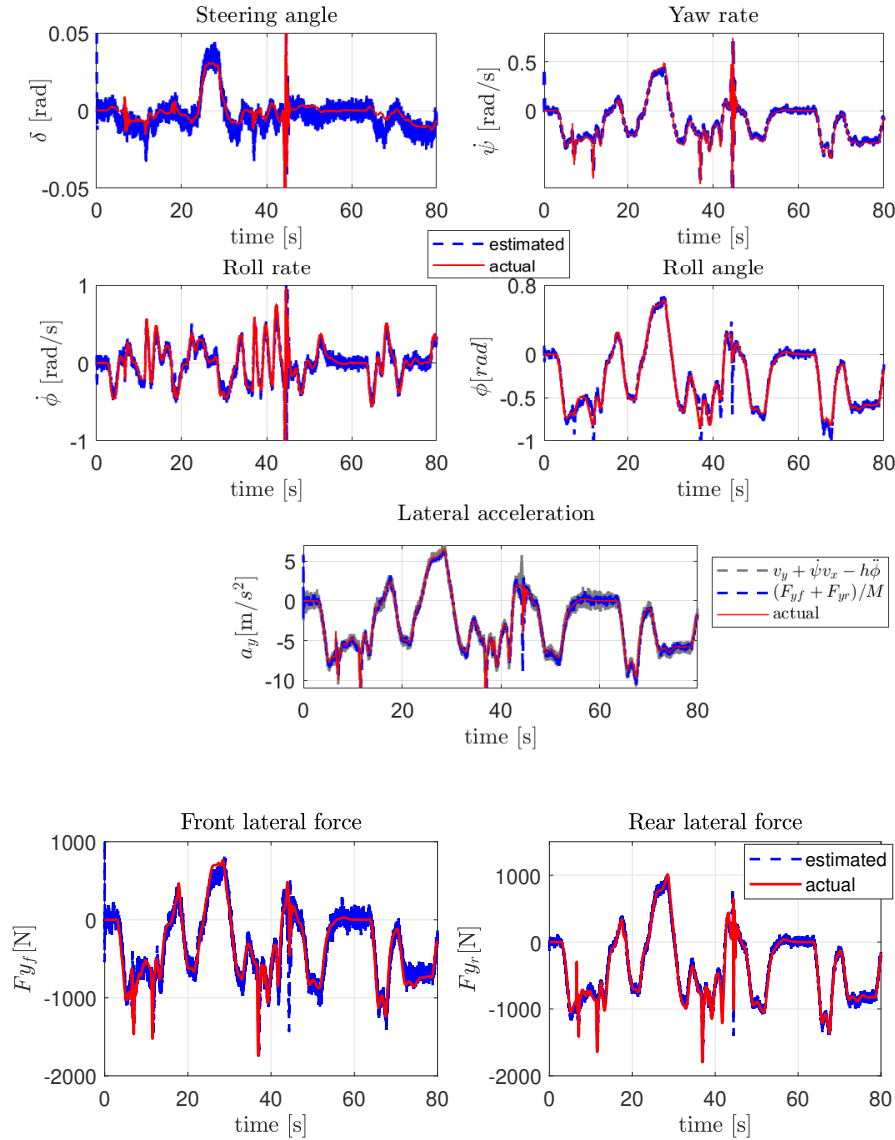


FIGURE 7.7: Robustness to noise: observer states estimation in presence of IMU measurements noise.

is more robust for tire parameters uncertainty. Therefore, the estimated values are generally small and does not exceed 10.87% between the proposed observer and actual data. One can see that the observer gives better estimation for the nominal case, where the *RMSE* values are the lowest. However, even with variations of the tires' parameters or the vehicle's mass, these errors are always lower than 13% which confirms that the performances of the observer are preserved even in the presence of parametric uncertainties. Despite modeling errors between synthesis model and data from simulator, the estimation error dynamics still have good performances and the observer ensures a good estimation.

## 7.5 Motorcycle Experimental Test

In this section, an assessment of the LPV-adaptive observer performance is presented using experimental log-data, using a fully electric propulsion scooter described in section (2.11). The test is carried out on an urban scenic road and performed with normal riding behavior and good environmental conditions. As depicted in figure 7.8c, the road is composed of straight line followed by a narrow turn and just after a big turn. This configuration allows to solicit the PTWV roll dynamics and to maximize as possible as the persistence condition.

State	RMSE				
	Nominal	$m^+$	$m^-$	$C_{fr_i} \times 1.5$	$C_{fr_i} \times 0.5$
$\phi$	6.195	6.369	7.9026	6.6251	7.0678
$\delta$	1.8521	1.8965	1.7682	1.8708	1.941
$\dot{\phi}$	4.8623	6.903	7.6141	6.1901	5.589
$\dot{\psi}$	8.5218	10.467	9.1085	9.0992	9.114
$a_y$	9.69	11.8859	13.7928	10.8682	10.66

TABLE 7.2: Robustness to motorcycle mass ( $m^+ = m + 50$ ,  $m^- = m - 50$ ), and tire parameters variation ( $C_{fr_i}$ ).

In figures 7.9, estimated steering angle, yaw rate and roll rate are compared to their respective measurements provided by the various sensors previously described. Once again, since these state variables are measured, we obtain a finite-time exact convergence. On the other hand, figures 7.11 report the estimation of unmeasured state variables namely the lateral velocity  $v_y$  and the front/rear tire forces  $F_{yf}$ ,  $F_{yr}$ . For validation, the estimation of unmeasured states are used to reconstruct the lateral acceleration  $a_y$  at the center of mass of the rear body  $G_r$  as shown in figures 7.10. Figure 7.12 shows the estimated tires stiffness deviations from their nominal values.

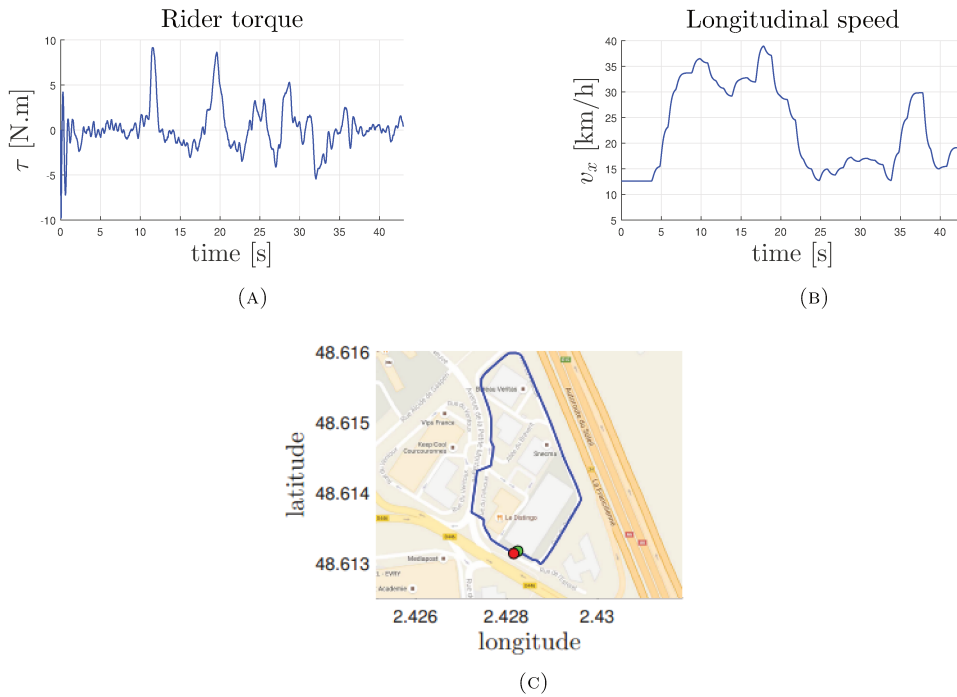


FIGURE 7.8: Experimental test: Vehicle trajectory, rider steering torque and longitudinal velocity.

Parameters	Estimated	Inversion	Direct
$\Theta_1$	178.6438	181.7665	184.5632
$\Theta_2$	2134	2065.7	2173.9
$\Theta_3$	2513	2496	2589.3
$\Theta_4$	643.2011	658.8327	618.1787

TABLE 7.3: Scooter Parameters Mean values comparison

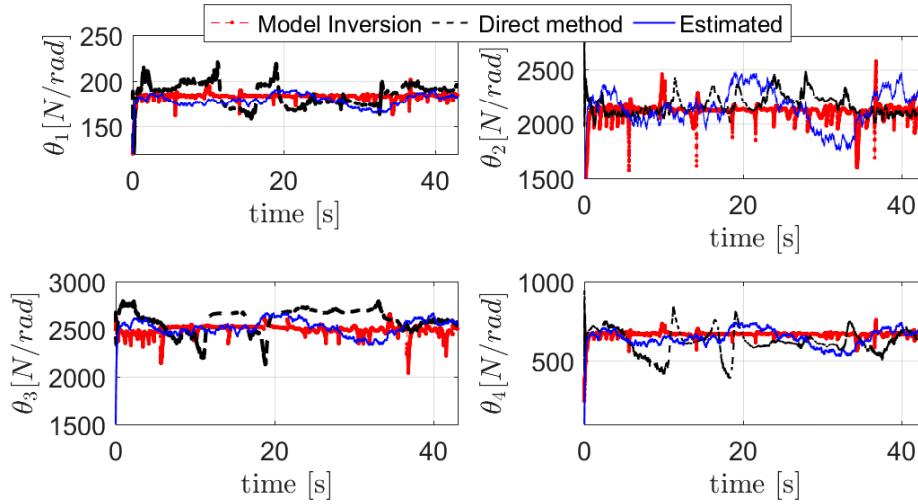


FIGURE 7.9: Test 2: Scooter Experimental test: Tire cornering stiffness Convergence  $\hat{\theta}_i = \hat{C}_{(f,r)i} - C_{(f,r)i_0}$  ( $f, r = \text{front, rear}$  and  $i = (1, 2, 3, 4)$ ).

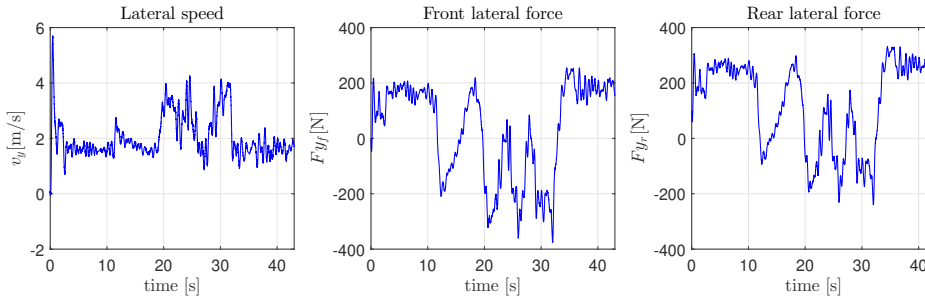


FIGURE 7.10: Test 2: Scooter Experimental test: Unmeasurable states estimation.

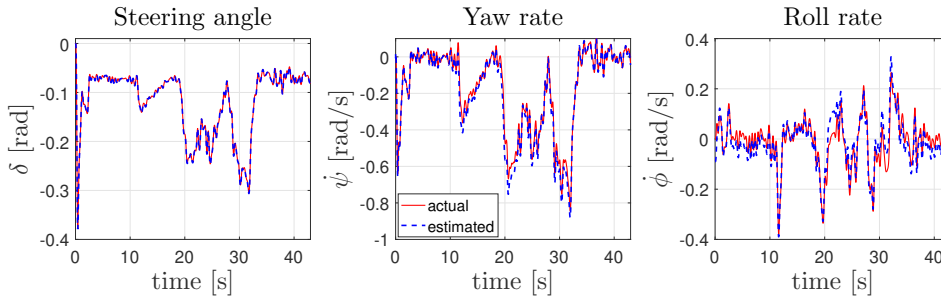


FIGURE 7.11: Test 2: Scooter Experimental test : Actual measures (red) and their estimation (dashed blue).

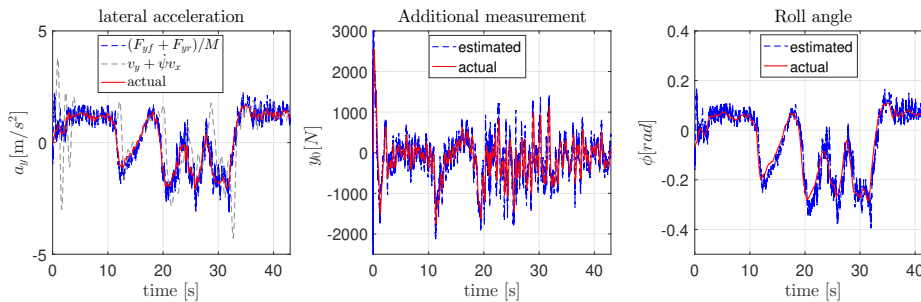


FIGURE 7.12: Real measurements (red) and observer estimation (dashed blue). Test 2: Scooter Experimental test: State estimates validation ( $v_y, F_{yf}, F_{yr}$ ) from the lateral acceleration and the additional measurement; and  $\phi$  from IMU roll angle.

According to these figures, it can be seen that the observer has a good dynamic transition and a finite-time convergence even for a riding scenario in the roll region away from the straight line dynamics linearization. In the experimental maneuver, it can be appreciated that the proposed observer shows a good estimation, however we note that the transient performance suffers slightly. It should be noted that in this maneuver, the true effective cornering stiffness should fluctuate somewhat.

In the experimental maneuver, it should be noted that, the true effective cornering stiffness are unknown. For more faithful estimations, the mean values of the estimated parameters are given in Table 7.3 to quantify the performances of the observer adaptive law through the mean values comparison. Comparing the adaptive law with the two others methods, one can see the small difference on the mean values results between estimated parameters, direct and inversion methods. This confirm the performance of the estimation scheme.

## 7.6 Conclusions

This chapter deals with observer-based identification framework to estimate both motorcycle lateral dynamics states and tires' cornering stiffness. Our main contribution concerns the design of an adaptive observer adapted to class of system problem in the context of ADAS design. For that purpose, an adaptive law is proposed, associated with an LPV formulation the observer to deals with the variable measured longitudinal velocity. An optimization problem in forms of LMI is resolved to compute the states observer gains.

An evaluation methodology based on a co-simulation with a high-end motorcycle simulator and with real experimental data-log are presented and discussed. The fundamental evaluation is made by estimating the tires' cornering stiffness using the adaptive law, a direct method and an inversion dynamic system. The direct method is simple and straightforward but it is very sensitive to states differentiation and singularities. The inversion based algebraic method requires the computation of the outputs derivatives which can be obtained for example by a high-gain second-order sliding mode observer. This method might be unrealistic in practical applications where measurements suffer noise and disturbances, leading also to singularities in the solution of the inverse problem. For the adaptive observer achieves a good estimation of unmeasured states and unknown parameters vector starting from self-integrated PTWV sensors.

# Chapter 8

## Interconnected Observers for PTWV

### Abstract

It is well known in vehicle community that the riding behavior is highly dependent on both tire-ground lateral and longitudinal forces, since these forces affect the comfort and safety of riders. The physical intuition suggests that the longitudinal and lateral friction phenomena are related since the two phenomena are produced in the tire contact area. Thereafter, the longitudinal and lateral models dependency and the tedious coupling features will be overcome here thanks to the estimation approach. The theoretical aspects and the validation of this idea were published in Fouka et al., 2019b. The chapter focuses on the estimation of the powered two wheelers vehicle states, including both the longitudinal and lateral dynamics. First, the linear parameter varying (LPV) of the two-sub models of the interconnected PTWV motion are transformed into a Takagi-Sugeno (TS) form. Secondly, the observer convergence study is based on Lyapunov theory associated with the Input to State Practical Stability (ISpS) to guaranty boundedness of the state estimation errors. Further, sufficient conditions are given in terms of linear matrix inequalities (LMIs). Finally, observer performances are tested and compared to the motorcycle model states and several simulation cases are provided to highlight the effectiveness of the suggested method using motorcycle Simulator Software *BikeSim*®.

### 8.1 Complete PTWV Model

Usually, the PTWV exhibits a coupled dynamics generating simultaneously the longitudinal and lateral tires forces. However, in the described observer based identification methods, the longitudinal dynamics are generally represented by the forward speed  $v_x$ . In this context, the main contribution of this work is to extend the estimation problematic of the PTWV lateral dynamics by including the longitudinal one. We will explore the ability of the concept of interconnected models to estimate the coupling dynamics while reducing the observability problem.

#### 8.1.1 State Space Representation

In most situation, the motorcycle develop a combined scenarios and applied simultaneously longitudinal forces (braking or acceleration) and lateral forces (cornering). Since this dependency in motorcycle motions, obtaining a “good” estimation require that the coupled behavior must be taken into account. Thereafter, this section is devoted to the modeling of the state space sub-models of the longitudinal and lateral dynamics.

In this work, the first sub-system of the rectilinear motion under the influence of lateral dynamics is considered, this analytic model is derived from the single-corner model (defined in section 2.9.4) to describe the rotations of the tires with respect to the front and rear braking systems. Thereby, the equations of the longitudinal motion will be modeled by the following quasi LPV sub-state space model:

$$\dot{\zeta}_1(t) = \bar{A}(\zeta_1)\zeta_1(t) + \bar{B}u_B(t) + \bar{D}(\zeta_2)\zeta_2(t) \quad (8.1)$$

Whereas the state vector  $\zeta_1(t) = [v_x, \omega_f, \omega_r, F_{xf}, F_{xr}]^T$  and the input vector is  $u_B = [B_f, B_r + T]^T$ . The estimation of this model required to know the longitudinal acceleration and the rotational speed of wheels, and to suppose that during the acceleration phase, the engine torque is applied only to rear wheel. We consider this sub-model to estimate the longitudinal speed and forces based on some of the lateral estimates under an acceptable convergence time. This quasi LPV sub-model (8.1) depends on longitudinal velocity  $v_x$ , the longitudinal front and rear stiffness  $\rho_{f,r}$ , which are considered as external varying parameters, with:  $\rho_i = \frac{1}{\max(R_i \omega_i, v_x)}$ ,  $i = f, r$ .

The lateral dynamics study quantifies the vehicle's ability to support lateral accelerations and to develop lateral forces to follow a steering rider input. The good compromise between simplicity and accuracy for the modeling of lateral dynamics is the Sharp two-body model, defined in section 2.9.1. Thereby, the quasi LPV sub-model of the lateral motion is described by:

$$\dot{\zeta}_2(t) = \check{A}(\zeta_1)\zeta_2(t) + \check{B}u_\tau(t) + \check{D}(\zeta_2)\zeta_1(t) \quad (8.2)$$

With  $\zeta_2(t) = [\phi, \delta, v_y, \dot{\psi}, \dot{\phi}, \dot{\delta}, F_{yf}, F_{yr}]^T$  and  $u_\tau = \tau(t)$ .

The motorcycle interconnected dynamics is given by:

$$\begin{cases} \dot{\zeta}_1(t) = \bar{A}(\zeta_1)\zeta_1(t) + \bar{B}u_B(t) + \bar{D}\zeta_2(t) \\ \dot{\zeta}_2(t) = \check{A}(\zeta_1)\zeta_2(t) + \check{B}u_\tau(t) + \check{D}\zeta_1(t) \\ y_x(t) = \bar{C}\zeta_1(t) \\ y_y(t) = \check{C}\zeta_2(t) \end{cases} \quad (8.3)$$

where :  $\xi(t) = [\zeta_1(t) \zeta_2(t)]^T$  and  $C = [\bar{C} \check{C}]^T$ . where  $\zeta_1(t) \in \mathbb{R}^5$  and  $\zeta_2(t) \in \mathbb{R}^8$  are the state vector, and  $y_x(t) = [\omega_f, \omega_r, a_x] \in \mathbb{R}^3$  and  $y_y(t) = [\delta, \dot{\psi}, \dot{\phi}, a_y] \in \mathbb{R}^5$  the output vector.

The design of the observer can be handled in the domain of polytopic models.

1. The longitudinal model has 8 sub-models comes from the fact that there is 3 nonlinearities on the model:

$$z_1 = v_x, \quad z_2 = \rho_f, \quad z_3 = \rho_r \quad (8.4)$$

$$z_1^{\min} \leq z_1 \leq z_1^{\max} \quad z_2^{\min} \leq z_2 \leq z_2^{\max} \quad z_3^{\min} \leq z_3 \leq z_3^{\max}$$

The membership functions of the fuzzy sets are defined as:

$$\sum_{\zeta_1} \begin{cases} h_{11} = \frac{z_{1max} - z_1}{z_{1max} - z_{1min}} & , \quad h_{12} = \frac{z_1 - z_{1min}}{z_{1max} - z_{1min}} \\ h_{21} = \frac{z_{2max} - z_2}{z_{2max} - z_{2min}} & , \quad h_{22} = \frac{z_2 - z_{2min}}{z_{2max} - z_{2min}} \\ h_{31} = \frac{z_{3max} - z_3}{z_{3max} - z_{3min}} & , \quad h_{32} = \frac{z_3 - z_{3min}}{z_{3max} - z_{3min}} \end{cases} \quad (8.5)$$

where the variables  $\eta_i(\rho)$  are computed as follows:

$$\begin{cases} \eta_1 = h_{11} \cdot h_{21} \cdot h_{31} & , \quad \eta_2 = h_{12} \cdot h_{21} \cdot h_{31} \\ \eta_3 = h_{11} \cdot h_{22} \cdot h_{31} & , \quad \eta_4 = h_{12} \cdot h_{22} \cdot h_{31} \\ \eta_5 = h_{11} \cdot h_{21} \cdot h_{32} & , \quad \eta_6 = h_{12} \cdot h_{21} \cdot h_{32} \\ \eta_7 = h_{11} \cdot h_{22} \cdot h_{32} & , \quad \eta_8 = h_{12} \cdot h_{22} \cdot h_{32} \end{cases} \quad (8.6)$$

2. The lateral model has 2 sub-models comes from the forward speed coupling. With regard to the motorcycle stability, this forward speed is considered bounded in the interval where the motorcycle is

stable. Consequently, the membership functions are given by:

$$\sum_{\zeta_2} \begin{cases} \vartheta_1 & = \frac{v_{xmax} - v_x}{v_{xmax} - v_{xmin}} \\ \vartheta_2 & = \frac{v_x - v_{xmin}}{v_{xmax} - v_{xmin}} \end{cases} \quad (8.7)$$

The variables  $\eta_i$  and  $\vartheta_j$  are called the weighing functions and they must satisfy the following convex sum property:

$$\begin{cases} 0 \leq \eta_i(z_1, z_2, z_3) \leq 1 \\ 0 \leq \vartheta_j(v_x) \leq 1 \\ \sum_{i=1}^8 \eta_i(z_1, z_2, z_3) = 1 \\ \sum_{j=1}^2 \vartheta_j(v_x) = 1 \end{cases} \quad (8.8)$$

For the quasi LPV interconnected model (8.1), applying TS representation would lead to an exact form well-suited to design the appropriate observer.

$$\begin{cases} \dot{\zeta}_1(t) = \sum_{i=1}^{p_1} \eta_i(\zeta_1(t)) (\bar{A}_i \zeta_1(t) + \bar{D}_i \zeta_2(t) + \bar{B}_i u_B(t)) \\ y_x(t) = \bar{C} \zeta_1(t), \quad p_1 = 8 \\ \dot{\zeta}_2(t) = \sum_{j=1}^{p_2} \vartheta_j(\zeta_1(t)) (\check{A}_j \zeta_2(t) + \check{D}_j \zeta_1(t) + \check{B}_j u_\tau(t)) \\ y_y(t) = \check{C} \zeta_2(t), \quad p_2 = 2 \end{cases} \quad (8.9)$$

With this model, we propose a Interconnected Fuzzy Observer (IFO) design for nonlinear systems whose TS form has unmeasured premise variables. In the next section, we derive the synthesis steps of the observer for joint states and time-varying parameter estimation. The observer for this type of system should take into account the fact that the weighing functions would be depending on estimated premise variables, rather than exact ones.

## 8.2 Observer Design

Motivated by the need of observers to acquire certain states used in safety and control systems to prevent possible dangerous situation, this section investigates the design of an interconnected observers. The design is done in two stages, first an observer is associated with the longitudinal subsystem, and then a second observer based on the results of the first observer is proposed for the estimation of lateral dynamics. Thereby, the sub-observer of the lateral dynamics gives the unmeasured variable, then, the lateral velocity is connected to the longitudinal sub-observer to estimate the forward speed and the longitudinal forces. An overall scheme of the system/observer structure is given in figure 8.1.

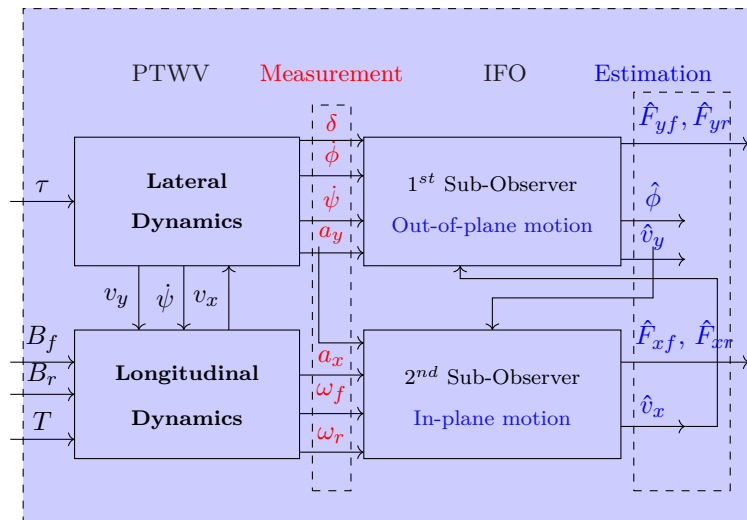


FIGURE 8.1: General diagram of the interconnected estimation of longitudinal and lateral dynamics

### 8.2.1 Preliminaries

The following nonrestrictive assumptions are considered:

**Assumption 8.1.** Assume that, for the design of each observer, the states of other subsystems are available.

**Assumption 8.2.** Suppose that the signals  $u_B$  and  $u_\tau$  are known, bounded and sufficiently persistent inputs for each observer respectively.

**Assumption 8.3.** The state vector  $\zeta_1$  and  $\zeta_2$  of the two models are considered bounded.

**Assumption 8.4.** The pair  $(\check{A}(\zeta_1), \check{C})$  and  $(\bar{A}(\zeta_2), \bar{C})$  are observable or detectable.

The following lemmas are used in the proof of the observer convergence study.

**Lemma 8.1.** Consider  $Y$  and  $\Xi$  matrices with appropriate dimensions. For every positive definite matrix  $\Lambda > 0$ . the following property holds (Boyd et al., 1994).

$$Y^T \Xi + \Xi^T Y \leq Y^T \Lambda Y + \Xi^T \Lambda^{-1} \Xi \quad (8.10)$$

**Lemma 8.2.** Given the following matrices  $Y$ ,  $\Xi$  and  $\aleph$ , with appropriate dimensions, where  $Y = Y^T$  and  $\aleph = \aleph^T$  (Boyd et al., 1994), the Schur's lemma apply:

$$\begin{bmatrix} Y & \Xi \\ \Xi^T & \aleph \end{bmatrix} < 0 \Leftrightarrow \begin{cases} \aleph < 0 \\ Y - \Xi \aleph^{-1} \Xi^T < 0 \end{cases} \quad (8.11)$$

**Definition 8.1.** The state estimation error verifies the Input To State Practical Stability (ISpS) if there exists a  $\mathcal{KL}$  function  $\beta : \mathbb{R}^n \times \mathbb{R} \rightarrow \mathbb{R}$ , and a  $\mathcal{K}$  function  $\alpha : \mathbb{R} \rightarrow \mathbb{R}$  such that for each input  $\Delta(t)$  satisfying  $\|\Delta(t)\|_\infty < \infty$  and each initial conditions  $e(0)$ , the trajectory of the system associated to  $e(0)$  and  $\Delta(t)$  satisfies (Lazar et al., 2008):

$$\|e(t)\|_2 \leq \beta(\|e(0)\|, t) + \alpha(\|\Delta(t)\|_\infty) \quad (8.12)$$

### 8.2.2 State Estimation

Based on the connection between the two lateral and longitudinal subsystems in equation (8.9), the following observer is proposed:

$$\begin{cases} \dot{\hat{\zeta}}_1 = \sum_{i=1}^{p_1} \eta_i(\zeta_1(t)) (\bar{A}_i \hat{\zeta}_1(t) + \bar{D}_i \hat{\zeta}_2(t) + \bar{B}_i u_B(t) - \bar{L}_i (y_x - \hat{y}_x)) \\ \dot{\hat{\zeta}}_2 = \sum_{j=1}^{p_2} \vartheta_j(\zeta_1(t)) (\check{A}_j \hat{\zeta}_2(t) + \check{D}_j \hat{\zeta}_1(t) + \check{B}_j u_\tau(t) - \check{L}_j (y_y - \hat{y}_y)) \\ \hat{y}_{\zeta_1}(t) = \check{C} \hat{\zeta}_1(t) \\ \hat{y}_{\zeta_2}(t) = \check{C} \hat{\zeta}_2(t) \end{cases} \quad (8.13)$$

Using equations (8.9) and (8.13), the state estimation error obeys the following differential equations:

$$\begin{cases} \dot{e}_{\zeta_1} = \sum_{i=1}^{p_1} \eta_i(\zeta_1(t)) (\bar{\Phi}_i e_{\zeta_1} + \bar{D}_i e_{\zeta_2}) + \Delta_{\zeta_1}(t) \\ \dot{e}_{\zeta_2} = \sum_{j=1}^{p_2} \vartheta_j(\zeta_1(t)) (\check{\Phi}_j e_{\zeta_2} + \check{D}_j e_{\zeta_1}) + \Delta_{\zeta_2}(t) \end{cases} \quad (8.14)$$

where:  $\bar{\Phi}_i = (\bar{A}_i - \bar{L}_i \bar{C})$ ,  $\check{\Phi}_j = (\check{A}_j - \check{L}_j \check{C})$ ,  $\Delta_{\zeta_i}(t) = \sum_{i=1}^{r_i} (\eta_i(\zeta_1) - \eta_i(\hat{\zeta}_1)) \bar{A}_i \zeta_1(t)$  and  $\Delta_{\zeta_2}(t) = \sum_{i=1}^{r_i} (\vartheta_j(\zeta_1) - \vartheta_j(\hat{\zeta}_2)) \check{A}_j \zeta_2(t)$ .

Notice that if the state estimation errors converge to zero, the terms  $\Delta_{\zeta_1}(t)$  and  $\Delta_{\zeta_2}(t)$  converge also towards zero. In addition, since the weighting functions are bounded and the state vector  $\zeta_1(t)$  and  $\zeta_2(t)$  are also bounded (see assumption 8.1), the term  $\Delta_{\zeta_i}(t)$  are thus bounded.

By considering the vector of the state estimation errors  $e_\zeta = (e_{\zeta_1}, e_{\zeta_2}) = (\zeta_1 - \hat{\zeta}_1, \zeta_2 - \hat{\zeta}_2)$  the errors dynamics are given by:

$$\dot{e}_\zeta = \begin{bmatrix} \sum_{i=1}^{p_1} \eta_i(\zeta) \bar{\Phi}_i & \eta_i(\zeta) \bar{D}_i \\ \sum_{j=1}^{p_2} \vartheta_j(\zeta) \check{D}_j & \sum_{j=1}^{p_2} \vartheta_j(\zeta) \check{\Phi}_j \end{bmatrix} e_\zeta + \begin{bmatrix} \Delta_{\zeta_1}(t) \\ \Delta_{\zeta_2}(t) \end{bmatrix} \quad (8.15)$$

**Theorem 8.1.** *The state estimation error between the system and the interconnected observers converges asymptotically to zero if there exists two symmetric and definite matrices  $P$  and  $Q$ , two diagonal positive matrices  $\Omega_1$  and  $\Omega_2$ , given a positive scalars  $\sigma, \alpha, a \in [0, 1]$  and gains  $\bar{K}_i, i = 1, \dots, p_1, \check{K}_j, j = 1, \dots, p_2$  such that the LMI conditions:*

$$\min_{P, Q, \Omega_1, \Omega_2} a\zeta_1 + (1-a)\zeta_2$$

s.t.

$$\begin{bmatrix} \bar{A}_i^T P + P \bar{A}_i - \bar{K}_i \bar{C} - \bar{C}^T \bar{K}_i^T + \Omega_2 + \alpha P & P \bar{D}_i + R_1 \\ \bar{D}_i^T P + R_1^T & -\Omega_1 \end{bmatrix} < 0 \quad (8.16)$$

$$\begin{bmatrix} \check{A}_j^T P + P \check{A}_j - \check{K}_j \check{C} - \check{C}^T \check{K}_j^T + \Omega_1 + \alpha Q & Q \check{D}_j + R_2 \\ \check{D}_j^T Q + R_2^T & -\Omega_2 \end{bmatrix} < 0 \quad (8.17)$$

The gains of the interconnected observer are obtained from the equations  $\bar{L}_i = P^{-1} \bar{K}_i, i = 1, \dots, p_1$  and  $\check{L}_j = Q^{-1} \check{K}_j, j = 1, \dots, p_2$ .

**Proof 8.1.**

The convergence analysis of the the interconnected observer (8.13) can be performed by considering the following quadratic Lyapunov function:

$$V(e(t)) = e_{\zeta_1}(t)^T P e_{\zeta_1}(t) + e_{\zeta_2}(t)^T Q e_{\zeta_2}(t) \quad (8.18)$$

The time-derivative of the Lyapunov function (8.18) is:

$$\begin{aligned} \dot{V}(e) = & \sum_{i=1}^{p_1} \eta_i(\zeta_1) ((\bar{\Phi}_i e_{\zeta_1} + \bar{D}_i e_{\zeta_2})^T P e_{\zeta_1} + e_{\zeta_1}^T P (\bar{\Phi}_i e_{\zeta_1} + \bar{D}_i e_{\zeta_2})) + \sum_{j=1}^{p_2} \vartheta_j(\zeta_1) ((\check{\Phi}_j e_{\zeta_2} + \check{D}_j e_{\zeta_1})^T Q e_{\zeta_2} \\ & + e_{\zeta_2}^T Q (\check{\Phi}_j e_{\zeta_2} + \check{D}_j e_{\zeta_1})) + e_{\zeta_1}^T P \Delta_{\zeta_1} + \Delta_{\zeta_1}^T P e_{\zeta_1} + e_{\zeta_2}^T Q \Delta_{\zeta_2} + \Delta_{\zeta_2}^T Q e_{\zeta_2} \end{aligned} \quad (8.19)$$

Considering  $\bar{\Gamma}_i = \bar{\Phi}_i^T P + P \bar{\Phi}_i$  and  $\check{\Gamma}_j = \check{\Phi}_j^T Q + Q \check{\Phi}_j$ , equation (8.19) lead to:

$$\begin{aligned} \dot{V}(e(t)) = & \sum_{i=1}^{p_1} \eta_i(\zeta_1) (e_{\zeta_1}^T \bar{\Gamma}_i e_{\zeta_1} + e_{\zeta_1}^T P \bar{D}_i e_{\zeta_2} + e_{\zeta_2}^T \bar{D}_i^T P e_{\zeta_1} + 2e_{\zeta_1}^T P \Delta_{\zeta_1}) + \\ & \sum_{j=1}^{p_2} \vartheta_j(\zeta_1) (e_{\zeta_2}^T \check{\Gamma}_j e_{\zeta_2} + e_{\zeta_2}^T Q \check{D}_j e_{\zeta_1} + e_{\zeta_1}^T \check{D}_j^T Q e_{\zeta_2} + 2e_{\zeta_2}^T Q \Delta_{\zeta_2}) \end{aligned} \quad (8.20)$$

Applying Lemma (8.1), inequality (8.20) yields:

$$\begin{aligned} \dot{V}(e(t)) < & \sum_{i=1}^{p_1} \eta_i(\zeta_1) \left( e_{\zeta_1}^T (\bar{\Gamma}_i + P \bar{D}_i \mathcal{G}_1 \bar{D}_i^T P + P \mathcal{F}_1 P) e_{\zeta_1} + e_{\zeta_2}^T \mathcal{G}_1^{-1} e_{\zeta_2} + \Delta_{\zeta_1}^T \mathcal{F}_1^{-1} \Delta_{\zeta_1} \right) + \\ & \sum_{j=1}^{p_2} \vartheta_j(\zeta_1) \left( e_{\zeta_2}^T (\check{\Gamma}_j + Q \check{D}_j \mathcal{G}_2 \check{D}_j^T Q + Q \mathcal{F}_2 Q) e_{\zeta_2} + e_{\zeta_1}^T \mathcal{G}_2^{-1} e_{\zeta_1} + \Delta_{\zeta_2}^T \mathcal{F}_2^{-1} \Delta_{\zeta_2} \right) \end{aligned} \quad (8.21)$$

where,  $\mathcal{G}_1$  and  $\mathcal{G}_2$  are positive definite matrices. Then, if inequality  $\dot{V}(e(t)) < 0$  holds, one have

$$\begin{aligned} \sum_{i=1}^{p_1} \eta_i(\zeta_1) \left( e_{\zeta_1}^T (\bar{\Gamma}_i + P \bar{D}_i \mathcal{G}_1 \bar{D}_i^T P + P \mathcal{F}_1 P + \mathcal{G}_2^{-1}) e_{\zeta_1} + \Delta_{\zeta_1}^T \mathcal{F}_1^{-1} \Delta_{\zeta_1} \right) + \\ \sum_{j=1}^{p_2} \vartheta_j(\zeta_1) \left( e_{\zeta_2}^T (\check{\Gamma}_j + Q \check{D}_j \mathcal{G}_2 \check{D}_j^T Q + Q \mathcal{F}_2 Q + \mathcal{G}_1^{-1}) e_{\zeta_2} + \Delta_{\zeta_2}^T \mathcal{F}_2^{-1} \Delta_{\zeta_2} \right) < 0 \end{aligned} \quad (8.22)$$

Let us define:

$$\begin{cases} \Xi_i &= \bar{\Gamma}_i + P \bar{D}_i \mathcal{G}_1 \bar{D}_i^T P + P \mathcal{F}_1 P + \mathcal{G}_2^{-1} \\ \Xi_j &= \check{\Gamma}_j + Q \check{D}_j \mathcal{G}_2 \check{D}_j^T Q + Q \mathcal{F}_2 Q + \mathcal{G}_1^{-1} \end{cases}$$

Then, the time-derivative of the Lyapunov function is bounded as:

$$\dot{V}(e(t)) < 0 \Leftrightarrow \begin{aligned} \dot{V}(e(t)) < & \sum_{i=1}^{p_1} \eta_i(\zeta_1) \left( e_{\zeta_1}^T \Xi_i e_{\zeta_1} + \Delta_{\zeta_1}^T \mathcal{F}_1^{-1} \Delta_{\zeta_1} \right) + \\ & \sum_{j=1}^{p_2} \vartheta_j(\zeta_1) \left( e_{\zeta_2}^T \Xi_j e_{\zeta_2} + \Delta_{\zeta_2}^T \mathcal{F}_2^{-1} \Delta_{\zeta_2} \right) < 0 \end{aligned} \quad (8.23)$$

The inequality (8.23) is equivalent to:

$$\begin{aligned} \dot{V}(e(t)) &< \sum_{i=1}^{p_1} \eta_i(\zeta_1)(e_{\zeta_1}^T \Xi_i e_{\zeta_1} + \Delta_{\zeta_1}^T \mathcal{F}_1^{-1} \Delta_{\zeta_1}) + \alpha(e_{\zeta_1} P e_{\zeta_1} + e_{\zeta_2} Q e_{\zeta_2}) - \alpha(e_{\zeta_1} P e_{\zeta_1} + e_{\zeta_2} Q e_{\zeta_2}) + \\ &\quad \sum_{j=1}^{p_2} \vartheta_j(\zeta_1)(e_{\zeta_2}^T \Xi_j e_{\zeta_2} + \Delta_{\zeta_2}^T \mathcal{F}_2^{-1} \Delta_{\zeta_2}) < 0 \\ &< \sum_{i=1}^{p_1} \eta_i(\zeta_1)(e_{\zeta_1}^T (\Xi_i + \alpha P) e_{\zeta_1} + \Delta_{\zeta_1}^T \mathcal{F}_1^{-1} \Delta_{\zeta_1}) + \sum_{j=1}^{p_2} \vartheta_j(\zeta_1)(e_{\zeta_2}^T (\Xi_j + \alpha Q) e_{\zeta_2} + \Delta_{\zeta_2}^T \mathcal{F}_2^{-1} \Delta_{\zeta_2}) - \\ &\quad \alpha(e_{\zeta_1} P e_{\zeta_1} + e_{\zeta_2} Q e_{\zeta_2}) < 0 \end{aligned} \quad (8.24)$$

Considering  $e_\zeta(t) = [e_{\zeta_1}^T(t) \ e_{\zeta_2}^T(t)]^T$ . The inequality (8.24) leads to:

$$\begin{aligned} \dot{V}(t) &\leq \sum_{i=1}^{p_1} \eta_i(\zeta_1) e_{\zeta_1}^T (\Xi_i + \alpha P) e_{\zeta_1} + \sum_{j=1}^{p_2} \vartheta_j(\zeta_1) (e_{\zeta_2}^T (\Xi_j + \alpha Q) e_{\zeta_2} \\ &\quad - \alpha(e_{\zeta_1} P e_{\zeta_1} + e_{\zeta_2} Q e_{\zeta_2}) + \Delta_{\zeta_1}^T \mathcal{F}_1^{-1} \Delta_{\zeta_1} + \Delta_{\zeta_2}^T \mathcal{F}_2^{-1} \Delta_{\zeta_2}) \end{aligned} \quad (8.25)$$

Then, the time derivative of the Lyapunov function (8.25) is then bounded as follows

$$\dot{V}(e(t)) < e_\zeta^T \Psi e_\zeta - \alpha e_\zeta^T(t) \mathcal{Q} e_\zeta(t) + \Delta_{\zeta_1}^T \mathcal{F}_1^{-1} \Delta_{\zeta_1} + \Delta_{\zeta_2}^T \mathcal{F}_2^{-1} \Delta_{\zeta_2} < 0 \quad (8.26)$$

where

$$\mathcal{Q} = \text{diag}(P, Q) \quad \text{and} \quad \Psi = \begin{bmatrix} \sum_{i=1}^{p_1} \eta_i(\zeta_1) \Xi_i + \alpha P & 0 \\ 0 & \sum_{j=1}^{p_2} \vartheta_j(\zeta_1) \Xi_j + \alpha Q \end{bmatrix} < 0 \quad (8.27)$$

Now, if  $e_\zeta^T \Psi e_\zeta < 0$ , the inequality (8.26) can be bounded as follows

$$\begin{aligned} \dot{V}(t) &\leq -\alpha e_\zeta^T(t) \mathcal{Q} e_\zeta(t) + \Delta_{\zeta_1}^T \mathcal{F}_1^{-1} \Delta_{\zeta_1} + \Delta_{\zeta_2}^T \mathcal{F}_2^{-1} \Delta_{\zeta_2} \\ &\leq -\alpha(e_{\zeta_1}^T P e_{\zeta_1} + e_{\zeta_2}^T Q e_{\zeta_2}) + \Delta_{\zeta_1}^T \mathcal{F}_1^{-1} \Delta_{\zeta_1} + \Delta_{\zeta_2}^T \mathcal{F}_2^{-1} \Delta_{\zeta_2} \end{aligned} \quad (8.28)$$

which is equivalent to

$$\dot{V}(t) \leq -\alpha V(t) + \Delta_{\zeta_1}^T \mathcal{F}_1^{-1} \Delta_{\zeta_1} + \Delta_{\zeta_2}^T \mathcal{F}_2^{-1} \Delta_{\zeta_2} \quad (8.29)$$

Regarding inequality (8.29), the asymptotic convergence is no longer ensured. Integrating (8.29) over the interval  $[0, t]$  implies that

$$\begin{aligned} V(t) &\leq V(0)e^{-\alpha t} + \mathcal{F}_1 \int_0^t e^{-\alpha(t-s)} \|\Delta_{\zeta_1}(s)\|_2^2 ds + \\ &\quad \mathcal{F}_2 \int_0^t e^{-\alpha(t-s)} \|\Delta_{\zeta_2}(s)\|_2^2 ds \\ &\leq V(0)e^{-\alpha t} + \frac{\mathcal{F}_1}{\alpha} \|\Delta_{\zeta_1}(s)\|_\infty^2 + \frac{\mathcal{F}_2}{\alpha} \|\Delta_{\zeta_2}(s)\|_\infty^2 \end{aligned}$$

The Lyapunov function can be bounded as:

$$\lambda_{\min}(\mathcal{Q}) \|e_\zeta(t)\|_2^2 \leq V(t) \leq \lambda_{\max}(\mathcal{Q}) \|e_\zeta(t)\|_2^2 \quad (8.30)$$

Now, thanks to inequality (8.30), one obtains:

$$\|e_\zeta(t)\|_2^2 \leq \frac{\lambda_{\max}(\mathcal{Q})}{\lambda_{\min}(\mathcal{Q})} \left( V(0)e^{-\alpha t} + \frac{\mathcal{F}_1}{\alpha} \|\Delta_{\zeta_1}(s)\|_\infty^2 + \frac{\mathcal{F}_2}{\alpha} \|\Delta_{\zeta_2}(s)\|_\infty^2 \right) \quad (8.31)$$

By using the square root on (8.31), one obtains

$$\|e_\zeta(t)\|_2 \leq \sqrt{\frac{\lambda_{\max}(\mathcal{Q})}{\lambda_{\min}(\mathcal{Q})}} \left( V(0)e^{-\frac{\alpha}{2}t} + \sqrt{\frac{\mathcal{F}_1}{\alpha}} \|\Delta_{\zeta_1}(s)\|_\infty + \sqrt{\frac{\mathcal{F}_2}{\alpha}} \|\Delta_{\zeta_2}(s)\|_\infty \right) \quad (8.32)$$

Hence, when  $t \rightarrow \infty$  the exponential error (8.32) converges to zero and knowing that  $\Delta_{\zeta_1}$  and  $\Delta_{\zeta_2}$  are bounded, one have

$$\lim_{t \rightarrow \infty} \|e_\zeta(t)\|_2 \leq \sqrt{\frac{\lambda_{\max}(\mathcal{Q})}{\lambda_{\min}(\mathcal{Q})}} \left( \sqrt{\frac{\mathcal{F}_1}{\alpha}} \|\Delta_{\zeta_1}(s)\|_\infty + \sqrt{\frac{\mathcal{F}_2}{\alpha}} \|\Delta_{\zeta_2}(s)\|_\infty \right) \quad (8.33)$$

According to Lyapunov formulation of Input To State Practical Stability (ISpS), the states converge to a region which will be minimized in order to achieve a more accurate estimation of the states of the motorcycle

longitudinal and lateral motions. This ball is smaller as the attenuation level of the transfer from  $\Delta_{\zeta_1}(t)$ ,  $\Delta_{\zeta_2}(t)$  to the state estimation errors is smaller. To enhance the performances of the observer, a minimal values of these quantities are studied.

Let us consider the quantity:

$$\sqrt{\frac{\lambda_{\max}(\mathcal{Q})}{\lambda_{\min}(\mathcal{Q})\alpha}} \leq \sqrt{\varsigma} \quad \text{with} \quad \mathcal{Q} = \text{diag}(P, Q) \quad (8.34)$$

where  $\varsigma = \text{diag}(\varsigma_1, \varsigma_2)$ ,  $\varsigma_i$  is a positive scalar. It is then sufficient to minimize the term  $\varsigma$ . Assume  $\lambda_{\min}(\mathcal{Q}) \geq 1$  ( $\mathcal{Q} > I$ ), leads to:

$$\sqrt{\frac{\lambda_{\max}(P)}{\alpha}} \leq \sqrt{\varsigma_1}, \quad \sqrt{\frac{\lambda_{\max}(Q)}{\alpha}} \leq \sqrt{\varsigma_2} \quad (8.35)$$

which is transformed easily into:

$$(\alpha\varsigma_1)^2 I - P^T P > 0, \quad (\alpha\varsigma_2)^2 I - Q^T Q > 0 \quad (8.36)$$

Using Shur's complement lemma:

$$\begin{pmatrix} \alpha\varsigma_1 I & P \\ P & \alpha\varsigma_1 I \end{pmatrix} > 0, \quad \begin{pmatrix} \alpha\varsigma_2 I & Q \\ Q & \alpha\varsigma_2 I \end{pmatrix} > 0 \quad P \geq I \quad Q \geq I \quad (8.37)$$

Now, using the convex sum propriety and the condition  $\dot{V}(e(t)) < 0$  ( $\Psi < 0$  holds). The condition  $\Psi < 0$  in equation (8.27) leads to the following optimization problem:

$$\begin{bmatrix} \Xi_1 + \alpha P & 0 \\ 0 & \Xi_2 + \alpha Q \end{bmatrix} < 0 \quad (8.38)$$

with

$$\begin{cases} \Xi_1 & = & \bar{\Gamma}_i + P\bar{D}_i\mathcal{G}_1\bar{D}_i^T P + P\mathcal{F}_1 P + \mathcal{G}_2^{-1} \\ \Xi_2 & = & \check{\Gamma}_j + Q\check{D}_j\mathcal{G}_2\check{D}_j^T Q + Q\mathcal{F}_2 Q + \mathcal{G}_1^{-1} \\ \bar{\Gamma}_i & = & \bar{\Phi}_i^T P + P\bar{\Phi}_i \\ \check{\Gamma}_j & = & \check{\Phi}_j^T Q + Q\check{\Phi}_j \\ \bar{\Phi}_i & = & (\bar{A}_i - \bar{L}_i\bar{C}) \\ \check{\Phi}_j & = & (\check{A}_j - \check{L}_j\check{C}) \end{cases}$$

which lead to:

$$\left[ \bar{\Gamma}_i + P\bar{D}_i\mathcal{G}_1\bar{D}_i^T P + P\mathcal{F}_1 P + \mathcal{G}_2^{-1} + \alpha P \right] < 0 \quad (8.39)$$

and

$$\left[ \check{\Gamma}_j + Q\check{D}_j\mathcal{G}_2\check{D}_j^T Q + Q\mathcal{F}_2 Q + \mathcal{G}_1^{-1} + \alpha Q \right] < 0 \quad (8.40)$$

The two matrix inequalities are connected by  $\mathcal{G}_1$  and  $\mathcal{G}_2$ . Using Schur Lemma (8.2), inequalities (8.39 and 8.40) yield to:

$$\begin{bmatrix} \bar{\Gamma}_i + \mathcal{G}_2^{-1} + \alpha P & P\bar{D}_i + P\mathcal{F}_1 \\ \bar{D}_i^T P + \mathcal{F}_1^T P & -\mathcal{G}_2^{-1} \end{bmatrix} < 0, \quad i = 1, \dots, p_1 \quad (8.41)$$

$$\begin{bmatrix} \check{\Gamma}_j + \mathcal{G}_1^{-1} + \alpha Q & Q\check{D}_j + Q\mathcal{F}_2 \\ \check{D}_j^T Q + \mathcal{F}_2^T Q & -\mathcal{G}_1^{-1} \end{bmatrix} < 0, \quad j = 1, \dots, p_2 \quad (8.42)$$

By using the definitions of the matrices  $\bar{\Gamma}_i$  and  $\check{\Gamma}_j$  and change of variables  $\bar{K}_i = P\bar{L}_i$ ,  $\check{K}_j = Q\check{L}_j$  and  $\Omega_1 = \mathcal{G}_1^{-1}$  and  $\Omega_2 = \mathcal{G}_2^{-1}$ , where  $\Omega_1$  and  $\Omega_2$  are diagonal and positive definite matrices  $R_1 = P\mathcal{F}_1$  and  $R_2 = Q\mathcal{F}_2$ . Finally, the gains of the interconnected observer are computed from the LMI conditions given in theorem (8.1).

## 8.3 Observer Evaluation and Simulation

In this section, the proposed interconnected observer for the combined longitudinal and lateral dynamics of PTWV is evaluated by co-simulation with *BikeSim*<sup>©</sup> software. A PTWV model is chosen from the dataset *Big Sport Baseline 8* bodies and default parameters. The simulations are carried out in two maneuvers:

**Maneuver 1:** Urban scenic road includes acceleration and braking scenarios with a high friction coefficient  $\mu = 0.9$ .

**Maneuver 2:** Handling road course with variable speed.

The motorcycle behavior, including longitudinal and lateral dynamics requires three inputs: the rider's steering torque applied on the handlebars and the two braking torques applied on both front and rear wheels to reduce the longitudinal velocity.

In the following, if the actual state  $v_y, v_x$  and  $F_{yf}, F_{yr}$  and  $F_{xf}, F_{xr}$  are unknown, the state estimation can be validated from lateral and longitudinal accelerations as follow:

$$\begin{aligned} Eq_1 : \hat{a}_y &= \frac{(\hat{F}_{yf} + \hat{F}_{yr})}{m}, & Eq_2 : \hat{a}_y &= \hat{v}_y + v_x \hat{\psi} \\ Eq_3 : \hat{a}_x &= \frac{(\hat{F}_{xf} + \hat{F}_{xr})}{m}, & Eq_4 : \hat{a}_x &= \hat{v}_x - v_y \hat{\psi} + C_d/m \cdot \hat{v}_x^2 \end{aligned} \quad (8.43)$$

The first simulation is carried out from FHWA (Federal Highway Administration), this maneuver demonstrates an acceleration and braking test includes three phases.

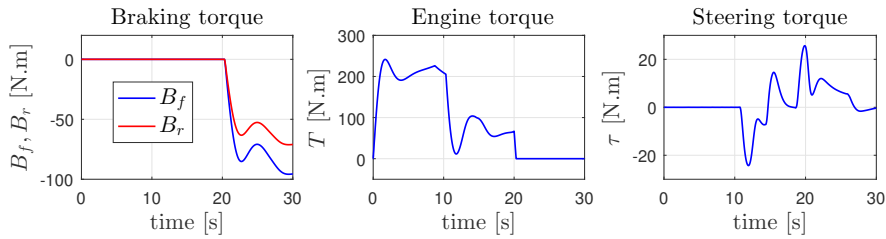


FIGURE 8.2: Maneuver 1: Inputs.

The first phase ( $0 < t < 10(s)$ ) is an acceleration phase, where only the drive torque  $T$  is applied on the rear wheel. In the second phase ( $10 < t < 20(s)$ ), no braking or engine torque is applied and the main body is subject to lateral motion in response to the generated tire forces whereas the front body is subject to steering motion as imposed by the applied rider's steering torque  $\tau$  on the motorcycle handlebar. The third phase ( $20 < t < 30(s)$ ), is the braking phase where a braking torque  $B_f$  and  $B_r$  are applied to both front and rear wheels to reduce the forward speed of the PTWV from  $35m/s$  to  $10m/s$ .

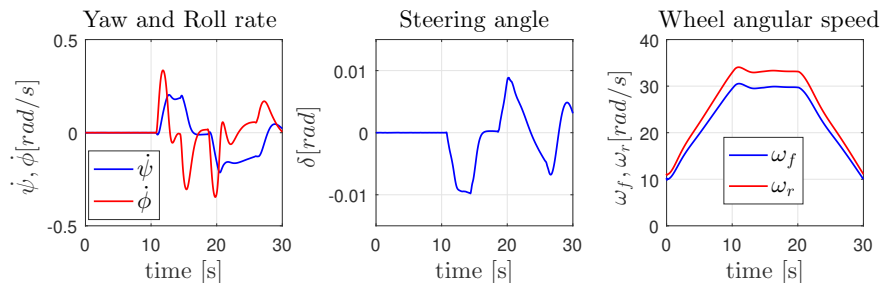


FIGURE 8.3: Maneuver 1: *BikeSim* measured states.

The inputs of the lateral and longitudinal models are the braking torques at the front and rear wheels, the drive engine torque and the steering torque depicted in figure 8.2. The measured state used in the observer design are given in figure 8.3. The lateral and forward accelerations ( $a_x$  and  $a_y$ ) are also used in the observer design as well as to validate the estimation of the unmeasured states from equation (8.43).

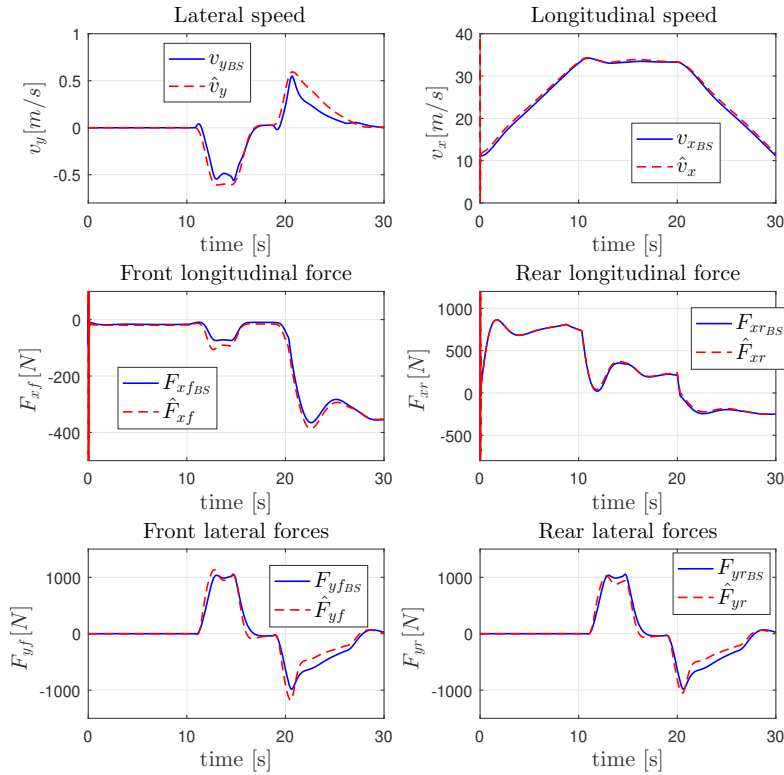


FIGURE 8.4: Maneuver 1: Actual states (in blue) compared to estimated states (dashed red).

Estimation results of this scenario are depicted on figure 8.4, which are the lateral and longitudinal speeds, the front and rear longitudinal forces, the front and rear cornering forces. From equation (8.43), the unmeasured state  $(v_x, v_y, F_{x_i}, F_{y_i})$  are validated and depicted in figure 8.5.

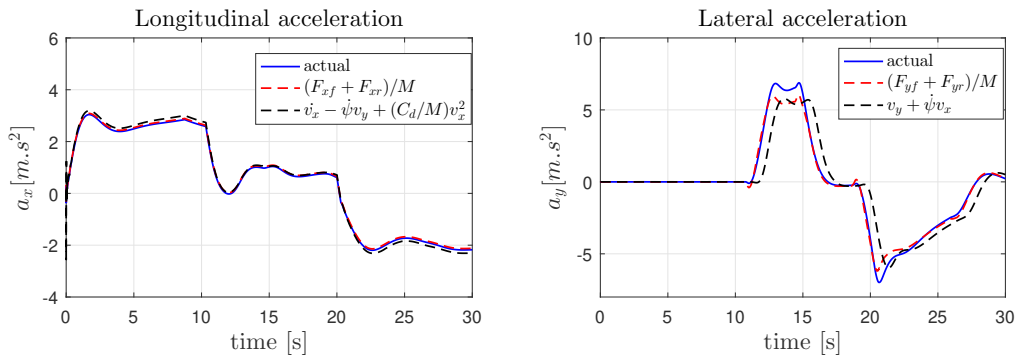


FIGURE 8.5: Maneuver 1: Validation of the estimated states.

We can see on figure (8.4) the non-measured states (the lateral and longitudinal speeds, the front and rear longitudinal forces, the front and rear cornering forces) compared to the actual data acquired from *BikeSim* sensors. These results show the ability of the designed observer to well recover simultaneously the interconnected longitudinal and lateral states of the motorcycle motion. Also we can remark a rapid transient phase of the observer. Indeed, these plots show some differences, in particular in the lateral speed and the lateral forces. This means that the lateral model is the most affected by the modeling errors between the *BikeSim* model and the sharp model used in the observer design. In fact, the two body sharp model is a pure lateral dynamic model valid for a various constant forward speeds. Indeed, the lateral model is slightly

affected by the longitudinal motion because it does not take into account speed variation when accelerating or braking. Despite modeling errors and the speed variation, the state estimation error still have ISpS performance and the interconnected observer still provide good estimation.

In the second maneuver, the motorcycle undergoes an oncoming traffic in road course with variable speed. The figures 8.6 show the input signals in the longitudinal and lateral models whereas figures 8.7 depict the measured states along the track. The unmeasured state are estimated, depicted in figures 8.8, and validated in figure 8.9.

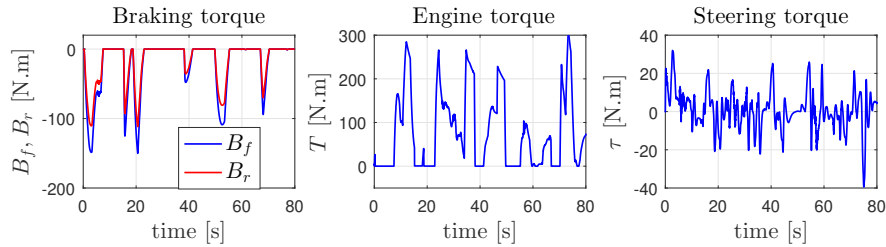


FIGURE 8.6: Maneuver 2: Inputs.

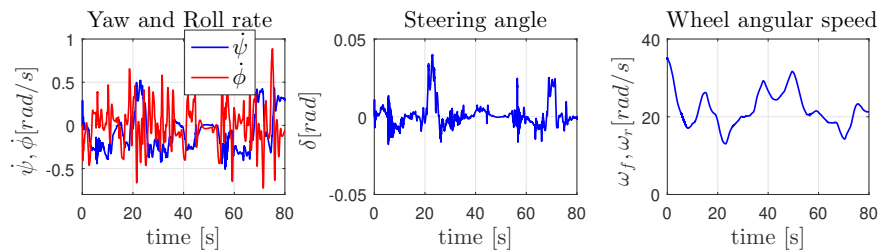


FIGURE 8.7: Maneuver 2: Measured states.

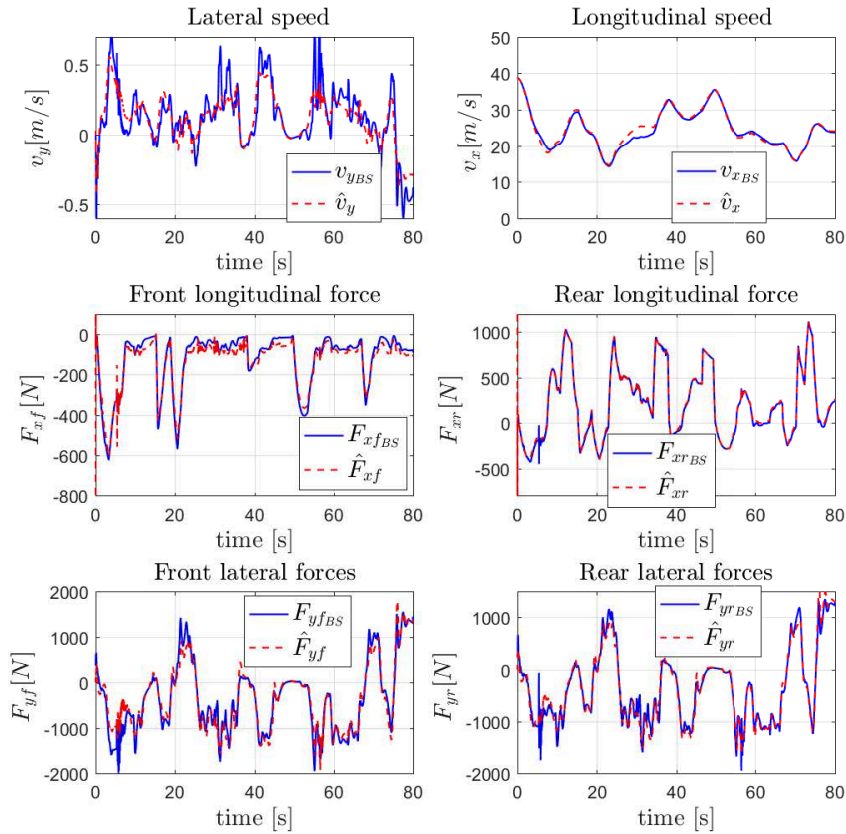


FIGURE 8.8: Maneuver 2: Actual states (in blue) compared to estimated states (dashed red).

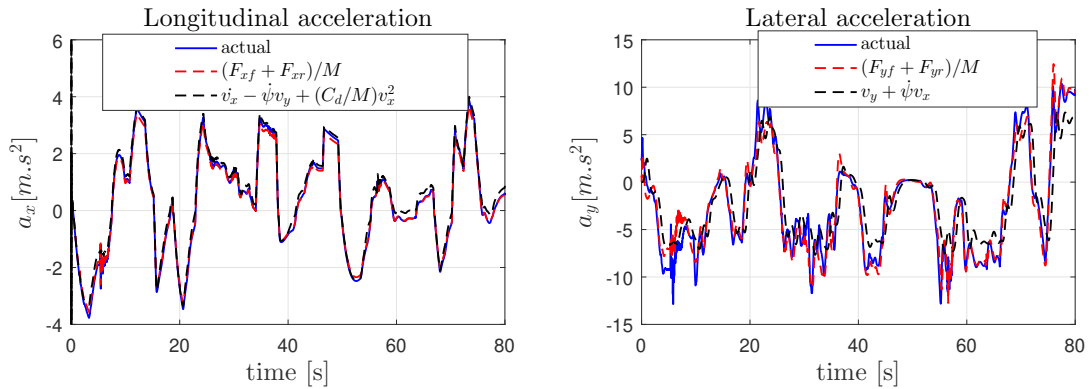


FIGURE 8.9: Maneuver 2: Validation of the estimated states.

This track test includes a speed variations, in which the rider alternate between acceleration and braking in turns, this maneuver is very common in riding situations. It clearly demonstrates all the capabilities of the interconnected observer of estimating the unknown states of both longitudinal and lateral motorcycle dynamics. Moreover, the forward speed is varying between 15 and 40m/s simultaneously with the braking and engine torques and with lateral rider action in order to test the estimation performances independently of the longitudinal velocity variations. As for the first test, this scenario illustrate that the observer rapidly and accurately estimates the state of the interconnected model with minimal error even for extreme riding situations. Despite some small estimation errors owing to modeling uncertainties, one can conclude that the interconnected observer provides satisfactory results.

## 8.4 Final Remarks

The main contribution of this work is to extend the existing works on the estimation of two-wheeled vehicle's lateral dynamics by the estimation of the longitudinal motion. The dependencies between these two motions interfere on the observability of the estimators. In this scope, this chapter dealt with the estimation of the quasi LPV out-of-plane and in-plane motorcycle motion. The interconnected observer formulation of the estimation problem is presented and evaluated throughout co-simulation with a high-end motorcycle simulation. This method is based on the decomposition of motorcycle model into two quasi LPV subsystems, then each quasi LPV subsystems model of the vehicle is transformed into Takagi-Sugeno (TS), the result is formalized using Lyapunov theory and the Input to State Practical Stability (ISpS) formulated as an optimization problem under Linear Matrix Inequalities (LMI) aiming to minimize the error estimation bound. The observer allows the reconstruction of relevant non-measurable states of the PTWV: the forward speed and the longitudinal tire forces from the first sub-observer and lateral speed, roll angle and the cornering forces from the second sub-observer.

## 8.5 Comparison and Analysis

From the previous chapters 5, 6, 7 and 8, the difference between the observers is not so trivial due to the fact that all the techniques achieve acceptable results. Nevertheless, these fourth observers have their advantages and disadvantages. For getting a close view, we recall the most important features of each of them in Table 8.1. To sum up, these observers successfully respond to a common problem, allowing to estimate the non-measurable PTWV states of the lateral dynamics such as the steering torque  $\tau$ , the lateral pneumatic forces  $F_{yf}$  and  $F_{yr}$ , the longitudinal forces  $F_{xf}$  and  $F_{xr}$ , lateral velocity  $v_y$  or roll angle noted  $\phi$ . In practice, it is hard to have exact knowledge of certain parameters of the model, either because they are not measurable (inertia, tire stiffness, model parameters  $a_{ij}$  etc.) or because they are not constant in time, such as the mass of the motorcycle and/or rider or even the mass of fuel. According to the motivations and objectives of this thesis, we also provide some solutions based on observer based identifier (LAO and DUIO), these methods deal with the estimation of both motorcycle states and parameters with the same design procedure. In addition, many scenarios have been considered in order to test the convergence of these techniques. Besides, these estimators require light instrumentation with very simple sensors that are widely used in vehicles (GPS, IMU and steering encoder). They are therefore perfectly integrated into the development of Advanced Rider Assistance Systems (ARAS) for PTWVs. However, the use of low-cost sensors generally degrades the quality of the measurements, which are then significantly affected by noise. Also, sensor alignment is never perfect causing bias in measurements. In this case, it would be interesting to quantify the estimation performance in the presence of noisy measurement or parameters uncertainties by mean of well-known index (RMSE, MSE, RMS).

Observer	Sensors	Advantages	Disadvantages
<i>Unknown Input Observer (UIO)</i>	IMU Steering encoder GPS	Road and Steering dynamics reconstruction $\tau, \phi, \phi_r, v_y, F_{yf}, F_{yr}$ Asymptotic convergence No knowledge about UI Lyapunov+ LMI region Real data validation	Structural constraint Using a differentiator $\dot{v}_x$ Nominal parameters
<i>Interconnected fuzzy Observer (IFO)</i>	Accelerometer Gyroscope Steering encoder	Lateral and longitudinal dynamics estimation $v_x, v_y, \phi, F_{yf}, F_{yr}, F_{xf}, F_{xr}$ Lyapunov+ ISpS stability Reduce observability problem Add DoFs in the reconstruction BS validation Does not require $\dot{v}_x$	Boundness of estimation errors Ideal sensors Nominal parameters
<b>Observer based Identifier</b>			
<i>LPV Luenberger adaptive Observer (LAO)</i>	IMU Steering encoder Virtual output GPS	State estimation $v_y, \phi, F_{yf}, F_{yr}$ Tire parameters identification $C_{f1}, C_{r1}, C_{f2}, C_{r2}$ Does not require $\dot{v}_x$ Evaluation scheme BS validation+ real data	Bounded Convergence Requires a pneumatic model Lipschitz condition PE condition
<i>Delayed Unknown Input Observer (DUIO)</i>	IMU Steering encoder Delayed outputs GPS	Mismatched condition $v_y, \phi, F_{yf}, F_{yr}$ state estimation $a_{ij}$ parametric identification Step-by-step algorithm DUIO BS validation	Using a differentiator Singularities due to inversion Complexity in TS form Ideal sensors

TABLE 8.1: Comparison table: Advantages / disadvantages of the presented observers for estimating of PTWV states and parameters.

## Conclusions

This section concludes the observer synthesis part based on the mathematical model of PTWV dynamics. Thereby, model-based state estimators are used to achieve a reliable estimation of both the motorcycle's unmeasured dynamics and the most important unknown parameters. The purpose of these observers is a concrete application. In this context, they take into account the real riding behavior of a PTWV, unknown parameters, the lack of accuracy of sensors or uncertainties either in the synthesis model or in the observer evaluation. Four observers of different purpose were presented:

- Unknown Input Observer (UIO), chapter 5.
- Delayed Unknown Input Observer (DUIO) with mismatched condition, chapter 6.
- LPV Luenberger-adaptive observer (LAO), chapter 7.
- Interconnected Fuzzy Observer (IFO), chapter 8.

The outlined observers were tested on the *BikeSim*<sup>©</sup> simulator for different scenarios such as a Double Line Change (DLC), handling road course, slalom maneuver and chirp test. These co-simulation tests aim to validate the observers by proving the convergence of the estimation error in cases of both normal (handling road course) and extreme (chirp, slalom and DLC) behavior. Finally, a much more realistic validations were made on experimental data from a test setup on the Scooter. These validations showed the potential of these observers in more real riding behavior to illustrate the effectiveness of the proposed observer in estimating the states, unknown input, unknown parameters and road geometry. One of the main contributions common to these four observers (UIO, IFO, LAO and DUIO) is the taking into account of the variations of the longitudinal velocity  $v_x$  during the design of the observer. In other words, there is no restriction on  $v_x$  as is the case in many works of literature. These observers has been designed subject to Lyapunov theory. Sufficient conditions for the existence of the estimator are given in terms of linear matrix inequalities (LMIs) to ensure the state and/or parameters estimation convergence. The simulation results showed satisfactory results that support the claims.

## Part IV

# Risk Assessment: Steering Behavior



## Introduction

THE study of the road accidents shows that human factors (57%) of accidents appear far before the meteorological or technical issues (Penumaka et al., 2014). The two most frequent human causes: alcohol and speed are responsible respectively of 31% and 25% of fatal accidents. Distraction or tiredness are also important human factors in a road accident that can be highlighted by, for example, lane crossing or abnormal steering behavior. Lane departures account for a significant percentage of roadway fatalities. According to Federal Highway Administration's Roadway (FHWA), from 2015 to 2017 an average of 19,23% traffic fatalities resulted from roadway departure crashes. This is why the last few years have seen the emergence of on-board roadway departure assistance systems in cars as a mean for improving security and helping to avoid damage or even fatal crashes in dangerous steering situations. Departure Lane Assist (DLA) systems make the vehicles more autonomous, allowing to inspect the surrounding vehicle's position and to detect the driver hypo-vigilance. These systems can be done through different technologies: Lane Departure Warning (LDW) system (Gonzalez Bautista, 2017) and Lane Keeping Assistance (LKA) system (Visvikis et al., 2008). All those systems have been discussed, as well as their interoperability issue in (Mammar et al., 2004; Mammar, Glaser, and Netto, 2006; Wang et al., 2018; Benine-Neto et al., 2014; Lefevre et al., 2013). In spite of the fact that road-departure systems are present in every modern car, they are not yet developed for motorcycle and those implemented for four-wheeled vehicles are not entirely transferable to motorcycles due to the fact that motorcycle dynamics is more complex and unstable. Therefore, departure avoidance systems for motorcycle are the next step, aimed to detect as early as possible, when the motorcycle is involuntary getting out of the lane. Then, the rider corrects his trajectory, maintain stability and keep acceptable performances by means of this early detection systems.

Currently, relevant works are planned to study the design of these systems for PTWV from the control point of view (Marumo and Katagiri, 2011b). In (Katagiri, Marumo, and Tsunashima, 2008b), the lane-keeping controller for motorcycles was evaluated through computer simulation with a rider-control model, in which the lane-following performance was improved by using a virtual-point regulator. In (Chung et al., 2006), the authors developed a Lane Change Decision Aid System (LCDAS), which detects backward vehicles and motorcycles taking into account weather and environmental conditions. Eventually, they used a change using single camera, in order to inform the driver of dangerous situations during lane change maneuvers. Furthermore, an optimal control theory to the lane keeping controller for motorcycles was presented in (Katagiri, Marumo, and Tsunashima, 2009). In (Damon et al., 2018b; Damon et al., 2018), authors study the motorcycle's steering behavior, achieved by a vision-based approach to define the motorcycle position on the road and detect under or oversteer situations. Lane Departure Warning System for a motorcycle is still under development and needs a more thorough investigation to be implemented in new bikes.

In some ways, the PTWV size can be seen as a weakness. In fact, they tend to frequently change travel direction and speed, regardless number of lanes or their width. Consequently, the lane crossing may create hazardous situations. To reduce safety risks, riders should try as much as possible to avoid the middle and the overtaking lanes since that would expose them to left side and right-side hazards posed by adjacent vehicles (A Hamzah, 2018). Furthermore, a key problem in building up departure warning systems for motorcycle or even vehicles is how to develop a driving risk function, which can be used to warn the rider in the case of passive assistance or engage the control action in the case of active assistance. A car roadway departure system usually defines a Lane Crossing Time (TLC) and Distance to Lane Crossing (DLC) as a risk index, to assess the time for involuntary trespassing the boundaries (Mammar, Glaser, and Netto, 2006; Wang et al., 2018).

Among others, steady-state analysis and handling capabilities issues are very related to vehicle safe trajectory and steering behavior. Many researches were devoted to study the steady-state handling for cars (Pacejka, 1973; Velenis, Frazzoli, and Tsiotras, 2009; Grigorievich, Igorevich, and Nikolayevich, 2018; Wasiwitono, Sutantra, and Triwinarno, 2015). These studies focus either to define the analytical handling criteria or the critical dynamic variables by which the divergent loss of handling occurs. The analysis of the properties of handling highlights certain dynamic aspects that are important to define dangerous/safe stability threshold conditions (Evangelou, 2004), as the neutral, overturning or underturning behaviors (Glaser, Mammar, and Sentouh, 2010; Velenis, Frazzoli, and Tsiotras, 2010; Evangelou, 2004; Grigorievich, Igorevich, and Nikolayevich, 2018; Wasiwitono, Sutantra, and Triwinarno, 2015). Unfortunately, this keen interest is not as evident to some other road users. In this context, there is a lack of literature review related to the problem of Lane Crossing Point (LCP) detection and steady-state steering analysis for motorcycles.

To sum up, the accidentology analysis and gaps have revealed two major categories: roadway departure and

---

unsuitable steering behavior, which need more thorough investigations. The purpose of this part is to provide solutions to both of these problems. We aim at identifying objective indicators for the quantification of risk as well as carrying out and discussing the design of possible warning system for riders of PTW vehicles. Risks considered here are related to unsuitable steering behavior, speeds profile and/or inadequate rider roll posture leading to a possible loss of control, lane departure or collision. The risk functions to be synthesized will be mainly based on purely dynamic considerations.

This design requires a precise knowledge of the various dynamic states and parameters of the motorcycle as well as the external efforts to which it is subjected. The calculation of the risk function can be achieved using existing instrumented PTWV, with the addition of systems that allow precise localization on the road based on vision. In what follows, we will describe two approaches proposed in order to detect risky riding situation and warn the rider to correct his trajectory. To do so, we divided this part into two chapters. First, a Neutral-path departure (NPD) is proposed. In this chapter, a detection approach towards getting circular stationary states and analytical handling conditions developed for PTWV. Based on the established motorcycle model combined with magic formula tire cornering forces, a Self Steering Gradient for motorcycles is proposed as a risk function. Hence, the NPD algorithm monitors signals from sensors and compares intended neutral and actual paths to characterize the steering behavior: over or under-steering situations. The second chapter focuses on Lane Crossing Prediction (LCP) for PTWV. The aim is to predict, with a simple perception system, the spatial and temporal lane change information (DLC and TLC) which are key components to be estimated in order to predict critical situations. The idea is based on data from Inverse Perspective Mapping (IPM) techniques for motorcycles developed in a previous thesis work (Damon et al., 2018a). These data are then used to discuss the distance to lane crossing estimation.

# Chapter 9

## On Steady-State Cornering Analysis

### Abstract

Inspired by steady-state and the handling analysis for cars, the following work tackles the question of the motorcycle's steering behavior based on the stationary cornering condition to describe neutral, under or over steering behavior. In this chapter, a neutral-path departure (NPD) algorithm is proposed to define safe handling conditions and dangerous steering situation for PTWV. Based on this study, a self steering gradient for motorcycles is proposed as a risk function for neutral-path departure detection. Furthermore, the motorcycle overturning or under-steering are analyzed based on the handling index. This index depends on the intrinsic motorcycle parameters, as well as, the outputs. The proposed neutral-path departure algorithm aims to assess the risk when the motorcycle begins to drift out of the neutral path. Finally, the effectiveness of the detection scheme is tested using a high-fidelity software *BikeSim*<sup>©</sup>. This work was published in Fouka et al., 2019c.

### 9.1 Lateral Motorcycle Dynamics

Riding assistive systems seek to improve the PTWV controllability and achieve the best dynamic behavior in all situations, from the most common to the most unexpected. Thereby, vehicles that are equipped with roadway assistive systems remain perfectly controllable whatever the physical limits of the rider. In this part, we are interested in the steady state cornering and neutral path departure, related to a problem of PTWV dynamics due to an excessive speed, overtaking in a bend or a failure in guidance system. In fact, the yaw rate combined with the longitudinal speed and the steering angle can represent the motorcycle steering tendency to oversteer or understeer. To solve this problem, we proposed risk indicators, related to the motorcycle lateral dynamics, in order to assess the severity of the situation and alert the rider if necessary.

The lateral cornering forces are given by:

$$\begin{cases} F_{yf} &= -C_{f1}\alpha_f + C_{f2}\gamma_f \\ F_{yr} &= -C_{r1}\alpha_r + C_{r2}\gamma_r \end{cases} \quad (9.1)$$

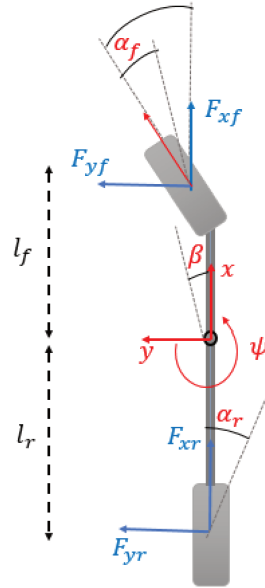


FIGURE 9.1: Motorcycle kinematics.

where  $C_{f1}$ ,  $C_{f2}$ ,  $C_{r1}$  and  $C_{r2}$  are the cornering stiffness and camber coefficients,  $\alpha_f$  and  $\alpha_r$  are sideslip angles,  $\gamma_f$  and  $\gamma_r$  are the camber angles of the front and rear tyres, respectively, with :

$$\begin{cases} \alpha_f = \frac{v_y + l_f \dot{\psi}}{v_x} - \delta \cos(\varepsilon) \\ \gamma_f = \phi + \delta \sin \varepsilon \\ \alpha_r = \frac{v_y - l_r \dot{\psi}}{v_x} \\ \gamma_r = \phi \end{cases} \quad (9.2)$$

After slight calculation, one can obtain:

$$\begin{cases} m(\dot{v}_y + \dot{\psi}v_x) = a_1 \frac{v_y}{v_x} + a_2 \frac{\dot{\psi}}{v_x} + a_3 \delta + a_4 \phi \\ I_z \ddot{\psi} = a_5 \frac{v_y}{v_x} + a_6 \frac{\dot{\psi}}{v_x} + a_7 \delta + a_8 \phi \\ I_x \ddot{\phi} + mh(\dot{v}_y + \dot{\psi}v_x) = mhg\phi \end{cases} \quad (9.3)$$

whereas,  $a_i$  are function of  $l_f$ ,  $l_r$ ,  $\varepsilon$ ,  $C_{fi}$  and  $C_{ri}$  with  $i = (1, 2)$ , given by:

$$\begin{cases} a_1 = -(C_{f1} + C_{r1}) \\ a_2 = -(l_f C_{f1} - l_r C_{r1}) \\ a_3 = (C_{f1} \cos(\varepsilon) + C_{f2} \sin(\varepsilon)) \\ a_4 = (C_{f2} + C_{r2}) \\ a_5 = a_2 \\ a_6 = -(l_f^2 C_{f1} + l_r^2 C_{r1}) \\ a_7 = (l_f C_{f1} \cos(\varepsilon) + l_f C_{f2} \sin(\varepsilon)) \\ a_8 = (l_f C_{f2} - l_r C_{r2}) \end{cases} \quad (9.4)$$

## 9.2 Steady Steering behavior and Handling Analysis

The aim of this section is to extract from the above model (9.3), the operating steady steering conditions. These characteristics are important and concur to define the sensitivity of the motorcycle's handling (Cosalter et al., 2006b), which is commonly judged by how a vehicle reacts to the rider inputs during cornering. Under a steady cornering scenario, the yaw rate  $\dot{\psi}$  as well as the steering angle, the lateral velocity and the side slip are constants, it follows:

$$\begin{cases} m\dot{\psi}v_x = a_1 \frac{v_y}{v_x} + a_2 \frac{\dot{\psi}}{v_x} + a_3\delta + a_4\phi \\ a_5 \frac{v_y}{v_x} + a_6 \frac{\dot{\psi}}{v_x} + a_7\delta + a_8\phi = 0 \\ \dot{\psi}v_x = g\phi \end{cases} \quad (9.5)$$

After simple manipulation, one can write :

$$\left( \underbrace{\left( a_5 m - \frac{a_5 a_4 - a_1 a_8}{g} \right)}_{K_1} v_x^2 - \underbrace{(a_5 a_2 - a_1 a_6)}_{K_2} \right) \frac{\dot{\psi}}{v_x} = \underbrace{(a_5 a_3 - a_1 a_7)}_{K_3} \delta \quad (9.6)$$

where

$$\begin{cases} K_1 = -(l_f C_{f1} - l_r C_{r1})m - \frac{(l_f + l_r)(C_{f2} C_{r1} - C_{f1} C_{r2})}{g} \\ K_2 = (l_f - l_r)^2 C_{f1} C_{r1} \\ K_3 = (l_f + l_r) C_{f1} (C_{r1} \cos(\epsilon) - C_{f2} \sin(\epsilon)) \end{cases} \quad (9.7)$$

The steering sensitivity  $\frac{\dot{\psi}}{\delta}$  is given by :

$$\frac{\dot{\psi}}{\delta} = \frac{\left(\frac{K_3}{K_2}\right)v_x}{[Kv_x^2 + 1]} \quad (9.8)$$

Where  $K = \frac{K_1}{K_3}$  is the handling factor. The aim of this part is to extract from the above model (9.3), the operating steady steering conditions. The motorcycle steering tendency depends on the yaw rate, the forward velocity  $v_x$  and the stability factor  $K$ , it follows:

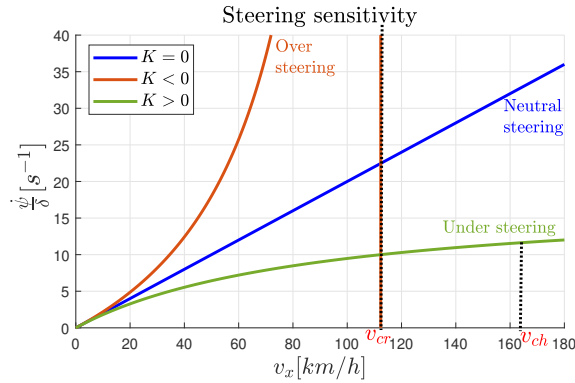


FIGURE 9.2: Motorcycle sensitivity gain.

1.  $K = 0$  for Neutral steering,  $\frac{\dot{\psi}}{\delta} = \frac{K_3}{K_2} v_x$  has a linear relation with motorcycle speed with  $\frac{K_3}{K_2}$  is the slope.
2.  $K > 0$  Under-steering, the steering sensitivity is below the neutral steering characteristics.  $\frac{d}{dv_x} \left( \frac{\dot{\psi}}{\delta} \right) = 0 \rightarrow v_{ch} = \frac{1}{\sqrt{K}}$ . It is interpreted as the motorcycle characteristic speed at which the vehicle reacts most sensitively to steering inputs.
3.  $K < 0$  Over-steering: when  $v_{cr} = \frac{1}{\sqrt{-K}}$ , the steering sensitivity strives toward infinity, where  $v_{cr}$  is the critical speed, for which a motorcycle becomes unstable because its steering is canceled, as even very small steering input would lead to infinite yaw rate.

### 9.3 Side Slip Dynamics

The following study defines a new handling factors proper to motorcycle. In steady cornering, the state variables are given by:

$$\phi = \frac{\dot{\psi}v_x}{g}, \quad \rho = \frac{\dot{\psi}}{v_x} = \frac{1}{R}, \quad a_y = \dot{\psi}v_x \quad (9.9)$$

The side slip relation can be expressed as a function of motorcycle intrinsic and dynamic variables from equations (3.4 and 9.1):  $\alpha_f - \alpha_r = f_1(\phi, \delta, a_y, \varepsilon, m, l_f, l_r, C_{fi}, C_{ri})$ , as well as from the kinematics equation (9.2):  $\alpha_f - \alpha_r = f_2(\delta, R, \varepsilon, l_f, l_r)$ . Now, replacing cornering forces (9.1) into (3.4), it follows:

$$\begin{bmatrix} \alpha_f \\ \alpha_r \end{bmatrix} = \begin{bmatrix} C_{f1} & C_{r1} \\ l_f C_{f1} & -l_r C_{r1} \end{bmatrix}^{-1} \left( \begin{bmatrix} ma_y \\ 0 \end{bmatrix} - \begin{bmatrix} C_{f2} & C_{r2} \\ l_f C_{f2} & -l_r C_{r2} \end{bmatrix} \begin{bmatrix} \gamma_f \\ \gamma_r \end{bmatrix} \right) \quad (9.10)$$

From the above equation:

$$\begin{cases} \alpha_f = \frac{(l_r m)}{(C_{f1} l_f + C_{r1} l_r)} a_y - \frac{C_{f2} l_r + C_{r2} l_f}{(C_{f1} l_f + C_{r1} l_r)} \gamma_f \\ \alpha_r = \frac{(l_f m)}{(C_{r1} l_f + C_{r1} l_r)} a_y - \frac{C_{r2} l_r + C_{r2} l_f}{(C_{r1} l_f + C_{r1} l_r)} \gamma_r \end{cases} \quad (9.11)$$

Replacing the camber angles ( $\gamma_f = \phi + \delta \sin(\varepsilon)$ ,  $\gamma_r = \phi$ ) in equation (9.11), one gets side slip relation:

$$\begin{aligned} \alpha_f - \alpha_r &= \underbrace{\left( \frac{C_{r2} C_{f1} - C_{f2} C_{r1}}{C_{r1} C_{f1}} \right)}_{EG_2} \phi - \underbrace{\frac{C_{f2}}{C_{f1}}}_{EG_3} \sin(\varepsilon) \delta + \\ &\quad \underbrace{\left( \frac{C_{r1} l_r - C_{f1} l_f}{C_{f1} C_{r1}} \right)}_{EG_1} \frac{m}{(l_f + l_r)} a_y \\ &= EG_1 a_y + EG_2 \phi - EG_3 \delta \end{aligned} \quad (9.12)$$

From the following kinematics equations:

$$\alpha_f = -\frac{v_y + l_f \dot{\psi}}{v_x} + \delta \cos(\varepsilon), \quad \alpha_r = -\frac{v_y - l_r \dot{\psi}}{v_x} \quad (9.13)$$

The side slip relation is also described as:

$$\begin{aligned} \alpha_f - \alpha_r &= -\frac{v_y + l_f \dot{\psi}}{v_x} + \cos(\varepsilon) \delta + \frac{v_y - l_r \dot{\psi}}{v_x} \\ &= -(l_f + l_r) \frac{\dot{\psi}}{v_x} + \cos(\varepsilon) \delta \\ &= -\frac{(l_f + l_r)}{R} + \cos(\varepsilon) \delta \end{aligned} \quad (9.14)$$

The self-steering behavior depends on the sideslip difference:

$$\begin{cases} \alpha_f - \alpha_r = EG_1 a_y + EG_2 \phi - EG_3 \delta \\ \alpha_f - \alpha_r = -\frac{(l_f + l_r)}{R} + \cos(\varepsilon) \delta \end{cases} \quad (9.15)$$

by identifying the above equations, one gets:

$$\begin{aligned} \delta &= \frac{(l_f + l_r)}{R(\cos(\varepsilon) + EG_3)} + a_y \frac{EG_1}{(\cos(\varepsilon) + EG_3)} + \phi \frac{EG_2}{(\cos(\varepsilon) + EG_3)} \\ &= \delta_A + a_y \frac{EG_1}{(\cos(\varepsilon) + EG_3)} + \phi \frac{EG_2}{(\cos(\varepsilon) + EG_3)} \\ &= \delta_A + \Delta \delta \end{aligned} \quad (9.16)$$

With

$$\delta_A = \frac{(l_f + l_r)}{R(\cos(\varepsilon) + EG_3)} \quad (9.17)$$

The steering angle  $\delta_A$  resulting from equation (9.16), is called the neutral steering angle. The additional  $\Delta \delta$  angle is caused by the motorcycle's dynamics.

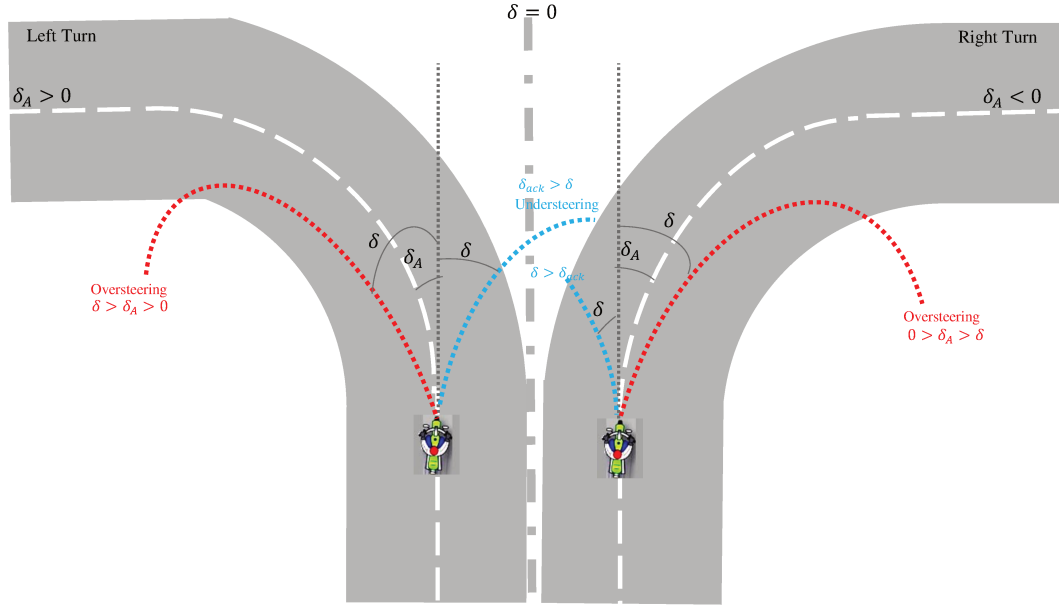


FIGURE 9.3: Over and Under steering situations.

Now, in order to propose a detection algorithm for the over and under steer situations, we propose a risk function defined from the self steer behavior in equation (9.16). Therefore, the steering behavior can also be described as follows:

$$S_S = \frac{\delta - \delta_A}{a_y (1 + \frac{EG_2 \phi}{EG_1 a_y})} \frac{(\cos(\epsilon) + EG_3)}{EG_1} \quad (9.18)$$

where  $S_S$  represents the Self-Steer Motorcycle Gradient. In the straight-line road, the lateral acceleration is small, and  $S_S$  values become very large. Thus we use the algebraic function  $\text{sign}(a_y)$  instead of  $a_y$  to avoid the detection of false alarms due to  $S_S \rightarrow \infty$ . Now, the expression of the steering behavior (9.18) is completely defined, a simple analysis of  $S_S$  allows to characterize the steering behavior of the PTWV.

## 9.4 Neutral Path Detection Algorithm

Neutral Path Departure algorithm aims at helping a rider in maintaining safe travel, where the goal is to detect an over or an understeer behavior compared with the neutral dynamics and to warn the rider of a loss of friction between the front and rear wheels. The NPD algorithm depends on a risk function  $S_S$  proper for a motorcycle, this index is required to detect the drift out from the neutral steady dynamics, the sign of the  $S_S$  signifies the understeer and oversteer behavior of the motorcycle in left and right turn. Then, the rider adjusts the steering angle, rider's posture and/or forward speed to recover the neutral trajectory without a controller. Moreover to improve the confidence of the results, the analysis of the derivative  $\dot{S}_S$  is of interest to detect the changing in the steering action if any correction is taken by the rider. This consideration is made to avoid false alarms when the driver is already correcting his maneuver. Therefore, the sign of  $S_S$  and derivative  $\dot{S}_S$  is used to define two decision variables  $(\zeta_1, \zeta_2)$ . The process of providing a neutral departure warning is summarized in the following cases:

1.  $S_S \approx 0$  ( $\dot{S}_S = 0$ ): The motorcycle is neutral-steering ( $\alpha_f = \alpha_r$ ). In this case, the cornering powers are equal at the front and rear wheels. When cornering, no change in steering angle is required to maintain the correct radius when the speed varies.
2. **Right turn**,  $\delta_A < 0$  (clockwise):

$-S_S < 0$  ( $\widehat{S_S} < 0$ ), when motorcycle steers towards the right: this reflects over-steering behavior. The actual cornering radius is smaller than the neutral one. Indeed, a decrease in lateral acceleration causes a greater increase in the radius of the trajectory. This phenomenon generates instability which can only be countered by a decrease in the steering angle to stay on the neutral radius.

$-S_S < 0$  ( $\widehat{S_S} > 0$ ) reflects counter-steering behavior (correction of the over steer).

$-S_S > 0$  ( $\widehat{S_S} > 0$ ) reflects under-steering behavior. It is necessary to steer the steering angle in the clockwise sense to stay on the right radius.

$-S_S > 0$  ( $\widehat{S_S} < 0$ ) correction of the under-steer.

### 3. Left turn, $\delta_A > 0$ (anticlockwise):

$-S_S > 0$  ( $\widehat{S_S} > 0$ ) reflects over-steering behavior, the actual cornering radius is smaller than the neutral one, the rider has to turn the front wheel in the right side, reduce roll angle or accelerate to increase the radius and catch the neutral path.

$-S_S > 0$  ( $\widehat{S_S} < 0$ ) counter-steering behavior.

$-S_S < 0$  ( $\widehat{S_S} < 0$ ) reflects under-steering behavior, the actual cornering radius is greater than the neutral path, the rider has to steer towards the left side or tilt to increase roll angle to reach the correct radius.

$-S_S < 0$  ( $\widehat{S_S} > 0$ ) under-steer correction.

**Remark 9.1.** Moreover, a hysteresis function  $Hys(S_S)$  or a memory block can be used to avoid multiple switching. This block holds the value of  $(S_S)$  when the algorithm switches to test the rider correction by  $\widehat{S_S}$ . The use of this block can minimize unwanted behaviors when switching between the algorithm loops.

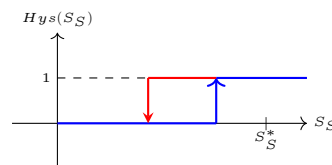


FIGURE 9.4: Memory block

## 9.5 Simulation Results

The proposed approach is evaluated by co-simulation with *BikeSim*<sup>©</sup> software under different riding maneuver. A PTWV model is chosen from the dataset *Big Sport Baseline* 8 bodies and default parameters. It will be assumed that:

- The road is flat with a high friction coefficient of  $\mu = 0.9$
- In these simulations, the motorcycle is riding at a constant speed of 50 km/h.

The simulations are carried out considering two scenarios:

**Scenario 1:** Three tests are conducted to evaluate the risk index: an oversteer scenario, a neutral turning scenario and an understeer maneuver.

**Scenario 2:** A mixed scenario including neutral, under, oversteer and rider correction with noise consideration to highlight the detection scheme and alarm generation.

Note that *BikeSim* offers several driver models with different control strategies. In our case, it is an open-loop control on the steering torque, more suitable to simulate steering behavior.

### 9.5.1 Scenario 1

In this scenario, it is proposed to validate the risk function selected for the detection of under and oversteer on the handlebar of a PTWV. To do this, we have simulated a circular trajectory with a constant radius of 61.4 meters for three different riding scenarios, conducted for different steering torques.

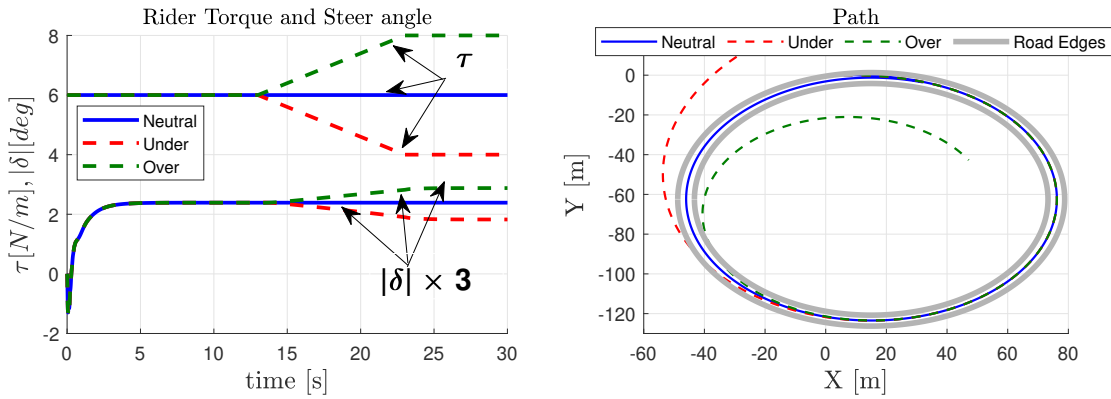


FIGURE 9.5: (right) Rider torque and steering angle (left) Neutral Path Departure.

Figure 9.5 (left) shows the steering torques applied to the PTWV. On the same figure, we can also see the steering angle corresponding to a scale factor of 3. The input steering angle used in this test is defined

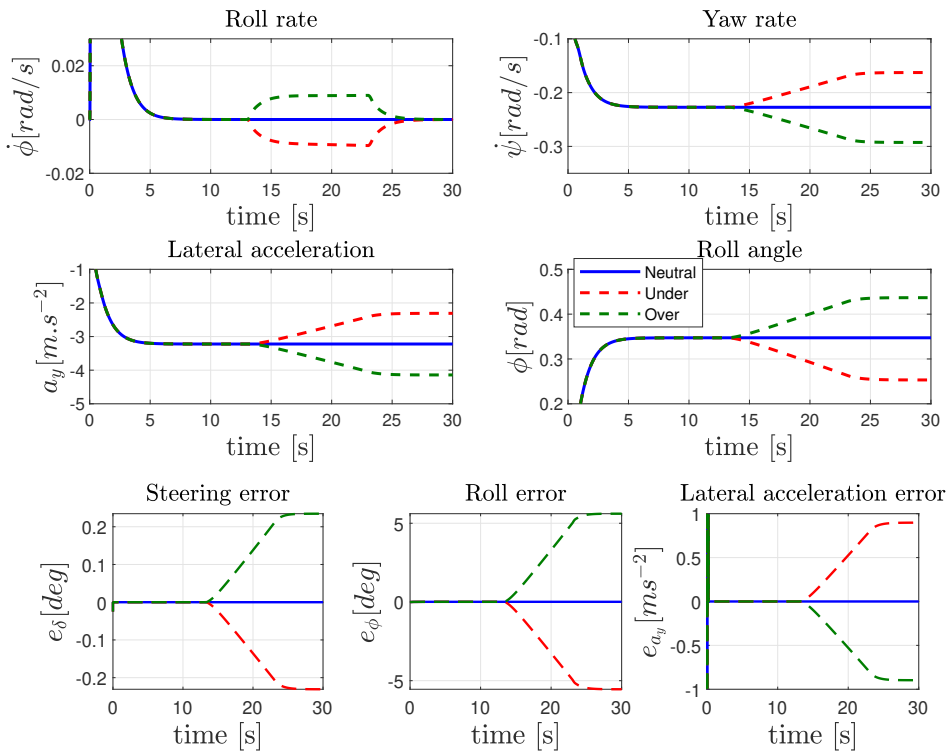


FIGURE 9.6: Steady Steering behavior: outputs and steering errors.

such that the wheel lift-off occurs at 13 sec, whereas in neutral test no wheel lift-off occurs. For the neutral

scenario, the torque applied to the handlebar is  $\tau = 6 \text{ N/m}$ . When a PTWV is oversteer, the torque applied by the rider on the handlebars is too large compared to the geometry of the turn. PTWV tends to turn inward of the curve. Conversely, when understeers the applied torque is lower than the neutral one, the PTWV tends to increase the trajectory to the road exit. The vertical dashed line refers to the time from which the steering behavior is significantly affected by the over or understeer phenomenon.

Figure 9.5 (right) shows the different trajectories of the PTWV during the constant turn. In blue, the motorcycle trajectory for a neutral turning. In which the motorcycle path is parallel to that of the road edges. While in red, we show the trajectories of over turning, respectively in black under turning.

Figures 9.6 plot the consequences of the over and under-steering phenomena on the steady state variables for the three cases. It can be seen that the slightest action on the handlebars when cornering has significant consequences on the complete dynamics of the PTWV ( $\psi$ ,  $a_y$ ,  $\phi$ , etc). In Figure 9.7, we present the steering index calculated from equation (9.18) for the three scenarios. It can be noted that the alarm and correction signals remain at zero when no wheel lift-off occurs. Then, these signals detect the motorcycle is drifting out:  $\zeta_1 = -1$  understeer or  $\zeta_1 = 1$  oversteer. In these scenarios, no correction is taken by the ride  $\zeta_2 = 0$ . The  $S_S$  shows good efficiency to early detect the steering errors from the neutral path. This advantage is very interesting since the neutral path departure has to be quickly avoided.

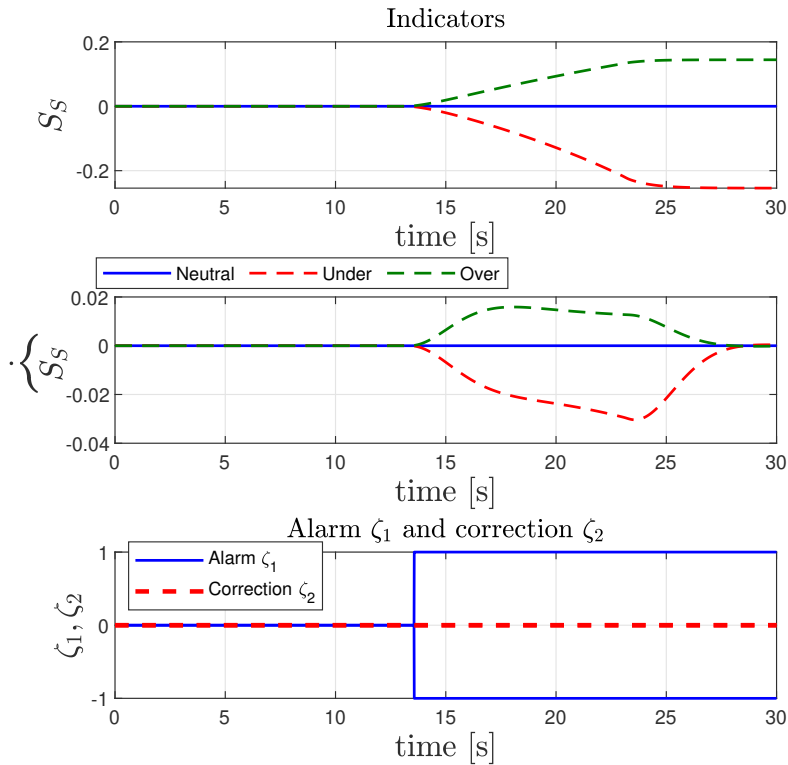


FIGURE 9.7: Alarm and corrections.

### 9.5.2 Scenario 2

This part is devoted to evaluating the neutral path departure warning algorithm in noisy case.

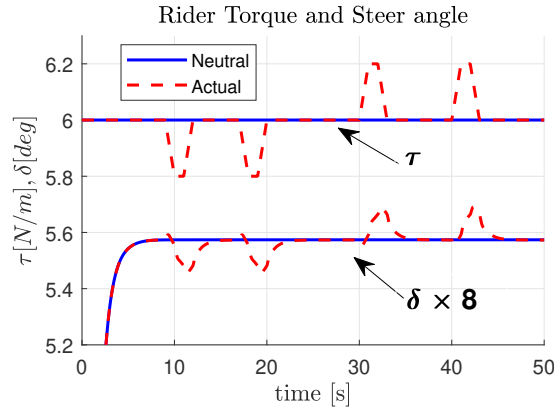


FIGURE 9.8: Steering behavior: Rider torque and steering angle.

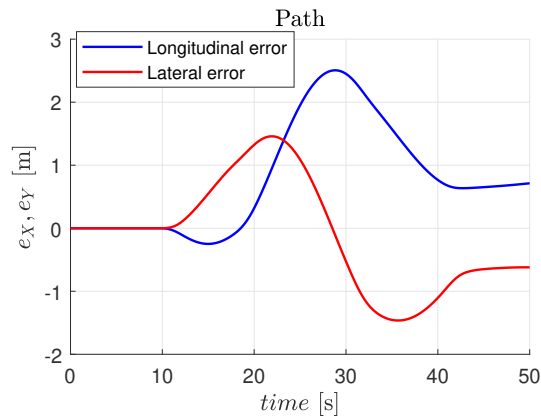


FIGURE 9.9: Trajectory departure errors.

During this scenario, the motorcycle is riding to perfectly follow the neutral path road until 9 sec. Then, the wheel drift will occur first as understeer until 30 sec including a rider correction, then as oversteer until 50 s with some adjustment from the rider, seeking to catch the neutral line. Figure 9.8 shows the steering torques applied by the rider and the corresponding steering angle.

Figure 9.9 shows the lateral and longitudinal errors. While, figures 9.10 show the consequences of the neutral path departure on the motorcycle states.

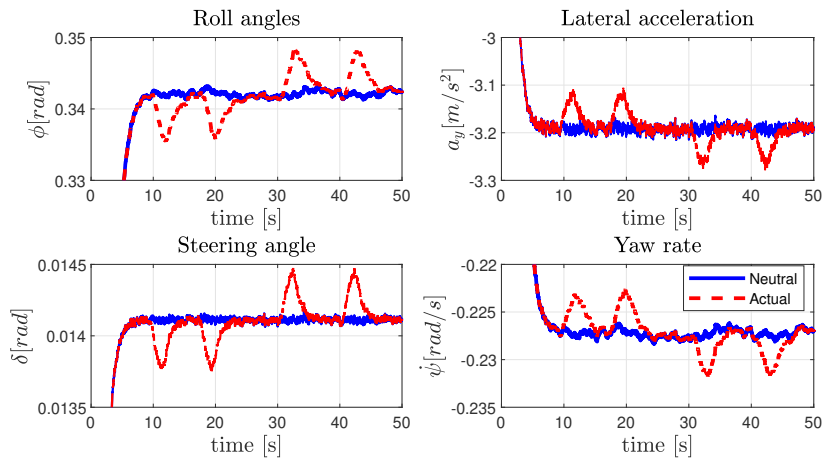


FIGURE 9.10: Noisy outputs.

Figure 9.11 illustrates the relevant indicators proposed for the characterization of steering behavior. The risk indicator  $S_S$  is computed here from the noisy measurement of the actual steering, lateral acceleration, and roll angle of the PTWV. Moreover, the analysis of  $\widehat{S}_S$  is very interesting to characterize the changing in the rider steering action. Note that the raw data (unfiltered) is difficult to exploit because of the noise amplified by the derivation. This is why the  $S_S$  has been filtered with a simple first-order filter. Therefore, we prefer to use the  $S_S$  and derivative  $\widehat{S}_S$  to define two levels of risk: the first level detects the over/understeering and the second level detects if any correction is taking by rider.

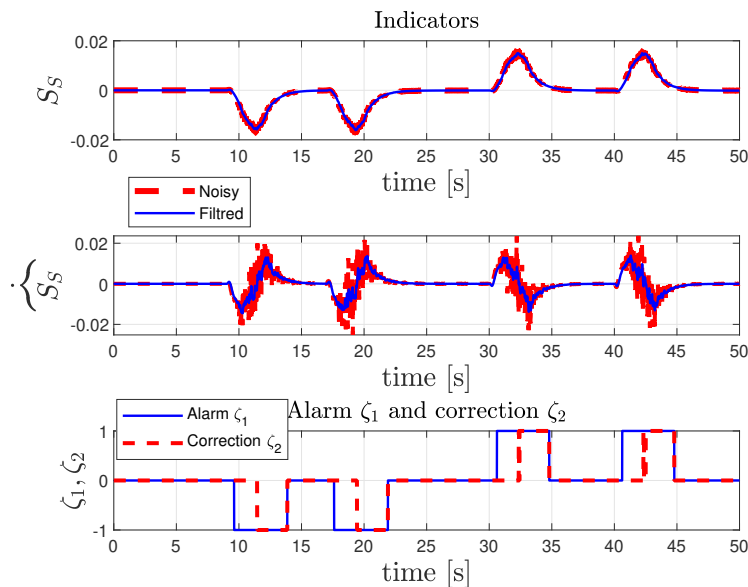


FIGURE 9.11: Risk functions, alarm and corrections.

One can see in figure (9.11) that the used steering risk indicators and the alarm signal given by the detection algorithm are very interesting to detect the rider errors and the neutral path drift out even with noisy outputs. It can be noted that the alarm signal remains at zero when no neutral path departure is detected  $S_S = 0$ . Then the alarm signals take the correct values depending on which direction the motorcycle is drifting out  $\zeta_1 = -1$  understeer or  $\zeta_1 = 1$  oversteer. Also, one can see the alarm corresponding to rider correction  $\zeta_2$  which means that the rider is trying to bring back the PTWV to the neutral path.

### 9.5.3 Results Discussion

Finally, simulation results from the *BikeSim*<sup>©</sup> software have shown that the synthesis of the detection algorithm-based risk function has undeniable potential to characterize the steering behavior. Indeed, it is much informative since it is based on the analysis of two parameters  $S_S$  and  $\widehat{S}_S$ . These results attest the effectiveness of the risk indicators developed for neutral path departure detection algorithm. These results highlight the effectiveness of the detection algorithm to detect in an early stage the steering deviation. This advantage is very interesting since the road departure has to be avoided earlier. Although the results are really encouraging, the idea presented in this thesis deserves to be deepened. Indeed, for the validation of the approach, we are limited to the co-simulation case and improvements should be made to avoid bad detection in case of using estimated data instead of measurement outputs in some situations.

## 9.6 Conclusions

In this chapter, we proposed a synthesis of a new risk function for the characterization of rider steering behavior. While conventional approaches use kinematics or geometric functions, to detect the intersection point on the road edges. The motorcycle tendency to under or oversteer in steady turning is also analyzed, based on handling conditions. We propose here a new neutral-path departure algorithm to overcome rider

steering errors when the rider drifts out of the neutral lane. The algorithm monitors signals from sensors and compares intended neutral (theoretical) and actual paths. If the trajectories differ from each other, this means that motorcycle is going out neutral path, in this case, the algorithm generates an alarm to warn the rider. Based on the established motorcycle model, combined with magic formula tire cornering forces, a Self Steering Gradient for motorcycles “ $S_S$ ” is proposed as a risk function. Besides, the NPD algorithm is designed based on the  $S_S$  and  $\widehat{S_S}$ . Then, the detection method was tested in co-simulation using *BikeSim*<sup>©</sup> under different steering maneuvers to highlight the effectiveness of the proposed algorithm to detect in an early stage the over/under steering deviation from the neutral path, to improve motorcycle handling and correct the unsafe maneuver. Indeed, the proposed solution is very economical, limiting the amount of energy needed since it only requires a conventional IMU and a steering encoder.

# Chapter 10

## Lane Crossing Tracking

### Abstract

Departure Lane Assist (DLA) systems for the PTWV are the next step in inspecting the motorcycle's position. Obviously, these departure avoidance systems were intended to warn the rider of an unintentional drift off the track. In this chapter, we investigate a vision-based approach for online lane change prediction and detection dedicated to motorcycles. The approach is composed of two steps. First, the road geometry (clothoid model) and the motorcycle position with respect to the road markers are deduced based an inverse perspective mapping (IPM) algorithm. The relative position is represented by the vehicle lateral displacement and heading estimated by means of an Inertial Measurement Unit and a monocular camera. The second step consists of predicting the Lane Crossing Point which allows to predict the distance and time before the motorcycle crosses the lane. The algorithm is achieved without the use of any steering sensor. The theoretical aspects and the validation of this idea were published in Damon et al., 2019.

### 10.1 Problem Statement

The detection and tracking of the Lane Crossing Point (LCP) involve several technical problems that must be overcome (Tapia-Espinoza and Torres-Torriti, 2013; Kumar and Simon, 2015). Whereas prediction is realized in most cases through monocular cameras by reconstructing the road profile as well as the current position of the vehicle. This is also done under some assumptions such as flat roads and perfectly parallel markings.

In the case of motorcycle riding, both previous assumptions are violated because of a bike dynamics. Indeed, the PTWV can reach significant roll angles (the world record is about  $68^\circ$ ) and undergo load transfers during braking or acceleration phases (pitch angle significant). Following this, the images recorded by the front camera undergo noteworthy deformations and do not allow a direct use without a projection in a more advantageous plan (bird-eye-view for example). The next section recalls previous work on a vision based approach for accurate vehicle position reconstruction, presented in Damon et al., 2018a; Damon et al., 2018c.

This allows to recover crucial information such that DLC or TLC proportional and the second being inversely proportional regarding the motorcycle speed.

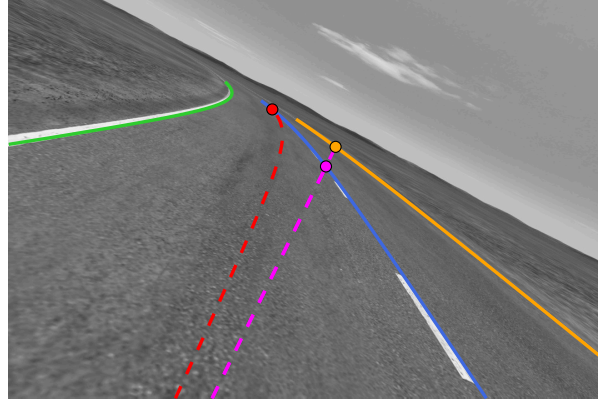


FIGURE 10.1: Captured camera image with reprojected road lanes, predicted trajectories and LCP

This work focuses on lane crossing prediction for powered two-wheeled vehicles. The aim is to predict, with a simple perception system, the spatial and temporal lane change information. Such information can be predicted using the Time to Lane Crossing (TLC) and the Distance to Lane Crossing (DLC) which are key components to be estimated in order to predict critical situations.

## 10.2 Vision-based Information

This chapter recalls the results initially introduced in Damon et al., 2018a. The reader could refer to the following videos <sup>1</sup> for visual illustrations. In Damon et al., 2018a, the authors used the IPM technique combined with a road lanes filter allowing to generate a bird-eye-view of the road markers (as presented in figure 10.3). Then, a clothoid model of the road is used to extract pertinent information such that the PTWV relative lateral displacement and heading angle to the road markers. They are respectively denoted  $\Delta Y_i$  and  $\Delta \psi_i$ , where  $i \in \{l, c, r\}$  indicates left, center and right markers. It allows to recover crucial information regarding the PTWV location on the road.

Furthermore, the clothoid model allows to predict the road curvature and its rate respectively named  $C_0$  and  $C_1$ . Both parameters allow to accurately reconstruct the road trajectory in the selected Region Of Interest (ROI). Note that, even if the ROI ahead limit of the PTWV is chosen about 30 meters (see Damon et al., 2018a), each road marker trajectory can be extended since we know its third degree polynomial approximation.

Let us remind that each road lane is approximated in the cartesian coordinate system with the following expression for  $i \in \{l, c, r\}$ :

$$y_i(x) \approx \Delta Y_i + \tan(\Delta \psi_i)x + \frac{1}{2}C_{0_i}x^2 + \frac{1}{6}C_{1_i}x^3 \quad (10.1)$$

Whereas, in the simulations discussed in Damon et al., 2018a, the right road marker is defined as a static reference, we proposed to introduce a dynamic reference. Indeed, the accuracy of the lane  $i$  trajectory reconstruction mainly depends on two factors: the proximity with this lane and its attribute (dashed or solid). Our strategy is to choose the reference among the right or left solid lanes regarding the estimated PTWV position on the road (given by  $\Delta Y$  and  $\Delta \psi$ ). Note that, choose the center marker is depreciated because it is often discontinuous leading to less accurate approximation. Then, if the PTWV is traveling in the right (respectively left) lane, the right (respectively left) road marker is set as the reference. Finally, since the road markers are assumed parallel and separated from each other by a distance  $L$ , the two others lanes trajectories are reconstructed from the reference road marker equation (10.1). At this point, we know an estimation of the three lanes trajectories in the vehicle frame  $F_v$  whose the origin is the projection of the camera center on the ground.

<sup>1</sup><https://www.youtube.com/playlist?list=PLRTI62SuvNymK2Dx-YKha-1a4Sp54IVs8>

## 10.3 Lane Crossing Point Tracking

Now, considering that the road lane trajectories are available, the LCP tracking problem consists of finding the intersection point coordinates between the predicted road lane and vehicle trajectories. For the latter, we addressed two cases. For both, the vehicle speed is assumed constant and positive. The first case considers a straight predicted vehicle trajectory which corresponds to a zero steering angle ( $\delta = 0$ ). Whereas for the second,  $\delta$  is assumed constant and non zero. Under these last assumptions, the predicted vehicle trajectory is a circular path with a constant radius. For what follows, we denoted  $DLC_0$  and  $DLC_\delta$  the predicted distances to the LCP respectively for straight and circular vehicle trajectories. Note that, the DLC is computed with respect to the vertical projection of the camera center on the ground which is the origin of the frame  $F_v$ .

Note that, for the case where  $\delta \neq 0$ , we systematically compute two DLC which are  $DLC_0$  and  $DLC_\delta$ . The first considering a straight predicted trajectory and the second based on a circular path prediction (see figure 10.3). This allows to get a surface containing all the LCP between the actual circular path and the straight one. In other words, it provides indications about the LCP location in case of the rider reduces the steering (increase of the trajectory radius).

Moreover, for both scenarios ( $\delta = 0$  and  $\delta \neq 0$ ), we solved the DLC algorithm for each detected road lane. Hence, the final LCP is the nearest point among the solutions as illustrated in figure 10.1 and 10.3.

### 10.3.1 Straight predicted vehicle trajectory ( $\delta = 0$ )

For straight predicted path, the computation of the DLC can be easily achieved by solving the equations for  $i \in \{l, c, r\}$ :

$$\Delta Y_i + \tan(\Delta \psi_i)x + \frac{1}{2}C_{0_i}x^2 + \frac{1}{6}C_{1_i}x^3 = 0 \quad (10.2)$$

Let us remind that equation (10.2) is expressed in the vehicle frame  $F_v$  where  $X_v$  corresponds to the vehicle longitudinal axis (refer to 10.3). Hence, if  $x_{DLC_{0_i}}$  is a solution of equation (10.2) then, the DLC with regards to the lane  $i$  is trivial. It can be directly deduced such that:  $DLC_{0_i} = x_{DLC_{0_i}}$ . Let us remind, the final DLC is computed such that  $DLC_0 = \min(DLC_{0_k})$  with  $k$  corresponding to the set of all the lane intersection points. In figure 10.3, the magenta line clearly illustrates the situation with  $k = \{\text{center, right}\}$ .

### 10.3.2 Circular predicted vehicle trajectory ( $\delta \neq 0$ )

In this case, we need to reconstruct the forward predicted vehicle trajectory based on its current dynamic states. To do so, it requires to compute the vehicle slip angle denoted  $\psi_s$ . It can be expressed as a function of the the measured yaw angle ( $\psi$ ) and the angle of the trajectory tangential vector ( $\psi_t$ ) as illustrated in figure 10.2.

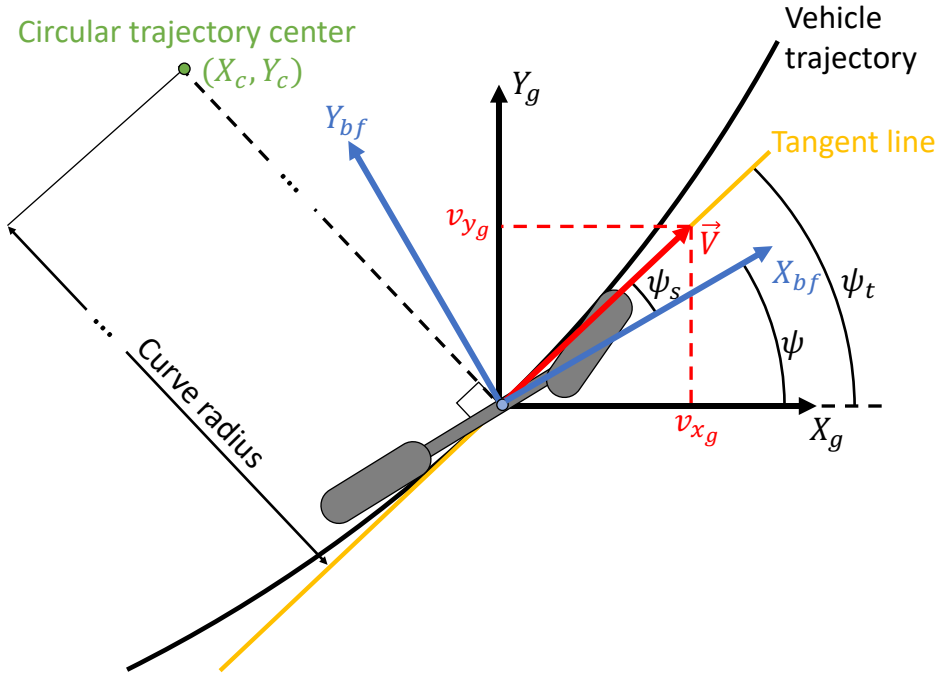


FIGURE 10.2: Scheme of the vehicle circular path prediction

Now, let us consider that the yaw angle, measured by the IMU, is included in the interval  $[-\pi, \pi]$ . To avoid any singularity, we introduced the following relation:

$$\begin{aligned}\psi_s &= \Psi_t(\psi, \psi_t) - \Psi(\psi) \\ &= \psi_t + \pi \text{sign}(\Psi(\psi)) \Theta(\psi_t, \psi) - \Psi(\psi)\end{aligned}\quad (10.3)$$

with  $\Theta$  and  $\Psi$  defined by the following functions:

$$\Psi(\psi) = \begin{cases} \psi - \text{sign}(\psi)\pi/2 & \text{if } |\psi| \geq \pi/2 \\ \psi & \text{if } |\psi| < \pi/2 \end{cases}\quad (10.4)$$

and

$$\Theta(\psi_t, \psi) = \begin{cases} 0 & \text{if } |\psi_t - \Psi(\psi)| \leq \pi/2 \\ 1 & \text{if } |\psi_t - \Psi(\psi)| > \pi/2 \end{cases}\quad (10.5)$$

At this step, the aim is to express  $\psi_t$  as a function of the IMU measurements such that the body-fixed accelerations  $(a_{x_{bf}}, a_{y_{bf}}, a_{z_{bf}})$  and the orientation angles  $(\phi, \theta, \psi)$ .

Let us define  $A_j = [a_{x_j}, a_{y_j}, a_{z_j}]^T$  and  $V_j = [v_{x_j}, v_{y_j}, v_{z_j}]^T$  as the acceleration and the speed vectors with  $j = g$  for the global frame and  $j = bf$  for the body-fixed one. Let us remind the following relations between the two frames:

$$\begin{cases} V_g &= \mathcal{R}V_{bf} \\ A_g &= \mathcal{R}A_{bf} \end{cases}\quad (10.6)$$

where  $\mathcal{R} = \mathcal{R}_\psi \mathcal{R}_\theta \mathcal{R}_\Phi$  is the rotation matrix. The terms  $\mathcal{R}_\psi$ ,  $\mathcal{R}_\theta$  and  $\mathcal{R}_\Phi$  denote the rotation matrices associated respectively to the yaw, pitch and roll Euler angles. Note that  $\Phi$  is the rotation angle about the axis which has been previously pitched of  $\theta$ . The real vehicle roll angle, denoted  $\phi$ , can be computed using the algebraic expression:

$$\phi = \text{asin}(\cos(\theta) \sin(\Phi))\quad (10.7)$$

Furthermore, the acceleration vector in the global frame can be obtain with the relation:  $A_g = \dot{V}_g$ . Combining the latter and (10.6) leads to:

$$A_g = \dot{\mathcal{R}}V_{bf} + \mathcal{R}\dot{V}_{bf} \quad (10.8)$$

Since we assumed that the vehicle motion is uniform and circular ( $\Phi = cst$ ,  $\theta = cst$ ,  $\dot{V}_{bf} = 0$ ), equation (10.8) can be reduced to:

$$A_g = \dot{\mathcal{R}}V_{bf} \quad (10.9)$$

where  $\dot{\mathcal{R}} = \dot{\mathcal{R}}_\psi \mathcal{R}_\theta \mathcal{R}_\Phi$  is the time derivative of the rotation matrix.

Using equations (10.6) and (10.9), we obtain the following expression:

$$\begin{aligned} \mathcal{R}A_{bf} &= \dot{\mathcal{R}}V_{bf} \\ &= \dot{\mathcal{R}}\mathcal{R}^{-1}V_g \end{aligned} \quad (10.10)$$

Afterwards, we get one expression of the speed vector in the global frame:

$$V_g = \mathcal{M}A_{bf} \quad (10.11)$$

where  $\mathcal{M} = \mathcal{R}\dot{\mathcal{R}}^{-1}\mathcal{R} = [m_{ij}]$  with  $i, j \in \{1, 2, 3\}$

Let us remind that, by definition, the speed vector, expressed in the global frame, is tangent to the vehicle trajectory. Since  $\psi_t$  is the angle of the tangential direction to the PTWV trajectory, it comes:

$$\begin{aligned} \psi_t &= \text{atan} \left( \frac{v_{yg}}{v_{xg}} \right) \\ &= \text{atan} \left( \frac{m_{21}a_{x_{bf}} + m_{22}a_{y_{bf}} + m_{23}a_{z_{bf}}}{m_{11}a_{x_{bf}} + m_{12}a_{y_{bf}} + m_{13}a_{z_{bf}}} \right) \end{aligned} \quad (10.12)$$

with:

$$\begin{aligned} m_{11} &= \sin(\psi) \cos(\theta) \\ m_{12} &= \cos(\psi) \cos(\Phi) + \sin(\psi) \sin(\theta) \sin(\Phi) \\ m_{13} &= -\cos(\psi) \sin(\Phi) + \sin(\psi) \sin(\theta) \cos(\Phi) \\ m_{21} &= -\cos(\psi) \cos(\theta) \\ m_{22} &= \sin(\psi) \cos(\Phi) - \cos(\psi) \sin(\theta) \sin(\Phi) \\ m_{23} &= -\sin(\psi) \sin(\Phi) - \cos(\psi) \sin(\theta) \cos(\Phi) \end{aligned}$$

At this point, the vehicle slip angle denoted  $\psi_s$  can be computed using equations (10.3), (10.4), (10.5), (10.7) and (10.12).

Now, let us consider the IMU measurements,  $A_{bf}$  and  $\dot{\psi}$ , are given at a fixed sample rate denoted  $\Delta t$ . Then, under the previous assumptions, at an instant  $t$ , the vehicle trajectory, defined by  $\hat{X}_{vh}$  and  $\hat{Y}_{vh}$ , can be predicted with the algorithm 4.

Note that, algorithm 4 predicts the discrete vehicle trajectory from its current position to the one with an angular horizon of  $\pi/2$ . The term  $D_{\Delta t}$  denotes the constant traveled distance along the circular path during  $\Delta t$ . Since the vehicle motion is assumed circular, uniform and forward, it comes:

$$V_{bf} = \frac{\|A_{bf}\|}{|\dot{\psi}|} \quad (10.13)$$

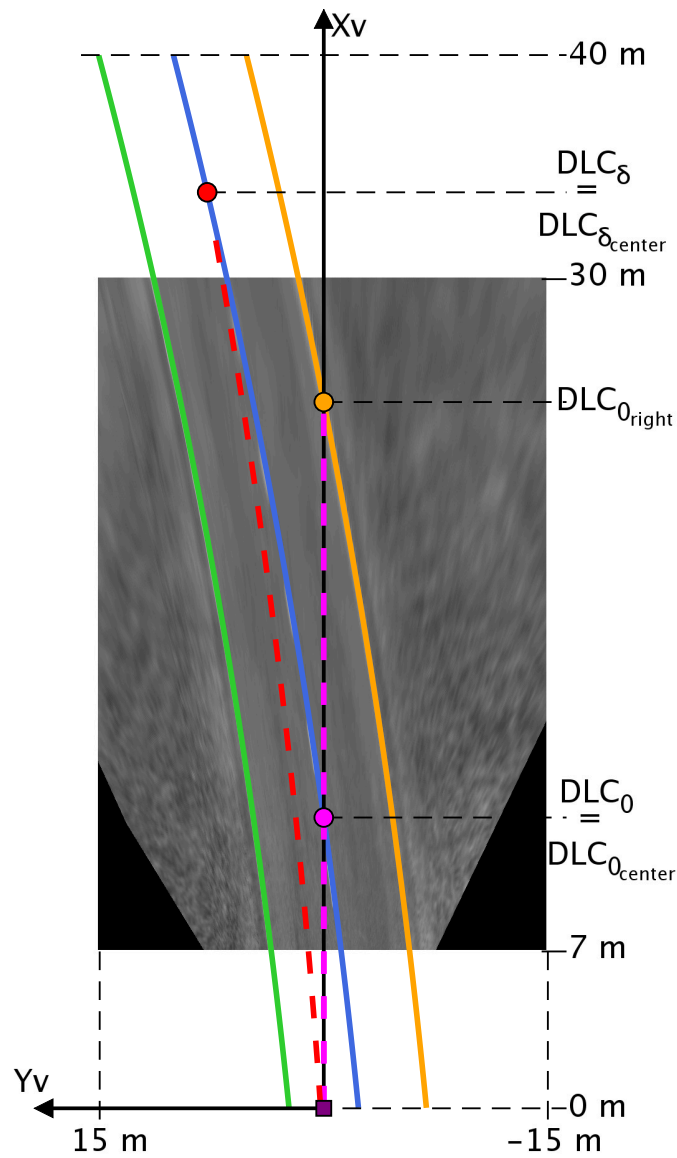


FIGURE 10.3: Road bird-eye-view with predicted vehicle trajectories and tracked LCP

Finally, in the case of non zero steering, the DLC is the numerical solution when solving the intersection between the road lane equations (10.1) and the discrete predicted trajectory given by algorithm 4 (see the red dot in figure 10.3). As for straight path, when several LCP are detected then  $DLC_{\delta} = \min(DLC_{\delta_k})$  with  $k$  a set of all LCP.

Notice that, since the longitudinal vehicle speed is available, the DLC can be trivially turned into a TLC using the equation:

$$TLC = \frac{DLC}{v_{x_{bf}}} \tag{10.14}$$

**Algorithm 4:** Motorcycle circular trajectory prediction

---

```

1: Inputs  $\psi_s, \dot{\psi}, A_{bf}, \Delta t$ 
2: Outputs  $\hat{X}_{vh}, \hat{Y}_{vh}$ 
3: Initialize  $D_{\Delta t} \leftarrow \frac{\|A_{bf}\|}{|\dot{\psi}|} \Delta t,$ 
    $\Delta\psi^1 \leftarrow -\psi_s,$ 
    $\hat{X}_{vh}^1 \leftarrow 0,$ 
    $\hat{Y}_{vh}^1 \leftarrow 0$ 
4: for  $i = 2$  to  $\frac{\pi}{2|\dot{\psi}(t)|\Delta t} + 1$  do
-
5:  $\Delta\psi^i \leftarrow \Delta\psi^{i-1} - \dot{\psi}(t)\Delta t$ 
6:  $\hat{X}_{vh}^i \leftarrow D_{\Delta t} \cos(\Delta\psi^i) + \hat{X}_{vh}^{i-1}$ 
7:  $\hat{Y}_{vh}^i \leftarrow D_{\Delta t} \sin(\Delta\psi^i) + \hat{Y}_{vh}^{i-1}$ 
8: End for

```

---

## 10.4 Simulation Results

This section discusses a validation of the proposed algorithm using the advanced motorcycle simulator *BikeSim*. Two scenarios are presented, the first one considers straight road and motorcycle trajectories with a constant relative heading deviation ( $\Delta\psi \neq 0$ ). Whereas, the second scenario deals with circular road and vehicle trajectories ( $\delta \neq 0$ ).

The hardware (camera and IMU) specifications and mountings are identical to the ones given in Damon et al., 2018a except the camera resolution which is  $1080 \times 720$ . Let us remind the ROI of the bird-eye-view is limited about 30 meters ahead of the vehicle. According to the fact that the road trajectory is slowly varying, we extended the road lane reconstruction to 40 meters that we defined as the maximum horizon for LCP tracking.

In the following simulations, we considered a two-way road separated with a dashed road marker whereas the extreme lanes are continued.

### 10.4.1 Case 1: Straight road with zero steering

In this scenario, we considered straight road markers and we simulated a constant heading deviation angle between the road lanes and the vehicle such that  $\Delta\psi = 3$  deg. In addition, the PTWV is traveling at 100 km/h without any steering action.

Figure 10.4-a and 10.4-b illustrate the simulated trajectory of the motorcycle as well as the lateral deviation with adjacent lanes (central and left one). From 0 to 75 first meters, on  $X$  axis, the PTWV reaches the first Lane Crossing Point with the central line within 3 seconds. The vehicle travels under the same conditions (DLC & TLC) the second portion, but this time between the center lane and the left one.

Figure 10.4-c gives the estimated DLC for the case of a pure longitudinal movement respectively with the central and left lanes. A comparison with the theoretical DLC, expressed by the equations 10.2, is given. It shows well the approximation of the DLC by our approach, although the resolution is not very high with a rather important speed, figure 10.4-d. Here, the average error is about 50 centimeters and decreases drastically when the LCP is approaching.

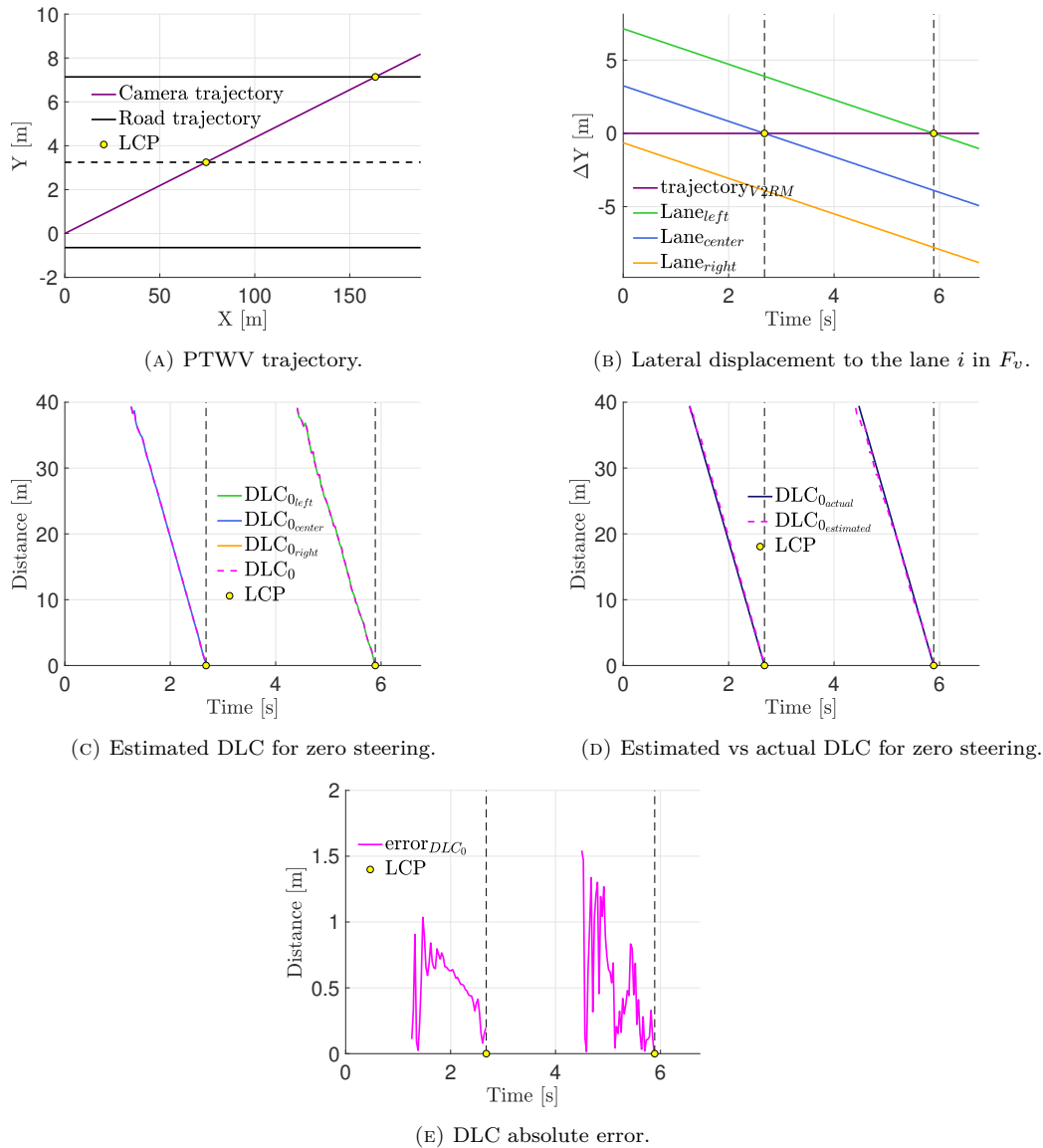


FIGURE 10.4: DLC for straight PTWV trajectory on straight road

### 10.4.2 Case 2: Curved roads with constant steering

In the next scenario, we assume bend case with curve radius 400 meters and we simulated a constant steering angle, figure 10.5-a. The longitudinal speed is fixed at 80 km/h.

In the present scenario, three LCP are detected, figure 10.5-b. The last one occurs with the right lane and the remains LCP with the center lane.

Figure 10.5-c gives the reconstructed DLC for the case of a pure lateral motion respectively with the central and right lanes. Whereas, the estimated DLC is compared to the theoretical one under a zero steering. Figure 10.5-d highlights a very good estimation of the DLC. The estimation under constant steering is depicted in figures 10.5-e and 10.5-d to show, at the same time, the performance of the proposed algorithm. Also, the average error is similar to the previous scenario and remains around 50 centimeters and decreases when the LCP is approaching, figure 10.5-g. These results are illustrated by the video at the following link : <https://youtu.be/K095a2SckWU>.

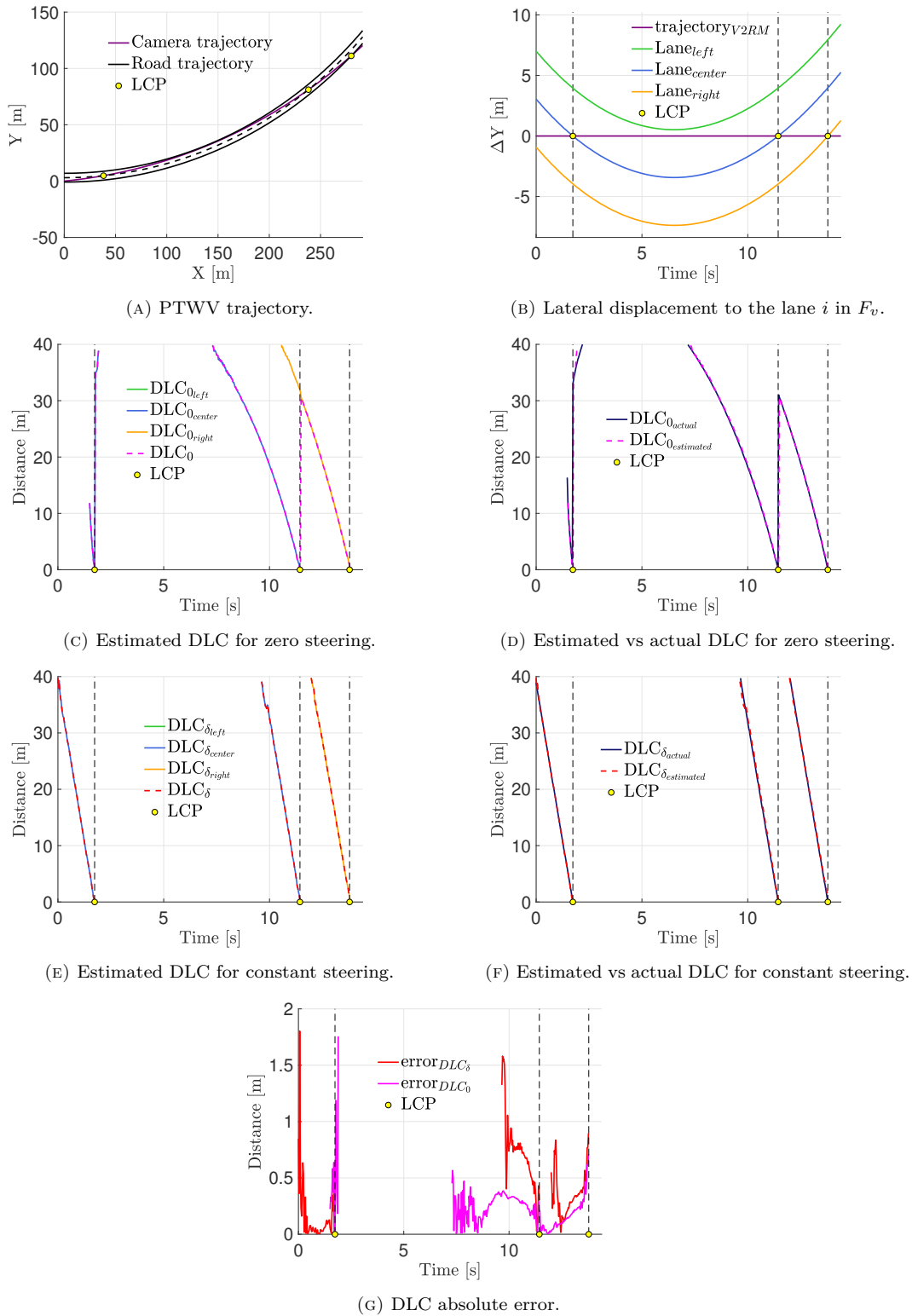


FIGURE 10.5: DLC for circular PTWV trajectory on curved road.

## 10.5 Conclusions

This work provided powerful video-based estimation algorithm for Lane Crossing Point tracking for powered two-wheeled vehicles. First we have recalled the Inverse Perspective Mapping technique, adapted to motorcycles, which allows the generation a bird-eye-view of the road markers. The advantage here is to extract

pertinent information such that the PTWV lateral displacement and heading angle to the road marker. Second, the Lane Crossing Point tracking problem is detailed. It consists of finding the intersection point coordinates between the predicted road lane and vehicle trajectories whether straight or circular. Then, the proposed algorithm is simulated towards several scenarios to show its great capabilities of tracking road lanes and compute the distance before crossing the marker. Finally, the proposed algorithm is an original contribution which allows to accurately compute, in real time, the DLC when lane change is occurring for motorcycles. This information is crucial for safety purposes like trajectory analysis.

In our future works, we plan to deal with the robustness (unfavorable camera light, undetected road markers, etc.) and to extend the algorithm to clothoid trajectories with various road curvature. We would like to take the proposed solution to the next step by integrating a risk function to create an alert system prototype. Finally, we would put all our effort into the experimental validation on our two-wheeled vehicle platform.

# General Conclusions & Perspectives

In this thesis, we are interested in the powered two-wheeled vehicle as it is among the most vulnerable road users. In fact, road traffic accident is now leading causes of violent death. The statistics analysis underline the importance of improving motorcycle safety as well as highlighting key safety concerns that new safety technologies should target. Towards this end, many research broadly seek to further investigate ITS technologies with the potential to enhance motorcycle safety. Therefore, involving riding assistance systems on this type of vehicle will bring notable benefits in terms of handling, stability and maneuverability. The main purpose of the work presented in this thesis is to contribute to the development of ARAS. The design of these systems, is a real challenge for researchers and automotive manufactures. Unlike four-wheeler vehicles, the roll motion of the PTWV plays a fundamental role in the lateral dynamics, it balances the lateral forces in turns. As a matter of fact, PTWVs are highly dynamic vehicles with a complex mechanism which gathers a set of actions, mechanical and physical phenomena during the riding task. These specifications does not allow the direct transposition of the developed cars safety systems to motorcycles. Thereby, it is very important to know how this motorcycle reacts, to design a more adequate safety systems able to transmit the good orders.

This manuscript outlines the various scientific contributions during this thesis, with the objective of developing a risk quantification through the synthesis of dynamic models and observation algorithms for the reconstruction of unmeasured variables. In this report, we have presented the context and the objective of the thesis as well as the different ways to approach the problem in order to provide estimation of the most pertinent states and parameters. In particular, a high fidelity simulator and an instrumented motorcycle are used to acquire data based on these latter, estimation schemes are achieved by designing observers. To sum up, the thesis project consists in designing and validating the proposed algorithms allowing the estimation of motorcycle states. It consists also on the study of appropriate methods to allow the estimation and identification. Throughout this research, we have targeted a particular type of scenario: cornering situations. In fact, accident studies have shown that bends are very risky for motorcycles, they noticed that motorcycles often losses control in this scenario. It is therefore one of the "typical" scenarios, for which adequate rider assistance systems could prevent the accident by alerting the rider and/or by acting on the dynamics of the PTWV via actuators.

On the basis of the existing literature, we have drawn up a generic modeling of motorcycle before adapting it to our concerns. The main objective is, in part, to develop the mathematical models of the motorcycles used in this thesis, in other parts, to validate these models. Three important steps have been identified: 1- define the complexity degree of the relevant models, 2- identify geometric and inertial parameters of the motorcycle 3- propose experiments exciting tests to identify modes of the dynamic models. Knowing that tire/ground contact play a fundamental role in the modeling and, in particular, in the study of the stability of the vehicle. The Part I of this thesis discussed the tire modeling (Chapter 2). In this part, we were also interested in deriving a complete dynamic model representing the PTWV and its rider as a set of eight bodies. The obtained model is very complex and strongly nonlinear, which is not adequate for the synthesis of the observation and control algorithms. The latter was introduced for simulations via the *BikeSim* software. Throughout this thesis, we have used *BikeSim* as a high-fidelity validation tool. After that, we have simplified the eight-body model, to derive a two-body Linear Parameter Varying Model (LPV) of the lateral dynamics and a one-body model of the longitudinal and lateral dynamics. In this modeling

phase, the main difficulty lies in the choice of the "precision" of the model. In other words, how much the mathematical model can be simplified while keeping a real dynamic representation? In our case, the model is simplified by reducing the number of bodies or by setting some simplifying assumptions. With regard to this modeling part, we have mostly used two types of state space models according to the expected fineness: firstly, the single-body model, also called inverted pendulum, which we have augmented with a linear model of the forces to validate identification and estimation algorithms. Then we studied an extended model, which is the two-body model according to our requirements. The validation of these models was handled in several phases, the first being to identify the pertinent parameters of each model. Afterwards, we selected the exciting maneuvers. In practice, even though we use a simplified two-body model of PTWV, it has more than 30 parameters. The proposed methods within Part II of this thesis are as follows:

- First, we considered the identification of the rigid body motorcycle model (chapter 3). Three design methods are studied in this chapter to identify the center of gravity (CoG) position and estimate motorcycle inertial and geometric parameters: using static test, an algebraic identification approach compared to an iterative gradient descent algorithm.
- Second, we focused on the identification of a mathematical two-bodies model of a two-wheeled vehicle (chapter 4). Concerning the Sharp model, two methods were proposed to identify a combined parameters of the motorcycle model. The first method was a cascade, multiple-objective optimization algorithm adapted to the complexity of our model. The second design process was a Levenberg-Marquardt identifier. This last method identified combined expression of inertial parameters, predicted the objective functions and improved convergence characteristics for state by updating coupled inertial parameters.

Identified models have been validated, through some riding scenarios with the Kawasaki ER6N motorcycle, the Scooter or even *BikeSim* simulator. Although these techniques have shown real potential for achieving some goals of this thesis, they may present some disadvantages to consider. The parameter identification problem requires persistence of excitation to reach an optimal solution. However, in practice, excitation signals can not be freely applied due to the motorcycle instability characteristics. Usually, identification is performed offline where online identification lays with some challenges. Furthermore, the identification problem is formulated assuming that all the system states are measured, which is really unrealistic. In this case, a reformulation of the identification problem is ineluctable. Alternative approaches suggest the use of observers based identifier to deal with both dynamics states and parameters estimation. These included the introduction of LPV adaptive observers or a novel method for unknown input observer with time delay concept. The proposed methods allow simultaneous on-line parametric identification and dynamic system estimation. They therefore prove to be perfectly suited to applications for PTWV, especially when we know that some of the parameters of the model are non-constant over time. All these arguments motivated the reorientation of the identification tools to model based observer methods to answer the issues of this thesis.

On the dynamic state reconstruction part III, we have implemented several new estimation approaches to reconstruct dynamic states of the motorcycle that can not be measured with physical sensors. With regards to the observer, the main concern is to develop techniques with good compromise permanence/robustness and simplicity for the sake of implementation. To ensure a good performance, we developed several estimation methods with different principles, in particular, we proposed two categories one of them deals only with observers for states dynamic estimation and the second one is more intuitive for observer based identifier to simultaneously estimate the model states and the parameters identification from measured data. The designed observers presented in the present manuscript are:

- Unknown Input Observer (UIO) which is proposed to estimate the pertinent dynamics with road geometry consideration and steering dynamics reconstruction.
- Interconnected Fuzzy Observer (IFO) which is a two sub-observer for estimating both lateral and longitudinal dynamics of the two wheeler.
- LPV Luenberger Adaptive Observer (LAO), for which we have suggested a different formulation based on a general Lipschitz condition and Lyapunov theory to estimate the PTWV dynamic states and then the tires' cornering stiffness identification from the adaptive law, which is compared to a direct estimation method and a dynamic inversion estimation scheme.

- Delayed Unknown Input Observer (DUIO) which is likely an extension of the well-known UIO for nonlinear system with mismatched condition, that we have proposed based on delay concept to define auxiliary outputs to fulfill the matching condition.

We have brought some new points of view concerning their formulations and therefore their application to ensure the desired performance by taking into account the forward speed as a varying parameter in the design procedure. We have considered several tests to validate the synthesized methods. Compared with some other works in the literature, the discussed algorithms have been developed with very clear objectives: to take into account realistic hypotheses during the synthesis of the observers and to propose a realistic validation on experimental data or on the *BikeSim* simulator. In addition, we have drawn up a table of comparison, between the proposed estimations methods to show the advantages and the drawbacks of each one. This table allows the selection of the adequate method for a given requirement and conditions. The estimation results are very promising even if they do not yet take into account the parametric uncertainties or the measurement noises in the synthesis design. Indeed, we studied robustness propriety related to noisy measurement and parameter variation. Nevertheless, it is obvious that a consideration of parameters uncertainties during the observer synthesis is necessary in order to face industrial applications. Furthermore, these designs require a set of sensors necessary to ensure observability conditions. Nonetheless, these sensors pose significant integration problems with respect to alignment, lack of space, etc. In fact, inertial sensors are strongly affected by mounting angles, and the correct rotation to be applied in order to recover an alignment to the vehicle motion. In the context of this work, we proposed an algorithm for self calibration to align data, the approach is tested and validated on another instrumented vehicle. The algorithm estimates the three mounting angles (roll, pitch, and yaw) of accelerometers and gyroscopes within Inertial Measurement Units. Such a self-calibration method is focused for telematic boxes (e-Boxes) installed on two-wheeled vehicles, whose IMUs' axes often result not to be aligned with the vehicle reference system. In this work we proposed an energy-efficient alignment procedure which limits the use of geolocation data. The aspects of data selection and real-time implementation of our method are taken particularly into account. The proposed approach is validated and its performance are analyzed on experimental data collected with tests performed with a motorcycle equipped with three e-Boxes mounted in different positions and orientations. The analysis of the real measured driving data proves the effectiveness of the approach in aligning the sensors' axes in all three directions.

The main element of the riding aid safety systems is the risk indicator and the warning algorithm that allows the two-wheeler vehicle to travel safely. Part IV aims to identify objective indicators for the quantification of risk as well as carry out and discuss the design of possible warning system for riders of PTW vehicles. Hence, the proposed indicators are studied in two chapters and mainly deal with the preventive safety considerations in order to assist the rider through warning system by detecting and/or generating alerts. In this scope, we described two approaches in order to detect risky riding situations and warn the rider to correct his trajectory. This solution is divided on two chapters:

- Neutral-path departure (NPD) algorithm, for which we have presented a detection approach towards getting circular stationary states and analytical handling conditions. Based on Self Steering Gradient proposed as a risk function, this NPD algorithm aims to characterize the motorcycle steering behavior: over or under-steering situations.
- Lane crossing prediction (LCP) which aimed to predict, with a simple perception system, the time and distance to lane crossing (TLC, DLC) in order to predict critical situations. Then, the proposed algorithm shows its great capabilities of tracking road lanes and compute the distance before crossing the road marker.

In this part, we proposed a synthesis of a new risk functions for the characterization of rider steering behavior. This design requires a precise knowledge of the various dynamic states and parameters of the motorcycle as well as the external effort acquired either from measurement, estimation or identification techniques. The main problem in building up warning systems for motorcycle is the design a driving risk function to warn the rider in assistive systems. The distance to line crossing DLC and time to line crossing TLC seem to play an important role as an indicator of steering performance, indicates that drivers can compensate for some errors of steering by decreasing their speed in order to maintain the TLC constant. These detection methods were tested in co-simulation using *BikeSim*<sup>©</sup> under different steering maneuvers. The results highlight the effectiveness of the proposed algorithm to detect in an early stage the over/under steering deviation from

the neutral path, or to predict the distance to edge crossing in order to improve motorcycle handling and correct the unsafe maneuver. During this thesis, we tried to put as much emphasis as possible on validation, hoping one day to see industrial use of these techniques. We are aware that this is only a first step of a long way. Nevertheless, the first validation results are very promising and the techniques presented clearly deserve to be further developed.

## Perspectives

To end up this manuscript, we would like to recall some of the perspectives and improvements we would like to bring in the future.

### Estimations and Identification:

- The analysis of stability, performance and robustness can be extended by considering other uncertainties such as the neglected dynamics. The observer will have to take into account, simultaneously, the parametric uncertainties of the model, the sensor biases and the measurement noises.
- The synthesis of robust observer, regarding measurement noises and/or uncertainties, includes to consider a linear term containing perturbations in the observation equation. This leads to an adaptation of the model-based observers to the case of uncertain matrices of the state space model.
- It would be very interesting to discuss the performance quantification and define a tolerance margins of parameters for which the estimation results remain acceptable.
- Moreover, IFO and DUIO have only been validated on *BikeSim*. It is therefore necessary to continue with validation on the laboratory platforms as for the UIO and LAO. It would also be interesting to diversify the scenarios and driving behaviors. In addition, the presented risk function have been only tested on BS. Once again, it is essential to extend the validation in case of non-constant turns and to continue with experimental tests.
- An alternative for calibration steps is the modeling transformation to the sensor reference frame. Indeed, when one is interested in the rewriting of the modeling expressions in the new sensor reference frame and not in the vehicle reference, this transformation add many non-linearities in the motorcycle model, and in particular, non-linearities appear in the the measurement equation, this leads to a new observer design taking the measurement matrix in the LPV observer design.

### Vision based approach:

Vision-based estimators have shown great potential in previous work (Damon, 2018) to estimate the position of the PTWV on the road. In future work, we would also like to combine the contributions presented in model-based estimation part with the vision-based approaches in order to obtain a unique algorithm capable of estimating the pertinent states and parameters as well as predicting the position of the PTWV, and the geometry of the road in order to characterize the steering behavior, alerting the rider and/or calculate the control orders in the case of active safety system.

### Trajectory generation:

We plan to design “safe” trajectory, the adoption of such a practice by PTW riders would improve their safety. Training that focuses on a safer riding style would also allow riders to be more aware of their own real handling ability and the breaking limits of their PTWs. The objective is then the reconstruction of reference trajectory which is the optimal path that a rider must follow to travel round corners safely and quickly. For that, the geometric model (imaginary racing line) can be a good solution to define a safety zone for cornering. The so-called “safe” trajectory is divided into four successive zones: 1)- Entry: where turning begins. 2)- Apex (discovery): where the motorcycle reaches the furthest point on the inside of the turn. 3)- Exit: where the motorcycle is in the end of the corner, and 4)- stability: where the motorcycle is driving straight again. For every bend (both left and right), it is possible to progressively read that bend and anticipate dangers and potential hazards. The core idea is to ride towards the bend tangent point only when one has “seen” the whole of the bend, up to its exit. Based on these recommendations, the rider must

---

makes use of the entire width of the track, entering at the outside edge, touching the "apex"-a point on the inside edge, then exiting the turn by returning outside, while maintaining a constant radius throughout from turn-in all the way to the exit point. With regard this description, one can draw up a mathematical model depending on the geometric characterization of the bend. To sum up, this safe trajectory allows riders to change from their current riding style (one where the rider adopts a more prone position on the bike, looking only a short distance ahead) to one that is less extreme (with a more upright posture, head erect and eyes looking as far ahead as possible). Taking the "reference" trajectories as a function of their beliefs, we plan to develop tools that will objectively rate the achieved performances (i.e., by measuring the deviation from the reference).

### **Rider state evaluation:**

Vulnerability of motorcycle riders is a leading cause of road accident death due to the static and dynamic instabilities of a PTWV, which require that the rider performs constantly a highly controlled tasks. One of the main challenges in motorcyclist safety is the rider state evaluation, which strongly depends on the individual abilities and the limits of riders skills. These evaluation offered the opportunity to analyze potentially critical situations in typical riding scenario involving rider posture. To improve the riders' skill level and reduce riding errors, safety trainings are the best way to enhance riding behavior. The idea is to give motorcycle riders useful feedback about their individual riding skills and about the occurrence of critical situations while riding in real time and thus support self-improvement. The key requirement for such an application is a procedure to capture the rider posture via reliable sensors and then to detect certain behaviors as indicators for riding errors. For this purpose, our perspectives is to use wireless inertial sensors, which are a well established solution to capture rider motion to estimate the rider skill in a variety of different traffic situations. Such wireless systems are designed to interact with the human motion and allow free body movement. Furthermore, analysis of motion tracking technologies can be an alternative to gold standard optical motion tracking and integration possibilities. Our near perspective is therefore to use Xsens MTw wireless technology to collect the motions of a motorcycle-rider wearing a motion-capture suit under the inertial sensor-based wireless network environment.

# Appendices



# Appendix A

## Definitions of observability and detectability

The simultaneous state and parameter reconstruction problem is closely linked to the problem of observability, as shown in Zhang and Zhu, 2018. Therefore, we recall some important definitions about strong observability and strong detectability of systems with unknown parameters.

Consider the following system with  $x(t)$  is the state vector,  $u(t)$  is the known inputs vector,  $\theta$  the unknown parameters vector and  $y(t)$  is the measurements vector:

$$\begin{cases} \dot{x}(t) &= f(x(t), u(t), \theta) \\ y(t) &= h(x(t), u(t), \theta) \end{cases} \quad (\text{A.1})$$

**Definition A.1.** (Moreno, Rocha-Cózatl, and Wouwer, 2014)

For every initial condition  $x(0)$ , any known input  $u(t)$  and any couple of unknown parameters  $(\theta, \bar{\theta})$ , the system (A.1) with two different trajectories  $x(t)$  and  $\bar{x}(t)$  is called:

- *state and unknown parameters strongly observable*: if  $y(t, x(t), u(t), \theta) = y(t, \bar{x}(t), u(t), \bar{\theta})$  implies that:  $x(t) = \bar{x}(t)$  and  $\theta = \bar{\theta}$ .
- *state and unknown parameters strongly detectable*: if  $y(t, x(t), u(t), \theta) = y(t, \bar{x}(t), u(t), \bar{\theta})$  implies that:  $x(t) \rightarrow \bar{x}(t)$  and  $\theta \rightarrow \bar{\theta}$  as  $t \rightarrow \infty$ .

Definition A.1 concerns the state and parameters observability or detectability. The unknown parameters observability (detectability) relates to the possibility of reconstruct the unknown part asymptotically having as information the known inputs and outputs.

Theoretical analysis of LPV system properties (stability, controllability, observability), often falls into the framework of LTV systems or of nonlinear ones. In the following, we will present the most important system properties definitions for LTI, LTV and LPV systems.

### A.0.1 LTI system properties

First, we recall some important definitions about strong observability and strong detectability of linear systems.

$$\dot{x}(t) = \tilde{A}x(t) + \tilde{B}u(t) + \tilde{D}F(t) \quad y(t) = \tilde{C}x(t) \quad (\text{A.2})$$

where the matrices  $\tilde{A}, \tilde{B}, \tilde{C}$  are constant of compatible dimensions.

**Definition A.2.** (Trentelman, Stoorvogel, and Hautus, 2012). System  $(\tilde{A}, \tilde{D}, \tilde{C})$  is called strongly observable if for any initial state  $x_0$  and any unknown input  $F$ ,  $y(t) \equiv 0$  for all  $t \geq 0$  implies that also  $x \equiv 0$ . Otherwise,

the system  $(\tilde{A}, \tilde{D}, \tilde{C})$  is called strongly detectable, if for any  $F$  and  $x(0)$ ,  $y(t) = 0$  for all  $t \geq 0$  implies that  $x \rightarrow 0$  as  $t \rightarrow \infty$ .

**Definition A.3.** (Strong detectability condition). Let  $s_0 \in \mathbf{C}$  be the invariant zero of the triplet  $(\tilde{A}, \tilde{D}, \tilde{C})$ , or, equivalently, the system  $(\tilde{A}, \tilde{D}, \tilde{C})$  is in the open left-hand complex plan  $s \in \mathbf{C}$  with  $\text{Re}(s) < 0$ , if:

$$\text{rank}(R(s_0)) < n + \text{rank}(\tilde{D}) = n + p$$

where,  $R(s)$  is the Rosenbrock matrix of system :

$$R_{(\tilde{A}, \tilde{D}, \tilde{C})}(s) = \text{rank} \left( \begin{bmatrix} sI_n - \tilde{A} & -\tilde{D} \\ \tilde{C} & 0 \end{bmatrix} \right)$$

## A.0.2 LTV/LPV system properties

Consider the time-varying system

$$\dot{x}(t) = \tilde{A}(t)x(t) + \tilde{B}(t)u(t) \quad y(t) = \tilde{C}(t)x(t) \quad (\text{A.3})$$

where  $x(t_0)$  is given, and the matrices  $\tilde{A}, \tilde{B}, \tilde{C}$  are of compatible dimensions and with bounded entries.

As far as the observability of LPV systems is concerned, the following theorem, borrowed from (Sename, Gaspar, and Bokor, 2013) and (Silverman and Meadows, 1967) are considered to study on observability for Linear Time-Varying Systems (LTV) which characterize also the observability of LPV systems. The following definitions introduce the concepts of observability Gramian and uniform complete observability for systems with bounded realizations (Kalman, 1960; Silverman and Meadows, 1967).

**Definition A.4.** (Observability Gramian). The observability Gramian associated with the system  $(\tilde{A}(t), \tilde{D}(t), \tilde{C}(t))$  on  $[t_0; t_f]$  is defined as

$$\mathbf{W}_o(t_0, t_f) = \int_{t_0}^{t_f} \Phi(t, t_0)^T \tilde{C}^T(t) \tilde{C}(t) \Phi(t, t_0) dt$$

where  $\Phi(t, t_0)$  is the state transition matrix associated with  $\tilde{A}(t)$  from  $t_0$  to  $t$ .

**Definition A.5.** (Uniform complete observability). The matrices  $(\tilde{A}(t), \tilde{D}(t), \tilde{C}(t))$  of the system in (A.3) is uniformly completely observable (UCO) if there exist positive constants  $\alpha > 0$  and  $\delta > 0$  such that, for all  $t \geq t_0$

$$\alpha_o \mathbf{I} < \mathbf{W}_o(t, t + \delta)$$

The LTV system (A.3) is observable on  $[t_0, t_f]$  if and only if the observability Gramian  $\mathbf{W}_o(t_0, t_f)$  is invertible. The following theorem corresponds to an alternative well known result on observability that does not require the computation of the observability Gramian.

**Theorem A.1.** Batista et al., 2017. Suppose that  $q$  is a positive integer such that, for all  $t \geq t_0$ ,  $\tilde{C}(t)$  is a  $q$  times continuously differentiable matrix and  $\tilde{A}(t)$  is  $(q - 1)$  times continuously differentiable matrix. Define

$$\mathcal{L}(t) = \begin{bmatrix} L_0(t) \\ \vdots \\ L_q(t) \end{bmatrix} \quad (\text{A.4})$$

Where

$$\begin{cases} L_0(t) &= \tilde{C}(t) \\ L_i(t) &= L_{i-1}(t)A(t) + \dot{L}_{i-1}(t), i = 1, \dots, q. \end{cases} \quad (\text{A.5})$$

Then, the linear system (A.3) is observable on  $[t_0, t_f]$  if, for some  $t_a \in [t_0, t_f]$ ,  $\text{rank } \mathcal{L}(t) = n$ .

For uniform complete observability of a LTV system with bounded realization, we will consider the following "folk" result, related to this Theorem.

**Theorem A.2.** *Batista et al., 2017. The bounded LTV system (A.3) is Uniformly Completely Observable if there exists a positive constant  $\alpha > 0$  and an integer  $q \in \mathcal{N}$  such that, for all  $t \geq t_0$ ,*

$$\mathbf{L}(t)^T \mathbf{L}(t) \geq \alpha \mathbf{I} \tag{A.6}$$

with  $\mathbf{L}(t) \in \mathcal{R}^{w \times n}$ ,  $w \geq n$ .

# Appendix B

## Motivating example of DUIO

In this section, an example is proposed to illustrate the estimation performance of DUIO observer. Consider the following matrices for system (6.1):

$$\bar{A} = \begin{bmatrix} -30 & 12 & -20 \\ -50 & -13 & 0 \\ 10 & 2 & -14 \end{bmatrix}, \bar{B} = \begin{bmatrix} 1.5 \\ 0 \\ 2 \end{bmatrix}, \bar{C} = \begin{bmatrix} 1 & 0 & 0 \\ 0 & 1 & -2 \end{bmatrix}, \bar{D}_{\bar{y}} = \begin{bmatrix} y_2 & 0 & 0 \\ 0 & 0 & y_1 \\ 0 & y_1 & y_2 \end{bmatrix}, \theta = \begin{bmatrix} \theta_1 \\ \theta_2 \\ \theta_3 \end{bmatrix}$$

For this given example, it is easy to verify that observer existence rank conditions is not fulfilled for the original system:  $\text{rank}(\bar{C}\bar{D}_{\bar{y}}) = 2 \neq \text{rank}(\bar{D}_{\bar{y}}) = 3, \forall (y_1, y_2) \neq (0, 0)$ .

It means the output vector is less than the unknown parameters:  $(n_{\bar{y}}, n_{\theta}) = (2, 3)$ .

The original system is augmented with  $m = 1$  delay in equation (6.9). Taking time delay  $\tau_m$  leads to  $\dim(y = [\bar{y}, \bar{y}_{\tau_m}]) = 4 > \dim(\theta) = 3$ . One get:  $C_y = [\bar{C}, 0; 0, \bar{C}]$ ,  $D_y = [\bar{D}_{\bar{y}}; \bar{D}_{\bar{y}_{\tau_m}}]$ . Therefore, the rank condition is fulfilled:  $\text{rank}(CD_y) = \text{rank}(D_y) = 3$ . The design of the DUIO observer has been achieved by considering the optimization problem under LMI constraints. Thus, the solution of theorem (6.21) is computed by using the procedure Yalmip-Sedumi Toolbox Löfberg, 2004. Since asymptotic convergence, unknown parameters are estimated from model inversion (6.26) assuming that all the states are available (either measurable or estimated). The initial condition are:  $\hat{x}_0 = \hat{x}_{\tau_{m_0}} = [0, 0, 0]^T$ ,  $\hat{x}_0 = \hat{x}_{\tau_{m_0}} = [0.75, -3, 0.15]^T$ ,  $\tau_m = 0.5(\text{sec})$ .

### B.0.1 The noise-free case

The first case is studied to illustrate the estimation performance and to corroborate the theoretical results obtained through the convergence analysis carried in the above sections. In this case, the input vector  $u(t)$ , state estimation error  $\tilde{x}(t)$  and the convergence of the estimated parameters, compared to nominal values are presented in Fig.B.1. the variations noted in the proximity of the time origin are due to the initial conditions of the observer which have been arbitrarily chosen. Fig. B.2 compares the states reconstructed by the DUIO observer with the corresponding states of system. The observer states starts from the initial condition and converge to the system state, the quality of the reconstruction is highlighted under  $RMS = \sqrt{\frac{\sum_{i=1}^n (x(i) - \hat{x}(i))^2}{n}}$  and  $MSE = \text{mean}(\sum_{i=1}^n (x(i) - \hat{x}(i))^2)$  to illustrate the convergence in the estimated states. The simulation results show that, the DUIO observer rapidly and accurately estimates the state of the model even if initial conditions are not the same. Moreover, parameters estimations lead to a peaking phenomenon in which initial estimator error can be prohibitively large, then, these parameters converge to true value after peaking has subsided. As a consequence, with small initial conditions, observer converge quickly to brings the estimated state's error to zero in small time.

### B.0.2 The noisy outputs case

During the design process of the observer, no perturbation was considered. In order to simulate practical situations, one considers the system affected by noise to test the robustness of the estimation approach. The

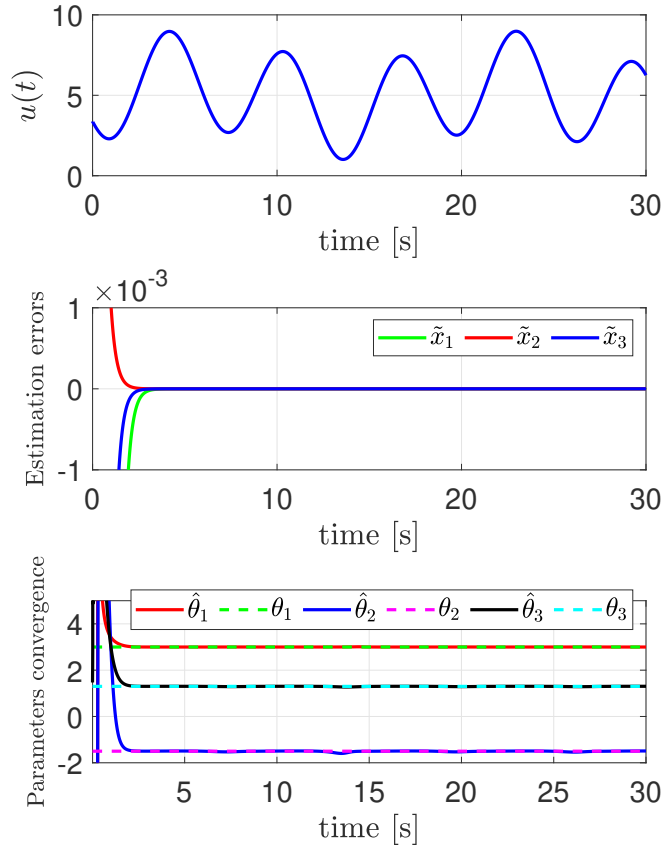


FIGURE B.1: Input-Estimation Errors- Parameters convergence. The convergence is compared with  $RMS = (0.0731, 0.2165, 0.0150)$ ,  $MSE = (0.0053, 0.047, 2.236 \cdot 10^{-4})$ .

outputs issued from the simulation of system are corrupted by additive noise bounded by a ratio around of 5%. Figure (B.3) shows the error in the estimated state, and the parameters convergence, both figures exhibit noisy case. Notice that the unknown parameters in figure B.3 are estimated with a good way even if we considered perturbed measures. One can remove the noise effect in parameters with a simple low-pass filter. Simulation result, shows that the DUIO observer is robust enough to handle the noisy case.

Summarizing this section, the estimation approach gives a solution even if the decoupling matrix is not of full rank in the original system. It can be appreciated that the observer performs as expected and the state errors reach zero asymptotically. This result proves the reliability of the approach to reconstruct unmeasured states and identify the unknown parameters.

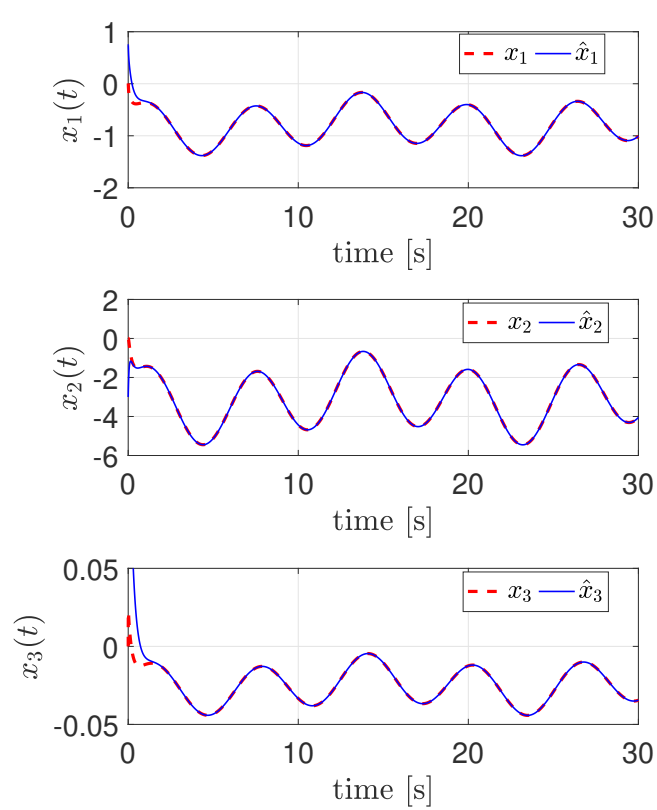


FIGURE B.2: State Estimation: Actual state (red) their estimates (blue)

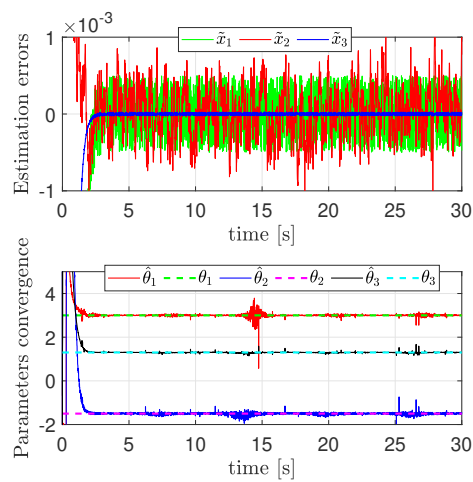


FIGURE B.3: The noise-corrupted case

# Appendix C

## Numerical Values of the PTWV

The parameters expressions for the identification algorithm of the two-bodies model are listed in table C.1:

TABLE C.1: Parameters expressions and numerical values

Parameters $\theta_i$
$\theta_1 = m_f k$ , $\theta_2 = m_f e$ $\theta_3 = m_f k^2 + I_{rz} + I_{fx} \sin^2 \epsilon + I_{fz} \cos^2 \epsilon$ , $\theta_4 = m_f j k - C_{rxz} + (I_{fz} - I_{fx}) \sin \epsilon \cos \epsilon$ $\theta_5 = m_f e k + I_{fz} \cos \epsilon$ , $\theta_6 = \frac{i_{fy}}{R_f} + \frac{i_{ry}}{R_r}$ , $\theta_7 = \frac{i_{fy}}{R_f} \sin \epsilon$ $\theta_8 = m_f j^2 + m_r h^2 + I_{rx} + I_{fx} \cos^2 \epsilon + I_{fz} \sin^2 \epsilon$ , $\theta_9 = m_f e j + I_{fz} \sin \epsilon$ $\theta_{10} = -(m_f j + m_r h + \frac{i_{fy}}{R_f} + \frac{i_{ry}}{R_r})$ , $\theta_{11} = -\frac{i_{fy}}{R_f} \cos \epsilon$ , $\theta_{12} = m_f e g - \eta Z_f$ $\theta_{13} = I_{fz} + m_f e^2$ , $\theta_{14} = -(m_f e + \frac{i_{fy}}{R_f} \sin \epsilon)$ , $\theta_{15} = -K$
Numerical values of the physical parameters deduced from $\theta$
$l = 1.3m$ , $m_f = 16kg$ , $m_r = 190kg$ , $m = m_f + m_r$ $K = 11.7332N.s/rad$ , $g = 9.81m/s^2$ $I_{fz} = 0.200kg/m^2$ , $i_{fy} = 0.4000kg/m^2$ , $i_{ry} = 0.4608kg/m^2$ $a = 0.949m$ , $e = 0.0079m$ , $f = -0.1527m$ , $h = 0.509m$ , $R_f = 0.2m$ , $R_r = 0.2m$ , $\eta = 0.08m$ , $\epsilon = 0.4363rad$ $k = 0.9168$ , $j = 0.2589$ $l_r = 0.35m$ , $l_f = 0.95m$ , $e = l_f + l_r$ , $Z_f = -491.25$ , $C_{f1} = 18592$ , $C_{f2} = 1195.2$ , $C_{r1} = 19209.58$ , $C_{r2} = 960.48$ $\sigma_f = 0.2$ , $\sigma_r = 0.2$

## Matrices expressions and BS numerical value for the two body-model

This section presents the numerical data of matrices and vectors of the state space representation used for the design of model-based observers.

TABLE C.2: Matrices expressions

$e_{ij} = e_{ji}$	
$e_{11} = 1$	$e_{22} = 1$
$e_{33} = m$	$e_{34} = m_f k$
$e_{35} = m_f j + m_r h$	$e_{36} = m_f e$
$e_{44} = m_f k^2 + I_{rz} + I_{fx} \sin^2 \epsilon + I_{fz} \cos^2 \epsilon$	
$e_{45} = m_f j k - C_{rxz} + (I_{fz} - I_{fx}) \sin \epsilon \cos \epsilon$	
$e_{46} = m_f e k + I_{fz} \cos \epsilon$	
$e_{55} = m_f j^2 + m_r h^2 + I_{rx} + I_{fx} \cos^2 \epsilon + I_{fz} \sin^2 \epsilon$	
$e_{56} = m_f e j + I_{fz} \sin \epsilon$	
$e_{66} = I_{fz} + m_f e^2$	
$e_{77} = 1$	$e_{88} = 1$
$a_{34} = -m v_x$	$a_{44} = -m_f k v_x$
$a_{45} = \left( \frac{i_{fy}}{R_f} + \frac{i_{ry}}{R_r} \right) v_x$	$a_{46} = \frac{i_{fy}}{R_f} \sin \epsilon v_x$
$a_{47} = l_f$	$a_{48} = -l_r$
$a_{51} = (m_f j + m_r h) g$	$a_{52} = m_f e g - \eta Z_f$
$a_{54} = - \left( m_f j + m_r h + \frac{i_{fy}}{R_f} + \frac{i_{ry}}{R_r} \right) v_x$	
$a_{56} = - \frac{i_{fy}}{R_f} \cos \epsilon v_x$	
$a_{61} = m_f e g - \eta Z_f$	$a_{62} = (m_f e g - \eta Z_f) \sin \epsilon$
$a_{64} = - \left( m_f e + \frac{i_{fy}}{R_f} \sin \epsilon \right) v_x$	
$a_{65} = \frac{i_{fy}}{R_f} \cos \epsilon v_x$	$a_{66} = -K$
$a_{67} = -\eta$	$a_{71} = \frac{C_{f2}}{\sigma_f} v_x$
$a_{72} = \frac{1}{\sigma_f} (C_{f1} \cos \epsilon + C_{f2} \sin \epsilon) v_x$	
$a_{73} = - \frac{C_{f1}}{\sigma_f}$	$a_{74} = - \frac{C_{f1}}{\sigma_f} l_f$
$a_{76} = \frac{C_{f1}}{\sigma_f} \eta$	$a_{77} = - \frac{1}{\sigma_f} v_x$
$a_{81} = \frac{C_{r2}}{\sigma_r} v_x$	$a_{83} = - \frac{C_{r1}}{\sigma_r}$
$a_{84} = \frac{C_{r1}}{\sigma_r} l_r$	$a_{88} = - \frac{1}{\sigma_r} v_x$
$B_6 = 1$	

TABLE C.3: Motorcycle parameters and numerical values

Numerical values for BikeSim
$e_{33} = 250$ , $e_{34} = 11.32$ , $e_{35} = 108.65$ , $e_{36} = 0.1765$ , $e_{44} = 23.73$ , $e_{45} = 3.97$ , $e_{46} = 0.66$ , $e_{55} = 66.02$ , $e_{56} = 0.183$ , $e_{66} = 0.614$ , $a_{34} = -250v_x$ , $a_{44} = -11.25v_x$ , $a_{45} = -3.665v_x$ , $a_{46} = 0.682v_x$ , $a_{47} = 0.856$ , $a_{48} = -0.624$ , $a_{51} = 1681$ , $a_{52} = 42.34$ , $a_{54} = -175.048v_x$ , $a_{56} = -1.4622v_x$ , $a_{61} = 62.34$ , $a_{62} = 69.45$ , $a_{64} = -1.8685v_x$ , $a_{65} = 1.47v_x$ , $a_{66} = -12.67$ , $a_{67} = -0.0894$ , $a_{710} = -5319v_x$ , $a_{720} = 104503v_x$ , $a_{730} = -112430$ , $a_{740} = -84997$ , $a_{760} = 10051$ , $a_{770} = -5v_x$ , $a_{810} = 3221.8v_x$ , $a_{830} = -100890$ , $a_{840} = 79098v_x$ , $a_{880} = -5v_x$ , $C_{f10} = 22408$ , $C_{f20} = -1056.4$ , $C_{r10} = 17657$ , $C_{r20} = -518.4$
Numerical values for scooter
$e_{33} = 221$ , $C_d = 0.19$ , $e_{34} = 6.97$ , $e_{35} = 92.386$ , $e_{36} = 0.126$ , $e_{44} = 24.73$ , $e_{45} = 5.0518$ , $e_{46} = 0.492$ , $e_{55} = 68.045$ , $e_{56} = 0.137$ , $e_{66} = 0.543$ , $a_{34} = -221$ , $a_{44} = -14.64v_x$ , $a_{45} = -3.87v_x$ , $a_{46} = 0.679v_x$ , $a_{47} = 0.95$ , $a_{48} = -0.42$ , $a_{51} = 1545$ , $a_{52} = 40.53$ , $a_{54} = 161.4v_x$ , $a_{56} = 1.567v_x$ , $a_{61} = 52.83$ , $a_{62} = 66.53$ , $a_{64} = -0.976v_x$ , $a_{65} = -1.525v_x$ , $a_{66} = -12.67$ , $a_{67} = -0.0489$ , $a_{71} = -5282v_x$ , $a_{72} = 104503v_x$ , $a_{73} = -112042$ , $a_{74} = -70644$ , $a_{76} = 10481$ , $a_{77} = -5v_x$ , $a_{81} = -2592v_x$ , $a_{83} = -98283$ , $a_{84} = 77078v_x$ , $a_{88} = -5v_x$

# Bibliography

- A Hamzah S Solah, N. F. Paiman (2018). “Motorcycles ?keep left? order: Is it viable?” In: *Vehicle Safety and Biomechanics Research Centre, Malaysian Institute of Road Safety Research, Malaysia*.
- Alam, Muhammad, Joaquim Ferreira, and José Fonseca (2016). “Introduction to intelligent transportation systems”. In: *Intelligent Transportation Systems*. Springer, pp. 1–17.
- ANR, Projects (2014). *Design of motorcycle training modules including simulation to the development of cognitive skills ? SIM2CO+*. <https://anr.fr/Project-ANR-10-VPTT-0005>.
- Arioui, Hichem, Pierre-Marie Damon, and Majda Fouka (2017). “Identification de Paramètres et Estimation des Etats dynamiques des véhicules à deux roues motorisés (V2RM)”. PhD thesis. Université d’Evry-Val-d’Essonne-IBISC Lab.
- (2019). “Quantification de risque pour les véhicules a deux-roues motorisés (V2RM): Aspects d’Estimation & de Perception”. PhD thesis. Université d’Evry-Val-d’Essonne-IBISC Lab.
- Bakker, Egbert, Lars Nyborg, and Hans B Pacejka (1987). *Tyre modelling for use in vehicle dynamics studies*. Tech. rep. SAE Technical Paper.
- Baronti, F et al. (2013). “Parameter identification of Li-Po batteries in electric vehicles: A comparative study”. In: *Industrial Electronics (ISIE), 2013 IEEE International Symposium on*. IEEE, pp. 1–7.
- Bartoli, Nathalie and Pierre Del Moral (2001). *Simulation et algorithmes stochastiques: une introduction avec applications*. Cépaduès-éd.
- Batista, Pedro et al. (2017). “Relaxed conditions for uniform complete observability and controllability of LTV systems with bounded realizations”. In: *IFAC-PapersOnLine* 50.1, pp. 3598–3605.
- Beanland, Vanessa et al. (2013). “Acceptability of rider assistive systems for powered two-wheelers”. In: *Transportation research part F: traffic psychology and behaviour* 19, pp. 63–76.
- Becedas, J et al. (2007a). “Algebraic identification method for mass-spring-damper system”. In: *WCECS 2007, Proceedings of the World Congress on Engineering and Computer Science 2007*. Citeseer.
- Becedas, Jonathan et al. (2007b). “Fast identification method to control a flexible manipulator with parameter uncertainties”. In: *Proceedings 2007 IEEE International Conference on Robotics and Automation*. IEEE, pp. 3445–3450.
- Bejarano, FJ, A Poznyak, and L Fridman (2006). “Observer for linear time invariant systems with unknown inputs based on the hierarchical super-twisting concept”. In: *International Workshop on Variable Structure Systems, 2006. VSS’06*. IEEE, pp. 208–213.
- Belov, Alexey et al. (2018). “Enhanced parameter convergence for linear systems identification: The DREM approach”. In: *2018 European Control Conference (ECC)*. IEEE, pp. 2794–2799.
- Benine-Neto, André et al. (2014). “Model reference-based vehicle lateral control for lane departure avoidance”. In: *International Journal of Vehicle Autonomous Systems* 12.3, pp. 284–306.
- Bertolazzi, Enrico et al. (2009). “Supporting drivers in keeping safe speed and safe distance: the SASPENCE subproject within the European framework programme 6 integrating project PReVENT”. In: *IEEE Transactions on Intelligent Transportation Systems* 11.3, pp. 525–538.
- Biral, Francesco et al. (2010). “An intelligent curve warning system for powered two wheel vehicles”. In: *European transport research review* 2.3, pp. 147–156.
- Bolandhemmat, Hamidreza, Christopher Clark, and Farid Golnaraghi (2012). “A solution to the state estimation problem of systems with unknown inputs”. In: *Recent Patents on Mechanical Engineering*.
- Boniolo, I., S. M. Savaresi, and M. Tanelli (2009a). “Roll angle estimation in two-wheeled vehicles”. In: *Control Theory Applications, IET* 3.1, pp. 20–32. ISSN: 1751-8644. DOI: [10.1049/iet-cta:20080052](https://doi.org/10.1049/iet-cta:20080052).

- Boniolo, Ivo, Sergio M Savaresi, and Mara Tanelli (2012). “Lean angle estimation in two-wheeled vehicles with a reduced sensor configuration”. In: *Circuits and Systems (ISCAS), 2012 IEEE International Symposium on*. IEEE, pp. 2573–2576.
- Boniolo, Ivo, SM Savaresi, and Mara Tanelli (2009b). “Roll angle estimation in two-wheeled vehicles”. In: *IET Control Theory & Applications* 3.1, pp. 20–32.
- Boyd, S. et al. (1994). *Linear Matrix Inequalities in System and Control Theory*. Ed. by Philadelphia SIAM. SIAM ed.
- Burgess, John C (1992). “Chirp design for acoustical system identification”. In: *The Journal of the Acoustical Society of America* 91.3, pp. 1525–1530.
- Cabrera, Juan A et al. (2014). “Evolutionary optimization of a motorcycle traction control system based on fuzzy logic”. In: *IEEE Transactions on Fuzzy Systems* 23.5, pp. 1594–1607.
- Cavallo, Viola and Maria Pinto (2012). “Are car daytime running lights detrimental to motorcycle conspicuity?” In: *Accident Analysis & Prevention* 49, pp. 78–85.
- (2014). “Visual factors affecting motorcycle conspicuity: Effects of car daytime running lights and motorcycle headlight design”. In:
- Chabane, Chenane et al. (2012). “Proportional two integral (P2I) observer synthesis for single track vehicle”. In: *20th Mediterranean Conference on Control and Automation (MED 2012)*, pp. 1530–1535.
- Chiu, Kuo-Yu and Sheng-Fuu Lin (2005). “Lane detection using color-based segmentation”. In: *IEEE Proceedings. Intelligent Vehicles Symposium, 2005*. IEEE, pp. 706–711.
- Chong, Michelle S et al. (2015). “Parameter and state estimation of nonlinear systems using a multi-observer under the supervisory framework”. In: *IEEE Transactions on Automatic Control*.
- Chung, E. Y. et al. (2006). “Vision Based for Lane Change Decision Aid System”. In: *2006 International Forum on Strategic Technology*, pp. 10–13. DOI: [10.1109/IFOST.2006.312232](https://doi.org/10.1109/IFOST.2006.312232).
- Cooper, KR (1974). “The effects of aerodynamics on the performance and stability of high speed motorcycles”. In: *Proc. 2nd AIAA Symp. Aerodynamics Sport Competition Automobiles*. Vol. 2.
- Corless, Martin and JAY Tu (1998). “State and input estimation for a class of uncertain systems”. In: *Automatica* 34.6, pp. 757–764.
- Corno, Matteo, Giulio Panzani, and Sergio M Savaresi (2013). “Traction-control-oriented state estimation for motorcycles”. In: *IEEE Transactions on Control Systems Technology* 21.6, pp. 2400–2407.
- Corno, Matteo and Sergio M Savaresi (2010). “Experimental identification of engine-to-slip dynamics for traction control applications in a sport motorbike”. In: *European Journal of Control* 16.1, pp. 88–108.
- Corno, Matteo, Sergio M Savaresi, and Gary J Balas (2009). “On linear-parameter-varying (LPV) slip-controller design for two-wheeled vehicles”. In: *International Journal of Robust and Nonlinear Control: IFAC-Affiliated Journal* 19.12, pp. 1313–1336.
- Cossalter, V et al. (2006a). “Measurement and identification of the vibration characteristics of motorcycle riders”. In: *Proc. ISMA 2006*.
- Cossalter, V et al. (2010). “Motorcycle steering torque decomposition”. In: *World Congress on Engineering*. Vol. 30.
- Cossalter, Vittore and Roberto Lot (2002). “A motorcycle multi-body model for real time simulations based on the natural coordinates approach”. In: *Vehicle system dynamics* 37.6, pp. 423–447.
- Cossalter, Vittore et al. (2006b). “A motorcycle riding simulator for assessing the riding ability and for testing rider assistance systems”. In: *9th Driving Simulation Conference, Paris, France*.
- Dabladji, M. E. H. et al. (2013). “Observer Based Controller For Single Track Vehicles”. In: *proc. of the IEEE Conference on Decision and Control*.
- Dabladji, Mohammed El-Habib et al. (2015). “On the estimation of longitudinal dynamics of powered two-wheeled vehicles”. In: *Control Conference (ECC), 2015 European*. IEEE, pp. 921–926.
- (2016). “Unknown-input observer design for motorcycle lateral dynamics: Ts approach”. In: *Control Engineering Practice* 54, pp. 12–26.
- Dahmani, Hamid et al. (2011). “Vehicle dynamics and road geometry estimation using a Takagi-Sugeno fuzzy observer with unknown inputs”. In: *2011 IEEE Intelligent Vehicles Symposium (IV)*. IEEE, pp. 272–277.
- Damon, P. et al. (2018). “Image-Based Lateral Position, Steering Behavior Estimation, and Road Curvature Prediction for Motorcycles”. In: *IEEE Robotics and Automation Letters* 3.3, pp. 2694–2701. ISSN: 2377-3766. DOI: [10.1109/LRA.2018.2831260](https://doi.org/10.1109/LRA.2018.2831260).
- Damon, Pierre-Marie (2018). “Estimation pour le développement de systèmes d’aide à la conduite des véhicules à deux-roues motorisés”. PhD thesis. Université Paris-Saclay; Université d’Evry-Val-d’Essonne.
- Damon, Pierre-Marie et al. (2017). “Lateral & Steering Dynamics Estimation for Single Track Vehicle: Experimental Tests”. In: *IFAC-PapersOnLine* 50.1, pp. 3400–3405.

- Damon, Pierre-Marie et al. (2018a). “Image-based lateral position, steering behavior estimation, and road curvature prediction for motorcycles”. In: *IEEE Robotics and Automation Letters* 3.3, pp. 2694–2701.
- Damon, Pierre-Marie et al. (Nov. 2018b). “Powered Two-Wheeled Vehicles Steering Behavior Study: Vision-Based Approach”. In: pp. 355–360. DOI: [10.1109/ICARCV.2018.8581298](https://doi.org/10.1109/ICARCV.2018.8581298).
- Damon, Pierre-Marie et al. (2018c). “Powered two-wheeled vehicles steering behavior study: Vision-based approach”. In: *2018 15th International Conference on Control, Automation, Robotics and Vision (ICARCV)*. IEEE, pp. 355–360.
- Damon, Pierre-Marie et al. (2019). “Vision-Based Lane Crossing Point Tracking for Motorcycles”. In: Darouach, Mohamed and Latifa Boutat-Baddas (2008). “Observers for a class of nonlinear singular systems”. In: *IEEE Transactions on Automatic Control*.
- Darouach, Mohamed, Michel Zasadzinski, and Shi Jie Xu (1994). “Full-order observers for linear systems with unknown inputs”. In: *IEEE transactions on automatic control* 39.3, pp. 606–609.
- De Filippi, Pierpaolo et al. (2011a). “Enhancing active safety of two-wheeled vehicles via electronic stability control”. In: *IFAC Proceedings Volumes* 44.1, pp. 638–643.
- De Filippi, Pierpaolo et al. (2011b). “Single-sensor control strategies for semi-active steering damper control in two-wheeled vehicles”. In: *IEEE Transactions on Vehicular Technology* 61.2, pp. 813–820.
- (2012). “Single-sensor control strategies for semi-active steering damper control in two-wheeled vehicles”. In: *IEEE Transactions on Vehicular Technology* 61.2, pp. 813–820.
- De Tommasi, Claudio (2014). *Method for calibrating inertial sensor installed in arbitrary position on board vehicle and sensor system of dynamics of vehicle able to be installed on board in arbitrary position*. US Patent 8,825,274.
- Dee, Thomas S (2009). “Motorcycle helmets and traffic safety”. In: *Journal of Health Economics* 28.2, pp. 398–412.
- Diederichs, JP et al. (2010). “SAFERIDER HMI Strategies for Motorcycles? ARAS and OBIS”. In: *17th ITS World Congress ITS Japan ITS America ERTICO*.
- Dixit, Amit and Shashikanth Suryanarayanan (2008). “Adaptive observers for servo systems with friction”. In: *Control Applications, 2008. CCA 2008. IEEE International Conference on*. IEEE, pp. 960–965.
- Eaton, DJ (1975). “Man-Machine Dynamics in the Stabilization of Single-Track Vehicles,” Univ. of Michigan”. PhD thesis. Ph. D. Thesis.
- Edwards, Dustin (2008). “Parameter estimation techniques for determining safe vehicle speeds in ugvs”. PhD thesis.
- Evangelos, B (2010). “Saferider project”. In: *French National Agency of Reaserch, Tech. Rep.*
- Evangelou, Simos (2004). “Control and stability analysis of two-wheeled road vehicles”. PhD thesis. University of London London.
- Faheem, Malik (Apr. 2017). “Road Accidents and Prevention”. In: *INTERNATIONAL JOURNAL OF ENGINEERING DEVELOPMENT AND RESEARCH* 5, pp. 40–46.
- Flanigan, Erin et al. (2018). *Motorcycle Safety and Intelligent Transportation Systems Gap Analysis, Final Report*. Tech. rep. United States. Joint Program Office for Intelligent Transportation Systems.
- Fliess, Michel and Hebertt Sira-Ramírez (2003). “An algebraic framework for linear identification”. In: *ESAIM: Control, Optimisation and Calculus of Variations* 9, pp. 151–168.
- Fouka, M et al. (2017a). “Mutiple-gradient descent algorithm for parametric identification of a powered two-wheeled vehicles”. In: *2017 IEEE International Conference on Systems, Man, and Cybernetics (SMC)*. IEEE, pp. 3231–3236.
- Fouka, Majda et al. (2019a). “Full Order Observer With Unmatched Constraint: Unknown Parameters Identification”. In: *IEEE Control Systems Letters* 3.4, pp. 1026–1031.
- Fouka, Majda et al. (2017b). “Parametric identification of a powered two-wheeled vehicles: Algebraic approach”. In:
- Fouka, Majda et al. (2018a). “Adaptive Observer for Motorcycle State Estimation and Tire Cornering Stiffness Identification”. In: *2018 IEEE Conference on Decision and Control (CDC)*. IEEE, pp. 3018–3024.
- Fouka, Majda et al. (2018b). “Motorcycle inertial parameters identification via algorithmic computation of state and design sensitivities”. In: *2018 IEEE Intelligent Vehicles Symposium (IV)*. IEEE, pp. 3926–3929.
- Fouka, Majda et al. (2018c). “Road Geometry and Steering Reconstruction for Powered Two Wheeled Vehicles”. In: *2018 21st International Conference on Intelligent Transportation Systems (ITSC)*. IEEE, pp. 2024–2029.
- Fouka, Majda et al. (2018d). “Self-calibration algorithm for an IMU in two-wheeled vehicles: design and experimental validation”. In: *2018 21st International Conference on Intelligent Transportation Systems (ITSC)*. IEEE, pp. 1751–1756.

- Fouka, Majda et al. (2018e). “Simultaneous parameters identification and state estimation based on unknown input observer for a class of lpv systems”. In: *2018 Annual American Control Conference (ACC)*. IEEE, pp. 1120–1125.
- (2019b). “Interconnected Observers for a Powered Two-Wheeled Vehicles: Both Lateral and Longitudinal Dynamics Estimation”. In: *2019 IEEE 16th International Conference on Networking, Sensing and Control (ICNSC)*. IEEE, pp. 163–168.
- Fouka, Majda et al. (2019c). “On Steady-State Cornering Analysis for Motorcycles”. In: Fridman, Leonid, Arie Levant, and Jorge Davila (2007). “Observation of linear systems with unknown inputs via high-order sliding-modes”. In: *International Journal of systems science* 38.10, pp. 773–791.
- Gail, Jost et al. (2009). “Anti lock braking and vehicle stability control for motorcycles—who or why not”. In: *21st International Conference on the Enhanced Safety of Vehicles (ESV), Stuttgart, Germany*.
- Garimella, Phanindra and Bin Yao (2003). “Nonlinear adaptive robust observer design for a class of nonlinear systems”. In: *American Control Conference, 2003. Proceedings of the 2003*. Vol. 5. IEEE, pp. 4391–4396.
- Gasbarro, L. et al. (2004a). “Motorcycle Trajectory Reconstruction by Integration of Vision and MEMS Accelerometers”. In: *Conference on Decision and Control*.
- Gasbarro, Luca et al. (2004b). “Motorcycle trajectory reconstruction by integration of vision and MEMS accelerometers”. In: *Proceedings of the 43th Conference on Decision and Control*, pp. 779–783.
- Georgi, Andreas et al. (2009). “New approach of accident benefit analysis for rear end collision avoidance and mitigation systems”. In: *21st International Technical Conference on the Enhanced Safety of Vehicles*, pp. 09–0281.
- Glaser, Sebastien, Saïd Mammar, and Chouki Sentouh (2010). “Integrated driver–vehicle–infrastructure road departure warning unit”. In: *IEEE Transactions on Vehicular Technology* 59.6, pp. 2757–2771.
- Gonzalez Bautista, David (Apr. 2017). “Functional architecture for automated vehicles trajectory planning in complex environments”. Theses. PSL Research University. URL: <https://pastel.archives-ouvertes.fr/tel-01568505>.
- Gordon, Robert (2016). “Intelligent Transportation Systems”. In: *Cham: Springer*.
- Grigorievich, Verbitskii Vladimir, Bezverhyi Anatoliy Igorevich, and Tatievskiy Dmitry Nikolayevich (2018). “Handling and Stability Analysis of Vehicle Plane Motion”. In: *Mathematics and Computer Science* 3.1, p. 13.
- Groves, P. D (2013). *Principles of GNSS, inertial, and multisensor integrated navigation systems*. Artech house.
- Groves, Paul D (2015). “Navigation using inertial sensors [Tutorial]”. In: *IEEE Aerospace and Electronic Systems Magazine* 30.2, pp. 42–69.
- Grzeżożek, Witold and Krzysztof Weigel-Milleret (2015). “Impact analysis of gyroscopic effects on motorcycle’s stability”. In: *Logistyka* 4, pp. 3556–3562.
- Hammar, Karima (2015). “Identification des systèmes non-linéaires à structure Wiener, Hammerstein, application au cas fractionnaire”. PhD thesis. Université Mouloud Mammeri.
- Herrero, JM et al. (2007). “Non-linear robust identification of a greenhouse model using multi-objective evolutionary algorithms”. In: *Biosystems Engineering* 98.3, pp. 335–346.
- Hildebrand, Roland and Michel Gevers (2002). “Identification for control: optimal input design with respect to a worst-case  $\nu$ -gap cost function”. In: *SIAM Journal on Control and Optimization* 41.5, pp. 1586–1608.
- Honda, By Loz Blain (2017). *Honda’s self-balancing motorcycle*. <https://newatlas.com/honda-self-balancing-motorcycle/47257/>.
- Huang, CK and MC Shih (2011). “Dynamic analysis and control of an anti-lock brake system for a motorcycle with a camber angle”. In: *Vehicle system dynamics* 49.4, pp. 639–656.
- Huth, Véronique et al. (2012). “Comparison of two warning concepts of an intelligent Curve Warning system for motorcyclists in a simulator study”. In: *Accident Analysis & Prevention* 44.1, pp. 118–125.
- Ichalal, D. et al. (2012). “Estimation de la dynamique latérale pour véhicules à deux roues motorisés”. In: *Septième Conférence Internationale Francophone d’Automatique*.
- Ichalal, Dalil and Saïd Mammar (2015). “On unknown input observers for LPV systems”. In: *IEEE Transactions on Industrial Electronics* 62.9, pp. 5870–5880.
- Imaizumi, Hirohide, Takehiko Fujioka, and Manabu Omae (1996). “Rider model by use of multibody dynamics analysis”. In: *JSAE review* 17.1, pp. 75–77.
- Ioannou, Petros A and Jing Sun (1996). *Robust adaptive control*. Vol. 1. PTR Prentice-Hall Upper Saddle River, NJ.
- Jakob, Wilfried and Christian Blume (2014). “Pareto optimization or cascaded weighted sum: A comparison of concepts”. In: *Algorithms* 7.1, pp. 166–185.

- James, Stephen R (2002). "Lateral dynamics of an offroad motorcycle by system identification". In: *Vehicle System Dynamics* 38.1, pp. 1–22.
- Kalman, Rudolf Emil et al. (1960). "Contributions to the theory of optimal control". In: *Bol. soc. mat. mexicana* 5.2, pp. 102–119.
- Kalsi, Karanjit et al. (2010). "Sliding-mode observers for systems with unknown inputs: A high-gain approach". In: *Automatica*.
- Katagiri, Nozomi, Yoshitaka Marumo, and Hitoshi Tsunashima (2008a). *Evaluating Lane-Keeping-Assistance System for Motorcycles by Using Rider-Control Model*. Tech. rep. SAE Technical Paper.
- (Sept. 2008b). "Evaluating Lane-Keeping-Assistance System for Motorcycles by Using Rider-Control Model". In: *SAE Technical Paper*. SAE International. DOI: [10.4271/2008-32-0056](https://doi.org/10.4271/2008-32-0056). URL: <https://doi.org/10.4271/2008-32-0056>.
- (2009). "Controller design and evaluation of lane-keeping-assistance system for motorcycles". In: *Journal of mechanical systems for transportation and logistics* 2.1, pp. 43–54.
- Katayama, T, A Aoki, and T Nishimi (1988). "Control behaviour of motorcycle riders". In: *Vehicle System Dynamics* 17.4, pp. 211–229.
- Khobotov, Evgenii Nikolaevich (1987). "Modification of the extra-gradient method for solving variational inequalities and certain optimization problems". In: *USSR Computational Mathematics and Mathematical Physics* 27.5, pp. 120–127.
- Kidane, Samuel et al. (2009). "Development and experimental evaluation of a tilt stability control system for narrow commuter vehicles". In: *IEEE Transactions on control systems technology* 18.6, pp. 1266–1279.
- Koenen, Cornelis (1983). *The dynamic behaviour of a motorcycle when running straight ahead and when cornering*. Tech. rep.
- Koenig, Damien (2006). "Observers design for unknown input nonlinear descriptor systems via convex optimization". In: *IEEE Transactions on Automatic control*.
- Kooijman, JDG and AL Schwab (2013). "A review on bicycle and motorcycle rider control with a perspective on handling qualities". In: *Vehicle system dynamics* 51.11, pp. 1722–1764.
- Kumar, Ammu M and Philomina Simon (2015). "Review of lane detection and tracking algorithms in advanced driver assistance system". In: *Int. J. Comput. Sci. Inf. Technol* 7.4, pp. 65–78.
- Kuschefski, Achim, Matthias Haasper, and André Vallese (2009). "Advanced Rider Assistance Systems for Powered Two-Wheelers (ARAS-PTW)". In: *Institut für Zweiradsicherheit eV, Germany, Paper* 11-0123.
- Lam, Hak Keung, Hongyi Li, and Honghai Liu (2013). "Stability analysis and control synthesis for fuzzy-observer-based controller of nonlinear systems: a fuzzy-model-based control approach". In: *IET Control Theory & Applications* 7.5, pp. 663–672.
- Lauffenburger, Jean-Philippe (2002). "Contribution à la surveillance temps-réel du système" Conducteur-Véhicule-Environnement": élaboration d'un système intelligent d'aide à la conduite". PhD thesis. Université de Haute Alsace-Mulhouse.
- Lazar, M. et al. (2008). "On input to state stability of min-max nonlinear model predictive control". In: *Systems & Control Letters* 57.
- LeBlanc, David (2006). "Road departure crash warning system field operational test: methodology and results. volume 1: technical report". In:
- Ledwidge, Jim (1995). "System identification and parameter estimation of a motorcycle suspension system". PhD thesis. Dublin City University.
- Lefevre, Stéphanie et al. (2013). "Lane keeping assistance with learning-based driver model and model predictive control". In: *12th International Symposium on Advanced Vehicle Control*.
- Levant, Arie (2003). "Higher-order sliding modes, differentiation and output-feedback control". In: *International journal of Control* 76.9-10, pp. 924–941.
- Limebeer, David JN, RS Sharp, and S Evangelou (2001). "The stability of motorcycles under acceleration and braking". In: *Proceedings of the Institution of Mechanical Engineers, Part C: Journal of Mechanical Engineering Science* 215.9, pp. 1095–1109.
- Limroth, John (2009). "Real-time vehicle parameter estimation and adaptive stability control". In:
- Ling, Bo, David RP Gibson, and Dan Middleton (2013). "Motorcycle detection and counting using stereo camera, IR camera, and microphone array". In: *Video Surveillance and Transportation Imaging Applications*. Vol. 8663. International Society for Optics and Photonics, 86630P.
- Liu, Hongbin et al. (2011). "Friction estimation based object surface classification for intelligent manipulation". In: *IEEE International Conference on Robotics and Automation*.
- Löfberg, Johan (2004). "YALMIP: A toolbox for modeling and optimization in MATLAB". In: *Proceedings of the CACSD Conference*. Vol. 3. Taipei, Taiwan, pp. 284–289.

- Lord, Dominique et al. (2011). *Analysis of roadway departure crashes on two lane rural roads in Texas*. Tech. rep. Texas Transportation Institute.
- Luenberger, David (1966). “Observers for multivariable systems”. In: *IEEE Transactions on Automatic Control* 11.2, pp. 190–197.
- Maeder, Urban and Manfred Morari (2011). “Attitude estimation for vehicles with partial inertial measurement”. In: *IEEE Transactions on Vehicular Technology* 60.4, pp. 1496–1504.
- Mamani, G et al. (2007). “Open-loop algebraic identification method for a DC motor”. In: *2007 European Control Conference (ECC)*. IEEE, pp. 3430–3436.
- Mammar, S., S. Glaser, and M. Netto (2006). “Time to line crossing for lane departure avoidance: a theoretical study and an experimental setting”. In: *IEEE Transactions on Intelligent Transportation Systems* 7.2, pp. 226–241. ISSN: 1524-9050. DOI: [10.1109/TITS.2006.874707](https://doi.org/10.1109/TITS.2006.874707).
- Mammar, S. et al. (2004). “Time-to-line crossing and vehicle dynamics for lane departure avoidance”. In: *Proceedings. The 7th International IEEE Conference on Intelligent Transportation Systems (IEEE Cat. No.04TH8749)*, pp. 618–623. DOI: [10.1109/ITSC.2004.1398972](https://doi.org/10.1109/ITSC.2004.1398972).
- Manzoni, Vincenzo et al. (2010). “A driver-to-infrastructure interaction system for motorcycles based on smartphone”. In: *13th International IEEE Conference on Intelligent Transportation Systems*. IEEE, pp. 1442–1447.
- Marumo, Yoshitaka and Nozomi Katagiri (2011a). “Control effects of steer-by-wire system for motorcycles on lane-keeping performance”. In: *Vehicle System Dynamics* 49.8, pp. 1283–1298.
- (2011b). “Control effects of steer-by-wire system for motorcycles on lane-keeping performance”. In: *Vehicle System Dynamics* 49.8, pp. 1283–1298. DOI: [10.1080/00423114.2010.515030](https://doi.org/10.1080/00423114.2010.515030). eprint: <https://doi.org/10.1080/00423114.2010.515030>. URL: <https://doi.org/10.1080/00423114.2010.515030>.
- Maruyama, Kazuyuki et al. (2014). “Vehicle-to-X functions for improved motorcycle safety”. In: *Auto Tech Review* 3.8, pp. 50–55.
- Møller, Martin Fodslette (1993). “A scaled conjugate gradient algorithm for fast supervised learning”. In: *Neural networks* 6.4, pp. 525–533.
- Montanari, Roberto, Andrea Borin, and Andrea Spadoni (2011). “SAFERIDER: results from Yamaha test site on advanced rider assistance system”. In: *Proceedings of the 9th ACM SIGCHI Italian Chapter International Conference on Computer-Human Interaction: Facing Complexity*. ACM, pp. 132–138.
- Moreno, Jaime A, Edmundo Rocha-Cózatl, and Alain Vande Wouwer (2014). “A dynamical interpretation of strong observability and detectability concepts for nonlinear systems with unknown inputs: application to biochemical processes”. In: *Bioprocess and biosystems engineering* 37.1, pp. 37–49.
- Muller, Alexander and Fevzi Yildirim (2011). “Bosch Motorcycle ABS: Safety for All”. In: *18th ITS World Congress TransCoreITS AmericaERTICO-ITS EuropeITS Asia-Pacific*.
- Murakami, Shintaroh, Hidekazu Nishimura, and Shaopeng Zhu (2012). “Front-Steering Assist Control System Design for a Motorcycle Stabilization during Braking”. In: *Journal of System Design and Dynamics* 6.4, pp. 431–446.
- Nehaoua, Lamri and Hichem Arioui (2008). “Parameters Identification for Motorcycle Simulator’s Platform Characterization”. In: *AIP Conference Proceedings*. Vol. 1019. 1. AIP, pp. 133–138.
- Nehaoua, Lamri et al. (2013a). “Dynamic modelling of a two-wheeled vehicle: Jourdain formalism”. In: *Vehicle System Dynamics* 51.5, pp. 648–670.
- Nehaoua, Lamri et al. (2013b). “Lean and steering motorcycle dynamics reconstruction: An unknown-input HOSMO approach”. In: *2013 American Control Conference*. IEEE, pp. 2821–2826.
- Neves, Aline (2005). “Identification Algébrique et Déterministe de Signaux et Systèmes à Temps Continu: Application à des Problèmes de Communication Numérique”. PhD thesis. Université René Descartes-Paris V.
- Ng, Hai Heng et al. (2018). “BESAFE: Design and Implementation of a DSRC-based Test-bed for Connected Autonomous Vehicles”. In: *2018 21st International Conference on Intelligent Transportation Systems (ITSC)*. IEEE, pp. 3742–3748.
- Oliveira, dmlaw (2013). *Motorcycle Accident Infographic from the personal injury firm d?Oliveira*. <https://newatlas.com/honda-self-balancing-motorcycle/47257/>.
- ONSIR, Observatoire national interministériel de la sécurité routière (2018). *Road Safety annual report*. <https://www.onisr.securite-routiere.interieur.gouv.fr/en/road-safety-performance/annual-road-safety-reports/2018-road-safety-annual-report>.
- Otte, Dietmar, Thorsten Facius, and Stephan Brand (2018). “Serious injuries in the traffic accident situation: definition, importance and orientation for countermeasures based on a representative sample of in-depth-accident-cases in Germany”. In: *International journal of crashworthiness* 23.1, pp. 18–31.
- Pacejka, Hans (2005). *Tire and vehicle dynamics*. Elsevier.

- Pacejka, Hans B (1973). "Simplified Analysis of Steady-state Turning Behaviour of Motor Vehicles. Part 1. Handling Diagrams of Simple Systems." In: *Vehicle System Dynamics* 2.3, pp. 161–172.
- Pacejka, Hans B and Robin S Sharp (1991). "Shear force development by pneumatic tyres in steady state conditions: a review of modelling aspects". In: *Vehicle system dynamics* 20.3-4, pp. 121–175.
- Park, Tae-Geon and Dongwon Kim (2014). "Design of unknown input observers for linear systems with unmatched unknown inputs". In: *Transactions of the Institute of Measurement and Control* 36.3, pp. 399–410.
- Patton, RJ, J Chen, and CJ Lopez-Toribio (1998). "Fuzzy observers for nonlinear dynamic systems fault diagnosis". In: *Proceedings of the 37th IEEE Conference on Decision and Control (Cat. No. 98CH36171)*. Vol. 1. IEEE, pp. 84–89.
- Penumaka, Avinash P. et al. (2014). "In-depth investigations of PTW-car accidents caused by human errors". In: *Safety Science* 68, pp. 212–221. ISSN: 0925-7535. DOI: <https://doi.org/10.1016/j.ssci.2014.04.004>. URL: <http://www.sciencedirect.com/science/article/pii/S0925753514000897>.
- Pertew, AM, HJ Marquez, and Q Zhao (2005). "Design of unknown input observers for Lipschitz nonlinear systems". In: *American Control Conference, 2005. Proceedings of the 2005*. IEEE, pp. 4198–4203.
- Piegay, Nicolas (2015). "Optimisation multi-objectif et aide à la décision pour la conception robuste.: Application à une structure industrielle sur fondations superficielles". PhD thesis. Bordeaux.
- Pietrasik, Tom (2018). *Road traffic injuries*. [https://www.who.int/violence\\_injury\\_prevention/road\\_traffic/en/](https://www.who.int/violence_injury_prevention/road_traffic/en/).
- Popov, AA, S Rowell, and Jacob Philippus Meijaard (2010). "A review on motorcycle and rider modelling for steering control". In: *Vehicle System Dynamics* 48.6, pp. 775–792.
- Rajab, Samer A, Ahmad S Othman, and Hazem H Refai (2012). "Novel vehicle and motorcycle classification using single element piezoelectric sensor". In: *2012 15th International IEEE Conference on Intelligent Transportation Systems*. IEEE, pp. 496–501.
- Rankine, William John Macquorn (1869). "On the dynamical principles of the motion of velocipedes". In: *The Engineer* 28.79, p. 129.
- Reger, Johann and Jerome Jouffroy (2009). "On algebraic time-derivative estimation and deadbeat state reconstruction". In: *Proceedings of the 48th IEEE Conference on Decision and Control (CDC) held jointly with 2009 28th Chinese Control Conference*. IEEE, pp. 1740–1745.
- Rizzi, Matteo et al. (2015). "Effectiveness of motorcycle antilock braking systems (ABS) in reducing crashes, the first cross-national study". In: *Traffic injury prevention* 16.2, pp. 177–183.
- Rodriguez-Vazquez, K and Peter J Fleming (1998). "Multi-objective genetic programming for nonlinear system identification". In: *Electronics Letters* 34.9, pp. 930–931.
- Roll, Georg, Oliver Hoffmann, and J Konig (2009). "Effectiveness evaluation of antilock brake systems (ABS) for motorcycles in real-world accident scenarios". In: *ESV Conference*.
- Roychowdhury, Sohini et al. (2018). "Machine Learning Models for Road Surface and Friction Estimation using Front-Camera Images". In: *2018 International Joint Conference on Neural Networks (IJCNN)*. IEEE, pp. 1–8.
- Sanchez, Julio C et al. (June 2018). "A Flatness-Based Predictive Controller for Six-Degrees of Freedom Spacecraft Rendezvous". In: *IFAC Workshop on Networked & Autonomous Air & Space Systems*. Santa Fe, Nouveau Mexique, United States.
- Savaresi, SERGIO et al. (2006). "Identification of tire-road contact forces by "in-tire" accelerometers". In: *14th IFAC Symposium on System Identification*, pp. 1–6.
- Savaresi, Sergio M et al. (2008). "New regressors for the direct identification of tire deformation in road vehicles via "in-tire" accelerometers". In: *IEEE Transactions on Control Systems Technology* 16.4, pp. 769–780.
- Savino, Giovanni et al. (2013a). "Evaluation of an autonomous braking system in real-world PTW crashes". In: *Traffic injury prevention* 14.5, pp. 532–543.
- Savino, Giovanni et al. (2013b). "Real-time estimation of road–tyre adherence for motorcycles". In: *Vehicle System Dynamics* 51.12, pp. 1839–1852.
- Schwab, AL, PDL De Lange, and Jason K Moore (2012). "Rider optimal control identification in bicycling". In: *ASME 2012 5th Annual Dynamic Systems and Control Conference joint with the JSME 2012 11th Motion and Vibration Conference*. American Society of Mechanical Engineers, pp. 201–206.
- Schwab, AL et al. (2012). "Rider control identification in bicycling, parameter estimation of a linear model using lateral force perturbation tests". In:
- Segel, Leonard and Robert Wilson (1975). "Requirements for describing the mechanics of tires used on single-track vehicles". In: *Vehicle System Dynamics* 4.2-3, pp. 115–115.

- Seiniger, Patrick, Kai Schröter, and Jost Gail (2012). “Perspectives for motorcycle stability control systems”. In: *Accident Analysis & Prevention* 44.1, pp. 74–81.
- Sename, Olivier, Peter Gaspar, and József Bokor (2013). *Robust control and linear parameter varying approaches: application to vehicle dynamics*. Vol. 437. Springer.
- Shabana, A. A (2013). *Dynamics of multibody systems*. Cambridge university press.
- Shahar, Amit et al. (2014). “Towards identifying the roll motion parameters of a motorcycle simulator”. In: *Applied ergonomics* 45.3, pp. 734–740.
- Sharp, R. S. (2001). “Stability, Control and Steering Responses of Motorcycles”. In: *Vehicle System Dynamics* 35, pp. 291–318.
- Sharp, Robin S (1971). “The stability and control of motorcycles”. In: *Journal of mechanical engineering science* 13.5, pp. 316–329.
- (1994). “Vibrational modes of motorcycles and their design parameter sensitivities”. In: *INSTITUTION OF MECHANICAL ENGINEERS CONFERENCE PUBLICATIONS*. Vol. 3. MEDICAL ENGINEERING PUBLICATIONS LTD, pp. 107–107.
- Sharp, RS (2012). “Rider control of a motorcycle near to its cornering limits”. In: *Vehicle system dynamics* 50.8, pp. 1193–1208.
- Sharp, RS, Simos Evangelou, and David JN Limebeer (2004). “Advances in the modelling of motorcycle dynamics”. In: *Multibody system dynamics* 12.3, pp. 251–283.
- Sharp, RS and CJ Jones (1977). “The straight-running stability of single track vehicles”. In: *Vehicle System Dynamics* 6.2-3, pp. 190–191.
- She, Jin-Hua, Xin Xin, and Yaodong Pan (2011). “Equivalent-input-disturbance approach? Analysis and application to disturbance rejection in dual-stage feed drive control system”. In: *IEEE/ASME Transactions on Mechatronics* 16.2, pp. 330–340.
- Sierra, C et al. (2006). “Cornering stiffness estimation based on vehicle lateral dynamics”. In: *Vehicle System Dynamics* 44.sup1, pp. 24–38.
- Silverman, Leonard M and HE Meadows (1967). “Controllability and observability in time-variable linear systems”. In: *SIAM Journal on Control* 5.1, pp. 64–73.
- Slimi, Hamid et al. (2009). “Advanced motorcycle-infrastructure-driver roll angle profile for loss control prevention”. In: *2009 12th International IEEE Conference on Intelligent Transportation Systems*. IEEE, pp. 1–6.
- Svendenius, Jacob (2007). “Tire modeling and friction estimation”. PhD thesis. Department of Automatic Control, Lund University Lund, Sweden.
- Syed, Zainab F et al. (2007). “A new multi-position calibration method for MEMS inertial navigation systems”. In: *Measurement Science and Technology* 18.7, p. 1897.
- Syed, Zainab F et al. (2008). “Civilian vehicle navigation: Required alignment of the inertial sensors for acceptable navigation accuracies”. In: *IEEE Transactions on Vehicular Technology* 57.6, pp. 3402–3412.
- Tanaka, Kazuo and Hua O Wang (2004). *Fuzzy control systems design and analysis: a linear matrix inequality approach*. John Wiley & Sons.
- Tanelli, Mara et al. (2009a). “Active braking control of two-wheeled vehicles on curves”. In: *International Journal of Vehicle Autonomous Systems* 7.3-4, pp. 243–269.
- Tanelli, Mara et al. (2009b). “Control-oriented steering dynamics analysis in sport motorcycles: modeling, identification and experiments”. In: *IFAC Proceedings Volumes* 42.10, pp. 468–473.
- Tapia-Espinoza, Rodolfo and Miguel Torres-Torriti (2013). “Robust lane sensing and departure warning under shadows and occlusions”. In: *Sensors* 13.3, pp. 3270–3298.
- Teerhuis, A. P. and S. T. H. Jansen (2012a). “Motorcycle state estimation for lateral dynamics”. In: *Vehicle System Dynamics* 50.8, pp. 1261–1276. eprint: <http://www.tandfonline.com/doi/pdf/10.1080/00423114.2012.656655>.
- Teerhuis, AP and STH Jansen (2012b). “Motorcycle state estimation for lateral dynamics”. In: *Vehicle system dynamics* 50.8, pp. 1261–1276.
- Touliou, Katerina et al. (2012). “Evaluation of rider’s support systems in Power Two Wheelers (PTWs)”. In: *Procedia-Social and Behavioral Sciences* 48, pp. 632–641.
- Trentelman, Harry L, Anton A Stoorvogel, and Malo Hautus (2012). *Control theory for linear systems*. Springer Science & Business Media.
- Varlakati, Sai Sandeep, V Yogaraja, and Sundaram Sudharsan (2013). *Self Adaptive Front Lighting Mechanism for the Fixed Headlamp Mounted Two Wheelers*. Tech. rep. SAE Technical Paper.
- Velenis, Efstathios, Emilio Frazzoli, and Panagiotis Tsiotras (2009). “On steady-state cornering equilibria for wheeled vehicles with drift”. In: *Proceedings of the 48th IEEE Conference on Decision and Control (CDC) held jointly with 2009 28th Chinese Control Conference*. IEEE, pp. 3545–3550.

- (2010). “Steady-state cornering equilibria and stabilisation for a vehicle during extreme operating conditions”. In: *International Journal of Vehicle Autonomous Systems* 8.2-4, pp. 217–241.
- Venture, Gentiane (2003). “Identification des paramètres dynamiques d’une voiture”. PhD thesis. Ecole Centrale de Nantes (ECN)(ECN)(ECN)(ECN); Université de Nantes.
- Verhaegen, Michel and Vincent Verdult (2007). *Filtering and system identification: a least squares approach*. Cambridge university press.
- Vinande, E., P. Axelrad, and D. Akos (2010). “Mounting-angle estimation for personal navigation devices”. In: *IEEE Transactions on Vehicular Technology*.
- Visvikis, C. et al. (2008). “Study on lane departure warning and lane change assistant systems”. In: *Final Report, Transport research laboratory*. Technical assistance and economic analysis in the filed of legislation pertinent to the issue of automotive safety PROJECT REPORT. URL: <http://www.sciencedirect.com/science/article/pii/S147466701638466X>.
- Wang, W. et al. (2018). “A Learning-Based Approach for Lane Departure Warning Systems With a Personalized Driver Model”. In: *IEEE Transactions on Vehicular Technology* 67.10, pp. 9145–9157. ISSN: 0018-9545. DOI: [10.1109/TVT.2018.2854406](https://doi.org/10.1109/TVT.2018.2854406).
- Wasiwitono, Unggul, I Nyoman Sutantra, Yunarko Triwinarno, et al. (2015). “Steady-state cornering modeling and analysis of three-wheel narrow vehicle”. In: *Applied Mechanics and Materials*. Vol. 758. Trans Tech Publ, pp. 173–178.
- Weir, David H and John W Zellner (1978). *Lateral-directional motorcycle dynamics and rider control*. Tech. rep. SAE Technical Paper.
- Weiss, Marie et al. (2000). “Investigation of a model inversion technique to estimate canopy biophysical variables from spectral and directional reflectance data”. In: *Agronomie* 20.1, pp. 3–22.
- Whipple, Francis JW (1899). “The stability of the motion of a bicycle”. In: *Quarterly Journal of Pure and Applied Mathematics* 30.120, pp. 312–348.
- WHO, World Health Organization et al. (2018). *Global status report on road safety 2018*. World Health Organization.
- Wilhelm, Erik et al. (2012). “Electric vehicle parameter identification”. In: *World Electric Vehicle Journal* 5.4, pp. 1090–1099.
- Woschnagg, ELISABETH and J Cipan (2004). “Evaluating forecast accuracy”. In: *University of Vienna, Department of Economics*.
- Xie, Lihua (1996). “Output feedback  $H_\infty$  control of systems with parameter uncertainty”. In: *International Journal of control* 63.4, pp. 741–750.
- Yang, Jun et al. (2011). “Robust control of nonlinear MAGLEV suspension system with mismatched uncertainties via DOBC approach”. In: *ISA transactions*.
- Yang, Jun et al. (2014). “High-order mismatched disturbance compensation for motion control systems via a continuous dynamic sliding-mode approach”. In: *IEEE Transactions on Industrial Informatics*.
- Yanhua, Yuan and Yan Zhibin (2015). “Revisiting the necessary condition for the existence of Luenberger observer”. In: *Control Conference (CCC), 2015 34th Chinese*. IEEE.
- Yousefi, Hassan, Heikki Handroos, and Azita Soleymani (2008). “Application of differential evolution in system identification of a servo-hydraulic system with a flexible load”. In: *Mechatronics* 18.9, pp. 513–528.
- Yu, Hao and Bogdan M Wilamowski (2011). “Levenberg-marquardt training”. In: *Industrial electronics handbook* 5.12, p. 1.
- Yuen, Choon Wah, Mohamed Rehan Karim, and Ahmad Saifizul (2014). “Investigation on motorcyclist riding behaviour at curve entry using instrumented motorcycle”. In: *The Scientific World Journal* 2014.
- Zhang, Jiancheng and Fanglai Zhu (2018). “Observer-based output consensus of a class of heterogeneous multi-agent systems with unmatched disturbances”. In: *Communications in Nonlinear Science and Numerical Simulation*.
- Zhang, Mei et al. (2017). “Unknown input reconstruction: A comparison of system inversion and sliding mode observer based techniques”. In: *Control Conference (CCC), 2017 36th Chinese*. IEEE, pp. 7172–7177.
- ZindaLawGroup, Zinda & Davis (2015). *Annual Global Road Crash Statistics for the world*. <https://injurylawfirmphoenix.com/car-accident/>.

**Titre :** Contributions à l'Identification Paramétrique et à l'Observation des Véhicules à Deux-Roues Motorisés.

**Mots clés :** Motos (V2RM), Systèmes d'aide à la conduite, Identification, Observation, Fonction de risque

**Résumé :**

Au cours des dernières années, la mobilité routière a été marquée par la croissance considérable du trafic des Véhicules à Deux-Roues Motorisés (V2RM), qui demeure désormais le mode de déplacement le plus dominant et convoité, notamment pour les possibilités qu'il offre d'esquiver les embouteillages de trafic. Cependant, les conducteurs de deux-roues motorisés sont considérés comme les usagers de la route les plus vulnérables. En effet, le risque d'être tué dans un accident est 29 fois plus élevé pour un cyclomoteur que pour un conducteur de voiture de tourisme. En plus, la nature instable des V2RM, les rend plus susceptibles aux pertes de contrôle. Ce problème est d'autant plus important lors du freinage d'urgence ou lors de la prise de virage. Alors que les systèmes de sécurité passifs et actifs (ABS, ESP, ceintures de sécurité, airbags, etc.) développés en faveur des véhicules de tourisme ont amplement contribué à la diminution des risques sur la route, cependant, le retard dans le développement de ces systèmes pour les motos est considérable. De plus, malgré quelques systèmes existants, les conducteurs de motos les utilisent mal ou pas du tout. Ceci est dû à une mauvaise formation et cela ne contribue donc pas à l'amélioration de leur sécurité. Par conséquent, il n'est pas anodin que ce retard, dans le développement des systèmes d'aide à la conduite, résonne avec un retard dans le développement des outils de recherches théoriques.

Dans ce contexte, l'objectif principal de la thèse est de concevoir des systèmes d'assistance à la conduite, ARAS (Advanced Rider Assistance Systems), pour les V2RM pouvant alerter ces conducteurs en amont des situations de conduite dangereuses. Ces dernières sont au cœur de nos travaux de recherche. En réalité, de nombreux défis sont encore ouverts en ce qui concerne la conception des systèmes ARAS comme l'accessibilité des états dynamiques et paramètres physiques des V2RM ainsi que la synthèse des indicateurs de risques en visitant tous les points d'intérêts. Pour cela, nous

nous intéressons alors à proposer des techniques d'estimation, tout en réduisant le nombre de capteurs et en contournant la problématique de non-mesurabilité de certains variables. Par ailleurs, la synthèse de ces approches répondant à certaines exigences (modélisation, structure simple, précision, instrumentation) constitue un défi supplémentaire.

La première partie de thèse est consacrée aux algorithmes d'identification classiques. Ces techniques sont conçues pour estimer les paramètres physiques inconnus des modèles paramétriques des V2RM. La deuxième partie concerne des observateurs basés modèles. Pour cela, un observateur à entrées inconnues (UIO) pour reconstruire la dynamique de la direction en tenant compte de la géométrie de la route, et, un observateur interconnecté (IFO) pour l'estimation de la dynamique longitudinale et latéral, ont été proposées. Ensuite, nous nous sommes penchés sur des méthodes alternatives aux approches d'identification, notamment des techniques d'estimations basées identification capable à la fois d'estimer les états et les paramètres au même temps. À cette occasion, un observateur retardé à entrées inconnues pour les systèmes avec un degré relatif arbitraire (DUIO), et, un observateur de Luenberger adaptative (LAO) pour l'estimation des raideurs pneumatiques ont été développées. Les méthodes proposées nécessitent une combinaison simple de capteurs et prennent en compte des hypothèses réalistes telles que la variation de vitesse longitudinale. Tous ces travaux ont été validés à l'aide de BikeSim et/sur des données expérimentales. En outre, ce manuscrit introduit un algorithme d'auto-calibration pour l'alignement des unités de mesure inertielle (IMU). Une telle méthode d'auto-étalonnage s'applique aux boîtiers télématiques (e-Box) installés sur des véhicules à deux roues, dont les axes des IMU sont souvent mal alignés avec le repère référentielle du véhicule.

La dernière partie de cette thèse traite des indicateurs objectifs (comportement sur/sous vireur de la moto et la distance de sortie de la voie de circulation) pour la quantification du risque.

**Title :** Contributions to Parametric Identification and Observation of Powered Two-Wheeler Vehicles

**Keywords :** Motorcycle (PTWV), Rider assistance system, Identification, Observation, Risk function

**Abstract :**

Nowadays, Powered Two-Wheeled Vehicles (PTWV) are an increasingly popular means of transport in daily urban and rural displacements, especially for the possibilities it offers to avoid traffic congestion. However, riders are considered as the most vulnerable road users. In fact, the risk of being killed in an accident is 29 times higher for a motorcycle than for a driver of a four wheeled vehicle. Therewith, the unstable nature of the PTWV makes them more susceptible to control loss. This problem is even more complex during emergency braking or on cornering maneuvers. As matter of fact, passive and active safety systems (Anti-Lock Braking (ABS), Electronic Stability Control (ESP), seat belts, airbags) developed in favour of passenger vehicles have largely contributed to the reduction of risks on the road. However, the delay in the development of security systems for motorcycles is notable. Moreover, despite some existing systems, motorcycle riders use them badly or they don't use them at all. Therefore, it is not trivial that this delay, in the development of Advanced Rider Assistance Systems (ARAS), coming from a delay in the development of theoretical and research tools.

This thesis fits into the context of designing ARAS for PTWV that can alert riders upstream of dangerous driving situations. Our work deals with observation and identification techniques to estimate the PTWV dynamic states and physical parameters. These latter are fundamental for risk quantification in ARAS design and to assess the safety of the PTWV, which are the main focus of our research work.

The first part of the thesis concerns classical identification techniques to estimate physical parameters of PTWV. The second part deals with model-based ob-

servers implemented to estimate the dynamic states of the PTWV. We proposed an unknown input observer (UIO) for steering and road geometry estimation and an interconnected fuzzy observer (IFO) for both longitudinal and lateral dynamics. An alternative methods for identification algorithms are observer based identifier which provide both parameters identification and states estimation. Therefore, a Luenberger adaptive observer (LAO) to estimate lateral dynamic states and pneumatic stiffness as well as a delayed unknown inputs observer (DUIO) with an arbitrary relative degree, have been developed in this thesis.

As matter of fact, all these techniques allow to estimate the vehicle dynamics while reducing the number of sensors and overcoming the problem of non-measurable states and parameters. These proposed methods require a simple combination of sensors and take into account realistic assumption like the longitudinal speed variation.

Among others, this manuscript introduces a self calibration algorithm for Inertial Measurement Units (IMUs) alignment. Such a self-calibration method is used for telematic boxes (e-Boxes) installed on two-wheeled vehicles, whose IMUs' axes are often result not to be aligned with the vehicle reference system.

Finally, objective indicators are setting up to quantify riding risks. These functions were studied for ARAS purpose.

To highlight the performance of these approaches, we have acquired data from high-fidelity motorcycle simulator and also with data from real motorcycles. To sum up, a comparison tables are drawn up for all the presented approaches. The results of both the numerical simulations and the performed experimentations seem to be quite promising.

